Contact Mechanics of Metal on Polyethylene Hip Replacements

By

Xijin Hua

Submitted in accordance with the requirements for the degree of
Doctor of Philosophy

The University of Leeds
School of Mechanical Engineering

Leeds, UK

July, 2013

The candidate confirms that the work submitted is his own, except where work which has formed part of jointly-authored publications has been included. The contribution of the candidate and the other authors to this work has been explicitly indicated below. The candidate confirms that appropriate credit has been given within the thesis where reference has been made to the work of others.

1. **Chapter 3** of this thesis is based on a jointly-authored journal paper: Hua, X., Wroblewski, B. M., Jin, Z. and Wang, L., "The effect of cup inclination and wear on the contact mechanics and cement fixation for ultra high molecular weight polyethylene total hip replacements", Medical Engineering & Physics, 2012, 34(3): 318-325. The candidate developed and solved the models and presented the results of the models. Professor Wroblewski, Professor Jin, and Dr Wang contributed ideas and valuable discussion of the paper.

2. **Chapter 3** of this thesis is based on a jointly-authored journal paper: Hua, X., Wroblewski, B. M., Wang, L., Jin, Z. and Fisher, J. "The cup outer diameter influences the cement fixation of Charnley total hip replacement", Journal of Biomechanics, 2012, 45(S1): S82. The candidate developed and solved the models and presented the results of the models. Professor Wroblewski and Professor Jin contributed ideas and valuable discussion of the paper. Professor Jin and Dr Wang contributed the review of the paper.

This copy has been supplied on the understanding that it is copyright material and that no quotation from the thesis may be published without proper acknowledgement.

The right of Xijin Hua to be identified as author of this work has been asserted by him in accordance with the Copyright, Designs and Patents Act 1988.

Acknowledgements

Firstly, I would like to thank my supervisors, Professor John Fisher, Professor Zhongmin Jin, Professor Ruth K Wilcox and Dr Ling Wang for their great supervision and professional guidance throughout my PhD. Without their help it would have been impossible to complete this work. From them I have learned an attitude towards scientific research that will benefit me for a lifetime.

Thanks to the University of Leeds for the financial support to my study.

I would also like to thank Dr Mazen Al-Hajjar for his patient guidance and help with the experimental work. Also, thanks to Dr Feng Liu and Dr Qingen Meng for their guidance and advice for developing modelling at the beginning of my PhD. Thanks to Dr Alison Jones for the thesis grammar checking.

I would like to thank the secretarial staff of the school especially Mrs Debra Baldwin and Mrs Cheryl Harris who provided administrative support throughout all my studies.

Thanks to all of the people in Office 442c. A supportive research atmosphere makes a positive PhD daily life. Thanks to Manyi, Wei, Junyan, Mazen, Raman, Abdellatif, Simon, Dawn, Phil, Adam, Stewart, Nick and Salah, who shared their experience and joyful time with me during my PhD study.

I would like to thank my sisters, my brother and all my friends for their help, care and love. Thank you to my parents for their unconditional support and constant love.

Most importantly, I would like to thank my wonderful wife, Dr Juanjuan Zhu, who is the most important person in my life. Thanks for her help, support, encouragement and company in the past four years during my PhD study.

Finally, I would like to dedicate this thesis to my lovely daughter, Qinyi Hua. Her birth has brought me great happiness and motivation during my thesis writing-up.

Abstract

Metal-on-ultra high molecular weight polyethylene (UHMWPE) total hip replacement (THR) has been the most popular and clinically successful hip prosthesis to date. The long-term performance of THR depends on both the tribological characteristics and biomechanical behaviour of the prosthesis. This project focused on understanding the contact mechanics and mechanical behaviour of cemented and cementless metal-on-UHMWPE THRs under different conditions using a computational approach.

Three-dimensional (3D) computational models of THRs with realistic pelvic bone were developed. Two typical bearings, the Charnley hip and the Pinnacle cup system, were investigated. The effect of different factors on the contact mechanics and cement stresses for Charnley THR were examined. Additionally, the contact mechanics and mechanical behaviour of Pinnacle THR under daily activities, standard and microseparation conditions were analysed.

The cup angles and penetration depths in the cup, and the sizes of the components were found to have a significant effect on the contact mechanics and cement stresses for Charnley THR. The stresses at the bone-cement interface for the Charnley THR with outer diameter of 40 mm were predicted to be higher than that of 43 mm, the difference was found to be consistent with the clinical observation of different aseptic loosening rates.

The cup angles and radial clearances were found to have a synergistic effect on the contact mechanics of Pinnacle THR. Edge loading on both articulating surface and backside surface of the liner was observed during some daily activities due to steep cup inclination angles and smaller radial clearance. The introduction of microseparation into the gait cycle, especially when combined with steep cup inclination angles, resulted in concentrated stresses and plastic deformation in the liner, which would cause potential damage to the liner. Therefore, it is critically important to reduce the levels of rotational and translational mal-positioning of the components clinically.

Table of Contents

List of Tables

List of Figures

List of Abbreviations

2D	two-dimensional
3D	three-dimensional
AoP	alumina-on-polyethylene
AVN	avascular necrosis
BW	body weight
CoC	ceramic-on-ceramic
CoCrMo	chrome cobalt molybdenum alloy
CoCr	cobalt chromium alloy
CoM	ceramic-on-metal
CoP	ceramic-on-polyethylene
CT	computed tomography
DOF	degree of freedom
FE	finite element
HA	hydroxyapatite
HIPed	Hot Isostatically Pressed
LFA	low friction arthroplasty
MoM	metal-on-metal
MoP	metal-on-polyethylene
OA	osteoarthritis
PMMA	polymethylmethacrylate
ROM	range of motion
PTFE	polytetrafluoroethylene
THR	total hip replacement
UHMWPE	ultra high molecular weight polyethylene
VIP	Variable Interface Prosthesis

Chapter 1
Introduction and Literature Review

1.1 Introduction

THR is one of the best solutions for hip joint diseases and the most successful surgical interventions in the orthopaedics field. It is a surgical technology that replaces the hip joint with artificial parts, aiming to reduce joint pain, restore hip function and improve the quality of life for patients with severe hip disease and injury. Several material combinations for hip joint replacements have been introduced, including metal-on-polyethylene (MoP), ceramic-on-polyethylene (CoP), metal-on-metal (MoM), ceramic-on-ceramic (CoC) and ceramic-on-metal (CoM). Each of them has its own benefits and limitations. Due to its durability and performance, MoP has been the leading bearing material combination chosen by surgeons for at least 30 years, and remains the gold standard for hip joint replacements today.

Hip replacements can fail for a variety of reasons, either biologically or mechanically. By far the most common cause is called "aseptic loosening" (Ingham and Fisher, 2005). Aseptic loosening occurs when the hip implants become loose within the bone as a result of focal periprosthetic inflammatory bone loss. This focal inflammation is induced by particulate wear debris, which is generated primarily on the articulating surface or other non-articular prosthesis or cement interface (Goldring et al., 1983). When failure of the implant occurs, a re-operation is required to replace the failed joint with a new prosthesis. This re-operation is called a "revision". Hip replacement revisions are often not as successful as the primary operations. Patients with revision operations tend to have less overall motion of the joint, and the longevity of the implant decreases with each revision. Aseptic loosening and revision of hip prostheses are caused by many reasons and involve many factors such as the component design, the fixation of the components, the conditions that the implants are subjected to, etc (Sundfeldt, et al., 2006).

For this reason, pre-clinical testing and evaluation of the THR are necessary and very important. The development of experimental tests to simulate *in*

vivo kinematics and loading conditions allow the performance of the implant system to be evaluated physiologically. However, experimental studies are complex, time consuming and expensive to conduct. Alternatively, computational simulation is an effective solution for assessing and evaluating the performance of THR. By modifying the input conditions and system parameters, the performance of the hip implant under different conditions can be evaluated and tested and the design can be optimized. With the help of computational simulation, the mechanical behaviour of hip prostheses, as well as the mechanism of the failure of the hip replacements can be better understood.

The computational analysis of contact mechanics and fixation of the THR is very important. Contact stress, one of the parameters from the contact mechanics analysis, is generally related to the fatigue-related wear mechanism and surface damage of hip prostheses (Rostoker and Galante, 1979; Rose et al., 1983; McNie et al., 1998). In view of this, to minimize the contact stresses has been the ultimate goal for design of the implants. In most cases, contact occurs within the surface of the cup and the contact stresses are at a low level in MoP THR due to the lower stiffness of the polyethylene of the cup compared to the metal of the femoral head. However, under certain circumstances, some unexpected consequences can occur. Contact may be extended to the edge of cup, namely "edge loading", which can lead to a stress concentration and potentially plastic deformation of the material, causing damage to the cup (Besong et al., 2001a; Williams et al., 2003). The scientific understanding of the contact mechanics of MoP THR undergoing edge loading is still in a preliminary stage and is the main focus of this research.

1.2 The Human Hip Joint

1.2.1 Synovial Joint

In the human body, a joint is the location at which two or more bones make contact. It is constructed to allow various movements and provide mechanical support. The most common type of joint in the human body is the synovial joint (Moor and Agur, 2002). In the synovial joint, the end of the

articulating surface is covered with hyaline cartilage - the articular cartilage. The articulating bones are separated by a space called the joint cavity but held together by the synovial membrane, which forms a synovial capsule and secretes synovial fluid into the joint cavity for lubrication and also provides a source of nutrition (Blewis et al., 2007). The outer layer of the capsule consists of the ligaments that hold the bones together, as shown in Figure 1.1. Movement of the joint is controlled by the action of the muscles, which are connected to the bone via tendons.
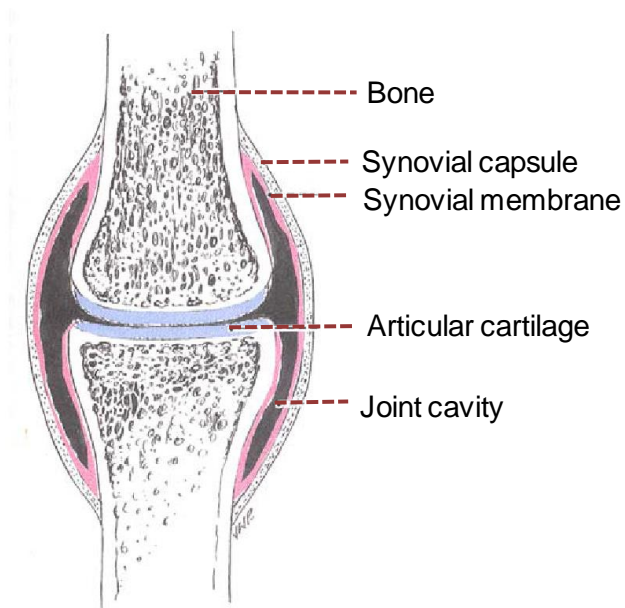
Figure 1.1 Typical synovial joints (Fisher, 2001).

1.2.2 Anatomy of The Hip Joint

The hip joint is a typical ball and socket type of synovial joint, which connects the lower extremities of the body to the pelvis and axial skeleton of the trunk. The hip joint is formed by the head of the femur (thigh bone) and the acetabulum of the pelvis (Figure 1.2 a), and as such it accommodates a wide range of movements, as well as transmits high dynamic loads (7-8 times the body weight (BW)) (Palastanga et al., 2006). The hip joint is wrapped in a capsule that contains the synovial fluid (Figure 1.2 b). The stability of the hip joint is mainly ensured by the strong ligaments, the joint capsule that surrounds the hip joint and the muscles that surround the hip.
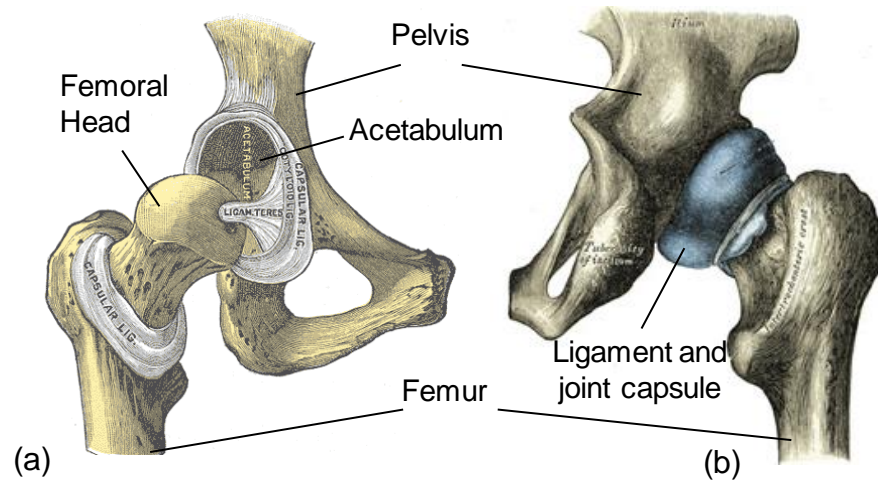
Figure 1.2 The nature hip joint. (a) dissected joint, (b) hip joint with synovial capsule (Gray, 2000).

The pelvis is a large semicircular complex structure, which comprises three bones: the ilium, ischium and pubis (Figure 1.3). The uppermost bone is the ilium which is formed in the shape of a wing. The ischium forms the middle portion of the pelvis, and the pubis is the lower, posterior part. The three bones are joined together and form the acetabulum.

The femur is the longest and strongest bone in the body and forms the thigh. Close to the top of the femur are two protrusions, known as the greater trochanter and lesser trochanter (Figure 1.3). The main function of the two trochanters is for muscle attachment. The femoral neck connects the head and the main femoral shaft. The angle between the femoral neck and the shaft is known as the inclination angle in the frontal plane and anteversion angle in the horizontal plane. In an average adult, the inclination angle of the femoral head is approximately 125⁰ and the anteversion angle is around 10⁰. However, these angles vary from one individual to another (Palastanga et al., 2006).
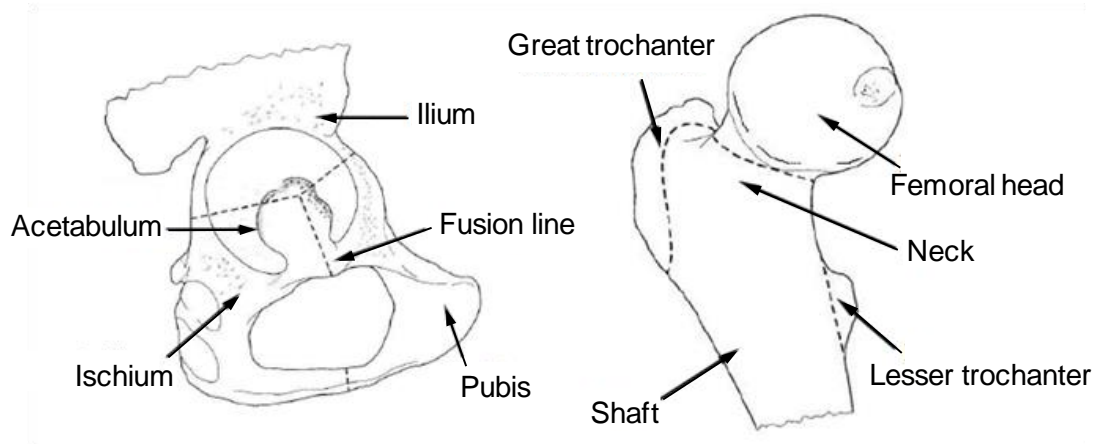
Figure 1.3 The bones of pelvis and femur (Norkin and Levangie, 1992).

1.2.3 Hip Joint Motion

The ball-in-socket configuration of the hip joint allows the head of the femur to rotate inside the socket of the acetabulum, resulting in three degrees of freedom (DOF) movement in three planes: flexion-extension in the sagittal plane, abduction-adduction in the coronal plane, and internal-external rotation in the transverse plane (Figure 1.4).

Hip flexion involves moving the femur forward/upward relative to the top of the pelvis while extension is moving the femur backward/downward. Abduction is lateral movement away from the midline of the body while adduction is medial movement towards it. Internal rotation or medial rotation is rotary movement around the longitudinal axis of the bone towards the centre of the body which will turn the thigh inward, while external rotation or lateral rotation is the rotary movement away from the centre of the body which will turn the thigh outward (Gray, 2000) (Figure 1.4). A mixture or a single contribution of these movements produces the range of movements that are experienced during daily life.

Flexion and extension   Abduction and adduction

Internal-external rotation
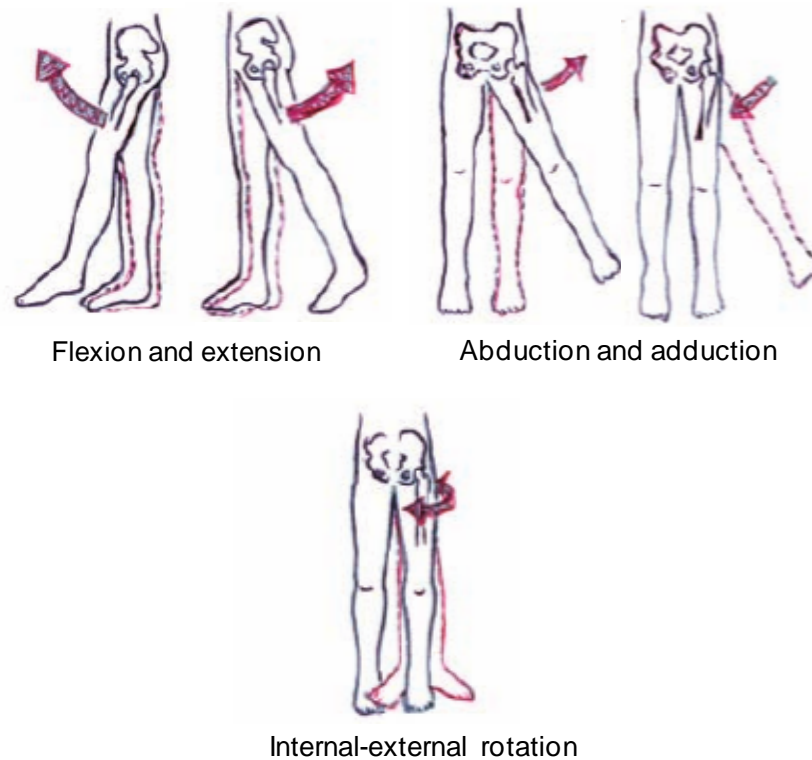
Figure 1.4 The anatomic movements for the hip joint (Neill, 2008).

Hip joint motion during normal walking has been measured using different methods and instruments, among which, two typical studies were conducted by Johnston and Smidt (1969), and Bergmann's group (Bergmann et al., 1993; 2001a; 2004). In 1969, Johnston and Smidt measured the hip joint motion during walking for thirty-three normal subjects by an electro goniometric method, and reported that the mean ranges of movement for the hip motion during walking were approximately 37° and 15° for flexion and extension, 7° and 5° for abduction and adduction, 5° and 9° for internal and external rotation respectively (Figure 1.5). Bergmann et al. (2001a) measured the patterns of hip motion *in vivo* from patients in several daily activities. According to their studies, the ranges of movement for the hip motions during walking were approximately between -6° and 26° for flexion-extension, -9° and 9° for adduction-abduction, -2° and 12° for internal-external rotation respectively. Other patterns and ranges of movement for hip motion during walking have also been reported, and these are summarised in Table 1.1.
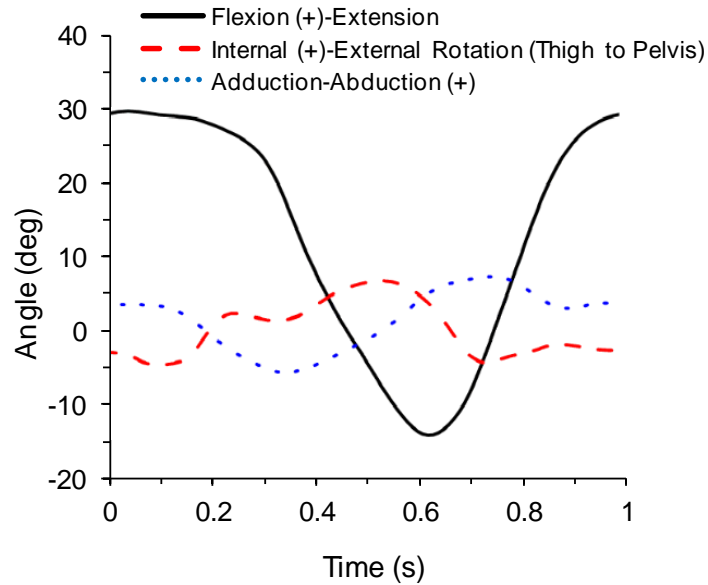
Figure 1.5 Normal pattern of hip joint motion (Johnston and Smidt, 1969).

Table 1.1 The mean total ranges of hip joint motion during the gait cycle.

Studies	Methods	Age	Mean ranges of motion		
			FE (⁰)	AA (⁰)	IER (⁰)
Sutherland et al, 1980	Cline film	19-40	43	14	9
Isacson et al., 1986	Goniometer	25-35	30.2	13.6	9.9
Kadaba et al., 1990	Vicon	18-40	43.2	11.6	13
Smidt, 1971	Electrogoniometer	23-56	42	12.2	10
Gore et al., 1984	Electrogoniometer	18-74	40	10-15	10
Apkarian et al., 1989	Video	21-26	25	13	18
Õunpuu, 1995	Cinematography	Adults	43	13	8

1.2.4 Hip Joint Loading

Daily activities such as normal walking, running, climbing and even standing and sitting can produce a broad range of forces that act upon the hip joint. These forces are mainly generated by the activity of muscles that cross the hip, the weight of the limbs and trunk, and the inertia forces caused by the mass of the body.

The studies that estimated the resultant forces acting on the hip joint during normal daily activities have been conducted using two main techniques. The first method was by mathematical calculation. This method is based on simplified muscle models and use a reduction method or optimisation technique (Paul, 1966; Fraysse et al., 2009). The musculoskeletal model is developed and the external forces (e.g. ground reaction force) are measured and are transmitted through the lower limb of the human body. Equilibrium is specified at each of the joints in the lower limb. Due to the redundancy of the muscles and other tissues, the number of variables generally exceeds the number of the equilibrium equations and cannot be solved with a unique solution. Two general approaches are used to overcome this problem: (1) the reduction technique, in which the number of variables is reduced so as to make exact solution of the equilibrium equations possible by making simplified assumptions about the anatomy and function of the load transmitting elements (Paul, 1966; Duda et al., 1997); or (2) the optimisation method, where all the variables are included and the equilibrium equations are solved by choosing a specified criteria, e.g., the minimisation of energy consumption (Stansfield et al., 2003; Hashimoto et al., 2005).

The second method was by using instrumented implants. This approach can provide the most accurate measurements and be used for different activities. However, such a method has ethical issues and some challenges, such as the cost and technical complexity. Importantly, this method cannot study truly normal hips. Nevertheless, this method has been widely used by Rydell (1966), English and Kilvington (1979) etc in early studies, and by Bergmann's group (Bergmann et al., 2001a; 2004) in more recent studies.

The hip resultant forces during different daily activities that have been reported are summarised in Table 1.2. Two typical studies should be noted. The first study was conducted by Paul (1966), who predicted the resultant forces that transmitted at the joints in the human body during walking. The hip resultant force curve obtained from this study is still regarded as one of the standard loading configurations for modern hip simulators. The second study was conducted by Bergmann's group (Bergmann et al., 1993; 2001a; 2004), in which, gait analysis data along with hip joint contact forces and ground reaction forces were documented for the most common human

activities like walking, stair climbing, standing up, etc. These data have been applied as inputs into computational models to study the biomechanics of both natural hip joints and artificial hip joints (Tong et al., 2008; Zant et al., 2008; Anderson et al., 2008; Harris et al., 2012).

Figure 1.6 shows a wave pattern of the hip resultant force during walking which was obtained from Bergmann's study (Bergmann et al., 2001a). It shows a double-peak pattern with the maximum force occurring at the first peak in the gait cycle. The hip resultant forces during level walking ranged from 2.64 BW to 7.6 BW, which were found to be dependent on the walking speed, muscle strength, gender and age of the studied subjects, as well as on the technique used (Bergmann et al., 1993; 2001a; Hashimoto et al., 2005).

Interestingly, the hip resultant forces during normal activities calculated by the mathematical method were consistently higher than those measured *in vivo* by using instrumented prostheses. This is likely because the instrumented prostheses studies were conducted on patients with medical conditions and hence could not be classified as 'normal' hips, whilst in mathematical studies, several assumptions were made which may affect the accuracy of the outcomes. (Brand et al., 1994; Stansfield et al., 2003).
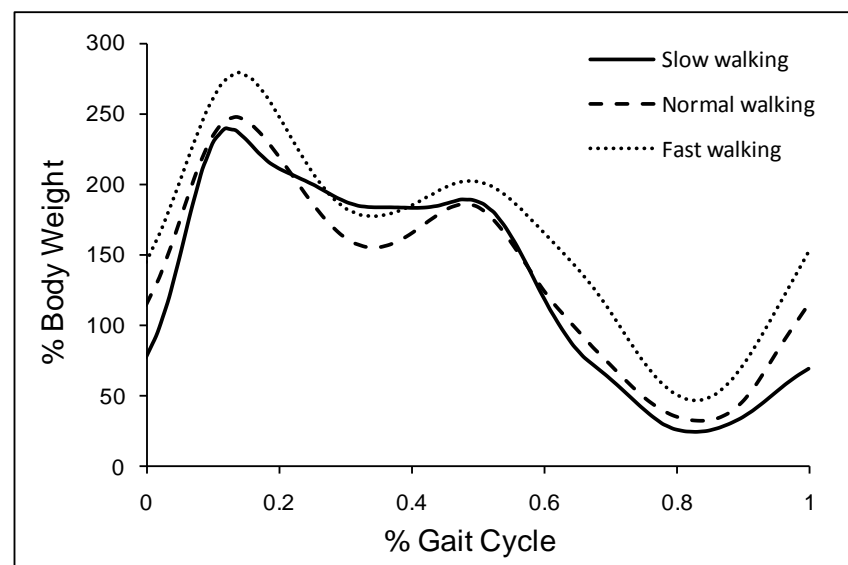
Figure 1.6 Averaged variation during the walking cycle of the resultant hip joint force at fast, normal and slow speeds (Bergmann et al., 2001a).

Table 1.2 Typical studies on hip joint forces during different activities.

Studies	Hip joint forces (BW)		Activities	Methods used
	Max	Average		
Rydell, 1966	3.3 2.9	-- --	Walking (1.4 m/s) One-legged stance	Instrumented implants
Paul, 1966	6.4	3.88	Walking	Reduction
Paul, 1976	--	4.9 4.9 7.6 7.2 7.1	Slow walking (1.10 m/s) Normal walking (1.48 m/s) Fast walking (2.01 m/s) Ascending stairs Descending stairs	Reduction
Crowninshield et al., 1978	5.0 7.6 3.9 3.7	4.3 -- -- --	Walking (0.95-1.05 m/s) Ascending stairs Descending stairs Rising from chair	Optimisation
English and Kilvington, 1979	2.7 3.59	-- --	Walking (0.73 m/s) One-legged stance	Instrumented implants
Davy et al., 1988	2.8 2.6 2.1	2.64	Walking (0.5 m/s) Stair climbing One-legged stance	Instrumented implants
Iglic et al., 1993	2.4	--	One-legged stance	Reduction
Brand et al., 1994	4.0	3.5	Walking (1.11-1.36 m/s)	Optimisation
Duda et al., 1997	3.8		Level walking	Reduction
Heller et al., 2001	3.1 3.2	2.7 2.7	Walking (1.08 m/s) Ascending stairs	Optimisation
Stansfield et al., 2003	3.2 2.8 2.2 4.5	3.1 2.6 2.2 3.8	Walking (1.43 m/s) Rising from chair Sitting on chair 2-1-2 leg stance	Optimisation
Fraysse et al., 2009	--	4.0	Walking	Optimisation
Bergmann et al., 1993	8.7 5.5	--	Stumbling Jogging	Instrumented implants
Bergmann et al., 2001a		2.33 2.32 2.52 2.60 1.90	Walking (1.08 m/s) One-legged stance Ascending stairs Desending stairs Rising from chair	Instrumented implants
Hashimoto et al., 2005		2.68 3.50 3.04	Normal walking Normal walking (young group) Normal walking (old group)	Optimisation
Simonsen et al., 1995		5.5	Walking	Optimisation

1.2.5 Hip Joint Disease

The hip joint is one of the strongest and most durable joints and serves a number of functions in the human body. However, it may suffer from disease or trauma, leading to joint pain, inflammation and even loss of the function and disability (Charlish, 1996). Hip joint disease can affect a variety of people from all age groups. The most common disease is hip arthritis, which is any condition that leads to degeneration of the joint and the cartilage surface (Charlish, 1996). Osteoarthritis (OA) is the most common arthritis form. It occurs when the equilibrium between the breakdown and repair of the joint tissues becomes unbalanced. It is a slow, progressive, ultimately degenerative disorder confined to movable joints. OA mainly affects older people and can range from mild to severe conditions. Apart from age-related reasons, it is also believed to be induced by high levels of stress in the joint causing structural and biomechanical changes (Hellio and Graverand-Gastineau, 2009). The end-stage of OA is the condition under which the cartilage is completely worn out, the femoral and acetabular subchondral bones are exposed and are directly in contact with each other (Muehleman and Arsenis, 1995).

Rheumatoid arthritis is an inflammatory condition that affects the lining of all joints in the body. It causes an inflammatory response in the joint lining which destroys the articular cartilage and surrounding tissues (Charlish, 1996).

Avascular necrosis (AVN), also known as osteonecrosis, is a disease which commonly involves the hip joint. The end result of this disease is the collapse and complete deterioration of the femoral head, commonly referred to as the "ball" of the hip joint (Charlish, 1996).

1.3 Artificial Hip Joint

1.3.1 Overview

The hip joint is expected to function in the human body for a lifetime. However, hip disease or trauma often require this natural bearing to be replaced by an artificial one. Hip joint replacement is currently the most

successful surgical treatment for hip joint disease, and the outcomes are excellent with a long-term survival rate of minimum 70% at 35 years for hip arthroplasty in the follow-up studies (Hardidge et al., 2003; Callaghan et al., 2009). Most patients with hip replacements have excellent pain relief and improved ability to perform routine daily activities.

There are two main choices that should be considered when a hip joint replacement is undertaken: the materials for the components and fixation methods for the prostheses. The most popular and favourite material combinations for the hip joint replacement are MoP, MoM and CoC. They are usually categorized into hard-on-soft combinations (e.g. MoP) and hard-on-hard combinations (e.g. MoM and CoC). Fixation of the implants can be achieved by using bone cement (referred as cemented hip replacement) or a porous sintered coating which allows bone in-growth (referred as non-cemented or cementless hip replacement) or combination of them (hybrid hip prostheses). The selection of the material combination and fixation method for the hip joint replacements depend on several factors, including the age and activity level of the patient, and the surgeon's preference.

1.3.2 History of Hip Joint Replacement

The earliest recorded attempt on hip joint replacement was in 1891, using ivory to replace the femoral head and fixing the implant to the bone with nickel-plated screws. However, the implant suffered extrusion after several months of wear (McKee, 1982). In 1938, Philip Wiles developed the first implanted MoM hip joint replacement, in which stainless steel was used for both the acetabular cup and femoral head. However, the materials had poor wear characteristics and the components of cup and head had matching sizes with no clearance between them. Therefore, these hip prostheses failed soon mainly due to excessive wear and equatorial binding.

The first generation of MoM hip joint replacement was introduced in 1960s. Designs included the Mckee-Farrar, Ring, Hugger and Müller. Figure 1.7 shows the design of Mckee-Farrar and Müller MoM hip joint replacement. However, by 1975, the MoM combination was abandoned due to poor prosthesis design, limited choice of materials, poor manufacturing processes, and more importantly, concerns over biological reaction to the

alloy constituents. However, merit exhibited in some of the first generation of MoM hip prostheses prompted the revival of the second generation of MoM hip joint replacement in late 1980s.

In late 1980s, concerns over osteolysis attributed to polyethylene wear debris, and improvements in technology, production tolerances and the material design prompted a renaissance of MoM bearings, particularly in Switzerland. These new-generation MoM joints have been more successful. Typical designs at this stage included the Müller prosthesis, the Ultamet hip joint replacement manufactured by Depuy International and the Metasul hip joint replacement by Zimmer Orthopaedics.
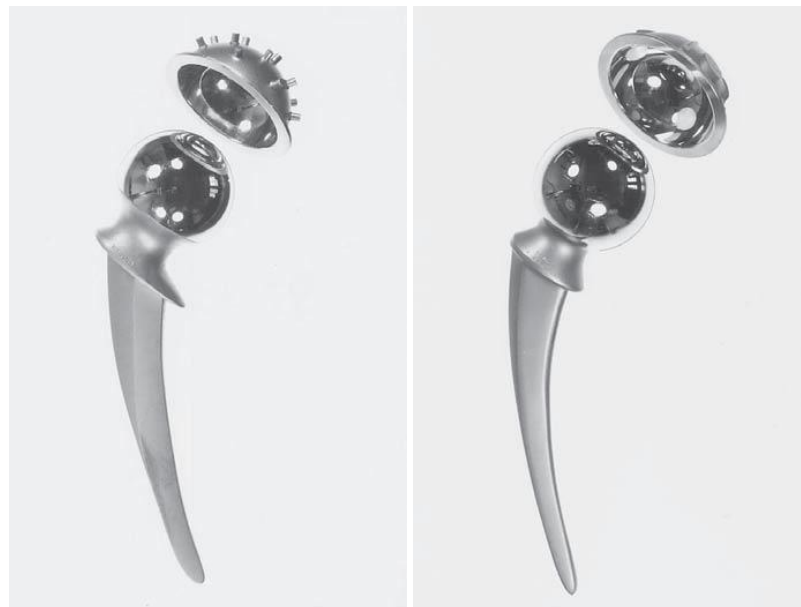
Figure 1.7 The first generation of MoM hip joint replacement. Left-McKee-Farrar design, right- Müller design (Semlitsch and Willert, 1997).

In 1960s, Sir John Charnley designed the first metal-on-polymer hip joint replacement, which has been a basis for existing designs of the modern Charnley total hip arthroplasty (Charnley et al., 1961). At the beginning, the bearing combination of polytetrafluoroethylene (PTFE) as the acetabular cup and stainless steel as the femoral head was used due to the low friction property of PTFE and the assumption that lower friction had lower wear. In order to minimize the mechanical loosening of the component fixation, a femoral head diameter of 22.225 mm was chosen in this low friction prosthesis. However, clinical results showed that the majority of these

prostheses failed due to complete penetration of the femoral head through the acetabular cup within three years (Charnley et al., 1969). Following the poor success of the PTFE replacement, a high density polyethylene (HDPE) was introduced in 1962 which articulated against a stainless steel head. The follow up studies had shown a 92.7% success rate for 379 hips between 4 and 7 years (Charnley, 1972) and a 92% success rate of 106 implants between 9 and 10 years (Charnley and Cupic, 1973). Later on, a more appropriate polymer known as UHMWPE with low friction coefficient, high resistance to wear and high impact resistance was introduced to replace the PTFE and HDPE cups. This prosthesis was called the "Low Friction Arthroplasty" (LFA), as shown in Figure 1.8, and has become the most widely used implant since then (Wroblewski et al., 2009a).

In the mid 1960s, Müller adopted Charnley LFA's concept and introduced his metal-on-UHMWPE hip prosthesis. The femoral head was made from a cast chrome cobalt molybdenum alloy (CoCrMo) and the diameter was increased from 22.225 to 32 mm. aiming to increase the range of motion (ROM) and reduce the risk of dislocation.

Figure 1.8 Charnley low friction metal-on-UHMWPE total hip joint replacement (Semlitsch and Willert, 1997).

In the early 1970s, CoC joints were first used by Boutin because of the favourable wear and frictional characteristics combined with good biocompatibility (Sedel et al., 1994). In CoC hip joint replacement, the articulating surfaces are made from aluminium oxide ceramic. Ceramic components are extremely wear resistant and have much smaller debris particles than those of the MoP components. The surfaces have a high wettability which also reduces friction in the articulating surfaces.

1.3.3 Cemented and Cementless Hip Joint Replacement

Two primary methods have been used to secure the fixation of a total hip prosthesis to the skeleton: the cemented method and the uncemented (cementless) method. The common aim of both fixation methods is to produce a strong, durable interface between the implant and the bone.

Cemented Hip Joint Replacement

The cemented approach for the fixation of hip joint replacements was introduced by Sir John Charnley in 1960 and has been the basis for the development of Charnley LFA over the following decades (Charnley et al., 1969). The rationale behind the cemented THR is to employ polymethylmethacrylate (PMMA) bone cement as a medium to fix the components to the bone. After the procedure, the bone cement completely fills the irregular gap between the bone and the implants and thus allows the smooth transfer of physiological loading from the prosthesis to the bone (Ries et al., 2006).

PMMA bone cement has been used in cemented THR for more than 50 years. The main mechanical function of PMMA bone cement is to transfer the stress across the interface between the components and the bone to ensure that the artificial implant remains in place over the long term (Ries et al., 2006). The yield strength for the regular PMMA bone cement is about 11.6 MPa (Boger et al., 2008a). However, the value is dependent on the quality of the cement, such as the porosity, viscosity, composition etc (Boger et al., 2007; Boger et al., 2008b).

PMMA bone cement itself is not a true glue and has poor adhesive properties (Kuehn et al., 2005). The fixation of the implant to bone was

implemented through the mechanical interlock between the porous cancellous bone and the geometric features of the prosthesis. To achieve this, it is absolutely necessary to ensure intimate contact between the bone and cement, and the cement and implant over the maximum possible area. The intimate contact between the bone and cement inevitably make the cement penetrate into the cancellous pore spaces or irregularities in cortical surfaces. Therefore, the true interface layer between the bone and cement is actually a transition region of a bone-cement composite, rather than a flat interface between cement on one side and bone on the other (Lewis, 1997). However, in computational modelling, the bone-cement interface has usually been considered to be a bilayer, which consists of the surface of bone and the surface of cement individually on two sides. (Lamvohee et al., 2009; Coultrup et al., 2010).

The cemented procedure is preferably recommended for older patients over age 60, all patients with cervical neck fractures, or younger patients with poor bone quality and density who cannot tolerate a long period of rehabilitation. Due to the improved cementing techniques, good outcomes of both short term and long term survivorship of cemented THR have been achieved and well documented (Schulte et al., 1993; Callaghan et al., 2009). However, aseptic loosening has been the major challenge for the durability of this kind of prosthesis. As the bone cement ages and cracks occur, the bond between the bone and the implant may be lost after the cemented operation, promoting the process of loosening of the hip prosthesis (Gardiner and Hozack, 1994; Mann et al., 2001). The unsatisfactory results of the cemented THR during a certain period prompted researchers to develop alternative methods for reliably and durably securing hip implants in bone, i.e. uncemented or cementless THR.

Cementless Hip Joint Replacement

The cementless hip joint replacement was introduced in orthopaedic fields during the 1970s. It was developed as an alternative method to cemented hip joint replacement, primarily aiming to improve long term success rates of implantation in younger patients (Rothman and Cohn, 1990).

The cementless cup system normally consists of an outer metallic layer and an inner layer made of polyethylene, metal or ceramic. The outer metallic layer, known as metal shell or metal-backing, is used to separate the bone and the polyethylene or ceramic material, as the direct contact between the bone and these materials would provoke bone resportion (Rothman and Cohn, 1990). The inner layer is usually called the liner or insert, which articulates with the femoral component.

The success and long term stability of the cementless hip joint replacement depends upon both the initial or primary stability and the secondary biological response between the bone and the prosthesis (Geesink et al., 1987). The initial stability of the implant is achieved by a purely mechanical fixation to the bone, normally using techniques such as additional screws, pegs or interference fit (press fit). The long term or secondary stability of cementless implant, however, relies on a favourable host bone response, the conditions for which must be achieved by the initial fixation (Kienapfel et al., 1999). As it is impossible to ensure perfect contact between bone and implant with current surgical techniques in the primary fixation, the long term success and stability of cementless implants requires a growth response and gap bridging by the bone to achieve osseointegration into the implant in the secondary fixation period, by means of improved coating materials and techniques such as porous and bioactive coatings (Kienapfel et al., 1999; Yamada et al., 2009).

The short-term performance of cementless hip joint replacement has been reported as good (Sakalkale et al., 1999; Gaffey et al., 2004), with revision rates of approximately 1.91% for MoP combinations and approximately 3.29% for MoM hip replacement in three years after primary hip replacement (National joint register, 9th annual report, 2012). However, the long-term clinical success is of major concern (Yamada et al., 2009), a revision rate of 12.48% was reported for uncemented MoM articulations in ten years after primary hip replacement (National joint register, 9th annual report, 2012). The predominant potential problems involved in these implants include the delamination or fragmentation of the coatings and subsequent exposure of metal beneath to the bone, causing particulate debris and invoking a foreign body host response (Yamada et al., 2009). The particulate debris could also

migrate into the joint articulation regions and act as third-body particles causing higher wear rates of the bearing surfaces and further consequences from the greater volumes of liberated wear debris (Kleinhans et al., 2009).

In summary, cementless hip prosthesis offers the advantage of fixation by direct bone-implant osseointegration, therefore avoiding the use of a synthetic intermediary material with limited mechanical strength, such as is used with the cemented hip prosthesis. Therefore, cementless hip joint replacement is preferably performed for younger patients with good bone quality. However, problems specific to cementless prosthesis have been reported. These include failure of the locking system of the polyethylene liner, which can cause dislocation of the liner from the metal backing and produce additional polyethylene wear particles (Diwan and Drummond, 1997); insufficient polyethylene thickness leading to the abrasion and breakage of the liner; the use of screws which promote osteolysis due to the dispersion of wear debris through the screw hole; and backside wear which can speed up the loosening of the hip prosthesis (Dorr et al., 1997; Yamada et al., 2009).

1.3.4 Failure of Hip Joint Replacement

Conventional, primary hip joint replacement is a durable operation in the majority of patients. While the hip replacement surgery has become more successful and safer, the hip implant is far from being perfect. Failure do occur and can be caused by a number of reasons.

Aseptic loosening

The most common cause of failure and revision of hip prosthesis is aseptic loosening. Aseptic loosening is related to the loosening of arthroplasty in the absence of infection and can be the result of poor initial fixation, mechanical loss of fixation or biological loss of fixation (Sundfeldt et al., 2006). Among these, the biological loss of fixation caused by the resorption of periprosthetic bone or osteolysis induced by the particulate debris is increasingly accepted as the main reason (Ingham and Fisher, 2005).

Clinically, the particulate debris can be accumulated due to implant interface wear, micromotion, minor pathogen contaminations, and oxidative reactions

(Maloney et al., 1995; Kadoya et al., 1998). It can be formed at the prosthetic joint articulations, or at non-bearing surfaces which rub together such as the backside of the acetabular liner, the modular interface, the bone-cement and cement-implant interfaces. However, wear debris caused by the articulating surface wear is considered as the main contribution, particularly the polyethylene debris in MoP hip joint replacement (Goldring et al., 1993; Harris, 1995). This particulate debris was found to vary in a wide range of size and shape, and accumulate over time after hip replacement surgery (Maloney et al., 1994; Campbell et al., 1995). The accumulated particulate debris then causes a tissue response and local osteolysis and bone resorption at the bone-implant interface.

The mechanisms of bone resorption and osteolysis of hip arthroplasty is actually an interaction of biological and mechanical processes (Sundfeldt et al., 2006). Mechanically, joint forces and kinematics combined with contact surface geometries and material properties determine the cyclic stresses that lead to the generation of particulate debris. Biologically, the ingress of accumulated particle debris to the bone-implant interface stimulates a foreign-body response, resulting in the release of bone resorption mediators and formation of a periprosthetic membrane with an abundance of macrophages, giant cells and particulate debris around the hip prosthesis (Ulrich-Vinther et al., 2002; Clohisy et al., 2004; Inhgam and Fisher, 2005). Subsequently, resultant bone loss occurs due to the phagocytosis of particulate debris by macrophages and other cells capable of phagocytosis at the bone-implant interface, which then cause the demarcation and migration of the hip prosthesis (Murray et al., 1990; Wang et al., 1993; Ingham and Fisher, 2005).

Many factors have been described as facilitating progression of the bone resorption or osteolysis events. Indeed, the process of aseptic loosening is a complex and multifactorial event, and is probably the result of a combination of different factors. Huiskes (1993) defined a series of "failure scenarios", which were useful to classify the potential failure processes for the cemented THR. These "failure scenarios" included: (a) the "implant reaction scenario", which is related to the particulate-induced bone resorption; (b) the "accumulated damage scenario", which is related to the bone-cement

interface failure due to the mechanical stresses upon it; (c) the "bone-adaptation scenario", where the bone responds to the uneven stress patterns caused bone hypertrophy in high stress areas and bone resorption in low stress areas; (d) the "destructive wear scenario", which involves the mechanical wear and eventually loss of continuity of the bearing surface. Sundfeldt et al. (2006) reviewed different theories about the cause of aseptic loosening, indicating that aseptic loosening was not only a question of wear and could not be explained by a single theory. It was a multifactorial etiology and a combination of macro-, micro- and nano- events, involving cell activation in particle disease, cement damage, micromotion, stress shielding, high fluid pressures etc.

Bone cement damage

Bone cement damage has been accepted as one of the main factors that causes the aseptic loosening and failure of hip prosthesis recently (McCormack and Prendergast, 1999; Sundfeldt et al., 2006). The main contributions of bone cement damage to loosening were confirmed in two ways: on one hand, the fatigue failure and defects of the cement mantle led to the release of cement particles, which would invade the articulating surface and act as third-body particles, causing severe articulating surface wear. It would also cause a foreign body reaction, promoting the osteolysis and loosening of the hip arthroplasty (Jones and Hungerford, 1987; Willert et al., 1990). On the other hand, the bone-cement demarcation or the crack of cement mantle, either by mechanical overload or due to the cement mantle damage, provided a pathway for the particulate debris to access the bone-cement interface directly, facilitating the propagation of inflammatory and eventual osteolytic events (Hirakawa et al., 2004).

The accumulated damage of the cement mantle is affected by the mechanical behaviour in the cement material and at the bone-cement or cement-implant interfaces (Tong et al., 2008; Coultrup et al., 2009). It is mainly determined by two factors - the stresses in the cement mantle and at the bone-cement or cement-implant interfaces, and the strength at these interfaces. If the stress levels in the materials or at the interfaces exceed the corresponding strength, cement damage or mechanical failure would be

initiated. Therefore, the probability of failure of the cement mantle can be decreased by reducing stresses and/or increasing strength of the interfaces (Gardiner and Hozack, 1994).

The accumulated damage of the cement mantle can also be caused by the fatigue failure of the cement mantle under cyclic loading, which has been shown to be closely related to the tensile stresses in the cement mantle. Murphy and Predergast (1999) applied a damage accumulated routine to simulate fatigue failure of the cement mantle using the fatigue data of specimens, in which the number of cycles to failure of the cement mantle was derived by:

$$\sigma = -4.395\log_{10}(N_f) + 40.42 \qquad (1.1)$$

Where σ is the stresses developed in the cement mantle, N_f is the number of cycles to fatigue failure.

Using this routine, the threshold value of 8.25 MPa which represents a 95% probability of survivorship of the cement mantle over 10 million cycles was determined (Lamvohee et al., 2009). Another cement damage accumulation method considering the porosity of the cement mantle was presented by Stolk et al. (2004) in which fatigue loading cycles were simulated incrementally in batches of thousands of cycles. In this study, the number of cycles to failure of cement mantle was calculated considering the element stress following the equation (Stolk et al., 2004):

$$\log N_f = (78.39 - \sigma) * 11.22 \qquad (1.2)$$

Where σ is the stresses developed in the cement mantle, N_f is the number of cycles to fatigue failure.

Based on this damage accumulation method, Coultrup et al. (2009) analyzed the mechanical fatigue failure of the cement mantle using a computational approach and indicated that both the increase of cup penetration depths from 0 mm to 4 mm and decrease of thickness of cement mantle from 4 mm to 2 mm led to increase of cement stresses, resulting in a reduction of the fatigue life of cement mantle by 9% to 11%.

The mechanical behaviour at the bone-cement interface and the load transfer between the prosthesis, cement and bone were widely investigated

on both a macroscopic level or a microscopic level, and using either experimental or finite element (FE) methods (Heaton-Adegbile et al., 2006; Zant et al., 2007; Wang et al., 2009; Tozzi et al., 2012). Different failure modes of cement mantle were reported based on these studies (Zant et al., 2007; Wang et al., 2009). Zant et al. (2007) developed an experimental multilayer model and a plane strain FE model to explore the fatigue failure of the cement mantle under peak contact force during normal walking. They indicated that radial fatigue cracks of cement mantle was observed and the location of the cracks was in the vicinity of the maximum tangential and compressive stresses as predicted by the FE model. This cracking pattern was found to be consistent with that observed in sections of cemented femoral replacements tested *in vitro* (Race et al., 2003) and retrieved samples (Jasty et al., 1991). However, different failure scenarios were observed for three-dimensional (3D) acetabular reconstruction models. Heaton-Adegbile et al. (2006) conducted an *in vitro* study to assess the fatigue behaviour of a cemented acetabular reconstruction under constant amplitude cyclic load, and demonstrated an extensive debonding at the bone-cement interface around the dome region of cement mantle. The same failure pattern was also observed in the studies conducted by Zant et al. (2008) and Wang et al. (2009), in which the fatigue behaviour of cemented acetabular replacement was tested using a hip joint simulator and the stress states in the reconstructions were analysed under long-term physiological loading conditions. It is reassuring in these studies that the location of the failure of the cement fixation seemed to be consistent with the high-stress region identified from FE analysis. Coultrup et al. (2009) focused on the mechanical fatigue failure of the cement mantle using a computational cement damage accumulation method, which was based on the damage accumulation routine published by Stolk et al. (2004). It was indicated that extreme combinations of a thin cement mantle and high cup penetration may result in mechanical failure of the cement mantle and a thin cement mantle itself may lead to the mechanical overload at the bone-cement interface.

Although a number of the studies were carried out to analyse the failure of cement fixation, they were at a macroscopic level and could not describe the mechanical response of the interface at a microscopic level. The

micromechanical behaviour at the bone-cement interface was studied recently by Wang et al. (2010) and Tozzi et al. (2012) using FE method. In these studies, the bone-cement interfaces were detailed on a microscopic level, where the bovine trabecular bone was interdigitated with bone cement. The FE models were developed from the CT images of the tested specimen. The bone-cement interface in the FE models was divided into four regions: (a) bone region, (b) bone-cement partially interdigitated region, (c) bone–cement fully interdigitated region and (d) cement region. Based on these studies, the fracture process of cement mantle, initial and propagation of the defects and failure at the bone-cement interface were described and analysed, which may be useful in moving towards a micromechanical understanding of the failure process at the bone-cement interface.

Other complications

After aseptic loosening, recurrent dislocation has historically ranked as the second leading cause of failure in total hip arhtroplasty (Woo and Morry, 1982). The contributing factors to dislocation include insufficient pseudo-capsular tissue, muscle weakness and imbalance due to inappropriate implant placement (Scifert et al., 1998; Bader et al., 2004). Dislocation usually occurs along with impingement which is caused by excessive joint motion. when impingement occurs, the centre of rotation moves from head centre to the rim of the cup. Recurrent impingement can result in material failure of the implant components, such as plastic damage of the polyethylene liner and fracture of the ceramic components (Pedersen et al., 2005). Further motion leads to subluxation of the femoral head and lever-out (Scifert et al., 1998). Instability of the hip prosthesis and inappropriate manoeuvres would also lead to dislocation (Barrack, 2003; Nadzadi et al., 2003). To avoid impingement and dislocation, advanced design and proper implant positioning are essential. Advanced design and surgical treatments for recurrent dislocation involve dual-head cups, larger heads, modular cups, high offset femoral necks and soft-tissue interventions such as posterior tissue or capsular repair (Kerschbaumer et al., 2007; Hummel et al., 2009; Konan et al., 2009).

Other factors that cause the failure of the hip prosthesis include avascular necrosis or osteonecrosis that will cause the collapse of the bone and periprosthetic fractures; the infection and fracture of the stem, which tend to occur at the early stage of the operation etc.

1.4 Biotribology and Biomechanics of Artificial Hip Joint

According to the concise Oxford English Dictionary, tribology is a study to deal with lubrication, friction, wear and other basic engineering subjects such as solid mechanics, lubricant chemistry, material science, heat transfer, etc. (Johnson, 1985).

Tribology applied to the biological systems is known as biotribology, which was first introduced by Dowson and Wright (1973) in 1970s. It covers all aspects of tribology related to biological systems such as the natural synovial joint and joint replacements.

1.4.1 Wear

Wear is defined as the progressive damage of surface or loss of materials from one or both solid surfaces as a result of relative motion on the surfaces (Rabinowicz, 1995). Wear of the joint replacement is vitally important as it is related to not only the decreased function and cost of implant, but also the adverse effects of wear particles in arthroplasty. For example, wear debris from hip implants has been proven to be the main reason for the bone resorption leading to the loosening of the hip prosthesis (Ingham and Fisher, 2005).

There are five types of wear mechanisms: adhesive, abrasive, fatigue, corrosive and erosive (Stachowiak and Batchelor, 2005). Adhesive wear refers to unwanted removal and attachment of wear debris, and transference of material from one surface to another. Abrasive wear is defined as the displacement of material due to hard particles or protuberances that force against and move along a solid surface. Fatigue is a process by which the material is weakened or fails by cyclic loading when a local stress exceeds the fatigue strength of that material. Corrosive wear is defined as the damage of the surface due to the mechanical and chemical or electrochemical combined reactions in a corrosive environment. Erosive

wear refers to the loss of the material from a solid surface due to relative motion in contact with a fluid which contain solid particles (Stachowiak and Batchelor, 2005).

A wide range of laboratory equipment and measuring systems, as well as computational modelling have been used to study the wear mechanisms of THR (Maxian et al., 1996a; Nevelos et al., 2000; Bowsher and Shelton, 2001). The three major forms of equipment used were pin-on-disc machines, pin-on-plate machines and hip joint simulators. Among them, hip joint simulators were mostly used to evaluate the hip joint devices with different designs and material combinations. Alternatively, computational approaches have also been applied to study the wear behaviour of the hip joint replacement (Maxian et al., 1996b; Kang et al., 2008; Liu et al., 2008). These computational simulations were conducted on the basis of sliding-distance coupled wear algorithms, which can be expressed mathematically as follows (Maxian et al., 1996a):

$$V = KFS \qquad\qquad (1.3)$$

$$W = K\sigma S \qquad\qquad (1.4)$$

Where V is the wear volume, K is the wear factor, F is the normal applied load, S is sliding distance, W is linear wear depth, and σ is the contact stress.

Based on these laboratory and computational studies, the typical wear rates among different bearings were reported and compared, as shown in Table 1.3. Generally, MoP hip implants exhibited the highest volume wear rate and linear wear rate, while the MoM hip implants showed the lowest volume and linear wear rate.

Table 1.3 Typical volumetric and linear wear rates for various hip implants (Salek, 2012).

Bearing couples	Volumetric wear rate (mm^3/year)	Linear wear rate (µm/year)
MoP	30-100	100-300
CoP	15-50	50-150
MoM	0.1-1	2-20
CoC	0.05-1	1-20

One year was assumed to be equal to 1 million cycles.

1.4.2 Friction

Friction is defined as the resistance to motion experienced when one solid body moves tangentially over another (Rabinowicz, 1995). For hip joint replacement, friction plays an important role in the load transmission from implant to the bone, and stresses generated on the bearing surface as well as the fixation interface. Generally, low friction is preferential on the bearing surface in order to reduce the stress transmitted to the fixation interface, and therefore reducing the likelihood of the interface failure. This has been the basic principle for LFA proposed by Sir John Charnley (Wroblewski et al., 2009a).

The friction experienced in artificial hip joints has been measured using pendulum simulators, in which simplified loading and motion was applied. A typical example was a simplified gait cycle consisting of a dynamic vertical load and a horizontal flexion and extension motion (Brockett et al., 2007). However, in order to investigate the potential squeeze-film effect in the friction measurement, a dynamic load that represents complete walking cycles was used (Scholes and Unsworth, 2000).

Friction of hip implants was found to vary greatly among different material combinations, as shown in Table 1.4. Under the same conditions, CoC and CoM couples produced a lower friction coefficient than other couples, while MoM couples exhibited the highest friction coefficient (Banchet et al., 2007).

Friction also serves as an important factor to assess the lubrication regimes, which can be reflected in the Stribeck curve, and will be discussed in the **section 1.4.3**.

Table 1.4 Typical friction factors for various bearings for hip implants in the presence of bovine serum (Jin et al., 2006).

Bearing couples	Friction factor
MoP	0.06-0.08
CoP	0.06-0.08
MoM	0.22-0.27
CoC	0.002-0.07
CoM	0.002-0.07

1.4.3 Lubrication

Lubrication refers to interposing a lubricant between two contacting solids for the purpose of reducing friction and wear (Bhushan, 2002). There are three distinct lubrication regimes in engineering: fluid-film lubrication, boundary lubrication and mixed lubrication.

The lubrication regimes are often determined using two major methods: experimental measurement and theoretical prediction (Dowson, 2001).

In the experimental method, a so-called Stribeck curve was used to compare the friction coefficient with the Sommerfield number (Dowson, 2001). The Stribeck curve is depicted in three phases, which correspond to three lubrication regimes respectively, as shown in Figure 1.9. The boundary lubrication regime occurs when the average surface roughness of the articulating surface is larger or equal to the thickness of fluid film. This lubrication regime is more likely to occur in rough bearing surface or the implants that remain *in situ* for a long time. As the thickness of the fluid film increases, the articulating surfaces become separated from each other, and the friction coefficient decreases sharply. At this stage, the mixed lubrication regime is achieved. The friction coefficient continues decreasing until the full fluid film lubrication is generated, where the articulating surface is separated

completely by the lubricant (Brown and Clarke, 2006). This is the ideal condition in which the hip implants are expected to work (Jin et al., 1997).

$$z = \frac{\text{viscosity} \times \text{sliding speed} \times \text{equivalent radius}}{\text{load}}$$
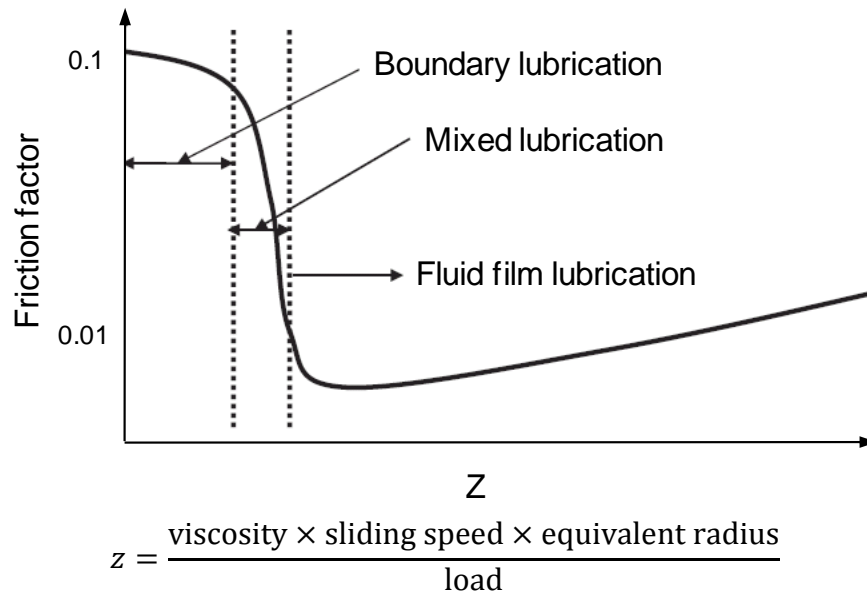
Figure 1.9 Typical strbeck curve (Jin et al., 2006).

The theoretical method to determine the lubrication regimes is based on the lambda ratio (λ) which is defined as (Dowson, 2001):

$$\lambda = \frac{h_{\min}}{R_a} = \frac{h_{\min}}{[(R_{a\_Head})^2 + (R_{a\_Cup})^2]^{\frac{1}{2}}} \tag{1.5}$$

Where R_{a_Head} and R_{a_Cup} are the average surface roughness for the head and cup respectively. $h_{\min}$ is the minimum film thickness between the two articulating surfaces.

The relationship between the values of the lambda ratio and the lubrication regimes is shown in Table 1.5.

The lubrication condition for the hip joint replacement is strongly dependent upon the design parameters, such as the femoral head diameter, the radial clearance and the materials used (Brown and Clarke, 2006). Under realistic loads and in the presence of synovial fluid, MoP hip joints are more likely to operate in the mixed or boundary lubrication regime, while CoC and MoM bearings primarily work in the mixed film lubrication regime (Jagatia et al., 2001; Dowson and Jin, 2006; Brockett et al., 2007).

Table 1.5 Lambda ratio and lubrication regimes (Jin et al., 2006).

Lambda ratio λ	Lubrication regime
λ≥3	Fluid film lubrication
3≥λ≥1	Mixed lubrication
λ≤1	Boundary lubrication

1.4.4 Contact Mechanics

Contact mechanics is the study of contact pressure and area when two bodies interact with each other under load (Johnson, 1985). The investigation of the contact mechanics of hip replacements is an important step to optimize the implant design, materials, surgical parameters, and provide better understanding of the long-term performance and success of the implants (Mak et al., 2002; Udofia et al., 2004; Korhonen et al., 2005).

Contact pressures and contact area

The main parameters determined from contact mechanics are the contact stresses and contact area. It has been shown that contact stresses are directly related to fatigue-related wear mechanisms (McNie et al., 1998; Orishimo et al., 2003). According to the Archard-Lancaster wear equation pioneered by Maxian et al. (1996a), the wear volume is proportional to the wear factor, the normal load and sliding distance, as demonstrated in **Section 1.4.1**. The normal load is normally obtained from the integration of the contact stresses over the contact area in the computational simulation (Liu et al., 2012). Recent studies have shown that the wear factor is dependent on the cross-shear motion and contact pressures for the polyethylene components. With increased contact pressures and cross-shear ratio, the wear factors increased (Kang et al., 2008; 2009). Therefore, with the same sliding distane, the increased contact pressures normally result in increased wear in the acetabular components (Mazzucco et al., 2003). More importantly, the high contact stresses in the UHMWPE components can exceed the yield stress of the UHMWPE, which would be decreased due to the oxidative degradation (Kurtz et al., 1999; McKellop et al., 2000), leading to plastic deformation and catastrophic rupture of the

components and potentially the failure of the implants. To this end, the investigation of the contact mechanics of the hip replacement is critically important and has been widely carried out through experimental studies (Plank et al., 2007; Müllera et al., 2004) and theoretical analysis (Korhonen et al., 2005; Plank et al., 2007).

Experimental studies

The experimental measurement of contact pressure and contact area on bearing surface of the hip prosthesis was usually conducted using a pressure sensitive film (Fuji film) (Hale and Brown 1992; Plank et al., 2007) or sensors (Müllera et al., 2004). The Fuji pressure sensitive film is usually composed of two layers, a colour developing layer and a microcapsule layer. Before loading, the film is folded spherically and placed between the two surfaces of the artificial joints. When the pressure is applied to the film, a local pressure-dependent colour reaction in the film is caused. The distribution of the colour reaction is then recorded by scanning the film to get the contact pressure distributions (Hale and Brown, 1992). The measurement data from Fuji film is usually used to validate the numerical methods, particularly the FE methods (Plank et al., 2007). The main problems with Fuji film are that it involves wrapping a flat surface onto a spherical ball of the femoral head, and changing the radial clearances of the bearings, which would affect the accuracy of the measurement (Hale and Brown 1992; Plank et al., 2007).

Apart from the pressure sensitive film, pressure sensors or transducers are alternative ways to obtain the pressure distribution on the bearing surface experimentally. The advantage of the sensors or transducers over the pressure sensitive film is that they can be used to measure how pressure changes as the joint moves in simulated activities, therefore providing the possibilities of both spatial and temporal resolution (Wilson et al., 2003; Müllera et al., 2004). However, both approaches have their limitations. The thickness of the film or sensor makes them not perfect methods for artificial hip joints with small clearances. Besides, the insertion of the film or sensor to the bearing surface would change the clearance of the bearing, reducing

the accuracy of the measured contact pressure and area (Wu et al., 1998; Liau et al., 2002).

Mathematical analysis

The typical theoretical method used to study the contact mechanics of artificial hip joints was simple elasticity analysis. It was originally developed by Bartel et al. (1985; 1986). The main assumption adopted in this method was that the contact pressure was dominated only by the radial displacement and therefore the contact analysis was simplified. This simple elasticity analysis was later applied by Jin *et al.* (1994) to undertake a parametric and design study in which a number of geometric parameters for artificial hip joints were investigated. This method was also used to compare with other numerical and analytical methods, such as modified Hertzian theory (Eberhardt *et al.*, 1990; 1991), the rigid-body-spring method and the FE method, and was shown to be reasonably accurate for close conformity contacts such as artificial hip joint (Li et al., 1997; Jin et al., 1999).

Another method of calculation for the contact pressure between a hard femoral head and soft plastic cup of an artificial hip joint was proposed by Keiji and his colleagues (Keiji et al., 2005). In this method, an equation of equilibrium in terms of a nondimensional parameter was derived, the contact pressure distribution was obtained once the magnitude of the parameter was determined through solving the equation. Unlike other methods, in this method, the pressure distribution can be directly obtained without any iterative calculation.

FE modelling

Although the experimental studies and mathematical analysis can provide some information on the contact mechanics of artificial hip joints, it is difficult to reproduce the physiological conditions of daily activities and examine the stress and strain inside the artificial hip joints and surrounding materials (bone, cement or metal backing). Numerical approaches, such as FE analysis, however, can make up for this insufficiency (Fuziansyah et al., 2006). FE analysis has also been an useful tool for parametric analysis, design optimization and pre-clinical testing for the artificial hip joint during the design phase (Korhonen et al., 2005; Plank et al., 2007).

There are three basic FE model types available for artificial hip joints: axisymmetric, two-dimensional (2D) and 3D models. The axisymmetric model is generally based on an axisymmetric configuration and used to replace the 3D model for saving computational resources. An early example of the axisymmetric model was used by Pedersen et al. (1982) who investigated the stress state within the acetabular region that was associated with some variations in prosthetic component design and surgical technique. Another axisymmetric model was presented by Jin et al. (1999) who investigated the stresses and contact areas within the components for eight combinations of femoral head and cups for MoP THR. In this study, the axisymmetric model was also validated by comparing the predicted results with the experiment measurements and simple elasticity analysis.

The 2D FE model for an artificial hip joint was initially presented by Vasu et al. (1982) who determined the alterations of stress patterns in the acetabular region caused by the implant. The model was based on a conventional UHMWPE cup, which was cemented with a 3 mm thick layer of PMMA bone cement. This model was further developed by altering the thickness of the cement layer and adding a 2 mm cobalt chromium alloy (CoCr) backing to the cup (Carter et al., 1982), aiming to explore the effect of cement thickness and metal backing on the stress distribution in the acetabular region. These studies showed that the von Mises equivalent stresses in the cancellous bone superior to the acetabular cup and stresses in the medial wall of the ilium increased immediately by approximately 30% after total joint replacement. Increasing cement thickness from 1 mm to 5 mm and adding a CoCr alloy backing to the cup caused a decrease of the von Mises equivalent stresses in the cement and surrounding cancellous bone by approximately 20%.

The advantage of the axisymmetric and 2D models was that by using a simple configuration, a relatively high computational efficiency was achieved and lower computational storage was required. Therefore, they were generally used as tools for the purpose of initial investigation before the more complex and expensive 3D analysis, and for computationally expensive problems such as non-linear interface analysis and shape

optimisation (Joshi et al., 2000). For the 'more realistic' configuration of the artificial hip joint and bone, 3D modelling should be used.

3D FE modelling can provide a rapid and relatively inexpensive estimation and evaluation for implanted factors, such as the geometry and design of the components, and surgery-related factors, such as abduction angle of the implant for THR (Korhonen et al., 2005). Korhonen et al. (2005) utilized 3D FE models to investigate the effect of geometrical design, thicknesses and abduction angles of the acetabular cup, as well as the radial clearances on the contact stresses on the cup/head and cup/cement interface for four designs of cemented THR. The FE analyses showed that an increase in the abduction angle led to mild increase of contact pressures at cup-head inferface, and increased clearance between head and cup resulted in market increase of contact pressure both at cup-head and cup-cement interfaces, whereas a decreased thickness of polyethylene layer increased contact pressure only at the cup-cement interface. For cementless THR, Kurtz et al. (1997) used 3D FE models to investigate the effect of liner thicknesses, shell/liner interface conditions and load application angles on the contact stresses on the articulating surface and backside surface of the liner. They found that among the variables that could be modified by either surgeon or engineer, liner thicknesses and cup angles (load application angles) played a greater role in determining the resulting contact stresses, compared to the shell/liner interface conditions.

The 3D models were also used to assess the contact stress of conventional and highly crosslinked UHMWPE liners for modular THR by Plank et al. (2007). Different combinations of head sizes and liner thicknesses were modelled in this study. It was indicated that the stresses at the articulating surface of highly crosslinked liners were lower compared to conventional polyethylene in every THR sizes examined. Specifically, the use of a large head against highly crosslinked material even at 3 mm thickness resulted in lower stresses than in a conventional 22 mm head and 5 mm thick combination. The innovation of this study was that a clearance between the shell and liner due to the manufacturing tolerance stack was modelled, and an increased stresses in the liner was observed. An asymmetrical distribution of stresses was predicted for this kind of modular THR in this

study which was not seen in the cemented THR. This contact pattern was also observed in the study conducted by Kurtz et al. (1998) who investigated the effect of backside nonconformity and locking restraints on the load transfer mechanisms and relative motion at the shell/liner interface in a modular THR.

Due to the versatility and capability of describing the detail of geometry and material features of the system, the pelvic bone has been integrated into the 3D FE models for artificial hip joints (Liu et al., 2005a; Udofia et al., 2007). The influence of the inclusion of pelvic bone in the 3D FE model on the computed contact pressure and wear was assessed by Barreto et al. (2010). It was indicated that inclusion of pelvic bone in the model led to decreased contact pressures and linear wear on the bearing surface for both all-polyethylene cup and metal backed cup. This is presumably due to the fact that in the model without pelvic bone, the outer surface of the cup was constrained rigidly while in the mode with pelvic bone, the elastic deformation of the bone allow the cup to deform more freely and the stresses to distribute on the bearing surface more evenly, which then resulted in decreased contact stresses on the bearing surface.

3D FE models were also adopted in MoM and CoC hip implants (Besong et al., 2001b; Verdonschot et al., 2002; Mak and Jin, 2002). Unlike the MoP combination, the deformation of both femoral head and acetabular cup in MoM and CoC bearings were considered. The design parameters such as clearances, head diameters and liner thicknesses, as well as the surgical parameters such as the cup angles were shown to have a marked effect on the predicted contact parameters (Udofia et al., 2004; Wang et al., 2012). The increased clearance, cup inclination angle and decreased head diameter and liner thickness were found to induce a marked increase of contact stresses (Mak and Jin, 2002; Udofia et al., 2004; Wang et al., 2012). Furthermore, different designs of the metallic and ceramic acetabular components such as taper-connected and sandwiched cups were modelled in the 3D FE model, and studies showed that the maximum contact pressures on the bearing surface of sandwiched design and taper-contected design were reduced by approximately 27% and 32.5% compared to other designs such as mono-block design. (Besong et al., 2001b; Liu et al., 2003).

1.4.5 Microseparation and Edge Loading

With the aid of fluoroscopy, microseparation of the head and cup during hip motion has been observed (Dennis et al., 2001; Glaser et al., 2008). Microseparation, combined with the cup inclination angle, has been considered as the main causes leading to edge loading in hip arthroplasty (Mak et al., 2002). Microseparation occurs during the swing phase and can be caused by different factors such as laxity of the joint, femoral head offset deficiency or medialised cups. These factors cause the femoral head to be moved laterally relative to the acetabular cup during swing phase. When a load is applied in the stance phase, the femoral head is moved vertically, leading to the contact between the femoral head and the rim of the acetabular cup (edge loading), as schematically illustrated in Figure 1.10 (Nevelos et al., 1999). This can result in accelerated wear of articulations for hard-on-hard bearings and increased stresses in the components of hip arthroplasty (Stewart et al., 2001; Mak et al., 2002).

Microseparation

(a) Swing phase

Rim contact

(b) Heel strike

Relocation
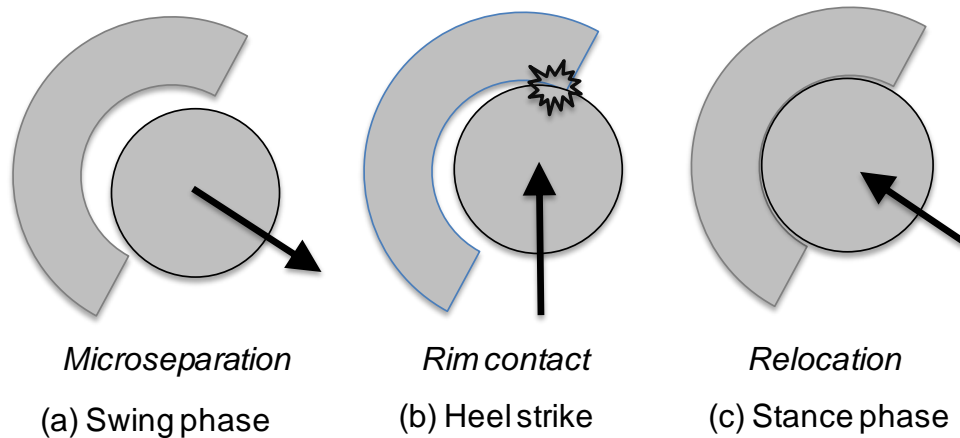
(c) Stance phase

Figure 1.10 A simple scheme shows the occurrence of microseparation during gait. Microseparation occurs at swing phase (a) followed by rim contact at heel strike (b) and relocation during the stance phase (c) (Nevelos et al., 1999).

Clinical retrievals have shown various stripe wear patterns on the femoral head which was not produced by *in vitro* simulatior studies under standard gait conditions even when steep cup inclination angles were simulated (Walter et al., 2004; Manaka et al., 2004). These observations prompted the

interest in quantifying *in vivo* hip kinematics (Nevelos et al., 1999; Stewart et al., 2001). Nevelos et al. (1999; 2000) were the first to introduce the microseparation motion in the hip simulator and reproduced clinically relevant wear rates, wear patterns, and wear particle distributions for CoC articulations. Following that, Stewart et al. (2001) presented the first long-term simulator study which incorporated microseparation motion during simulation. Subsequently, the microseparation motion was repeated by many researchers in the form of retrieval (Walter et al., 2004) and laboratory studies (Manaka et al., 2004; Affatato et al., 2004).

Fluoroscopic imaging was used to obtain the microseparation levels of the hip arthroplasty during hip motion, which were reported to be variable among different bearing materials (Komistek et al., 2004). Lombardi et al. (2000) determined the hip joint separation levels during normal gait on a treadmill and in abduction/adduction leg-lift manoeuvres, and reported that the average separation of head and cup was 1.2 mm (range 0.8 – 2.8 mm) and 2.4 mm (range 1.7 – 3.0 mm) for normal gait and abduction/adduction manoeuvres respectively. In this study, a computer automated model-fitting technique was used to convert 2D fluoroscopic images into 3D images. The same technique was applied by Komistek et al. (2002) who compared the hip separations during normal gait for MoM and MoP THRs. The results showed that the average separation in the subjects with MoM implants was 0.38 mm (range 0.3 – 0.51 mm), while the average separation in the subjects with MoP prostheses was 2.0 mm (range 0.8-3.1 mm). When considering the abduction/adduction leg lift manoeuvre, the maximum amount of separation of head and cup was reported to be 7.4 mm for a subject with alumina-on-polyethylene (AoP) THR and 3.1 mm for a subject with MoP THR (Komistek et al., 2004).

Microseparation of the head and cup in THRs have been replicated experimentally in hip joint simulators and the results have been compared with the retrievals (Nevelos et al., 2000; Shishido et al., 2006). Microseparation has been shown to produce both edge wear and accelerated general wear in CoC and MoM articulations. Stewart et al. (2001) tested Hot Isostatically Pressed (HIPed) alumina on alumina joints to 5 million cycles at two microseparation levels and reported that the wear rates

increased from 0.11 mm^3/million cycles in the bedding-in phase and 0.05 mm^3/million cycles in the steady-state phase under standard conditions to 0.55 mm^3/million cycles and 0.1 mm^3/million cycles respectively under mild microseparation conditions. These continued to increase to 4 mm^3/million cycles and 1.3 mm^3/million cycles respectively under severe microseparation conditions. Stripe wear was observed under both mild and severe microseparation conditions after the initial 1 million cycles. Compared to retrieved implants, Stewart et al. (2001) reported that the simulator implants had narrower stripe wear scars compared to the first general non-HIPed Mittelmeier replacements. However, similar stripe wear patterns were observed compared with the early retrieved HIPed alumina implants (Nevelos et al., 2000; 2001b).

Shishido et al. (2006) compared two types of retrieved hip prosthesis with the simulator joints under standard and microseparation conditions. The wear rates of the simulator joints were 0.011 mm^3/million cycles in steady-state phase under standard conditions, compared to a range from 0.16 to 0.65 mm^3/million cycles under microseparation conditions. Different stripe wear scars of the simulator and retrieved joints were observed in this study.

For MoM combination, Williams et al. (2004) tested the prostheses to 5 million cycles with a low (100 N) and ISO (280 N) swing phase loads (standard conditions), and under microseparation conditions. The results showed that the overall mean wear increased from low swing phase load to ISO standard load, and to microseparation conditions further with wear rates of 0.06 ±0.05 mm^3/million cycles, 0.58 ±0.53 mm^3/million cycles and 1.58 ±0.85 mm^3/million cycles respectively. Stripe wear was observed on the femoral head, as seen in the ceramic joints. However, the metal scars were wider and fatter than those found on the ceramic joints (Smith et al., 2002).

Microseparation conditions were also applied on simulators to test CoP combination. Williams et al. (2003) examined the wear of CoP artificial hip joints under standard and microseparation conditions using an *in vitro* simulator. Different from hard-on-hard combinations, the volume change of the polyethylene cup in CoP bearings was decreased from 25.6 ±5.3 mm^3/million cycles under standard conditions to 5.6 ±4.2 mm^3/million cycles

under microseparation conditions. No damage to the ceramic head was observed due to the softer polyethylene cup. However, there was local deformation at the rim of the cup and reduction of scratching within the wear patch which resulted in a decreased wear rate.

FE studies have also been widely carried out to examine the contact stress on the articulating surface due to microseparation (Mak et al., 2002; Sariali et al., 2012). It has been shown that the introduction of microseparation would induce edge contact between the femoral head and superior rim of the acetabular cup, leading to a substantial increase in the contact stresses on the bearing surface. The edge contact induced by microseparation was shown to be dependent upon the microseparation levels, radial clearances and cup inclination angles (Mak et al., 2002). The concentrated stress due to edge loading under a larger microseparation level could be reduced by the introduction of a fillet at the mouth of the acetabular cup. Mak et al. (2011) conducted 3D FE analysis to investigate the contact stresses in three acetabular cups with different rim designs (new, worn, and chamfer) under microseparation conditions. The results showed an approximately 5-8 fold increase in predicted contact stress when a microseparation distance of 250 µm was introduced. However, introducing a 2.5 mm radius chamfer reduced the maximum contact stress, von Mises stress and tensile stress by about 35%, 63% and 60% respectively.

The combined influence of the head lateral microseparation and the cup abduction angles on the contact stress in CoC THR was evaluated by Sariali et ai. (2012). It was indicated that as the microseparation distances increased, the maximal contact stress increased and converged to an asymptotic value. Both the lateral microseparation of the head and high cup abduction angle above 75⁰ induced a large increase in the stress in the CoC articulation. However, the increase in contact pressures induced by a high abduction angle became negligible as the lateral separation increased.

A comparison of the contact mechanics for different bearing couples under microseparation conditions was conducted by Besong et al. (2001a). The study showed that the introduction of microseparation with distance of 35 µm resulted in an increase of contact pressures at the bearing surface by about

56% for MoP bearings. The limitation of this study was that the polyethylene in the MoP hip replacement was modelled as elastic material. However, it is expected that the substantial increase of stress in the polyethylene liner under microseparation conditions could exceed the yield strength of the material, leading to plastic deformation of the liner. The plastic deformation in the polyethylene liner would weaken the mechanical properties of the polyethylene, leading to the rapid fatigue of the material when subjected to cyclic stress.

1.5 Summary of Literature and Rationale

The ball and socket configuration of the hip joint allows it to provide the second largest ROM after the shoulder joint in the human body and make it capable of supporting a larger load, even more than seven times BW for fast walking (Paul, 1966), as discussed in **Section 1.2.4**. However, the hip joint will have severe functional limitations when suffering from hip disease or trauma. At this time, the natural bearing of the hip joint is required to be replaced by an artificial one. Hip joint replacement is the most effective way to restore hip function and mobility.

Whilst hip joint replacements provide substantial benefits, the failure of these devices still occurs too frequently, placing a significant burden on the patient and the adjunct health care system. Therefore, the failure mechanism of the hip prosthesis and the performance of implants under different conditions should be investigated for the purpose of improving their longevity and reliability.

The major problem with the application of the hip joint replacements is that they are prone to wear, releasing wear debris which will cause loosening of the implants. For this reason, major efforts have been made to explore the wear mechanism for the hip prosthesis. Contact mechanics analysis is one such attempt as contact stress on the bearing surface has been shown to be associated with fatigue-related wear mechanisms and surface damage of the prosthesis (Rostoker and Galante, 1979; McNie et al., 1998).

For cemented THR, bone cement damage is one of the main factors that cause the loosening and failure of the hip prosthesis, as discussed in

Section 1.3.4. The bone cement damage is closely related to the mechanical stresses experienced in the cement mantle which has been shown to be affected by cement mantle thickness, porosity, cup penetration and bone quality etc. as reviewed in **Section 1.3.4**. It is important to recognize that the stress experienced in the cement mantle is associated with the contact mechanics on the bearing surface, since the contact stresses on the bearing surface are directly transmitted to the cement and *vice versa*. However, few studies have addressed these two problems interactively. Additionally, the synergistic effect of cup inclination angle, components size and cup penetration depth on the contact mechanics and cement stresses for cemented MoP THR has not been investigated comprehensively and is one of main focuses in this thesis.

Modular acetabular cup systems have been widely used for hip replacement with the advantage of providing not only biological and mechanical fixation but also a wide range of cup options depending on the patients' individual needs. However, due to the engineering manufacturing tolerances, there is clearance between the shell and liner in the modular THR. It has been shown that the nonconformity between the shell and liner make the contact mechanics and biomechanical behaviour of the modular THR quite sensitive to the cup inclination angles and load directions, which was largely different from non-modular THR (Kurtz et al., 1998; Plank et al., 2007). However, few studies have focused on this. The effect of cup inclination angles and normal activities on the contact mechanics of modular THR is still to be determined.

Edge loading would occur in the THR and can be the result of different factors, such as smaller radial clearances, steep cup inclination angles, microseparation and daily activities undertaken. Edge loading can induce some adverse complications such as concentrated stresses, high wear rates and unexpected damage in the components. This has been extensively investigated for the hard-on-hard combinations (MoM and CoC) (Williams et al., 2006; Al-Hajjar et al., 2010; Al-Hajjar et al., 2013), as reviewed in **Section 1.4.5.** However, limited works have been conducted for MoP THR, especially modular MoP THR. The investigation of edge loading in MoP THR deserves further attention and is another main focus in this thesis.

1.6 Aims and Objectives

The primary aims of this study were to investigate the contact mechanics of the bearings and the mechanical behaviour in the cement mantle as well as at the bone-cement interface for a cemented MoP THR (Charnley THR), and to investigate the contact mechanics and biomechanical behaviour of the bearings for a cementless modular MoP THR (Pinnacle THR), both using computational modelling.

The aims of this study were achieved through the following objectives:

- To develop a 3D anatomic FE model for a cemented MoP THR (anatomic Charnley THR model).
- To examine the effect of penetration depths, cup angles and sizes of the components on the contact mechanics of the bearings and the stresses in the cement mantle as well as at the bone-cement interface for Charnley THR using the anatomic Charnley THR model.
- To determine the wear depths, wear directions and the radial clearances between the head and worn surface of the cup based on the retrieved Charnley cups using CMM and surface-fitting technique. To examine how these factors affect the contact mechanics and cement stresses of Charnley THR.
- To develop a 3D anatomic FE model for a modular MoP THR which incorporates a high level of geometric details (anatomic Pinnacle THR model).
- To measure the contact areas of a Pinnacle THR system using the ProSim hip joint simulator to provide confidence in the validity of the FE predictions from anatomic Pinnacle THR model by comparing the contact areas from experimental measurements and FE predictions.
- To apply physiological loads from different daily activities to the anatomic Pinnacle THR model to analyse the contact mechanics and plastic behaviour of the modular MoP THR during different daily activities.
- To analyse the contact mechanics and plastic behaviour of the modular MoP THR under standard and microseparation conditions.

Chapter 2
Materials and Methods

2.1 Introduction

The development of general anatomic FE modelling is introduced in this chapter. The model includes the pelvic bone and hip replacement components, as well as the fixation between the bone and components. The realistic geometries, the material properties of the pelvis in terms of cortical and cancellous bones and the components themselves are detailed. Two types of total hip systems, which are often used in hip replacement, are considered. The first one is Charnley THR, which consists of an UHMWPE cup and a stainless steel femoral head, with the acetabular cup fixed to the pelvic bone by using cement ('cemented THR'). The second one is Pinnacle THR, which consists of a titanium shell, a UHMWPE liner and a CoCr femoral head, which is intended for uncemented fixation ('cementless THR'). The boundary and loading conditions used in the model, as well as the contact simulation are also presented.

2.2 Materials

2.2.1 Geometric Properties

The general anatomic model considered in this study is composed of the anatomic pelvic bone, the acetabular and femoral components as well as the fixation between the bone and the components.

Pelvic bone

The geometry of the anatomic hemi-pelvic bone used in this study was taken from the literature (Liu et al., 2005a; Udofia et al., 2007), which was reconstructed from computed tomography (CT) scans. However, the meshing and the assignation of materials properties for the pelvic bone were undertaken in this study and are described in this chapter. As shown in Figure 2.1, the pelvic bone was modelled as a cancellous region surrounded by a cortical bone layer with a thickness of 1.5 mm (Liu et al., 2005a; Udofia

et al., 2007), the cortical bone in the acetabulum was removed for the purpose of cement fixation. The acetabular components were usually fixed into the pelvic bone by using either a cemented or a cementless approach.
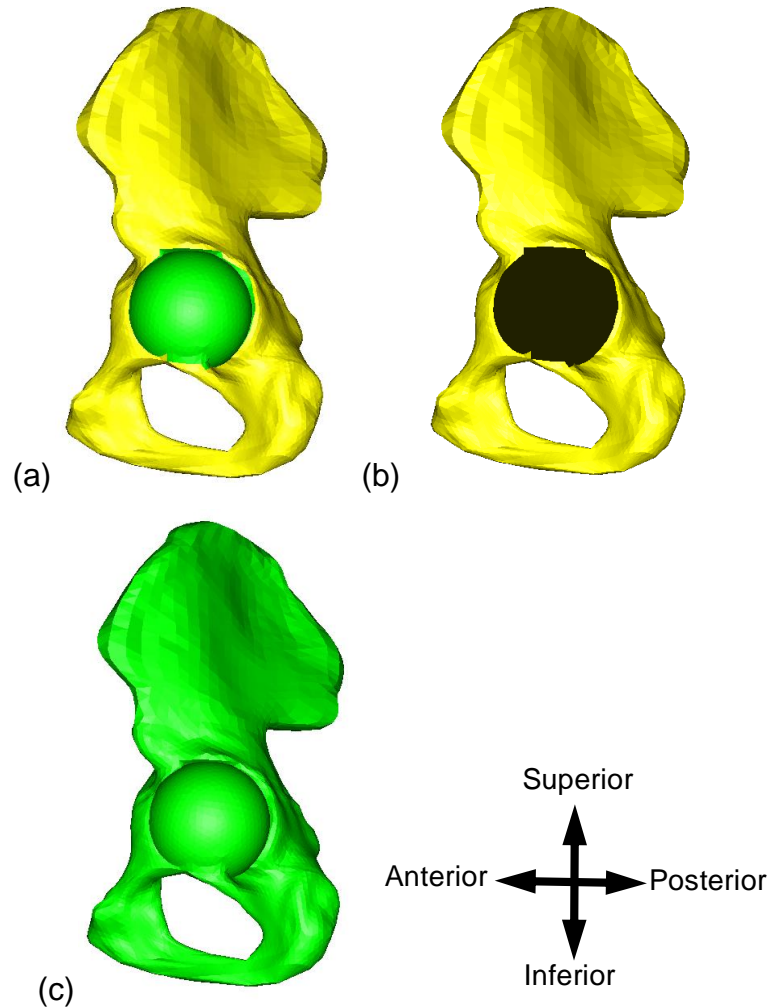
Figure 2.1 The anatomic pelvic bone model (a), including the cortical region (b), and the cancellous region (c).

Charnley THR

A standard 22.225 mm diameter Charnley bearing system, consisting of an UHMWPE acetabular cup and a stainless steel femoral head was considered (Jin et al, 1999). The main geometric parameters for the Charnley bearing were the radius of femoral head (R_1), the radius (R_2) and thickness (d_1) of the acetabular cup, as shown in Figure 2.2. The radial clearance C ($C=R_2-R_1$) between the acetabular cup and femoral head thus was obtained from the two radii. In the present study, the radius was considered as 11.1125 mm for the femoral head and 11.295 mm for the

inner surface of the acetabular cup, giving a nominal radial clearance of 0.1825 mm (Jin et al, 1999). The nominal outer diameter of the UHMWPE cup was 40 mm, giving a cup thickness of 8.705 mm.

The acetabular component was implanted into the pelvic bone by using PMMA bone cement. The thickness of the bone cement (d_2) was selected as 2 mm in the present study (Coultrup *et al.*, 2010).
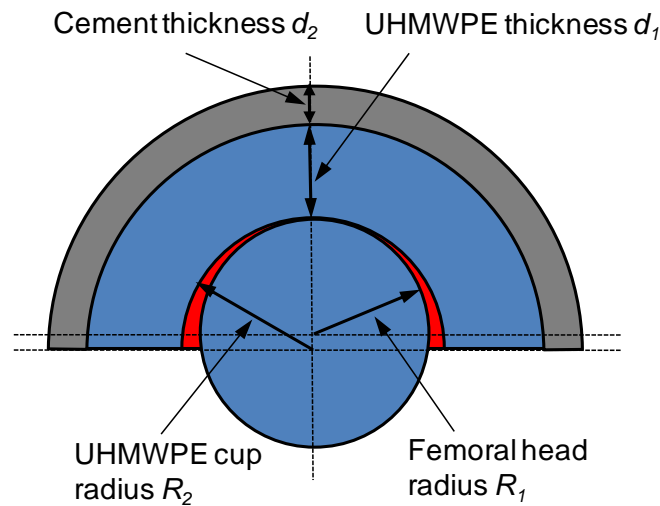
Figure 2.2 The main geometric parameters of Charnley THR considered in the present study.

Pinnacle THR

A typical MoP Pinnacle THR (DePuy Orthopaedics, Inc.), consisting of acetabular shell, polyethylene liner and femoral head, was analysed. Figure 2.3 (a) is the cross-section of the Pinnacle system, showing the geometric characteristics of the components. The inside of the acetabular shell is comprised of two distinct regions: the central dome region and the Variable Interface Prosthesis (VIP) taper. The central dome region covers approximately 140 degrees of the interior of the shell, providing backside support to the liner. Peripheral to the dome is the patented VIP taper, which extends to the face of the acetabular shell. This VIP taper provides advanced modularity - allow the acetabular cup system to offer multiple liners and advanced bearing options, including MoM, CoC, MoP, CoP or CoM bearing combinations. The polyethylene liner mechanically locks with the acetabular shell via the VIP taper junction and articulates with the

femoral head which is fixed to the thigh bone through a metallic femoral stem.

The fixation of the Pinnacle acetabular cup system is achieved through 180 degrees of either Porocoat Porous Coating or plasma sprayed Hydroxyapatite (HA) over Porocoat Porous Coating. Since its introduction, the Porocoat Porous Coating has established a clinically successful record of more than 20 years (Bobyn and Engh, 1984; Engh et al., 1995). HA Coating has been in use for over eight years (Frayssinet et al., 1995).

The geometry of the Pinnacle THR was provided by the manufacturer as an I-DEAS file, which was pre-processed using I-DEAS (Version 11, EDS, USA). Figure 2.3 (b) shows the detailed geometric dimension of the Pinnacle cup system. The radii of the femoral head (R_1) and polyethylene liner (R_2) were measured in I-DEAS as 18 mm and 18.542 mm respectively, giving a radial clearance of 0.542 mm between the inner surface of liner and the femoral head. The inner radius of the central dome region of the acetabular shell (R_3) was measured as 24.14 mm and outer radius of the polyethylene liner (R_4) was measured as 24 mm, giving a gap of 0.14 mm between the acetabular shell and polyethylene liner. A polar fenestration with radius of 10 mm was also considered in the central dome region of the acetabular shell.
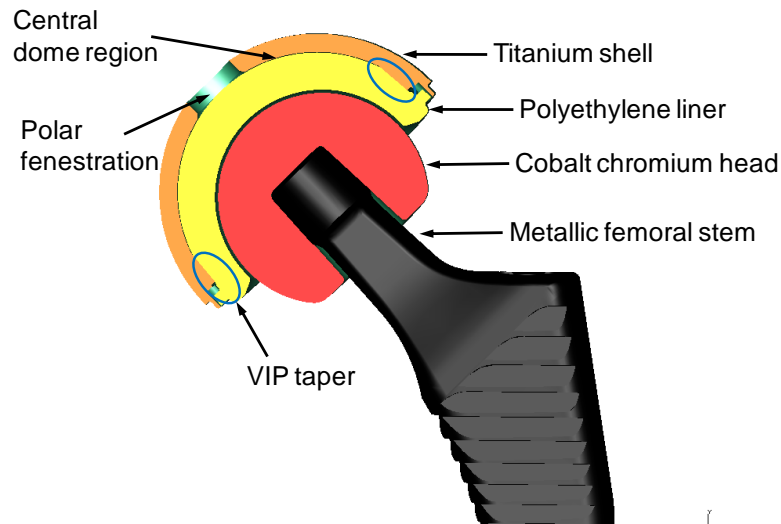
(a)
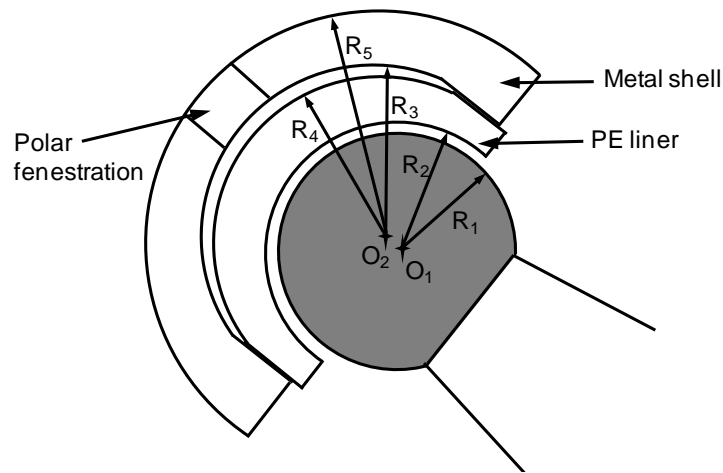
(b)

Figure 2.3 (a) The cross-section of the Pinnacle system showing the detailed structure and features of the Pinnacle cup system, (b) a schematic diagram showing the geometric dimensions of Pinnacle cup system. In order to clearly show the dimensions, just the main features of the acetabular shell and polyethylene liner are displayed. Note the eccentricity of inner surface of polyethylene liner and acetabular shell, as well as the gap between the outer surface of liner and acetabular shell.

2.2.2 Material Properties

All the materials considered in the present study were modelled as homogeneous, isotropic and linear elastic, except the UHMWPE for the Charnley cup and Pinnacle acetabular liner. It should be pointed out that the real pelvic bone has a non-homogeous, anisotropic property (Dalstra et al.,

1993), and previous studies have shown that the thickness of the cortical bone layer and the material properties of the cancellous bone are site-dependent and bone density-dependent (Dalstra et al., 1995; Anderson et al., 2005; Leung et al., 2009). However, as using fixed thickness for the cortical bone and uniform modulus for the cortical bone and cancellous bone were found to have negligible effect on the biomechanical behaviour of THRs (Liu et al., 2005a; Udofia et al., 2007), these values were assumed to be uniform in the present study. The elastic modulus and Poisson's ratio of 17 GPa and 0.3, and 0.8 GPa and 0.2 were assigned for cortical bone and cancellous bone respectively.

The femoral head for the Charnley hip replacement was made of stainless steel with Young's modulus of 190 GPa and Poisson's ratio of 0.3, and for the Pinnacle hip prosthesis was made of CoCr with Young's modulus of 220 GPa and Poisson's ratio of 0.3. However, as the elastic modulus for femoral head is about 200 times that for polyethylene, it was assumed to be rigid in the present study. The acetabular shell in the Pinnacle cup system was made of titanium with Young's modulus of 116 GPa and Poisson's ratio of 0.25. All the material properties of the components are summarised in Table 2.1.

In order to realistically investigate the mechanical behaviour of the polyethylene components, the UHMWPE cup for Charnley THR and polyethylene liner for Pinnacle hip prosthesis was considered as nonlinear elastic-plastic with the plastic stress-strain constitutive relationship showing in Figure 2.4 (Liu et al., 2005b).

Table 2.1 Material properties for the components used in the present study (Liu et al., 2005b; Udofia et al., 2007).

Components	Materials	Young's modulus (GPa)	Poisson's ratio
Metallic head (Charnley)	Stainless Steel	190	0.3
Metallic head (Pinnacle)	CoCr	220	0.3
UHMWPE cup and liner	UHMWPE	1	0.4
Bone cement	PMMA	2.5	0.254
Cortical shell	Cortical bone	17	0.3
Cancellous bone	Cancellous bone	0.8	0.2
Metal shell	Titanium	116	0.25
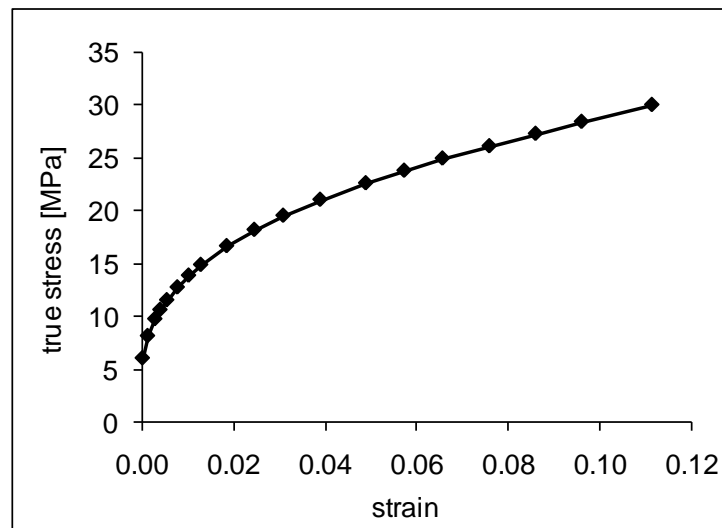
Figure 2.4 The plastic stress-strain relationship for polyethylene (Liu et al, 2005b).

2.3 Methods

2.3.1 FE Modelling

Anatomic Charnley THR model

The first FE model in the present study was anatomic Charnely THR model, which consisted of a hemi-pelvic bone, the cement mantle, the UHMWPE cup as well as the stainless steel femoral head, as shown in Figure 2.5. The geometries and mechanical properties for the pelvic bone and components were described in **Section 2.2**. The backside of the UHMWPE cup was bonded with a layer of cement, which was then attached to the pelvic bone.

The 3D anatomic FE model for Charnley THR and the mesh for the components is shown in Figure 2.5. Three-noded thin shell elements were used to model the layer of cortical bone in the pelvis with a uniform thickness of 1.5 mm (Liu et al., 2005a; Udofia et al., 2007). For the cancellous bone, four-node solid tetrahedron elements were employed. In order to achieve a trade-off between the accuracy of the results and computer resources as well as the simulation time, the pelvic bone was partitioned into two volumes as upper volume and lower volume, and meshed with different element sizes, as shown in Figure 2.5.

For the cement and prosthesis components, a "dual-poled" mesh design was selected. It was achieved by meshing the cross section of the cement and acetabular cup first to produce a plane mesh and then revolving the plane mesh around an angle of 180º to form the 3D mesh, as shown in Figure 2.6. Following a mesh sensitivity analysis which will be discussed in **Section 2.4**, the FE model consisted of a total of approximately 50, 000 nodes and 13, 000 elements, including 'brick' and 'wedge' elements for the cancellous bone, cement and prosthetic components, and 'thin-shell' elements for the cortical bone. The 'brick' and 'wedge' elements used here may have 4, 5, 7, 8, 15 or 20 nodes and are normally used to model solid objects. The 'thin-shell' elements are 3 or 4 node 2D elements that can be oriented anaywhere in 3D space. It is usually used to model thin shell and membrane material such as fabric, thin metal shell and cortical shell as in the present study. The thickness of the shell must be small relative to its length or width.
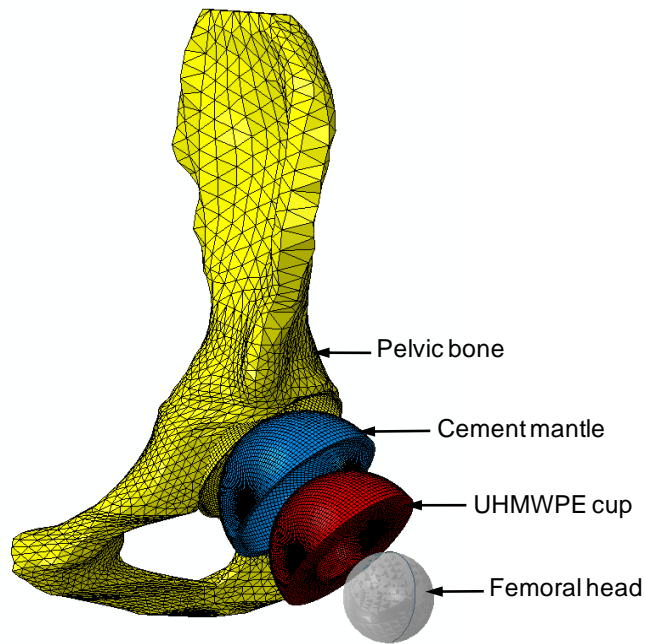
Figure 2.5 The FE model of the Charnley THR in an exploded view, the metallic femoral head was considered to be rigid.
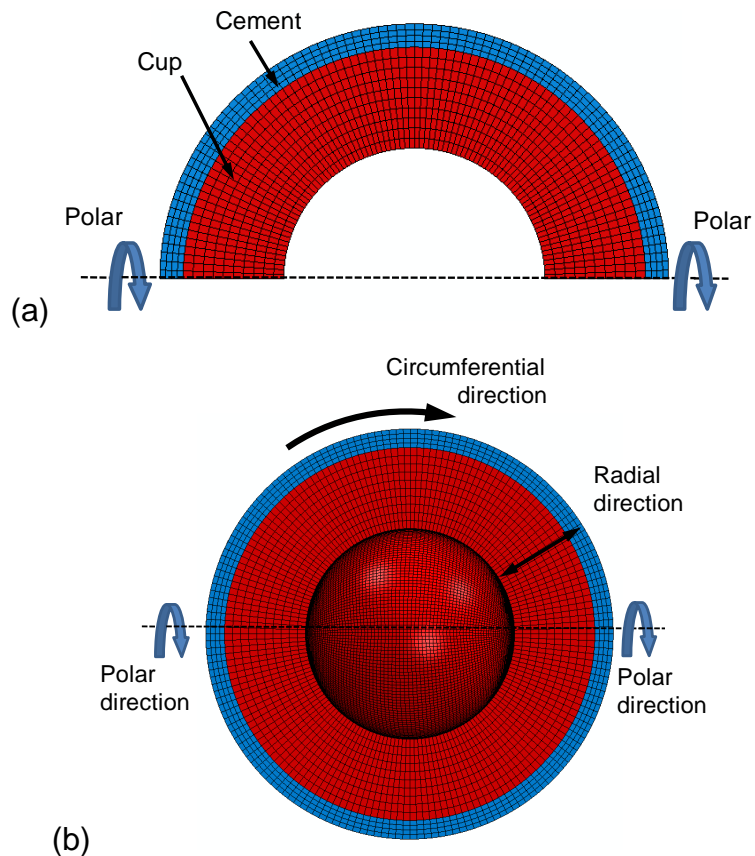
Figure 2.6 The "dual-poled" mesh for the Charnley cup and cement. The cross section of the cup and cement was first meshed to produce planar elements (a), and then the planar elements of the cup and cement were revolved around the pole by 180º to form the 3D FE model (b).

Anatomic Pinnacle THR modelling

The second FE model in the present study was anatomic Pinnacle THR model, as shown in Figure 2.7. As described above, the cortical bone and cancellous bone in the pelvis were meshed with three-noded thin shell elements and four-noded tetrahedron elements respectively. Because of the axisymmetry of the shell, polyethylene liner and femoral head in the Pinnacle system, a "unipolar" mesh was selected, as shown in Figure 2.8. It should be noted that finer mesh was used in the expected loaded region and coarse mesh was applied in the non-loaded region for the polyethylene liner to reduce the simulation time further. Four-noded tetrahedron elements were also applied to mesh the femoral stem. However, during the processing, the femoral head and the femoral stem were constrained to be rigid body. Following a mesh sensitivity analysis which will be discussed in **Section 2.4**, the total number of the nodes and elements for the FE model were approximately 120,000 and 95, 000 respectively, including 'brick' and 'wedge' elements for the cancellous bone and prosthetic components, and 'thin-shell' elements for the cortical bone.
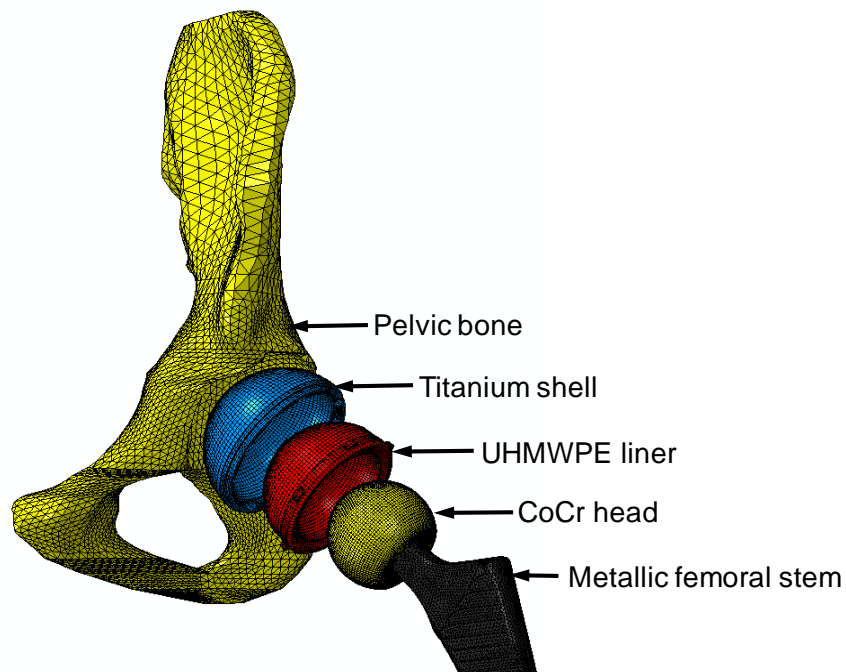
Figure 2.7 The FE model of the Pinnacle THR in an exploded view, the femoral head and femoral stem were considered to be rigid.
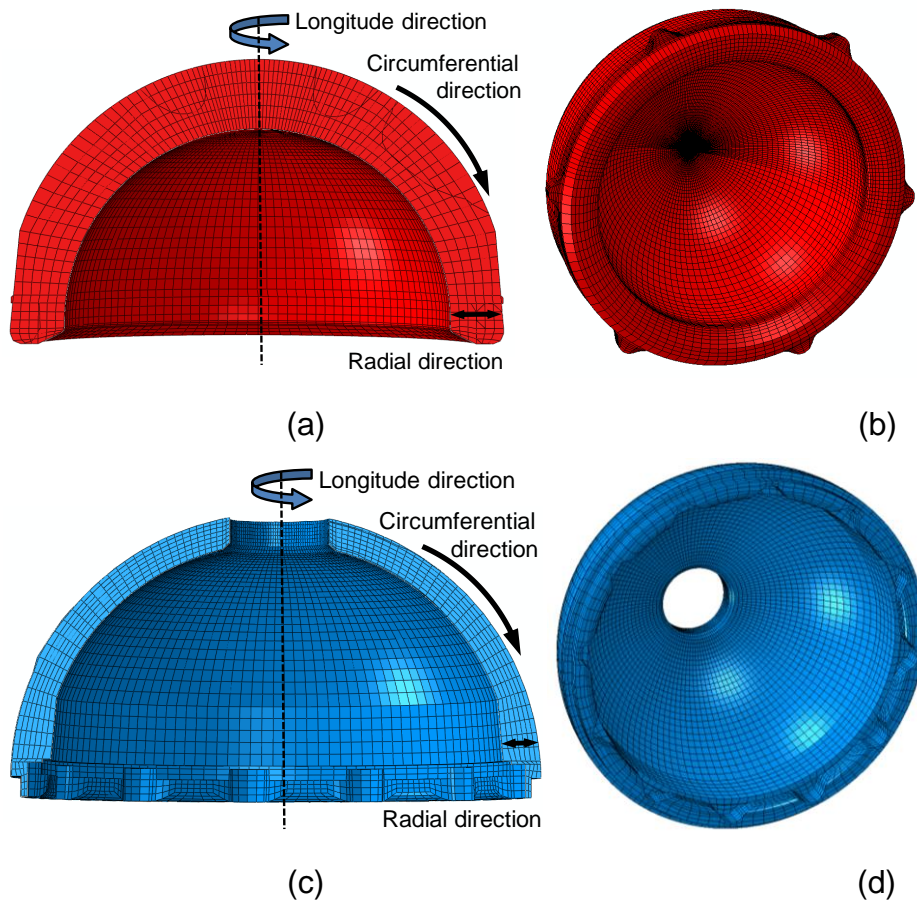
Figure 2.8 The mesh for the Pinnacle acetabular cup system, (a) the cross-section of the mesh for UHMWPE liner showing the element numbers in radial, circumferential and longitude directions, (b) the integral mesh for the UHMWPE liner, (c) the cross-section of the mesh for metal shell showing the element numbers in radial, circumferential and longitude directions, (d) the integral mesh for the metal shell.

The solid models for both the Charnley THR and Pinnacle THR were meshed in I-DEAS (Version 11, EDS, USA) and the FE models were solved using ABAQUS (Version 6.9, Dassault Systèmes Simulia Corp., Providence, United States).

2.3.2 Boundary Conditions and Contact Simulation

In both anatomic models, the nodes situated at the sacroiliac joint and about the pubic symphysis were fully constrained to simulate the sacral and pubic support of the pelvic bones (Udofia et al., 2007; Coultrup et al., 2010), as shown in Figure 2.9. However, it should be pointed out that the real constrain on the bone is elastic by the ligaments and other tissues rather

than rigid. While the difference of boundary conditions between FE modelling and real reconstructions should be recognized and considered, the effect of these differences may not be as significant when only the implants is considered. (Hao et al., 2011).

In the anatomic Charnley THR model, the contact interfaces between the bone and the cement as well as between the cement and the acetabular cup were assumed to be firmly bonded to simulate a full cement interlock and perfect fixation (Coultrup et al., 2010; Zant et al., 2008). A sliding contact formulation was adopted on the bearing surface between the cup and femoral head, and a frictionless behaviour was modelled on the bearing surface as coefficient of friction less than 0.1 was found to have negligible effect on the predicted contact mechanics in the artificial hip joint (Udofia et al., 2004) (Figure 2.9 a).

In the anatomic Pinnacle THR model, the interface between the bone and the implant was assumed to be fully bonded to simulate a situation where the porous sintered coating and in-grown bone were well bonded. A sliding contact formulation was used on both the bearing surface between the femoral head and polyethylene liner, and at the interface between the liner and metal shell, with friction coefficients of 0.083 and 0.15 respectively (Figure 2.9 b). The friction coefficients used on the bearing surface and shell/liner interface were taken from the literature (Ramero et al., 2007; Amirouche et al., 2008) and will be discussed in **Chapter 5**.
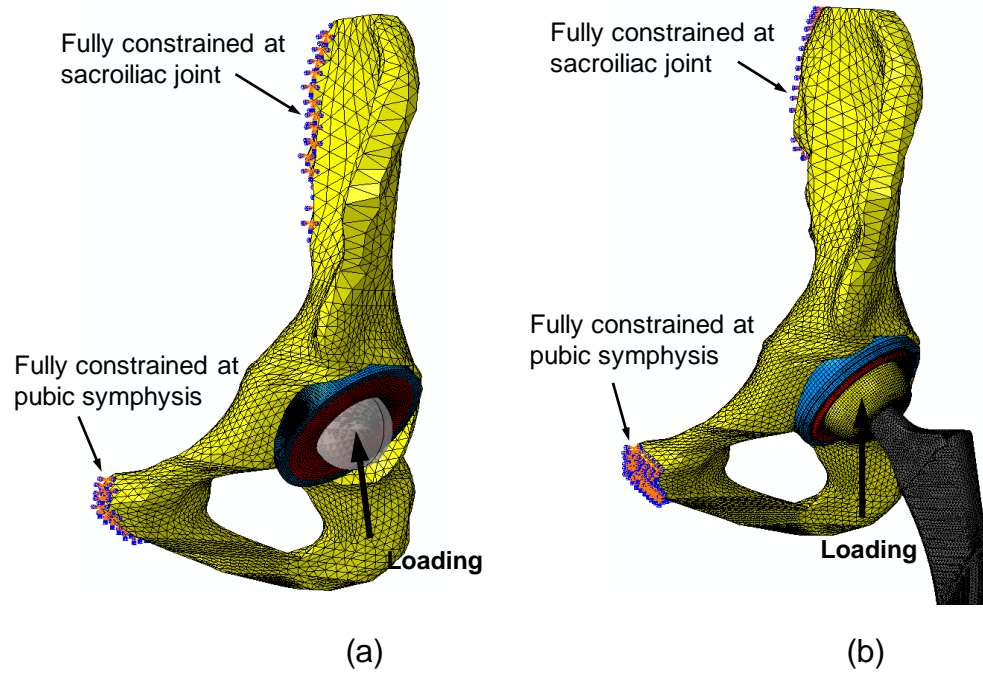
Figure 2.9 The boundary conditions for the anatomic FE Charnley THR model (a) and the anatomic FE Pinnacle THR model (b). The nodes situated at sacroiliac joint and about pubic symphysis were fully constrained in both models.

2.4 Mesh Convergence Analysis

Mesh convergence analysis was conducted in the present study in order to obtain the balance between the accuracy of results and computer resources. For this purpose, different element numbers used in the pelvic bone, Charnley THR components and Pinnacle THR components were analysed and the parameters of interest for both models were examined.

Anatomic Charnley THR model

Both the pelvic bone and components of the Charnley THR were considered in the mesh convergence analysis for the anatomic Charnley THR model. For the purpose of this, a series of meshes with increasing elements numbers in the pelvic bone, cup and cement for the anatomic Charnley THR model were applied. Different combinations of the element numbers for the pelvic bone, cup and cement for Charnley THR were considered.

Firstly, the mesh convergence analysis was conducted for the pelvic bone. This was achieved by keeping the element numbers of the cement and cup constant with large numbers (20, 736 for cement and 51, 840 for cup) and

applying different element numbers to the pelvic bone. Once the element number for the pelvic bone was determined, the mesh convergence analysis was conducted for the cement and the cup. Different combinations of the element numbers for the cement and cup were considered.

Just one case of simulations was conducted in the mesh convergence analysis, and once the element numbers for the components in the model were determined, they were then applied for the other simulation cases. The model used for the mesh convergence analysis has been described previously in **Section 2.3**. In the model, the cup was positioned with inclination angle of 45° and no penetration was considered within the cup. A load of 2500 N with direction of 10° medially was applied in the model. The maximum von Mises stress and peak max principal stress in the cement mantle, as well as the maximum contact pressure on the bearing surface were examined, since the maximum von Mises stress and contact pressure is associated with the tribological performance of the bearings and the max principal stress is closely related to the functional performace of the cement fixation (Maxian et al., 1996a; Coultrup et al., 2009). The convergence of these parameters against the element numbers are shown in Figure 2.10 and Figure 2.11.

As can be seen from Figure 2.10, the changes of all parameters examined in the mesh convergence analysis were within 5% when the element numbers for pelvic bone increased from 5, 608 to 11, 204. Hence, the former was used in all subsequent models. Similarly, the element number of 2, 076 and 5, 184 were applied for the cement and cup respectively as the changes of all parameters examined were within 5% when the numbers were nearly doubled.
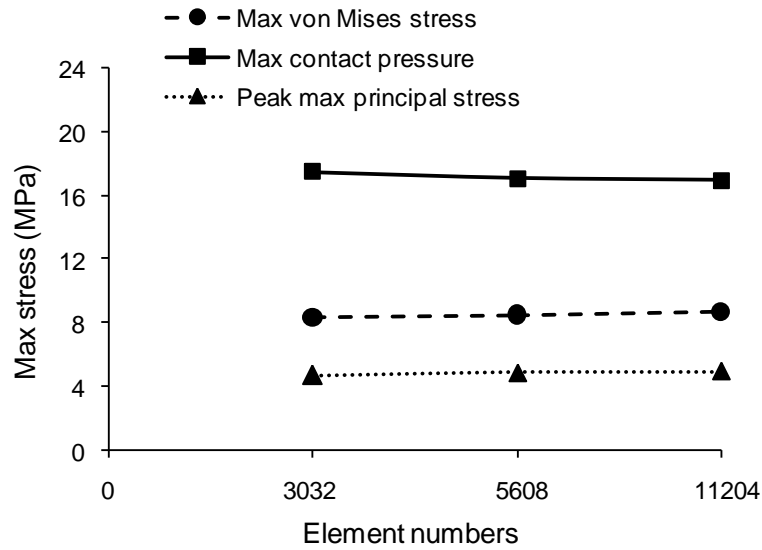
Figure 2.10 The convergence of maximum von Mises stress, peak max principal stress in the cement mantle and maximum contact pressure on the bearing surface as a function of element numbers for pelvic bone (keeping the element numbers of cement and cup as 4416 and 10720).
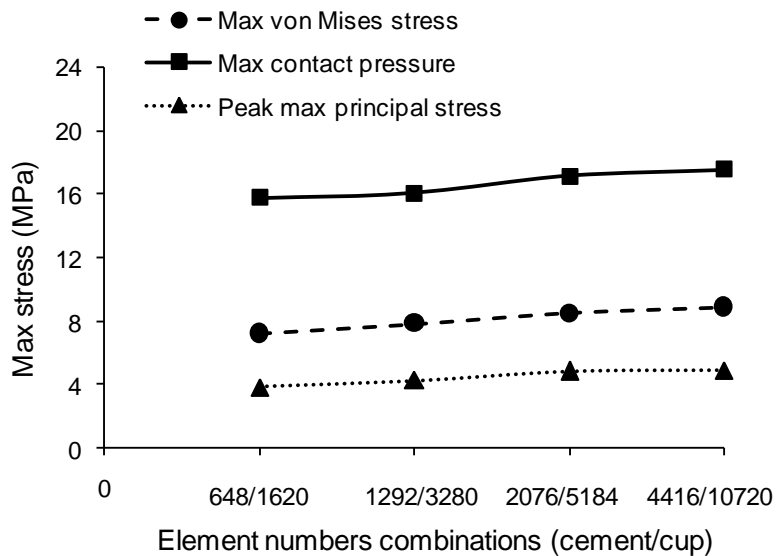
Figure 2.11 The convergence of maximum von Mises stress, peak max principal stress in the cement mantle and maximum contact pressure on the bearing surface as a function of combination of element numbers for cement and cup (keeping the element numbers of pelvic bone as 5608).

Anatomic Pinnacle THR model

The mesh convergence analysis for the anatomic Pinnacle THR model was conducted under both standard and microseparation conditions. Under standard conditions, the contact areas were mainly located within the inner surface of the liner, so the element numbers used at the rim of the liner would have negligible effect on the results. This case was considered to determine the element numbers used for the entire articulating region. However, under large microseparation conditions, the contact areas were concentrated at the rim of the liner, so the mesh density in this region would markedly affect the simulation results. Therefore, the element numbers used at the rim of liner were determined from the microseparation case. Similar to the anatomic Charnley THR model, just one simulation case was considered for both conditions.

Under the standard condition, a series of meshes with increasing element numbers for the components of Pinnacle THR were applied. The model was conducted with the metal shell and liner positioning with an inclination angle of 45° and no microseparation was considered. A vertical load of 2500 N was applied. The radial clearance between the liner and the head was 0.3 mm. The maximum von Mises stress in the liner and maximum contact pressure on the articulating surface were examined and the results are shown in Figure 2.12.

Subsequent anatomic Pinnacle THR models were meshed with element numbers of about 53, 000 for the liner and about 37, 000 for the metal shell because the change in the parameters of interest were within 5% when the element numbers were nearly doubled, as shown in Figure 2.12.
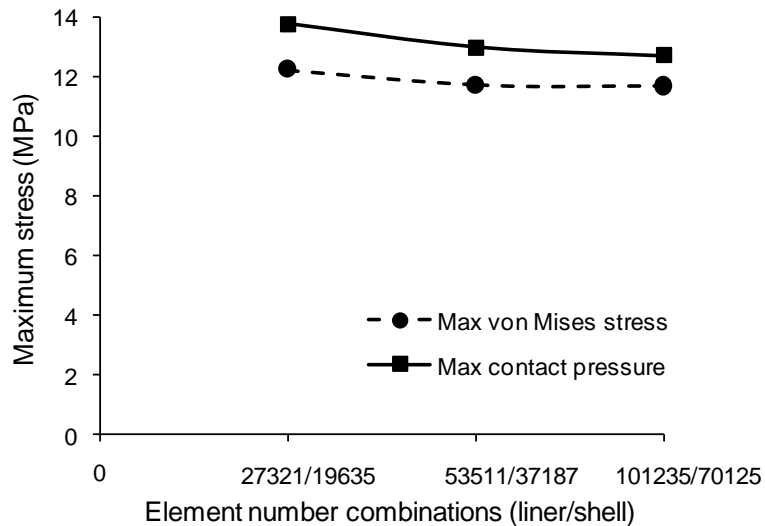
Figure 2.12 The convergence of maximum von Mises stress in the liner and maximum contact stress on the articulating surface as a function of combination of element numbers for liner and shell (keeping the element numbers of pelvic bone as 5608).

Under microseparation conditions, the meshes at the rim of the liner were refined. Therefore, keeping the element numbers for the metal shell and most part of liner the same as under standard conditions, a series of different element numbers along the arc of the rim of the liner were considered during the mesh convergence analysis, as shown in Figure 2.13.

The model was tested under a cup inclination angle of 45⁰ and microseparation level of 1500 μm. The definition of the microseparation level will be discussed in **Chapter 7**. A vertical load of 2500 N was applied. The maximum von Mises stress in the liner and maximum contact pressure on the articulating surface were examined and the results are shown in Figure 2.14.

From Figure 2.14, element numbers of 720 were used at the rim of the liner because the change of all parameters examined were within 5% when the element numbers were doubled.
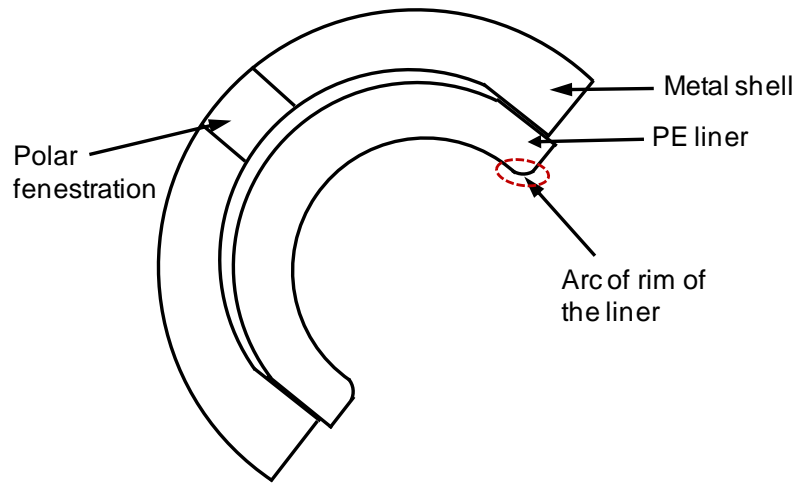
Figure 2.13 The cross-section of the Pinnacle cup system showing the arc of rim of the liner. Different element numbers were applied along the arc of the rim of the liner during the mesh convergence analysis.
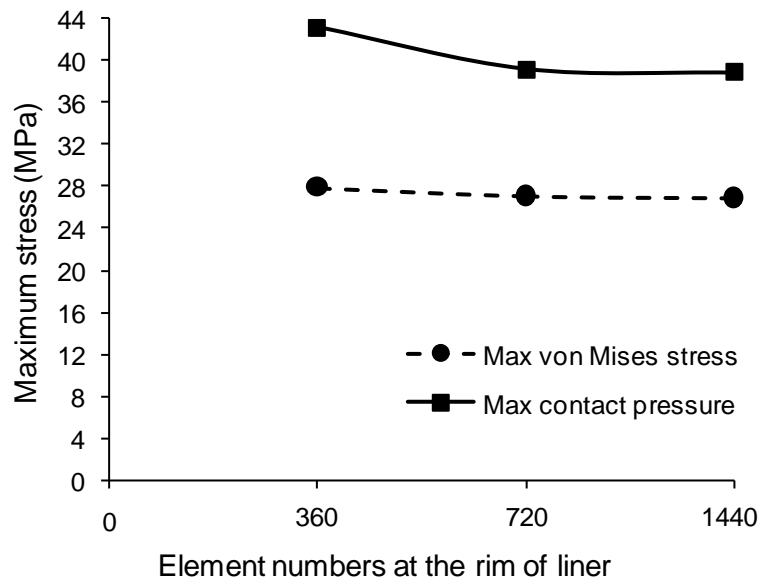
Figure 2.14 The convergence of maximum von Mises stress in the liner and maximum contact stress on the articulating surface as a function of element numbers used along the arc of the rim of the liner.

Chapter 3
Contact Mechanics and Cement Fixation Studies of Charnley THR

3.1 Introduction

The long-term clinical performance of artificial hip joints depends on both the tribology of the bearings and the fixation of the components. For cemented THR, the main reasons that caused the failure of the prosthesis are bone resorption due to the wear particles (Ingham and Fisher, 2005) and bone cement damage which is associated with the mechanical behaviour upon it (Crowninshield et al., 1983; Coultrup et al., 2009), as reviewed in **Section 1.3.4**. It is generally believed that the mechanical behaviour in the cement mantle and at the bone-cement interface is closely related to many factors such as head diameters (Mai et al., 1996; Morrey et al., 1989), penetration depths (Coultrup et al., 2009), outer diameters of the acetabular cup (Wroblewski et al., 2009a) etc. All these parameters can affect not only the contact mechanics and tribology on the articulating surfaces but also the mechanical characteristics in the fixation at the bone-cement interface, which are two main factors influencing the failure of the cemented THR. It is particularly important to recognize the interaction between the contact mechanics and the fixation, since the contact stresses on the articulating surface are directly transmitted to the interface and vice versa. Therefore, these parameters may have a synergistic effect on the performance of hip prostheses. However, to the author's knowledge, few studies reported in the literature have addressed the two problems interactively. Furthermore, the effect of cup inclination angles on the contact mechanics and especially the fixation of a MoP THR, with respect to the cement mantle, has not been investigated comprehensively. Therefore, the aims of this chapter were to investigate the individual and combined influence of different factors, including the cup inclination angles, penetration depths, outer diameters of the acetabular component and the head diameters on the contact mechanics and cement fixation of cemented MoP THRs using anatomic Pinnacle THR model.

3.2 Materials and Methods

3.2.1 FE Model

A typical Charnley THR was considered in this chapter. The geometries and nominal sizes of the components for the Charnley THR have been illustrated in **Chapter 2**. In order to examine the effect of cup inclination angles, different cup orientations of 45⁰, 55⁰ and 65⁰ were modelled. In order to study the effect of outer sizes of the acetabular components, two typical designs of acetabular cup sizes for the Charnley THR with outer diameter of 40 mm and 43 mm were modelled under these three different cup angles. Different head diameters of 22.225, 28, 32, 36, and 38 mm were also modelled to investigate the effect of head sizes.

Different liner penetration depths of 1, 2 and 4 mm in the acetabular cup were considered for each case described above. Geometrical characterization of the penetration on the acetabular cup was performed by intersecting the cup using the femoral head in the direction of the resultant load, as illustrated in Figure 3.1 (Coultrup et al., 2009). The maximum penetration depth of 4 mm was considered as the limit beyond which impingement between the neck and cup would occur (Wroblewski et al., 2009b). For a linear penetration rate of 0.1-0.2 mm/year (Wroblewski et al., 2009c), this would represent a maximum service life of 20-40 years.
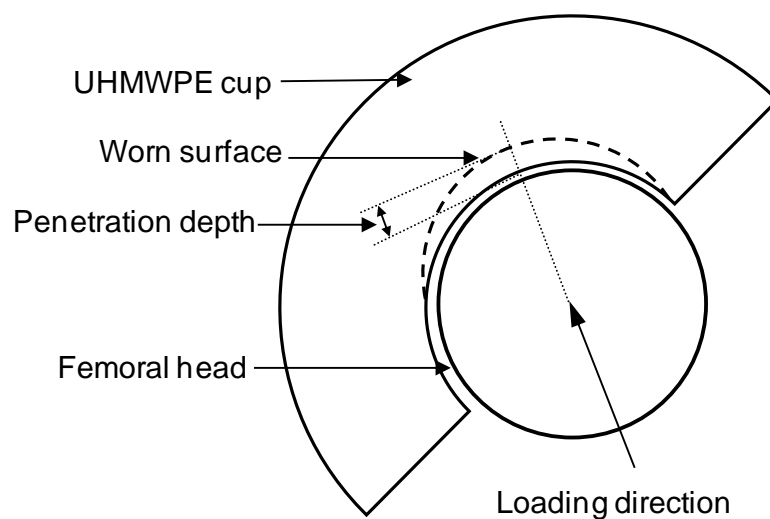
Figure 3.1 A schematic diagram (cross-section) shows the femoral head and UHMWPE cup with penetration indicated.

An anatomic Charnley THR model was developed. The FE model, mechanical properties of the components and the boundary conditions for the model were discussed in **Chapter 2**. A fixed resultant hip joint contact force of 2, 500 N with direction of 10⁰ medially was applied through the centre of the femoral head, simulating the mid-to-terminal stance loading of the gait cycle (Udofia et al., 2005), as shown in Figure 2.9. This hip joint contact force corresponds to about 3-4 times BW for a patient weight of 80 kg, which is close to the average weight for both males and females between the ages of 20 and 74 (Ogden et al., 2004).

The von Mises stress of the cement material and the max principal stress in the cement mantle, as well as the shear stress at the bone-cement interface were examined in the present study. The reason for this was that the von Mises stress is directly related to the fatigue of the cement mantle which could lead to the failure of the cement mantle, the max principal stress in the cement mantle and shear stress at the bone-cement interface could be an important contributor to the shear damage at the bone-cement interface and tensile damage in the cement mantle which can consequently lead to loosening of cemented acetabular components (Kim et al., 2004; Arola et al., 2005), especially since the PMMA cement is weak in tension and strong in compression (Kuehn et al., 2005). However, it should be noted that all the stresses were used as an indication of potential failure of the cement mantle, rather than using a damage accumulation approach (Coultrup et al., 2009), and also the present study focused on the medium to long-term period rather than the long-term when cement failure ultimately occurs. The bone-cement interface was examined in detail, since the cement failure is likely to be initiated at this interface (Tong et al., 2008; Zant et al., 2008).

3.2.2 Model Validation

The validation of the anatomic Charnley THR model was carried out by comparing the present study with a previous study (Jin et al., 1999). The main features of the components in the present anatomic Charnley THR model were identical with those in the axisymmetric model in the previous study. However, there are some differences between the two models regarding to the boundary and loading conditions, as well as the component

positions. The comparison of the two models is shown in Figure 3.2 and Table 3.1.

An experimental measurement of the contact areas using a pigmented paste (engineering blue) was also conducted in the previous study (Jin et al., 1999). By doing this, the cup was placed horizontally and the vertical load of 2, 500 N was applied at a loading rate of 1 mm/min, as shown in Figure 3.3. After the load was removed, the contact areas on the bearing surfaces were then measured in terms of half contact angle and the contact radius. These parameters were then converted into contact areas and compared with the contact areas predicted in the present study.
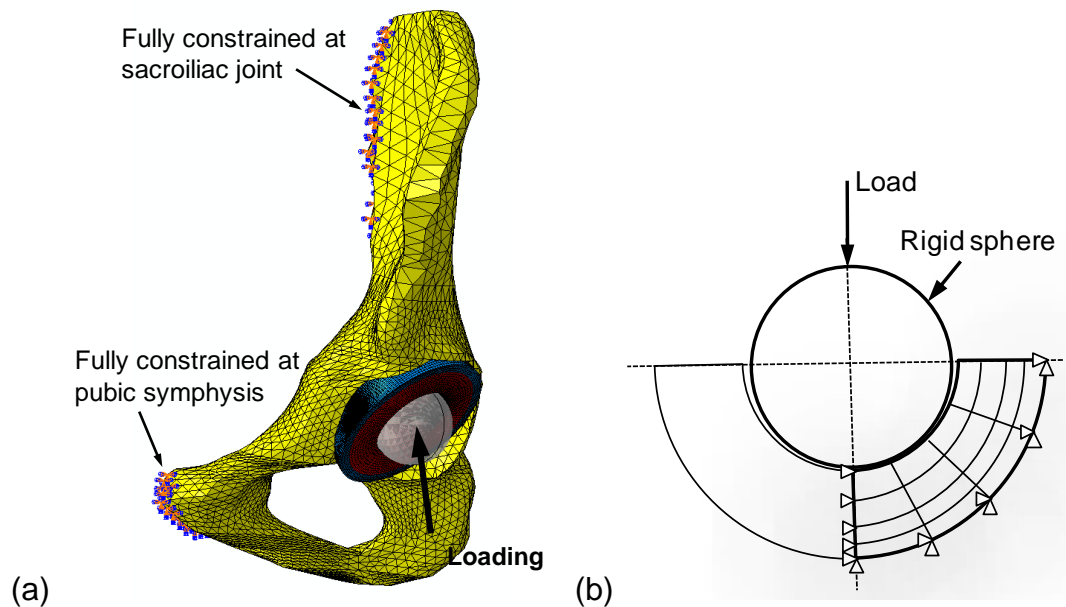
Figure 3.2 The comparison of the anatomic Charnley THR model with the axisymmetric model: (a) the anatomic Charnley THR model in the present study, (b) the axisymmetric model in the previous study (Jin et al., 1999).

Table 3.1 The comparison of the model, dimensions of the components and the loading conditions between the present study and previous study (Jin et al., 1999).

	Model in the present study	**Model in previous study**
Model	Anatomic model with pelvic bone	Axisymmetric model without pelvic bone
Head diameter (mm)	22.225	22.225
Radial clearance (mm)	0.1825	0.1825
Cup thickness (mm)	8.705	8.705
Cup inclination (º)	45	0
Load (N)	2500	2500
Load direction	10º medially	vertical
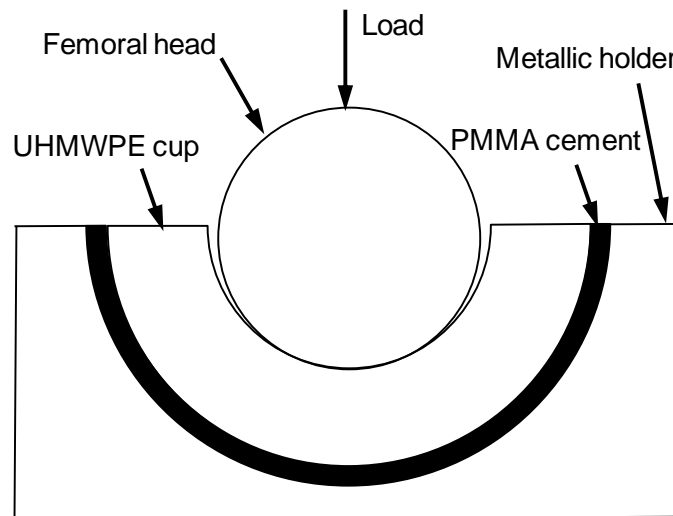
Figure 3.3 The experimental configuration to measure the contact areas on the bearing surface between the femoral head and cup in the previous study (Jin et al., 1999).

3.3 Results

3.3.1 Validation

The validation of the anatomic Charnley THR model was conducted by comparing the predicted contact pressures and contact areas on the bearing

surfaces between the present study and previous study, which included both simulation predictions and experimental measurements (Jin et al., 1999).

The difference in the predicted maximum contact pressures and contact areas on the bearing surfaces between the anatomic Charnley THR model in the present study and the axisymmetric model in the previous study were about 4.7% and 10.3% respectively. However, the difference in contact areas between the prediction from the anatomic Charnley THR model in the present study and the experimental measurement in the previous study was about 5.5% (Table 3.2).

Table 3.2 The comparison of maximum contact pressure and contact area on the bearing surface between the anatomic Charnley THR model in the present study, the axisymmetric model and the experimental measurement in the previous study (Jin et al., 1999).

	Max contact pressure		Contact area	
	Values (MPa)	Difference (%)	Values (mm^2)	Difference (%)
Anatomic Charnley THR model	17.1	--	268	--
Axisymmetric model	17.9	4.7	243	10.3
Experimental measurement	--	--	254	5.5

3.3.2 Effect of Wear and Cup Angles

Generally, for all conditions considered, the predicted contact areas were located about the superior region of the cup in the loading direction (Figure 3.4 and Figure 3.5). Contact area was shifted towards the edge of the cup as the inclination angle was increased (Figure 3.5). Both the maximum contact pressure on the bearing surface and von Mises stress in the acetabular cup were reduced markedly by ~30% and ~20% respectively when even a small penetration depth of 1 mm occurred. However, there was no large difference among different cup penetration depths with regard to either contact pressures or von Mises stress (Figure 3.6). Furthermore, the increase in the

cup inclination angles only resulted in a modest increase in the maximum contact pressure and von Mises stress (less than 10%) (Figure 3.6). These values were predicted corresponding to the mid-to-terminal stance portion of the gait cycles, and might not be the same when considering other instants of the walking cycle or other activities such as sitting, standing and the use of stairs.

(a) (b)
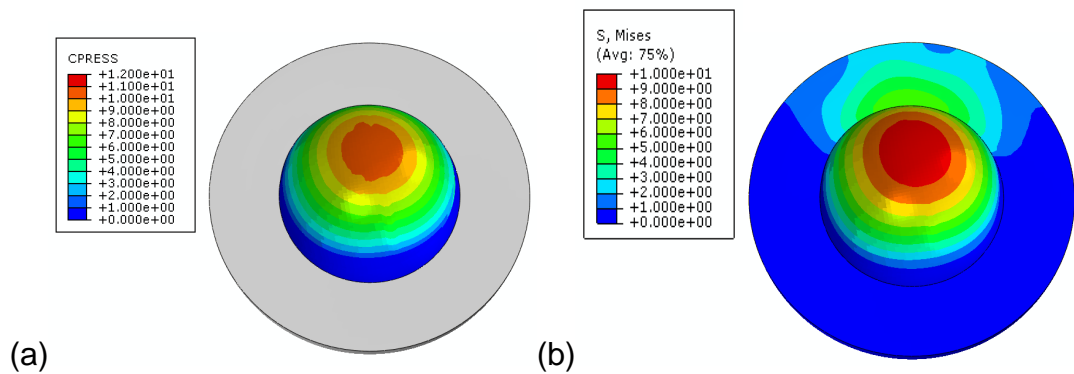
Figure 3.4 Contour plots of the predicted stresses (MPa) for the acetabular cup under cup inclination angle of 45⁰ and with penetration depth of 1 mm: (a) contact pressures on the bearing surface, (b) von Mises stresses in the acetabular cup.

	45°	55°	65°
No penetration	17.1 MPa 268 mm2	17.2 MPa 261 mm2	18.1 MPa 240 mm2
Penetration 1mm	11.1 MPa 557 mm2	11.7 MPa 499 mm2	13.4 MPa 432 mm2
Penetration 2mm	11.0 MPa 592 mm2	11.4 MPa 530 mm2	13.0 MPa 456 mm2
Penetration 4mm	11.2 MPa 645 mm2	11.2 MPa 583 mm2	12.4 MPa 501 mm2

CPRESS

0 MPa   19 MPa
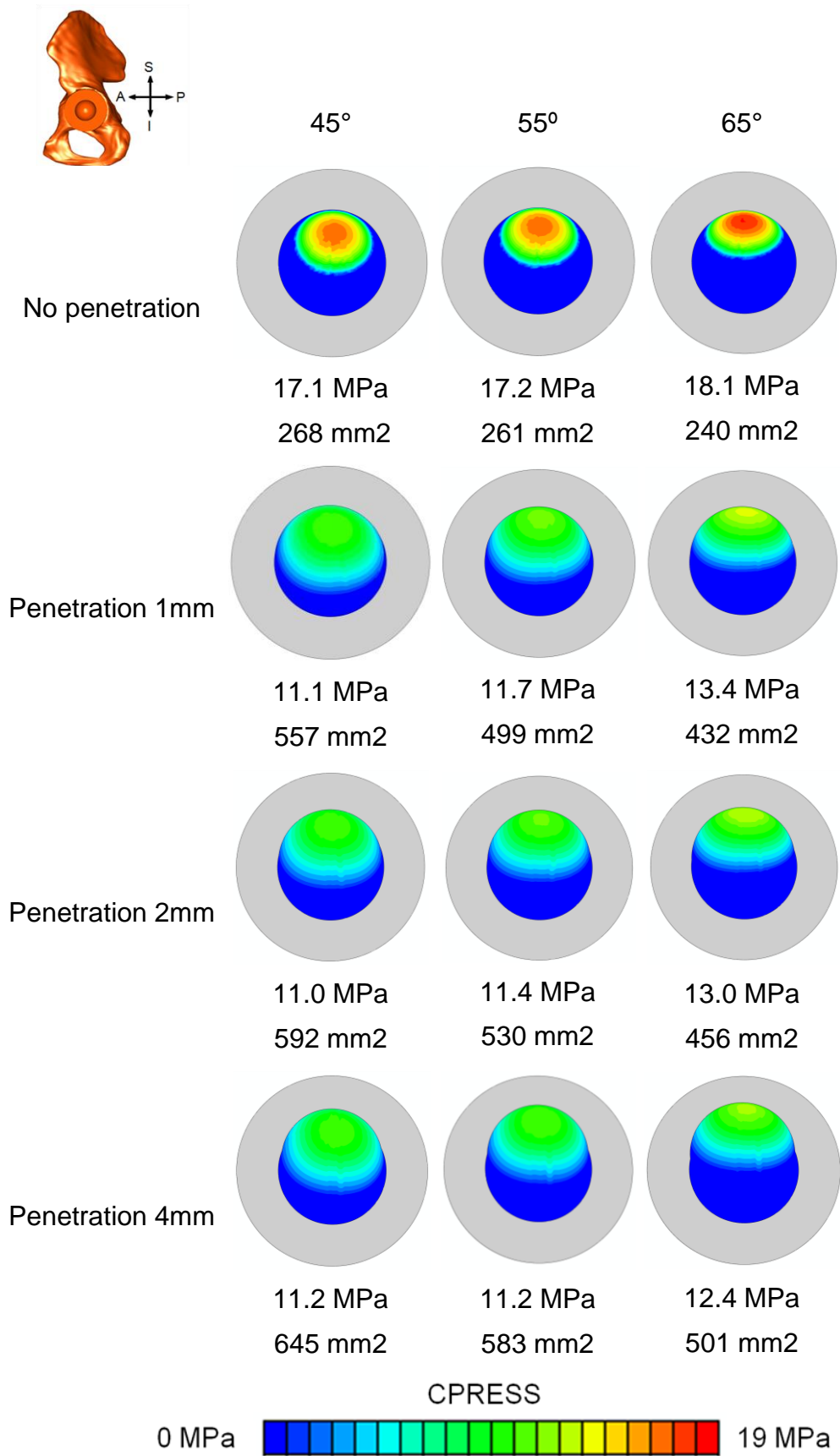
Figure 3.5 The distributions of predicted contact pressures (MPa) and contact areas as a function of cup inclination angles for the UHMWPE cup with different penetration depths.
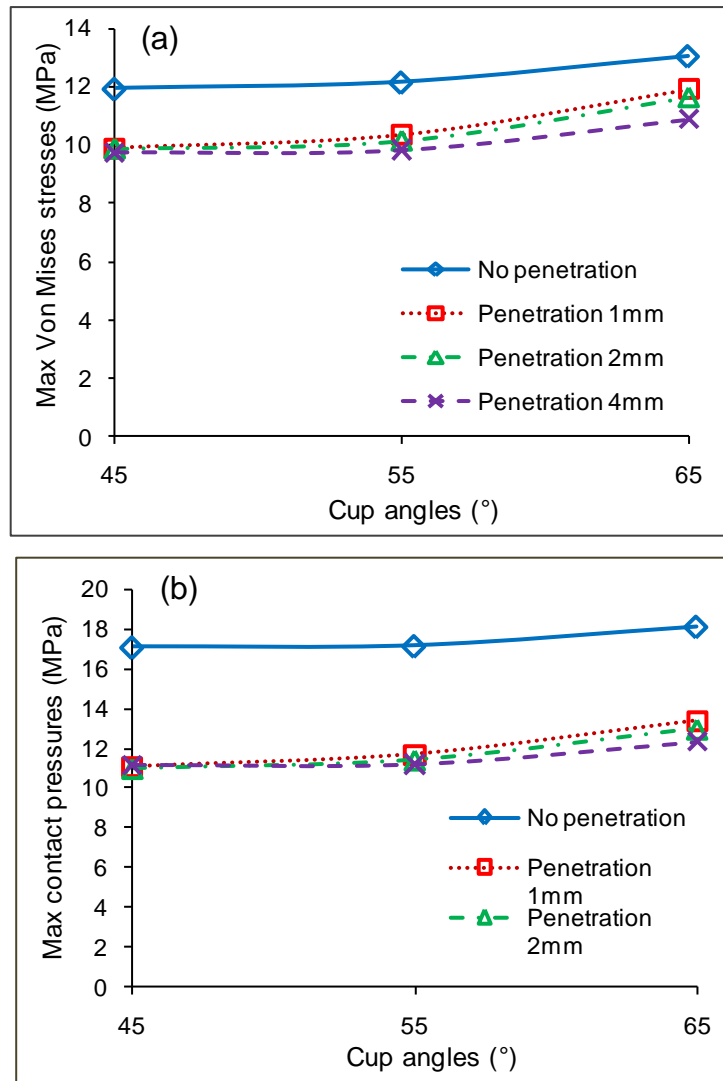
Figure 3.6 (a) the predicted maximum Von Mises stress (MPa) in the UHMWPE cup, (b) The predicted maximum contact pressure (MPa) on the bearing surface with different cup inclination angles and penetration depths.

The distributions of predicted von Mises stress in the cement mantle and at the bone-cement interface, as well as the max principal stress in the cement mantle for 1 mm penetration depth model and 45⁰ cup inclination angle condition is shown in Figure 3.7. It is noted that both the peak von Mises stress and max principal stress in the cement mantle and at bone-cement interface seem to occur in the superior region of the cement mantle.

With increased cup inclination angles, the distribution of von Mises stresses over the cement mantle at the bone-cement interface was shifted towards the edge of the cement as well (Figure 3.8). Both the cup inclination angles

and penetration depths in the acetabular cup had a marked effect on the peak von Mises stress over the cement mantle at the bone-cement interface (Figure 3.9 a). When the cup inclination angles increased from 45⁰ to 65⁰, the peak von Mises stress was elevated moderately by about 18%-46% for all the cup penetration depths. When minor wear in the acetabular cup occurred, i.e. with a wear depth of 1 mm and 2mm, the peak von Mises stress at the bone-cement interface was reduced and the reduction varied among different cup inclination angles. For example, the peak von Mises stress was reduced by about 18%-32% for cup angles of 45⁰ and 55⁰, and below 5% for cup angle of 65⁰ (Figure 3.9 a). An increase of penetration depths in the acetabular cup led to an increased von Mises stress (by approximately 15%-37% when the wear depth increased from 1 mm to 4 mm). Typically, a combination of a maximum penetration depth of 4 mm and a cup angle of 65⁰ resulted in a large increase in the predicted von Mises stress by more than 40%, slightly above the unworn cup (Figure .9 a).

With increased cup angles from 45⁰ to 65⁰, for all the cup penetration depths, the maximum shear stress at the bone-cement interface increased markedly by about 26%-32%, while the peak max principal stress in the cement mantle increased slightly by approximately 4%-12% (Figure 3.9 b and c). It is also interesting to note that a modest penetration depth in the acetabular cup resulted in a decreased shear stress at the bone-cement interface and peak max principal stress in the cement mantle, however, if the penetration depth was continuously increased to 4 mm, higher peak shear stresses and max principal stresses were observed (Figure 3.9 b and c).
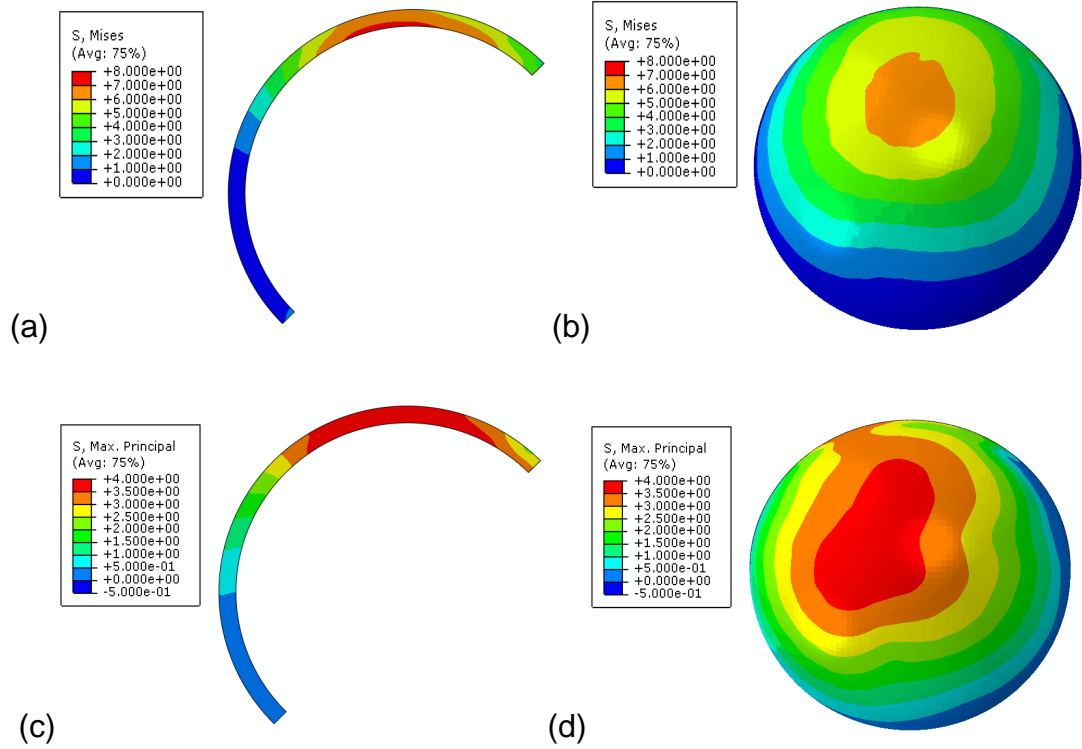
Figure 3.7 The predicted stresses (MPa) for the cement mantle under cup inclination angle of 45⁰ and with penetration depth of 1 mm: (a) Von Mises stresses in the cement mantle (cross-section), (b) Von Mises stresses at the bone–cement interface, (c) max principal stresses in the cement mantle (cross-section), (d) max principal stresses at the bone-cement interface.

	45°	55º	65°
No penetration			
	8.49	8.50	9.79
Penetration 1mm			
	6.46	6.72	9.44
Penetration 2mm			
	6.99	7.21	9.91
Penetration 4mm			
	8.50	8.61	10.61

S, Mises

0 MPa ■■■■■■■■■■■■ 12 MPa
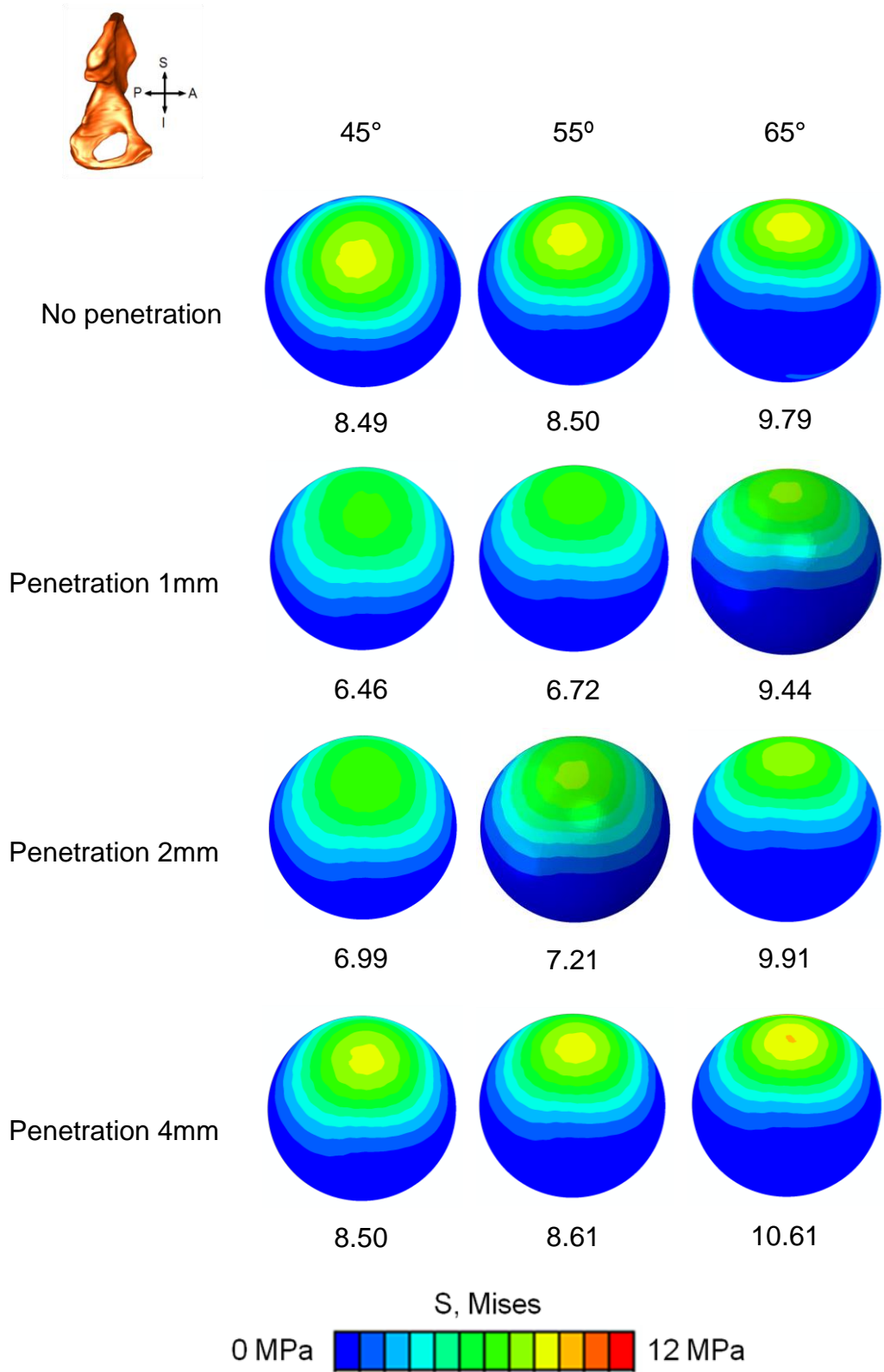
Figure 3.8 The distributions of predicted Von Mises stresses (MPa) at the bone-cement interface as a function of cup inclination angles for the UHMWPE cup with different penetration depths.
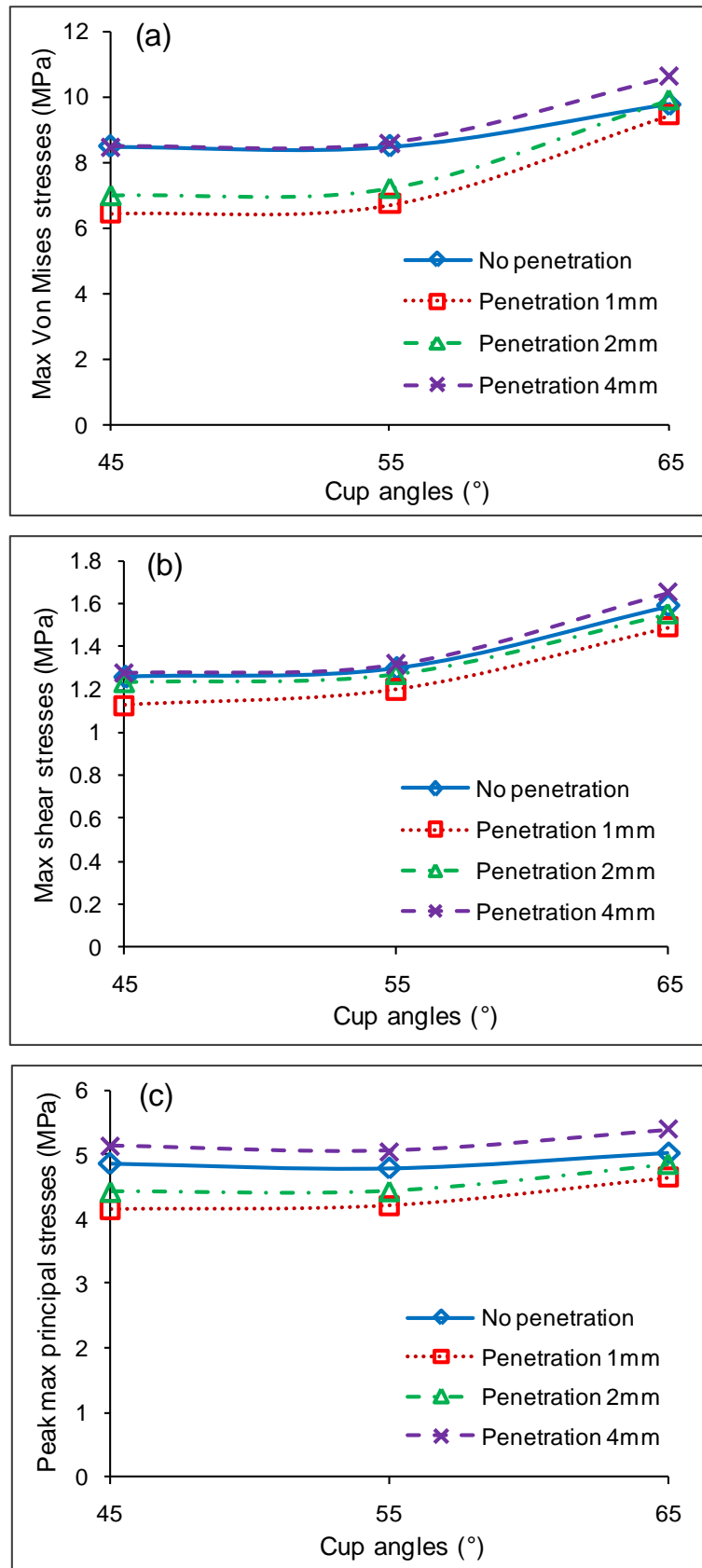
Figure 3.9 The predicted peak stress (MPa) for the cement mantle with different cup inclination angles and penetration depths: (a) von Mises stress at the bone-cement interface, (b) shear stress at the bone-cement interface, (c) max principal stress in the cement mantle.

3.3.3 Effect of Acetabular Cup Sizes

The maximum contact pressure on the bearing surface for both the two models with cup outer diameters of 40 mm and 43 mm were located at the superior region of the acetabular cup in line with the load vector, and the same pattern of the contact pressures was observed between the two models (Figure 3.10).

For all cup angle conditions, an increase in the penetration depth in the acetabular cup to 4 mm led to a marked decrease of both the maximum von Mises stress in the acetabular cup and maximum contact pressure on the bearing surface by approximately 20% and 50% respectively (Figure 3.11). At the same level of penetration depth, the maximum von Mises stress in the acetabular cup and contact pressure on the bearing surface for cup outer diameter of 40 mm were observed to be higher than that for cup outer diameter of 43 mm. However, the discrepancy was negligible (less than 5%) (Figure 3.11).

(a)   (b)
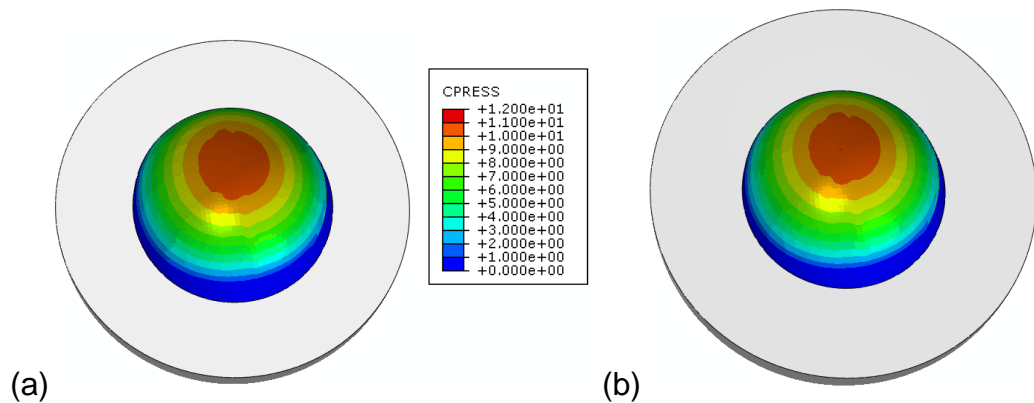
Figure 3.10 Contour plots of the predicted contact pressures (MPa) on the bearing surface at cup inclination angle of 45º and penetration depth of 1 mm with cup outer diameters of (a) 40 mm, (b) 43 mm.
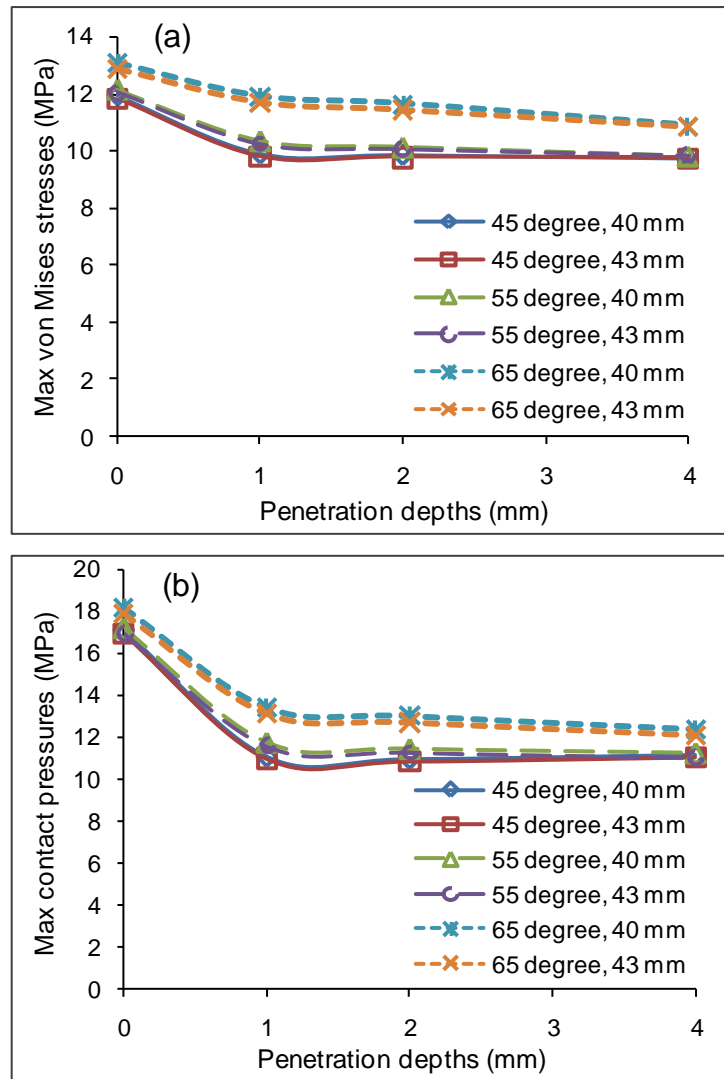
Figure 3.11 The predicted peak stress (MPa) for the acetabular cup as a function of penetration depths with different cup inclination angles and cup outer diameters: (a) von Mises stress in the acetabular cup, (b) contact pressure on the bearing surface.

The same pattern of the von Mises stresses and max principal stresses in the cement mantle was observed in both cup design models (cup outer diameter of 40 mm and 43 mm). However, the values for the cup design with outer diameter of 40 mm were higher than that with outer diameter of 43 mm (Figure 3.12 and Figure 3.13).

The peak von Mises stress and shear stress at the bone-cement interface, and max principal stress in the cement mantle for the model with cup outer diameter of 40 mm were observed to be higher compared with that of 43 mm, at a given penetration depth and cup inclination angle (Figure 3.14). It is also interesting to note that for all cup angles conditions, with the

increased penetration depths (from 1 to 4 mm), the discrepancies in the peak von Mises stress and max principal stress between the two cup designs were also increased (from about 15% to19% for von Mises stress, and about 15% to 22% for max principal stress when the penetration depths increased from 1 mm to 4 mm). However, no such difference for the shear stresses was observed (Figure 3.14).
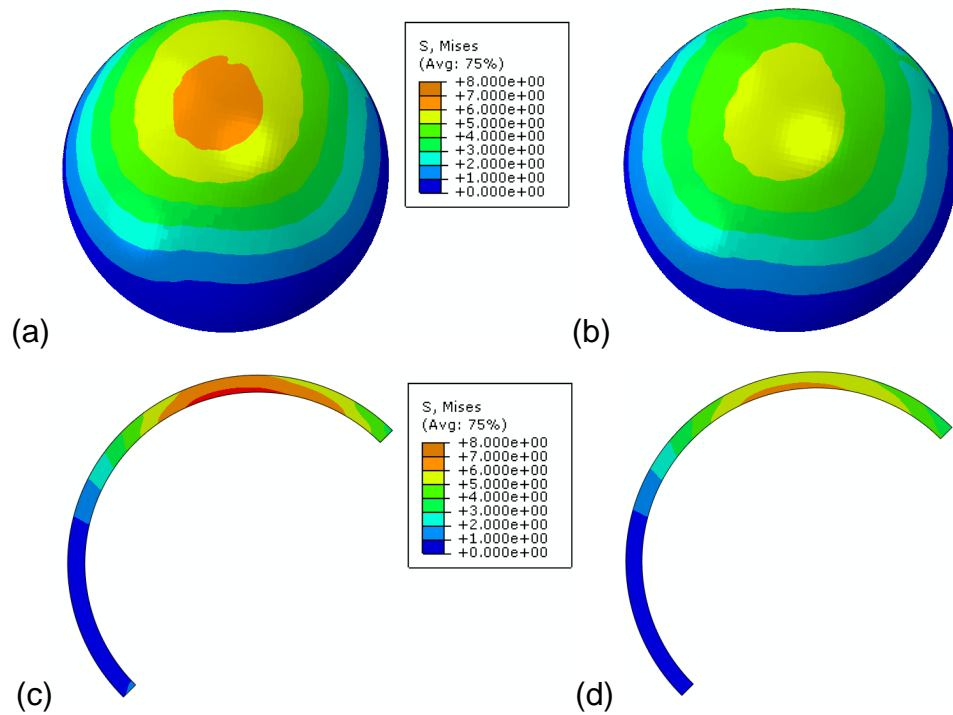
Figure 3.12 Comparison of the predicted von Mises stresses in the cement mantle (MPa) at 45⁰ cup inclination angle and 1 mm penetration depth for different cup outer diameters: von Mises stresses at the bone-cement interface for cup outer diameter of (a) 40 mm, (b) 43 mm; von Mises stresses in the cement mantle for cup outer diameter of (c) 40 mm, (d) 43 mm.
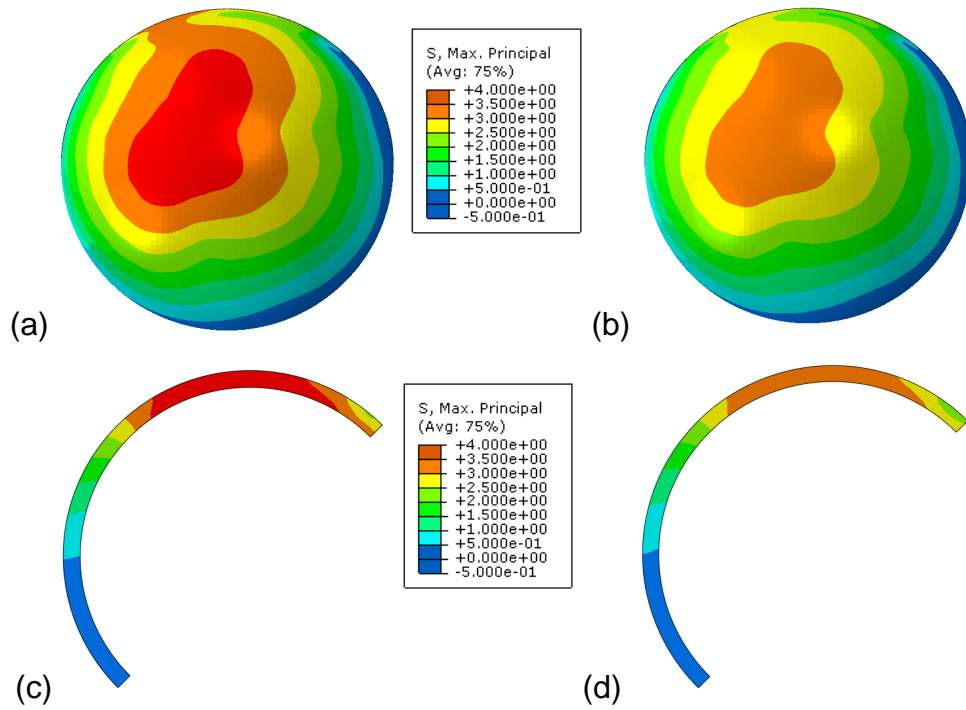
Figure 3.13 Comparison of the predicted max principal stresses (MPa) in the cement mantle at 45⁰ cup inclination angle and 1 mm penetration depth for different cup outer diameters: max principal stresses at the bone-cement interface for cup outer diameter of (a) 40 mm, (b) 43 mm; max principal stresses in the cement mantle for cup outer diameter of (c) 40 mm, (d) 43 mm.
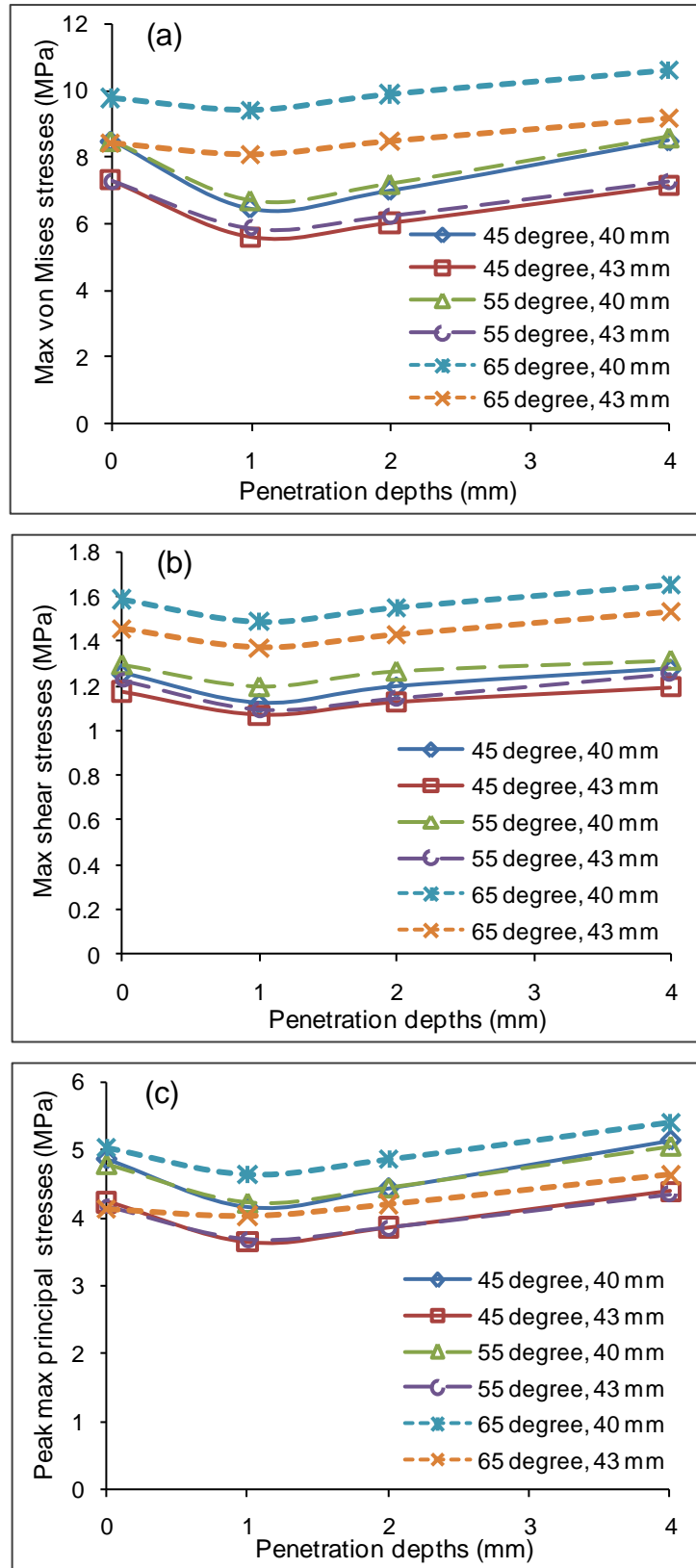
Figure 3.14 The predicted peak stress (MPa) for the cement mantle as a function of penetration depths with different cup inclination angles and cup outer diameters: (a) von Mises stress at the bone-cement interface, (b) shear stress at the bone-cement interface, (c) max principal stress in the cement mantle.

3.3.4 Effect of Head Diameters and Cup Thicknesses

An increase in the sizes of femoral head, hence a decrease in the thickness of acetabular cup, resulted in an increase in the contact area and a marked decrease in the contact pressure on the bearing surface and von Mises stresses in the acetabular cup (Figure 3.15 and Figure 3.16), and both stresses were reduced by nearly 50% (Figure 3.16). However, when the head diameters increased from 22.225 mm to 36 mm, the peak von Mises stress and shear stress at the bone-cement interface, and the max principal stress in the cement mantle were predicted to increase by about 30%, 25% and 11% respectively, followed by a slight decrease when the head sizes increased up to 38 mm (Figure 3.17, Figure 3.18 and Figure 3.19).
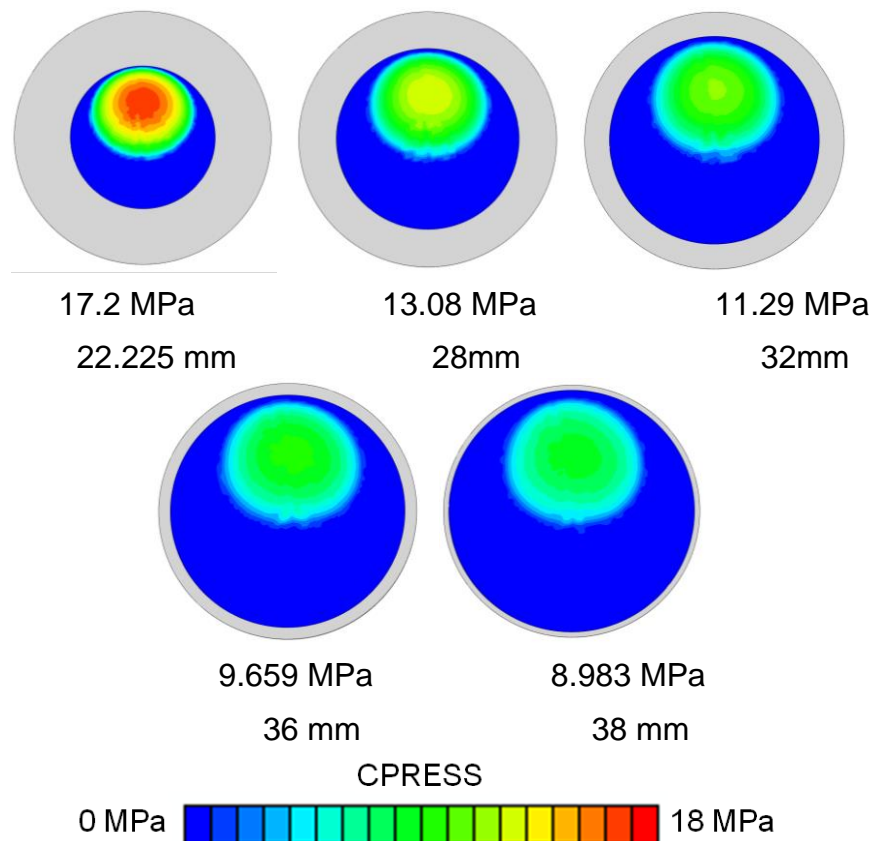
Figure 3.15 Contour plots of contact pressures (MPa) on the bearing surfaces with different head diameters.
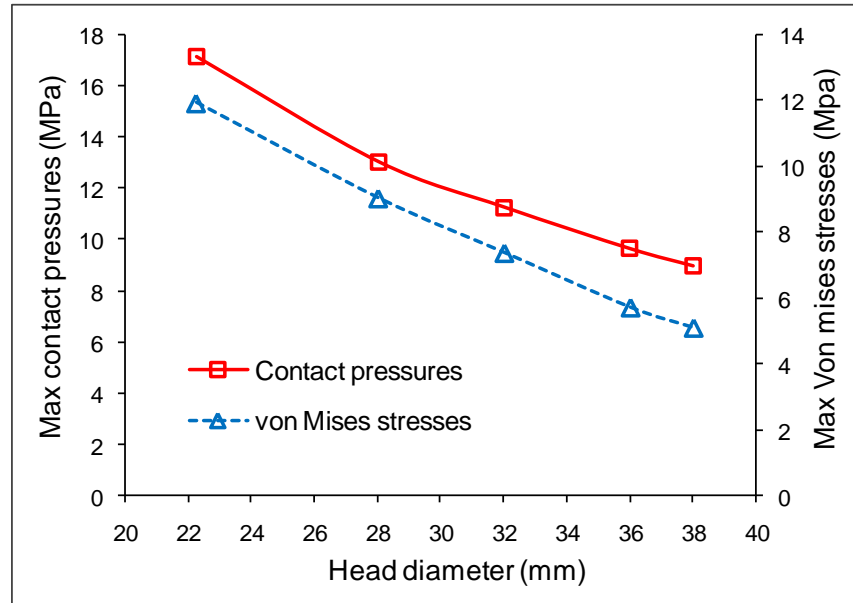
Figure 3.16 The predicted maximum contact pressure (MPa) on the bearing surface and von Mises stress (MPa) in the acetabular cup with different head diameters.
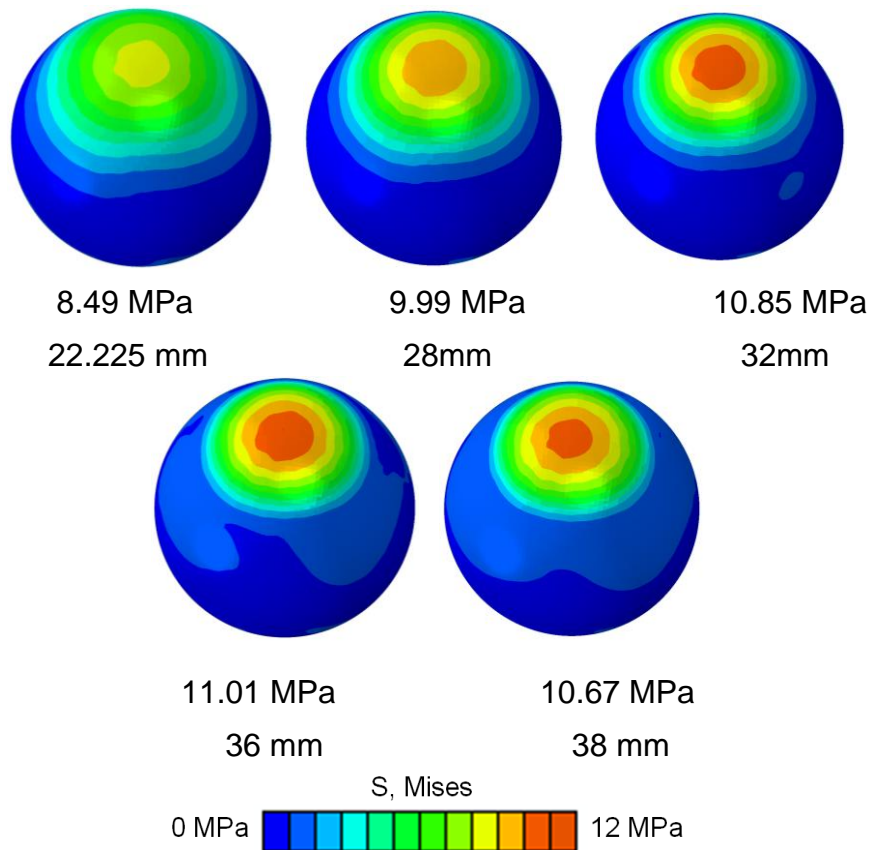
Figure 3.17 Contour plots of von Mises stresses (MPa) at the bone-cement interface with different head diameters.
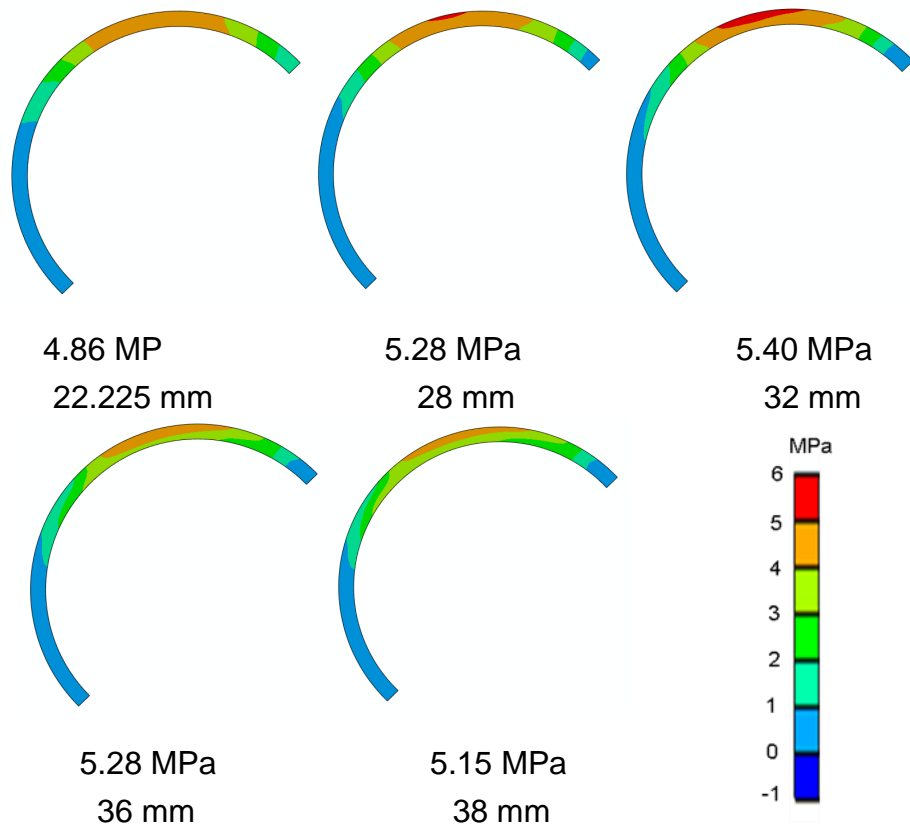
Figure 3.18 The predicted max principal stresses (MPa) in cement mantle with different head diameters (cross-section view for the cement mantle).
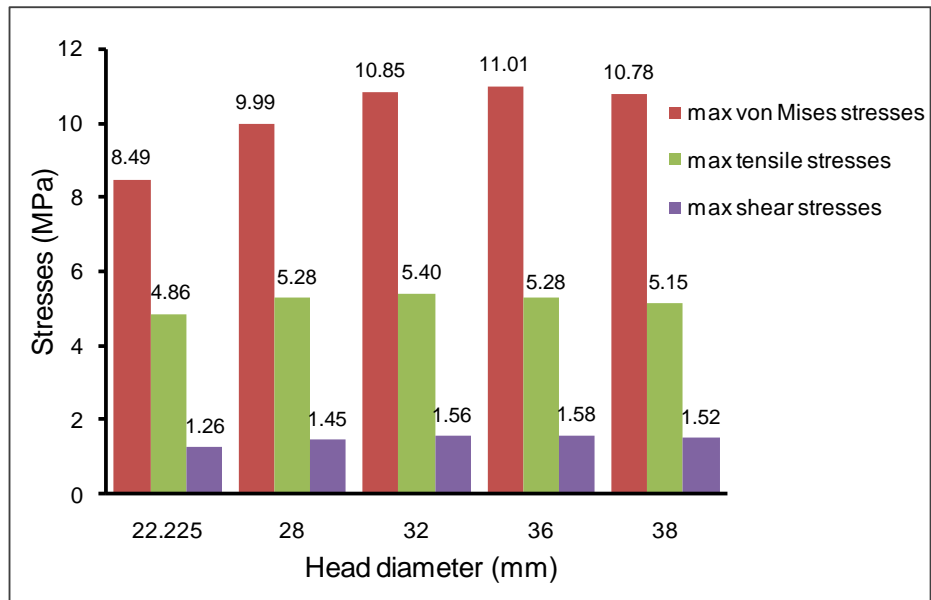
Figure 3.19 The predicted peak von Mises stress (MPa) and shear stress (MPa) at the bone-cement interface, and max principal stress (MPa) in the cement mantle with different head diameters.

3.4 Discussion

Results of this study showed that both the contact mechanics of the bearings and the mechanical behaviour in terms of von Mises stresses, shear stresses and max principal stresses for the cement mantle in the cemented MoP THR were influenced by the cup inclination angles, the wear in the acetabular cup and the sizes of both acetabular and femoral components. The validation of the model was conducted by comparing the present predictions with the previous FE predictions and experimental measurements (Jin et al., 1999) for the same design of components and under the same conditions. The slight difference between the present results and the previous results may be due to the fact that in the previous study, the FE model was an axisymmetric contact model without pelvic bone, while in the present study, a 3D FE model including the pelvic bone was considered. Indeed, a previous comparison study (Barreto et al., 2010) has proved that the contact pressures on the bearing surface and the wear generated in the acetabular cup for a MoP THR modelling without pelvic bone was predicted to be higher than that with pelvic bone. Therefore, the results presented in this chapter were considered to be fairly reasonable.

3.4.1 Effect of Wear and Cup Angles

Under all cup inclination angles, when penetration in the acetabular cup occurred, a large reduction in both the maximum von Mises stress in the acetabular cup and contact pressure on the bearing surface was observed. This is largely due to the increased conformity between the acetabular cup and femoral head as a result of wear. However, the difference was almost negligible between different penetration depths, and between different cup angles. This indicated that the soft-on-hard Charnley hip system is rather in-sensitive of wear on the polyethylene cup to both the wear rate and cup angles, as compared with the running-in wear of hard-on-hard articulations of MoM and CoC.

The outcomes of this FE study showed that the peak von Mises stress and max principal stress in the cement mantle and at the bone-cement interface occurred in the superior quadrant of the cement mantle, which was found to coincide with the location where the initial debonding of the cement mantle

was observed *in vitro* (Heaton-Adegbile et al., 2006; Wang et al., 2009). It is also interesting to note that the peak von Mises stress and shear stress within the cement mantle were observed at the prosthesis-cement interface. However, as failure in the acetabular implants was generally observed to initiate from the bone-cement interface(Tong et al., 2008), and the stress variation across the thickness of the cement mantle was found to be within 10%, the peak von Mises stresses and shear stresses at the bone-cement interface were examined in this study.

The FE results in this study also showed that a modest penetration depth (1 mm and 2 mm) in the acetabular cup actually resulted in a reduction in the predicted peak von Mises stress and max principal stress in the cement mantle. There are two competing factors in this process. The cement stresses depend on both the contact pressure on the articulating surfaces and how the contact stresses are transferred to the bone-cement interface. Although the increased penetration depths in the acetabular cup resulted in a potential increase in the cement stresses due to the reduction of the cup thickness, the improved conformity and the corresponding reduction in the contact pressure actually resulted in a reduction in the cement stresses. However, both the von Mises stresses at the bone-cement interface and max principal stress in the cement mantle increased with increased penetration depths. This was attributed to the reduced thickness of the cup due to the increased penetration depths and consequently, the stresses was getting closer to the bone-cement interface. A similar FE simulation study conducted by Coultrup et al. (2010) supported this observation that the increased cup penetration was associated with increased cement mantle stresses, resulting in a reduction of the cement mantle fatigue life of 9% to 11% for a high cup penetration depth. However, it is only limited to small penetration depths. When the penetration depth was increased to 4 mm, the effect of the cup thickness reduction became more dominant and consequently, the cement stresses were increased correspondingly. This is particularly evident, when combined with a steep cup inclination angle of 65º, that the peak von Mises stress was increased well above that of the un-worn cup.

For the conditions considered in the present study which represented the successful Charnley cups, neither the cup inclination angles nor the penetration depths affected the contact mechanics and the cement fixation markedly. These observations are consistent with the clinical observations reported in the literature (Wroblewski et al., 2009a; 2009c). However, beyond these conditions when the penetration or the inclination angle is increased further, a marked increase in the cement stresses would be predicted from the trend observed in Figure 3.7. These may cause rim crack and the rapid failure of the cement mantle. Furthermore, it should be pointed out that although the results in the present study reinforced the robustness of the Charnley THR, every effort should still be made to select the correct implant and to position the prosthesis correctly.

3.4.2 Effect of Acetabular Cup Sizes

Under all conditions considered, the differences in the von Mises stresses in the acetabular cup and contact pressures on the bearing surface between the hip prostheses with outer diameter of 40 mm and 43 mm were negligible. This can be explained from the consideration of the cup thickness and conformity. Due to the sufficient thickness of the acetabular cup, for the 40 mm prostheses, the cup thickness is approximately 8.7 mm, an increased diameter of 43 mm results in an increase in the cup thickness to around 10.2 mm. However, such an increase in the cup thickness is unlikely to cause large changes in the contact mechanics at the articulating surfaces (Bartel et al., 1985). Even though the severe penetration contributes to the decrease of the cup thickness, the improved conformity could compensate such a loss. Furthermore, it is expected from the present study that wear would not be influenced by the cup outer diameters, since neither the contact area, contact pressure nor the motion between the head and cup were altered markedly by the increased cup outer diameter.

The stresses in the cement mantle and at the bone-cement interface for the hip prosthesis with outer diameter of 40 mm were predicted to be higher compared to that with outer diameter of 43 mm for all cup inclination and penetration conditions. This observation was confirmed by the previous studies conducted by Lamvohee et al. (2007; 2009), who reported that both

the maximum tensile stress and shear stress in the cement mantle were decreased with an increased acetabular component sizes. This is presumably due to the fact that for a given penetration depth, a larger outer diameter of the acetabular cup implies an increase in the thickness of the acetabular component which helped to distribute the stresses better in the acetabular component itself rather than transferring the compressive loading to the cement mantle directly.

Clinical studies have shown that under similar conditions, a cup with outer diameter of 43 mm had smaller chance of aseptic loosening with increasing penetration depths compared to that of a 40 mm diameter cup. This was attributed to the lower friction torque with larger outer diameter of the acetabular cup (Wroblewski, et al., 2009a). However, the etiology of the aseptic loosening is multifactorial, and recent studies have particularly shown that high stress at the bone-cement interface would lead to premature failure of the fixation and the loosening of hip prosthesis (Kuehn et al., 2005; Coultrup et al., 2010). Whether other factors, such as the wear at the bearing surfaces or the mechanical behaviour at the bone-cement interface (Coultrup et al., 2010), will contribute to the difference of aseptic loosening observed clinically should be recognized. The present study showed that similar tribological characteristics in terms of contact pressures and contact areas were predicted on the bearing surfaces between the hip prostheses with outer diameter of 40 mm and 43 mm under all conditions considered. Therefore, it is supposed that wear is not the major contribution factor to the difference of aseptic loosening incidence between 40 mm and 43 mm diameter cup of Charnley THR observed clinically. However, it is interesting to note that the differences of the peak von Mises stress at the bone-cement interface and max principal stress in the cement mantle between the two cup designs were predicted to be between ~15-19% and ~15-22% respectively, and such differences were found to be similar to the clinical observations from Wroblewski et al. (2009a) who reported a difference of aseptic loosening incidence of ~20% between the acetabular components with outer diameter of 40 mm and 43 mm in favour of the cup with outer diameter of 43 mm clinically. Therefore, it is proposed that besides the friction torque, the difference of stress amplification in the cement mantle or at the bone-cement

interface between the two cup designs could also be responsible for the different incidence of aseptic loosening observed clinically.

3.4.3 Effect of Head Diameters and Cup Thicknesses

Previous studies have shown that the size of the femoral head and the thickness of the acetabular cup were key factors that influenced the biomechanics and long-term performance of THRs (Crowninshield et al., 2004; Lamvohee et al., 2009). This is due to the fact that the thickness of the acetabular component plays an important role in transferring the compressive forces acting on the pelvis (Lamvohee et al., 2007). The present study showed that an increase in the diameter of the femoral head, hence a decrease in the thickness of the polyethylene cup resulted in a decrease in both the maximum von Mises stress in the acetabular cup and the contact pressure on the bearing surface, yet led to an increase in the stresses in the cement mantle and at the bone-cement interface when the head diameters increased from 28 mm to 32 mm. This is due to the fact that the decrease of the thickness of the cup make the maximum stress closer to the bone-cement interface for head diameter of 28 mm compared to that of 32 mm. However, if the head diameter increased further to 38 mm, the von Mises stresses at the bone-cement interface and maximum principal stresses in the cement mantle decreased. This is because the decrease of the contact stress on the bearing surface is becoming dominant, making the stresses transferred to the interface decreased. These observations agree with the previous studies (Crowninshield et al., 2004; Lamvohee et al., 2007; Lamvohee et al., 2009). Crowninshield et al. (2004) investigated the biomechanics of THR with larger femoral heads and found that the stresses in the acetabular component were decreased with increased femoral head sizes. The FE study conducted by Lamvohee et al. (2009) showed that with increased sizes of femoral head, the max tensile stress in the cement mantle was increased, although there was a reduction in the stress experienced in the acetabular component. However, if the femoral head

Although the present study seemed to show that the larger femoral head was generally associated with better performance in terms of the contact stresses at the bearing surfaces, the increased sliding distance and contact

area contributed by the larger femoral head may result in increased wear of the UHMWPE cups (Kang et al., 2009). Indeed, a FE study to investigate the wear of the THR by Maxian et al. (1996b) demonstrated that an implant with 28 mm femoral head generated 25% more volumetric wear than that a 22 mm femoral head and an implant with 32 mm femoral head produced even more volumetric wear. Besides, the present FE results showed that the peak von Mises stress, shear stress and max principal stress in the cement mantle or at the bone-cement interface were predicted to increase with larger femoral head, which indicated that there is an increasing probability of fatigue failure of the cement mantle and mechanical loosening of the hip prostheses clinically as the head diameter was increased. From this point of view, it seems that a small head implant should be recommended for the patient. However, studies to investigate the biomechanics of the prosthesis with larger femoral head found that an increase in the femoral head size could result in an increase in prosthetic impingement-free ROM (Burroughs et al., 2005; Hammerberg et al., 2010) and decreased incidence of dislocation (Berry et al., 2005; Ng et al., 2011). Thus, it could be argued that a balance should be found when choosing a hip system relating to the femoral head sizes. However, as aseptic loosening has been the most commom cause of the failure of hip implant, the smaller femoral head should be considered preferentially clinically.

There are a number of limitations in the present study. Firstly, in the present simulation, the cup was assumed to be bonded to the bone cement using a tied contact formulation rather than modelling the macro-features on the cup external surface explicitly. Although this geometric simplification was reasonable in the computational simulation to study the contact mechanics at the bearing surfaces (Zant et al., 2007; Tong et al., 2008; Coultrup et al., 2010), it would inevitably affect the stress in the cement mantle. Besides, one of the most important concepts in the Charnley hip system is the low frictional torque. This was not simulated in the present FE modelling. A typical friction coefficient for a MoP combination is 0.08. Assuming a uniform shear stress at the bone-cement interface, the additional shear stress induced as a result of the frictional torque was estimated to be approximately 0.04 MPa. Therefore, considering the effect of friction is unlikely to affect the

major conclusions made from the present study. Additionally, as the model considered in the present study was a staic model rather than dynamic one, the effect of friction coefficient on the preditions is negligible.

The penetration of the acetabular cup was simulated towards the direction of the resultant load in the present study, which was 10⁰ medially. However, it is interesting to note that in retrieval studies, the direction of wear was generally observed to be lateral (Wroblewski et al., 1985). This may be due to the complex motion occurring during the different daily activities. The specific direction of the wear needs to be further studied. Furthermore, a simple worn geometry with a zero clearance to the head was considered, which may affect how the contact pressure distributes at the articulating surfaces and potentially the stress in the cement mantle. It has been shown in a retrieval study (Wroblewski et al., 1985) that there were clearly clearances between the worn area of the cup and the femoral head which were close to the clearance between the unworn area and the head. More adverse conditions such as large penetration and potential impingement and higher cup inclination angles as well as anteversion angles should also be simulated. Other cup designs, particularly a thicker polyethylene cup or different cement thicknesses should also be investigated to further understand the clinical observations (Wroblewski et al., 2007).

3.5 Summary

A general methodology combining contact mechanics between the articulating surfaces and fixation of the cement mantle was developed for a MoP hip system. The effect of wear depths, cup inclination angles, sizes of both the acetabular and femoral component on the contact mechanics of bearings and mechanical behaviour in the cement fixation for a MoP THR were analysed. The following conclusions can be drawn from this study:

1. Both the cup inclination angles and wear in the acetabular cup had a marked effect on the contact mechanics at the bearing surfaces and the stress states in the cement mantle. Typically, a combination of cup angle of 65⁰ and penetration depth of 4 mm generated a marked increase in the

contact pressures and cement stresses, compared with the cup angles of 45º and no penetration conditions.

2. Similar tribological characteristics were predicted at the bearing surfaces between the hip implants with outer diameter of 40 mm and 43 mm. However, the cement stresses for the hip implants with outer diameter of 40 mm were predicted to be higher than that of 43 mm, the difference was found to be consistent with the clinical observations of different aseptic loosening rate.

3. The increase of the femoral head diameters resulted in deceased contact pressures on the bearing surface and von Mises stress in the acetabular cup. However, the maximum stress in the cement mantle or at the bone-cement interface were increased with the increase of the head sizes.

Chapter 4
Surface Geometry and Contact Mechanics Analysis on
Retrieved Charnley THRs

4.1 Introduction

The contact mechanics and stability of the cemented THR in terms of the cement stresses were investigated using FE methods in **Chapter 3**. Particularly, the effect of wear depths in the acetabular cup was assessed. However, in the FE model, the geometrical characterization of the wear in the acetabular cup was simplified. The clearance between the femoral head and worn region of the cup was assumed as zero and the wear direction was assumed towards the direction of the resultant load. This would not be the normal case in retrieved components as clinical studies have shown that there was actually a gap between the femoral head and worn region of the cup, and the wear direction was normally observed to be lateral with respect to the cup position in the body. (Wroblewski et al., 1985; Hall et al., 1998). Therefore, the simplification of the worn surface geometry made in the FE model should be clarified with respect to retrieved components and the effect of these parameters needs to be examined. The aim of this chapter was therefore to develop a methodology to determine the geometric characteristics of worn components, i.e. the wear direction and the gap between the femoral head and worn region of the cup, for retrieved Charnley THRs using surface fitting technique, and to investigate how these factors affect the contact mechanics and mechanical behaviour of the cement fixation for cemented THR using FE methods.

4.2 Materials and Methods

4.2.1 Surface Geometry Prediction

The surface geometry prediction was conducted to determine the geometric characteristic of the worn surface of the cup with respect to the wear

direction and radial clearance between the femoral head and worn region of the cup from two retrieved Charnley sockets using surface fitting technique.

Data collection

Two retrieved Charnley acetabular cups, one had severe wear (severely worn cup) and another had mild wear (mildly worn cup), were considered in the present study. A coordinate measuring machine (CMM, Legex 322, Mitutoyo, UK) was used to scan the cups in the form of traces starting at the pole and ending at the rim. The CMM machine had a resolution of 0.8 µm. However, this value increased depending on the probe/stylus combination and measurement parameters.

A single straight stylus configuration with stylus diameter of 2 mm was used to measure the retrieved cups. Al-Hajjar (2012) compared the accuracy of different styli configurations by using an unworn ceramic femoral head and showed a form error in the range of ±2 µm for this stylus configuration. The definition of accuracy in ISO 10360-4:2000 (Geometrical product specification (GPS)-Acceptance and re-verification tests for coordinate measuring machines (CMMs)-part 4: CMMs used in scanning measuring mode) was accepted in the present study to evaluate the measurement accuracy. For the present set-up, the accuracy stated by Mitutoyo is $(0.8+2L/1000)$ µm, where L is the measurement length in mm (Lord et al., 2011). The largest value of L for 22.225 mm diameter cup was 17.45 mm, which corresponded to a measurement accuracy of 0.804 µm in the present study.

At the beginning of scanning, the retrieved cup was placed on the slate bed of the machine with its rim plane parallel to the machine's XY plane. It was critical to create an individual co-ordinate system on the component before the measurement. For the purpose of this, a reference plane was first identified from the measurement of the rim of the cup and aligned as the XY plane of the co-ordinate system. The origin of the coordinate system was determined by taking 25 points over the unworn part of the component's surface. Alignment of the X-axis was achieved by measuring a line through the introducer holes in the cup.

Once the co-ordinate system was developed, the acetabular cup was scanned by taking 2, 304 points in the form of 36 traces rotated by 10 degrees from each other about the Z-axis passing through the origin of the defined coordinate system. Each trace consisted of 64 points with a pitch of 0.5 mm starting at the pole and finishing at the rim of the cup. The last three points of each trace lay on the chamfer of the rim (Figure 4.1). All the points were recorded as X, Y and Z co-ordinates relative to the defined origin.
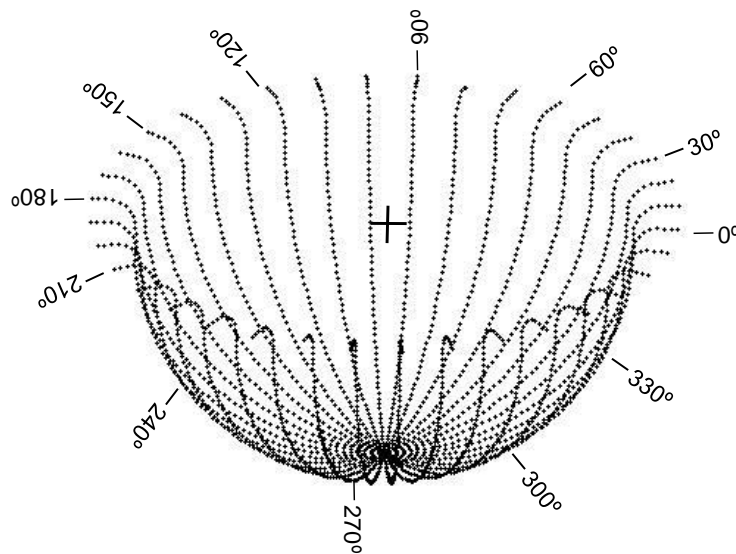
Figure 4.1 Data points taken on the surface of the Charnley cups using CMM by taking traces about the vertical axis.

Surface geometry prediction

Co-ordinate data collected from the CMM was read in to a MATLAB program to predict the surface geometry. The flowchart for the entire prediction process is shown in Figure 4.2. The program code is present in Appendix A.
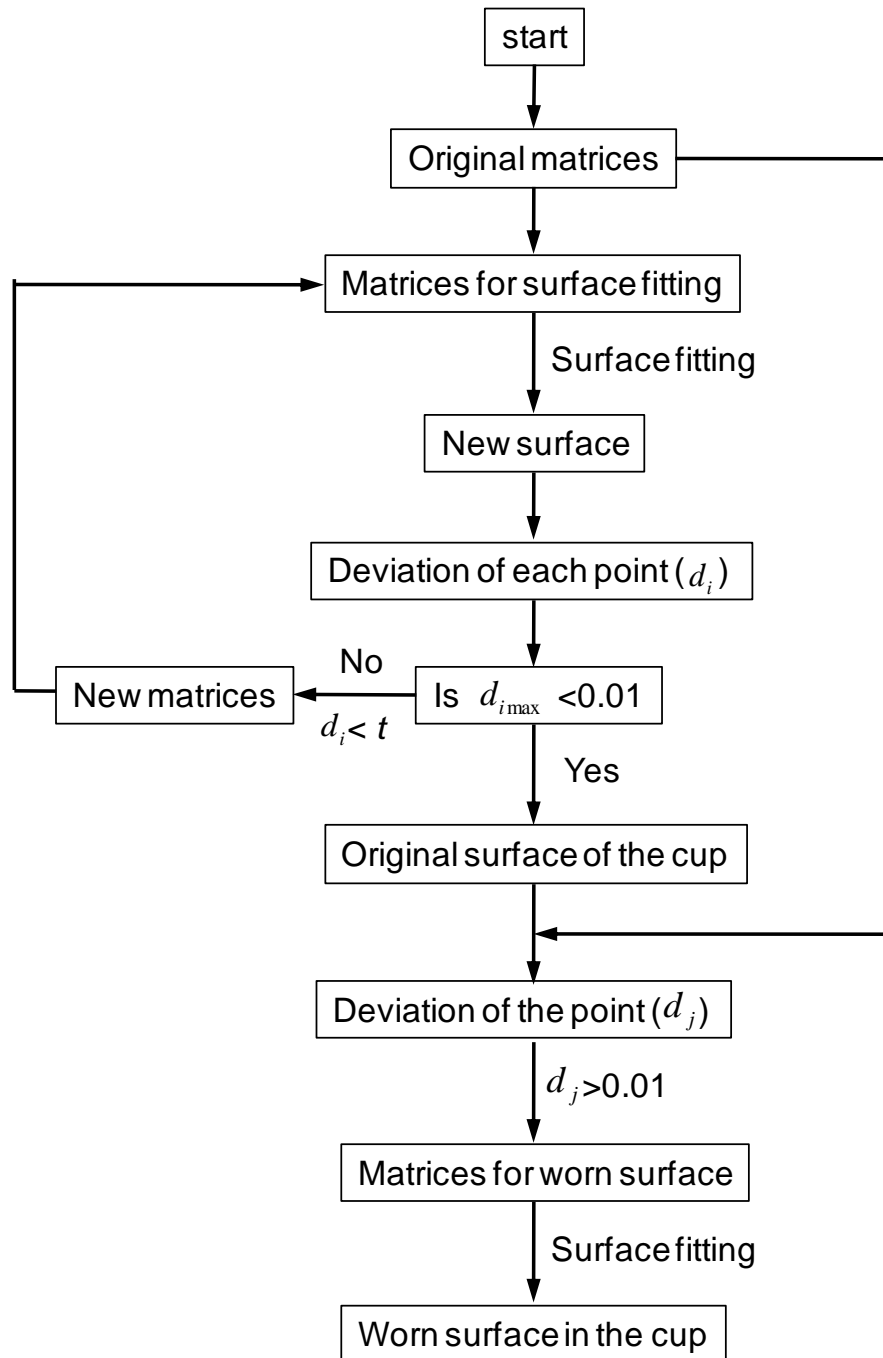
Figure 4.2 Flowchart for entire surface fitting process (*t* was the threshold value which was decreased for each iteration).

The data was split into 36 traces and each trace was split into three matrices (original matrices) which represented the Cartesian co-ordinates at each measured point. To determine the original surface of the cup, the traces that included the matrices representing the unworn region of the surface were selected. To do this, all the traces were imported in a co-ordinate system. The traces that coincided with each other were assumed to represent

unworn surface and the matrices of these traces were selected for the first surface fitting (Figure 4.3).

(a)

(b)
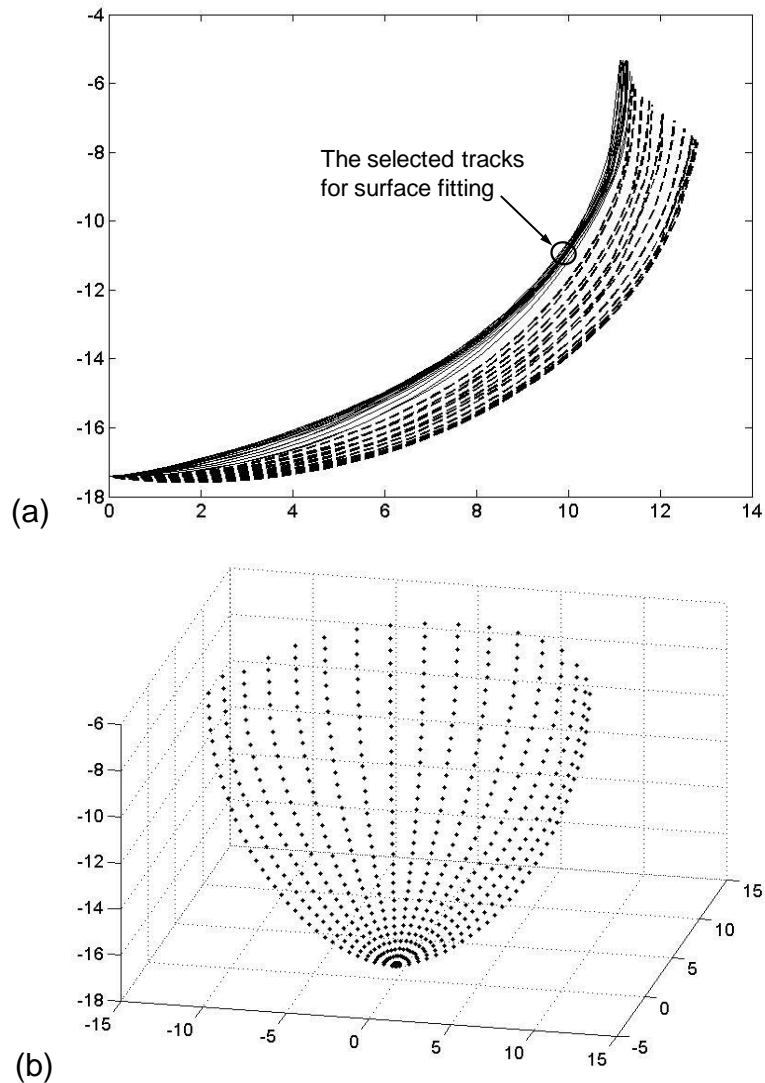
Figure 4.3 (a) The tracks of the collected data in a 2D co-ordinate system. The tracks that represented the unworn surface coincided with each other in the co-ordinate system; (b) the points selected for surface fitting.

Surface fitting was conducted based on the selected matrices. A new spherical surface was then reconstructed. The deviation of each point in the selected matrices (the error between the radius of the new spherical surface and the distance from the point to the centre of the new spherical surface) was calculated. If the maximum deviation of the points was larger than manufacturing tolerance of 10 µm, a threshold value was set based on the maximum deviation of the points. Any point for which the calculated

deviation was greater than the threshold value was discarded. The remaining points were retained to form new matrices and used in the fitting of the second sphere. The process was repeated until the maximum deviation of the points was smaller than 10 μm, and the sphere fitted at this stage was assumed as the original surface of the cup.

Once the original surface of the cup was determined, the deviation of each point in the original matrices to the original surface was calculated. All the points for which the calculated deviation greater than 10 μm were picked out. These points were then used in the calculation of a new spherical surface which was considered as the worn surface of the cup. The clearance between the femoral head and the worn surface of the cup was then determined. The maximum deviation was assumed as the maximum penetration depth and the wear direction was calculated based on the maximum deviation.

The wear direction was defined using the angle between the rim plane of the cup and vector from centre of the cup to the maximum deviation point, as shown in Figure 4.4.
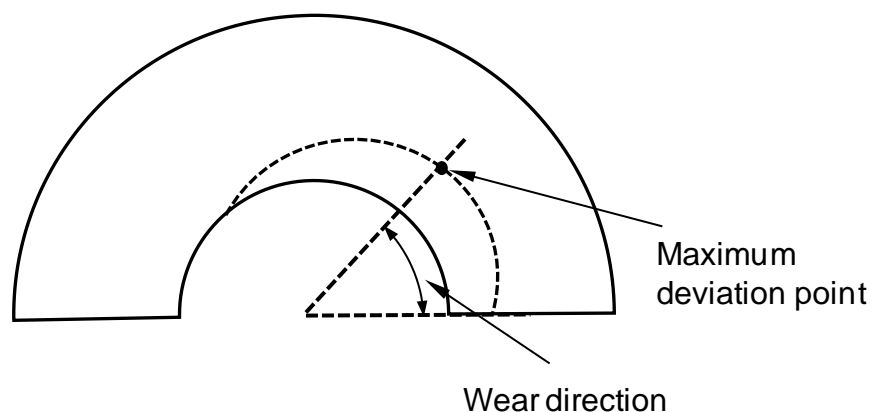
Figure 4.4 The definition of the wear direction in the surface fitting progress.

4.2.2 FE Modelling

The FE modelling was developed to conduct a parametric study for assessing the effect of wear direction and radial clearance between the femoral head and the worn region of the cup (C_w) on the contact mechanics

of the bearing and mechanical behaviour of the cement mantle for cemented THR.

The anatomic Charnley THR model used in **Chapter 3** was used once more in this Chapter. The FE modelling, mechanical properties of the components and the boundary conditions for the model were detailed in **Chapter 2**.

The geometries and structures of the components for the Charnley THR were described in **Chapter 2**. The nominal diameters of the femoral head and original surface of the cup were 22.225 mm and 22.59 mm respectively, giving a radial clearance of 0.1825 mm between the femoral head and original surface of the cup (C_0). The outer diameter of the acetabular cup was considered as 40 mm. The cup inclination angle was considered as 45⁰.

The wear depth in the acetabular cup was modelled as 2 mm. The method to simulate the wear in the acerabular cup was illustrated in **Chapter 3**. The parametric study was conducted separately. Firstly, keeping the radial clearance between the femoral head and worn region of the cup (C_w) as 0 mm invariably, different wear directions of -10⁰, 0⁰, 15⁰ and 30⁰ were modelled. The wear direction was defined as the angle between the superior axis and the vector from centre of the cup to the maximum deviation point, as shown in Figure 4.5. The negative value of the angle represented the medial direction while the positive value of the angle mean the lateral direction. The angle of 0⁰ represented vertical wear direction. Afterward, keeping the wear direction constant at -10⁰, different radial clearances of 0 mm, 0.1825 mm and 0.27 mm between the femoral head and worn region of the cup (C_w) were modelled. These radial clearances were considered correspond to 0, 1 and 1.5 times as the radial clearance between the femoral head and the original surface of the cup (C_0) respectively.
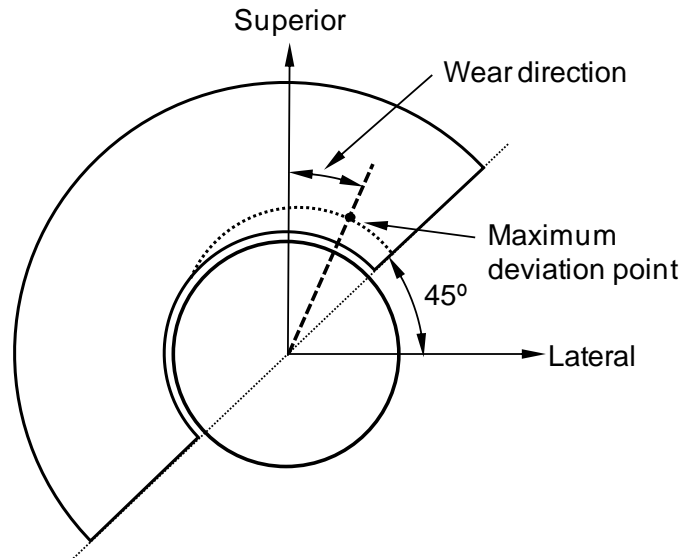
Figure 4.5 The definition of the wear direction in the FE modelling. Negative
value represented the medial direction while the positive value
represented the lateral direction.

4.3 Results

4.3.1 Wear and Surface Geometry Prediction for Retrieved Charnley THRs

Figure 4.6 shows the wear maps at the bearing surface in the acetabular
cups in terms of linear penetration for the two retrieved cups. The
characteristics of the surface geometry for the worn surfaces for the
retrieved cups is summarized in Table 4.1.

The severely worn cup had a linear penetration of approximately 1.85 mm
while the mildly worn cup had a linear penetration of about 0.23 mm. The
maximum penetration for the severely worn cup was offset at an angle of
approximately 32.5º from the rim plane while for the mildly worn cup, the
maximum penetration was predicted at the rim of the cup.

The radial clearance between the head and worn region of the cup (C_w) was
predicted as 0.15 mm for the severely worn cup, which was slightly smaller
than the radial clearance between the head and original surface of the cup
(C_0). For the mildly worn cup, the radial clearance C_w was predicted to be
0.23 mm, which was slightly bigger than the radial clearance C_0.
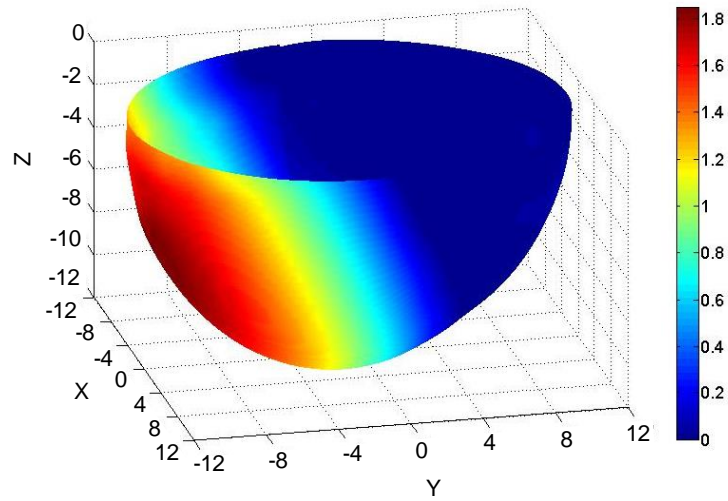
(a)
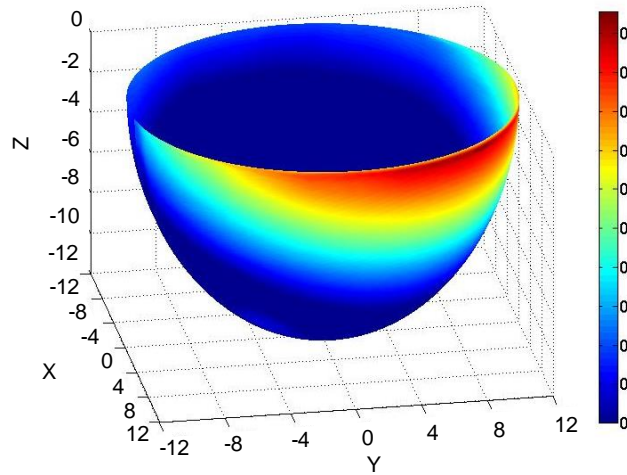
(b)

Figure 4.6 Wear maps of bearing surfaces in acetabular cups: (a) the severely worn cup, (b) the mildly worn cup. Dark blue represents the unworn surface, dark red represents the deepest wear areas, the vertical colour scales show wear depth in mm.

Table 4.1 The predicted wear and surface geometry of the retrieved Charnley cups. C_0 was the radial clearance between the femoral head and original surface of the cup, C_w was the radial clearance between the femoral head and the worn region of the cup.

Components	Radius of the original sphere (mm)	Maximum penetration (mm)	Wear angle (º)	Radial clearance C_0 (mm)	Radial clearance C_w (mm)
Severely worn cup	11.19	1.85	32.5	0.19	0.15
Mildly worn cup	11.21	0.23	3.9	0.21	0.23

4.3.2 Contact Mechanics and Cement Stresses Analysis

Effect of wear direction

With the penetration depth of 2 mm in the acetabular cup, the maximum contact pressure on the bearing surface was increased by approximately 1.2% when the wear directions changed from 10^0 medially to 15^0 laterally, and about 11.3% when the wear directions changed from 10^0 medially to 30^0 laterally (Figure 4.7 and 4.8). However, the change of wear directions from 10^0 medially to 30^0 laterally had negligible effect on the maximum von Mises stresses in the acetabular cup (Figure 4.8).

(a)   (b)
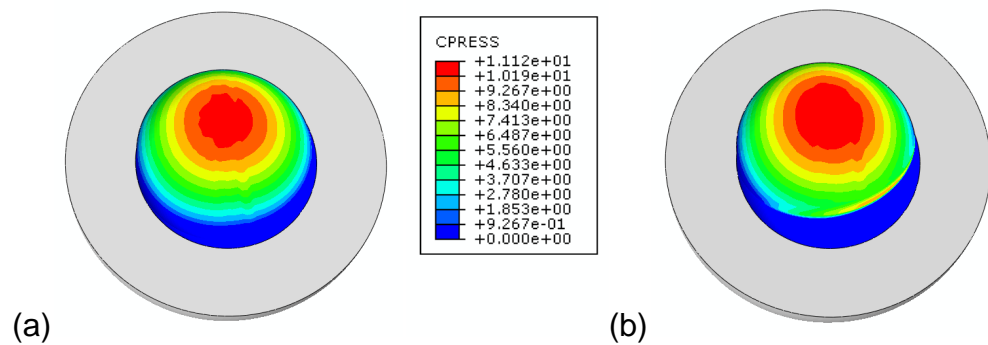
Figure 4.7 The predicted contact pressure (MPa) distributions on the bearing surface with penetration depth of 2 mm in the cup with wear direction of (a) 10^0 medially and (b) 15^0 laterally (Clearance C_w: 0 mm, cup inclination angle: 45^0).
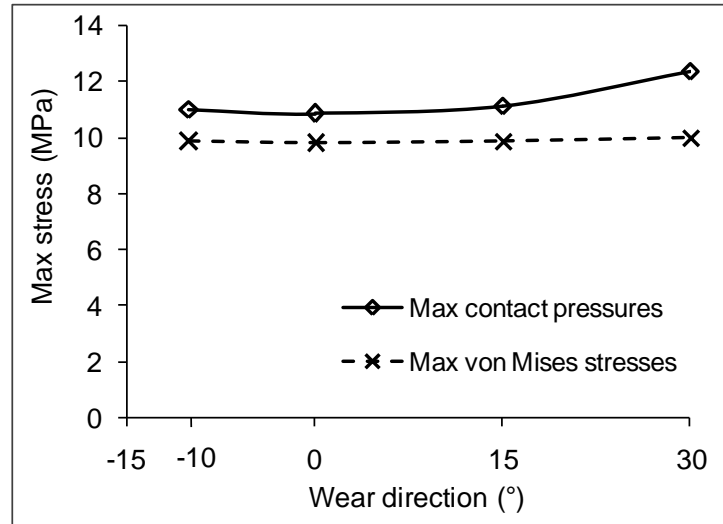
Figure 4.8 The predicted maximum contact pressure (MPa) on the bearing surface and maximum von Mises stress (MPa) in the acetabular cup with different wear directions. Negative value represented the medial wear direction, 0⁰ represented vertical direction and positive value represented the lateral wear direction, as shown in Figure 4.5. The penetration depth of the cup was 2 mm (Clearance C_w: 0 mm, cup inclination angle: 45⁰).

With the penetration depth of 2 mm in the acetabular cup, the change of wear directions from 10⁰ medially to 30⁰ laterally had negligible effect on the maximum von Mises stress at the bone-cement interface (Figure 4.9 and 4.11). However, it led to a slight increase of peak max principal stress in the cement mantle of about 4.0% (Figure 4.10 and 4.11) and moderate increase of maximum shear stress at the bone-cement interface of about 23.4% (Figure 4.11).

(a)   (b)
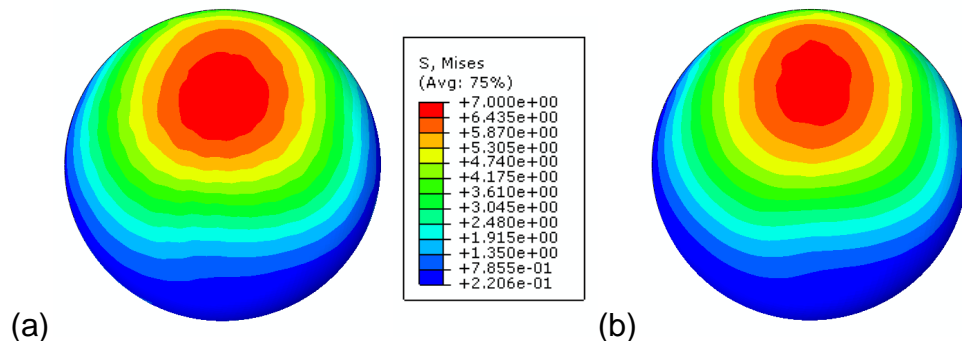
Figure 4.9 The predicted von Mises stresses (MPa) in the cement mantle at the bone-cement interface with wear depth of 2 mm in the cup with wear direction of (a) 10⁰ medially and (b) 15⁰ laterally (Clearance C_w: 0 mm, cup inclination angle: 45⁰).

(a)   (b)
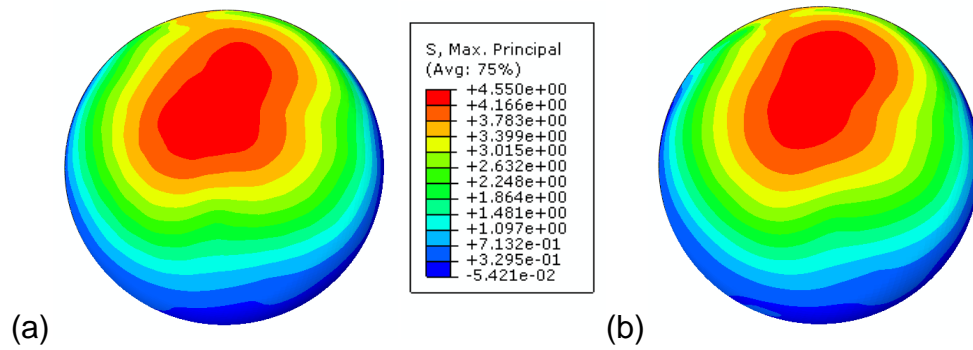
Figure 4.10 The predicted max principal stresses (MPa) in the cement
mantle with wear depth of 2 mm in the cup with wear direction of (a) 10⁰
medially and (b) 15⁰ laterally (Clearance C_w: 0 mm, cup inclination
angle: 45⁰).
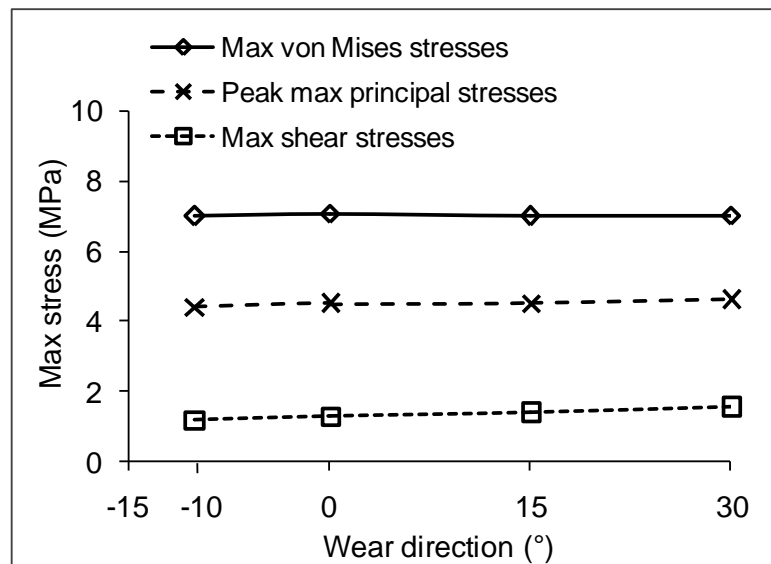
Figure 4.11 The predicted peak von Mises stress (MPa) and shear stress
(MPa) at the bone-cement interface, and max principal stress (MPa) in
the cement mantle with different wear directions. Negative value
represented the medial wear direction, 0⁰ represented vertical direction
and positive value represented the lateral wear direction, as shown in
Figure 4.5. The penetration depth of the cup was 2 mm (Clearance C_w:
0 mm, cup inclination angle: 45⁰).

Effect of radial clearance C_w

The increase of radial clearance C_w between the femoral head and worn
region of the cup from 0 mm to 0.27 mm resulted in a moderate increase of
maximum von Mises stress in the acetabular cup of approximately 15.3%
and markedly increase of maximum contact pressure on the bearing surface
of about 70.2% (Figure 4.12 and 4.13).

(a)   (b)
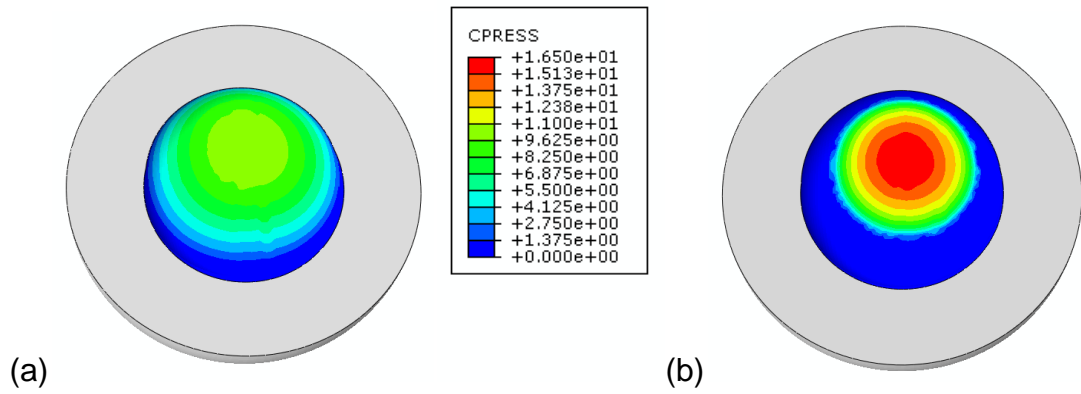
Figure 4.12 The predicted contact pressure (MPa) distributions on the
bearing surface with radial clearance C_w of (a) 0 mm and (b) 0.1825
mm between the femoral head and worn surface of the cup under cup
inclination of 45⁰. The penetration depth of the cup was 2 mm with wear
direction of 10⁰ medially.
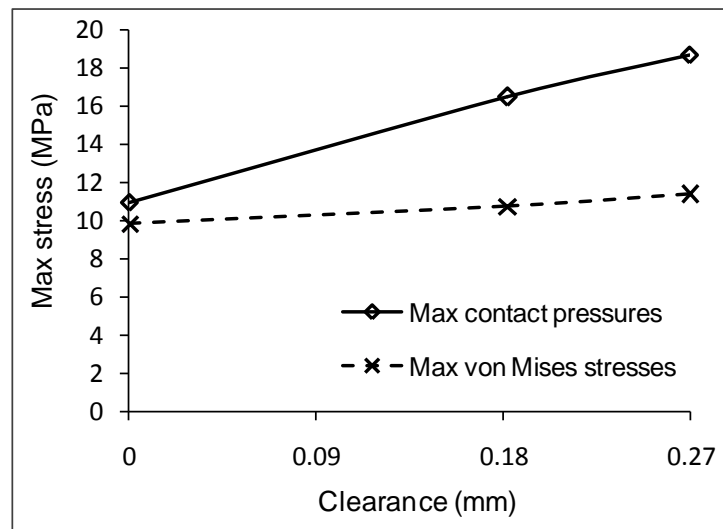
Figure 4.13 The predicted maximum contact pressure (MPa) on the bearing
surface and maximum von Mises stress (MPa) in the acetabular cup
with different radial clearances C_w under cup inclination of 45⁰. The
penetration depth of the cup was 2 mm with wear direction of 10⁰
medially. C_w was the radial clearance between the femoral head and
worn region of the cup.

With the penetration depth of 2 mm in the acetabular cup, and the radial
clearance C_w between the femoral head and the worn region of the cup
increased from 0 mm to 0.27 mm, the peak von Mises stress at the bone-
cement interface and peak max principal stresses in the cement mantle
increased markedly by approximately 68% (from 6.9 MPa to 11.6 MPa) and
40% (from 4.2 MPa to 5.9 MPa) respectively (Figure 4.14, 4.15, and 4.16).

The maximum shear stress at the bone-cement interface increased mildly by about 20.9% (Figure 4.16).
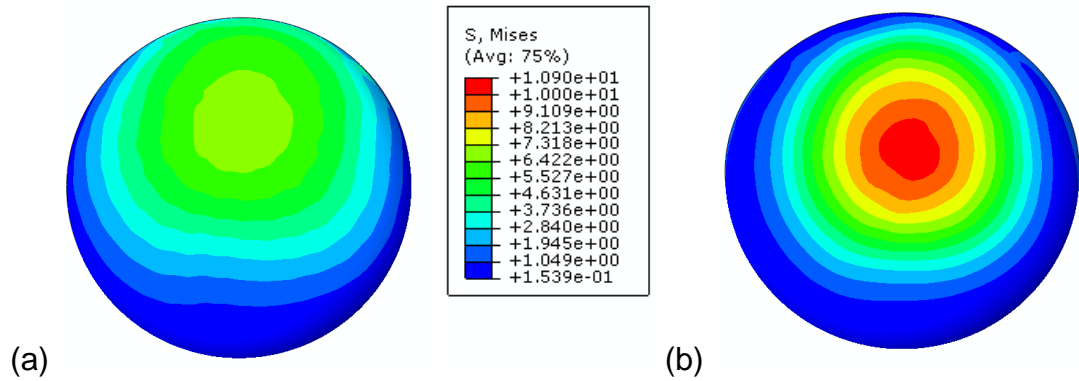
Figure 4.14 The predicted von Mises stresses (MPa) at the bone-cement interface with radial clearance C_w of (a) 0 mm and (b) 0.1825 mm between the femoral head and worn region of the cup under cup inclination of 45⁰. The penetration depth of the cup was 2 mm with wear direction of 10⁰ medially.
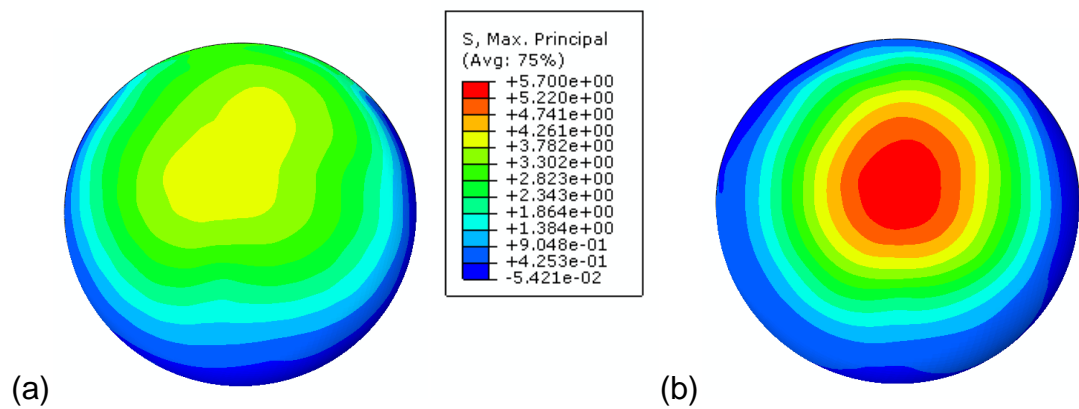
Figure 4.15 The predicted max principal stresses (MPa) in the cement mantle with radial clearance C_w of (a) 0 mm and (b) 0.1825 mm between the femoral head and worn surface of the cup under cup inclination of 45⁰. The penetration depth of the cup was 2 mm with wear direction of 10⁰ medially.
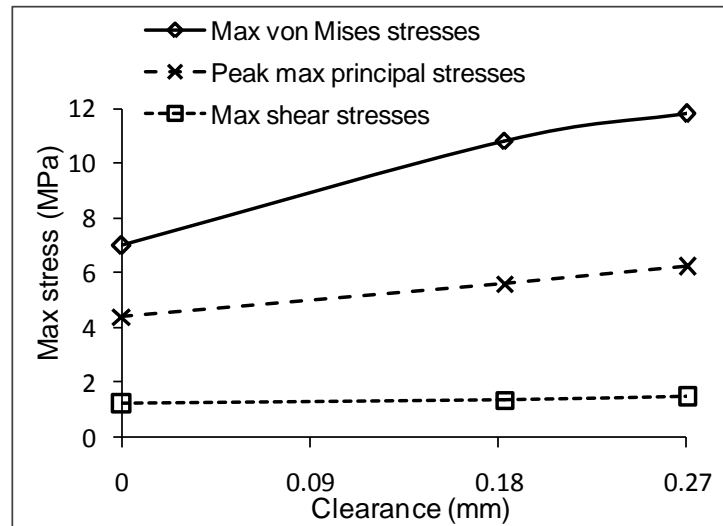
Figure 4.16 The predicted peak von Mises stress (MPa) and shear stress (MPa) at the bone-cement interface, and max principal stress (MPa) in the cement mantle with different radial clearances C_w under cup inclination of 45⁰. The penetration depth of the cup was 2 mm with wear direction of 10⁰ medially. C_w was the radial clearance between the femoral head and worn surface of the cup.

4.4 Discussion

To model the real-life wear of the components in the FE model is a challenge as it is difficult to obtain enough geometric information for the worn components for THRs. In our previous studies (**Chapter 3**) and other previous study (Coultrup et al., 2010), the wear of the component in the FE model was simplified, as discussed in **Chapter 3**. However, this geometric simplification of the worn component should be clarified, and the effect of the simplification should be evaluated. This chapter, therefore, presented a novel approach to assess the wear and surface geometries of two worn cups from retrieved Charnley THRs. With the aid of the method, the geometric information of the worn cup, in terms of wear depth, wear direction and the clearance C_w between the femoral head and worn region of the cup, was obtained. The effect of the worn surface geometries on the contact mechanics and cement fixation for a cemented THR was then evaluated.

A maximum penetration depth of 1.85 mm with wear direction of approximately 33⁰ from the rim plane was predicted for the severely worn cup. It should be noted that the definition of wear direction in the surface

geometry prediction was different from that in the FE model (as seen in Figure 4.3 and 4.5) and the initial orientation of the retrieved cup in the human body was not known when the explants were analysed. Considering a cup inclination angle of 45⁰, the wear direction of 33⁰ in the surface geometry prediction corresponded to a wear direction of 12⁰ laterally in the FE model. This was found to be in keeping with the observations of wear directions from retrieved Charnley sockets conducted by Hall et al. (1998). A maximum penetration depth of 0.23 mm was predicted for the mildly worn cup at the very rim of the cup. This rarely happens. However, two cases were reported by Wroblewski (1985) where extreme wear was found at the very rim of the socket when 22 Charnley sockets were considered. This occurred probably due to the steep inclination of the cup or microseparation taking place on the bearing.

It is interesting to notice that the maximum penetration in the mildly worn cup was much closer to the rim compared to the severely worn cup, and the radial clearance C_w between the femoral head and worn region of the cup was predicted to be higher for mildly worn cup than that for the severely worn cup. This showed a potential relationship between the penetration depths and wear directions, as proposed by Hall et al. (1998), as well as a relationship between the penetration depths and radial clearances C_w between the femoral head and worn region of the cup. However, more data should be analysed before any conclusions are drawn. Nevertheless, the radial clearance C_w between the femoral head and worn region of the cup was predicted to be close to the gap C_0 between the femoral head and original surface of the cup for both retrieved components.

The contact mechanics analysis showed that the wear directions did not affect the contact mechanics of the THR. However, if the wear direction was too lateral, i.e. over 30⁰ laterally, the contact stress would be increased. This is probably due to the fact that with a too lateral wear direction, the contact pitch moved to the transition zone between the worn region and unworn region in the cup thus the contact areas decreased, leading to an increase in the contact stress. However, it should be pointed out that the load direction considered in this study was 10⁰ medially, and the findings may not be the same when different load directions are considered.

The effect of the wear directions on the von Mises stresses at the bone-cement interface and the max principal stresses in the cement mantle was negligible. However, the change of the wear direction from medial to lateral resulted in a marked increase of the shear stresses at the bone-cement interface. Again, this may not be true if load with different directions was considered.

Compared to the wear direction, the radial clearance C_w between the femoral head and worn region of the cup had marked effect on the contact mechanics of the THR, as well as the von Mises stresses at the bone-cement interface and max principal stresses in the cement mantle. This was reasonable as the radial clearance is a key factor that affects the biomechanics of the THR (Jin et al., 1994; Chen et al., 2012). However, the change of the radial clearance between the femoral head and worn region of the cup had negligible effect on the shear stresses at the bone-cement interface.

The method presented in this Chapter was used to assess the linear penetration depth for the retrieved cup. However, it can be further developed to assess the volumetric wear of the retrieved components. The advantages of this method over the gravimetric analysis method are that it could provide a 3D construction of the component showing the area, depth and location of the wear patch on the components, and more importantly, it could be used reliably to determine the linear and volumetric wear in components where there is no pre-wear or 'zero-cycle' data.

4.5 Summary

A novel approach that can be used to assess the wear of the THR and characterise the surface geometry of the worn component was developed in this Chapter. Two retrieved Charnley acetabular components were analysed to get the geometric information of the worn cup. The effect of the surface geometry of worn cup in terms of wear direction and radial clearance between the femoral head and worn region of the worn cup was then evaluated. The following conclusions can be drawn from this study:

1. The wear directions for the two retrieved cups were predicted to be lateral, rather than medial with respect to the wear direction defined in the FE modelling. The radial clearances C_w between the femoral head and worn region of the cup for the two retrieved components were close to the radial clearances C_0 between the femoral head and original surface of the cup.

2. The wear direction had negligible effect on the contact mechanics of the bearings, the von Mises stresses and the max principal stresses for the cement mantle. However, if the wear direction was too lateral (i.e., over 30^0 laterally), the contact stresses on the bearing surface would increase markedly.

3. The radial clearance C_w between the femoral head and worn region of the cup had marked effect on the contact mechanics of the bearings, the von Mises stresses and the max principal stresses for the cement mantle. However, it had negligible effect on the shear stresses at the bone-cement interface.

Chapter 5
Experimental Study and Contact Mechanics Analysis of Pinnacle THR

5.1 Introduction

As discussed in **Section 1.4.1**, FE models, as an alternative to the experiment, are becoming increasingly useful tools to conduct parametric analysis, design optimization and pre-clinical testing for hip joint replacements (Huiskes and Chao, 1983; Saha and Roychowdhury, 2009; Laz and Browne, 2010). However, the level of confidence in the FE model depends upon how the FE predictions agree with the experimental or clinical observations (Okrajni et al., 2007; Lerch et al., 2012). Therefore, the experimental validation for the FE model is very important.

In this Chapter, an attempt was made to validate the methodology used in the 3D anatomic Pinnacle THR model by comparing the contact areas on the articulating surface between the experimental measurements and FE predictions from an experimentally-matched model. The experimentally-matched model used the same methodology as that used in the anatomic Pinnacle THR model. The methodology was further supported by conducting a parametric analysis to investigate the influence of friction coefficients at the shell/liner interface using the experimentally-matched model. The anatomic Pinnacle THR model with validated methodology will then be used to investigate more complications in the hip prostheses such as edge loading and microseparation in **Chapter 6 and Chapter 7**.

5.2 Materials and Methods

The validation of the methodology was undertaken in three steps: (1) the contact areas on the articulating surfaces for Pinnacle bearings were measured for a variety of different radial clearances and loadings; (2) the contact areas on the articulating surfaces were predicted from an experimentally-matched model which used the same methodology as the 3D anatomic Pinnacle THR model and had the same constructions with

experiemental set-up, (3) the contact areas were compared between the experimental measurements and the FE predictions from the experimentally-matched model.

5.2.1 Experimental Measurement

Hip joint simulator

The Leeds Prosim hip joint simulator (Prosim Limited, Manchester, UK) was used in the experimental measurement. The simulator consists of ten stations that can generate multi-direction motion between the femoral head and the acetabular cup (Goldsmith and Dowson, 1999). It has three axes, a single vertical load axis and two independently controlled axes of motion, extension/ flexion (-15°/+30°) and internal/external rotation (+/-10°) (Figure 5.1). The load is applied vertically through the centre of the femoral head. Under standard gait conditions, the machine is running at a frequency of 1 Hz with a twin peak loading cycle with a peak load of 3 KN and swing phase load of 0.3 KN, as recommended by ISO 14242-1 (2002). The loading and motion profiles are shown in Figure 5.2.

Rotation about the centre of the femoral head-X Axis
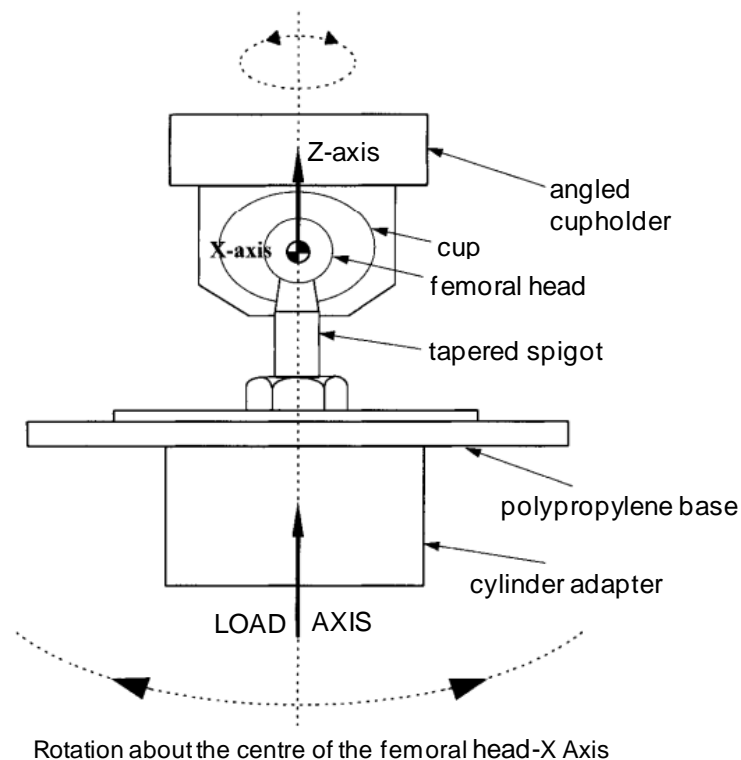
Figure 5.1 Schematic diagram of load axis and rotational axes of a test station of the hip joint simulator from the front view (Goldsmith and Dowson, 1999).
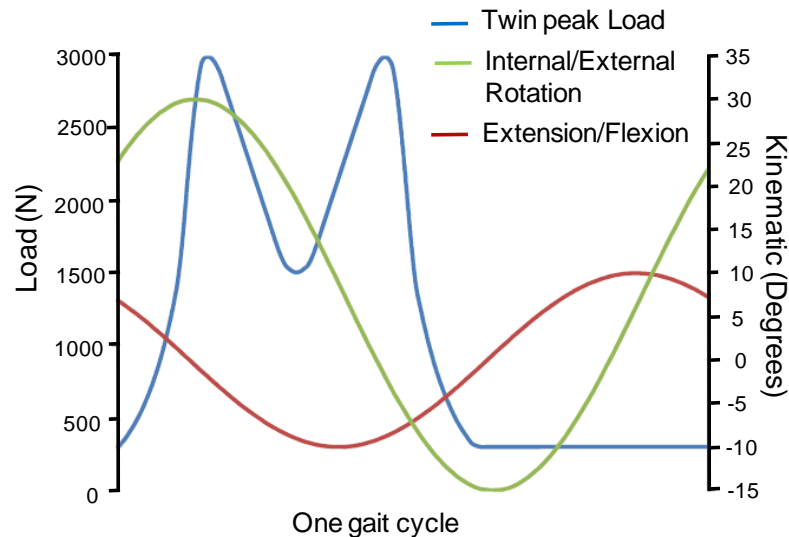
Figure 5.2 Loading and motion profiles on the Leeds ProSim hip simulator. One gait cycle takes one second.

Specimens

Three specimens of Pinnacle polyethylene liner (DePuy Orthopaedics, Inc.) in conjunction with 36 mm CoCr femoral heads were considered in this Chapter, as shown in Figure 5.3. The specimens were processed using three different approaches before test. The first specimen was soaked in deionised water for approximately 16 weeks to allow moisture uptake to stabilize prior to the test, it was then soaked in 25% serum with 0.03% sodium azide during the test. This specimen was termed as "soak control liner". The second specimen was loaded using the Leeds Prosim hip joint simulator (Prosim Limited, Manchester, UK) by the twin peak load (Figure 5.2) for 4.8 million cycles at frequency of 1 Hz without any articulations on the bearing surface, this specimen was termed as "load control liner"; The third specimen was loaded and wear-tested in Leeds Prosim hip joint simulator (Prosim Limited, Manchester, UK) under standard gait cycle conditions for 4.8 million cycles. The input of loading and motion is shown in Figure 5.2. This specimen was termed as "worn liner". These processed liners were used in order to represent three types of Pinnacle liners with three different clearances.

A coordinate measuring machine (CMM, Legex 322, Mitutoyo, UK) which was describe in **Chapter 4** was used to obtain the clearances of the contact

surfaces between these polyethylene liners and the femoral head. Before the test, the crept area of the load control liner and the worn region of the worn liner were identified. Thirty-two data points were taken in these regions and in the inner surface of the soak control liner. The diameters of the inner surface of soak control liner, crept region of the load control liner and the worn region of the worn liner were then measured based on these data points and are summarised in Table 5.1.
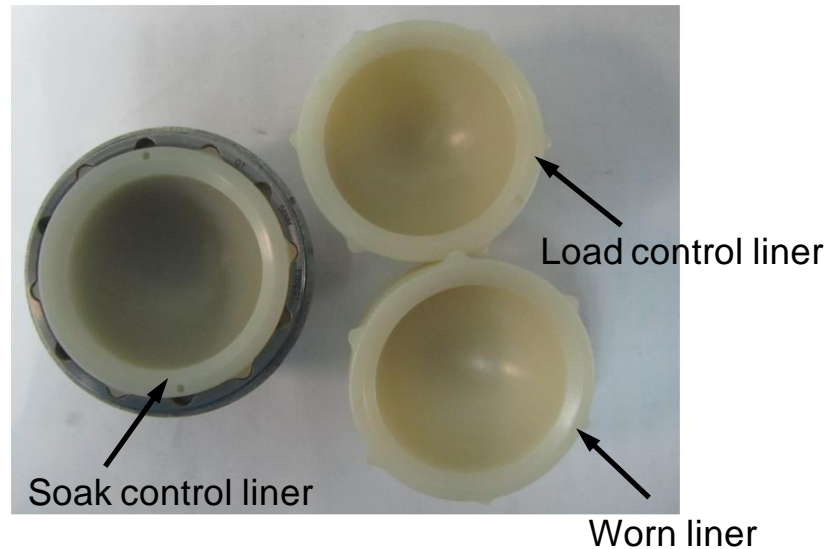
Figure 5.3 The Pinnacle liner specimens used in the experimental measurement.

Table 5.1 The sizes of the three polyethylene liner specimens measured using CMM.

Pinnacle liner specimens	Diameter of inner surfaces (mm)	Raidal clearances (mm)
Soak control	36.932	0.932
Load control	36.727	0.727
Worn	36.514	0.514

Experimental set up and measurement

A station of the Leeds Prosim hip joint simulator (Prosim Limited, Manchester, UK) was used to undertake experimental measurement. The

polyethylene liner specimen was taper locked to the metal shell, which was mounted to the stainless steel cup holder using PMMA resin. The cup holder was fixed to the station of the hip simulator to ensure that the centre of the cup was at the centre of rotation of the simulator. The metal shell was securely mounted in the cup holder with a hole drilled from the back and blocked with a grub screw for the liner specimen to be pushed out when needed for measurement. During mounting up, the cup was positioned at the desired inclination angle to the horizontal plane using a bespoke fixturing jig.

The CoCr femoral head of 36 mm diameter was screwed into the stainless steel head holder which was attached in the machine, making sure the centre of the femoral head was positioned on the centre of rotation of the machine through which the load was applied. By doing this, the concentricity between the femoral head and polyethylene liner was maintained. The whole experimental set-up is shown in Figure 5.4.
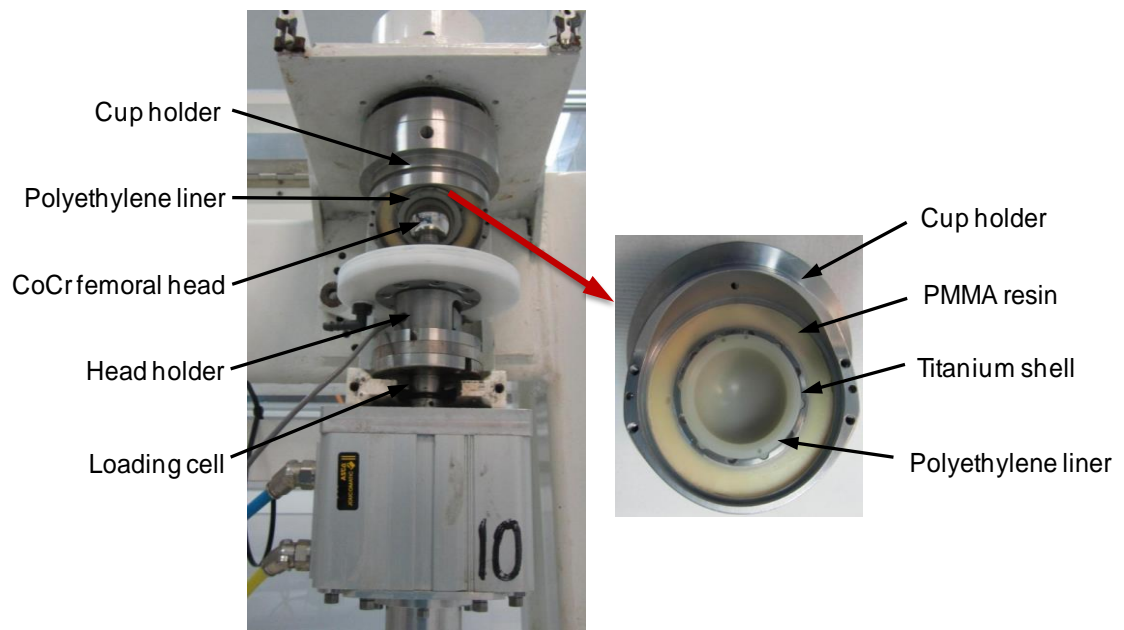
Figure 5.4 The experimental set up for the tests and cup holder for the acetabular components.

A pigmented paste (MicroSet, Warwickshire, UK) was used to mark the contact areas on the articulating surfaces between the femoral head and liner when the system was loaded. Before loading, the femoral head was coated with a uniform thin layer of MicroSet and articulated with the liner with

a uniform clearance. The whole system was first loaded with a small compressive force to make sure the femoral head contacted with the liner without dynamic impact. It was then loaded with a series of vertical compressive forces stock-still for 2 minutes to allow for the contact pattern in the liner to stabilize. The load was then moved immediately. The MicroSet was shifted from the femoral head to polyethylene liner during this process, as shown in Figure 5.5.
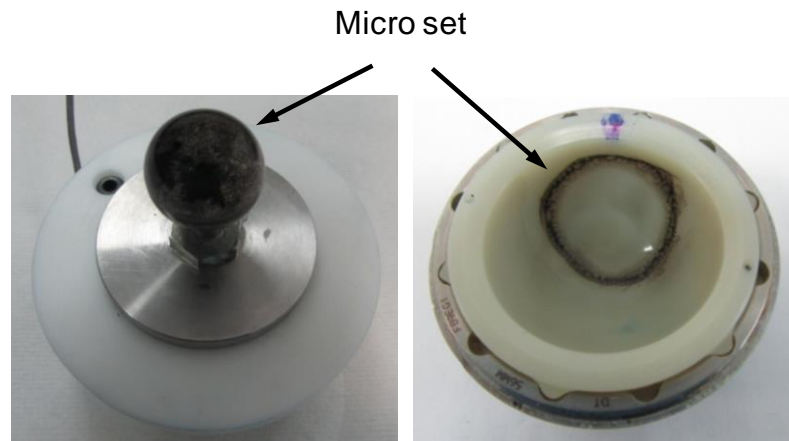
Micro set

Figure 5.5 The MicroSet was coated on the femoral head and shifted from femoral head to the cup when the loading was removed.

Various compressive forces from 500 N to 2500 N at regular intervals of 500 N were applied in the tests. Different cup inclination angles of 35º and 50º to the horizontal plane were considered in the experimental tests.

The photos of the liners with MicroSet were collected and post-processed. The contact areas at the liner were then calculated using Image ProPlus V3.0 (Media Cybernetics, Inc., MD, USA). For each specimen and a given loading, the experiment was repeated three times to obtain an average value.

5.2.2 FE Modelling

Model development

The experimentally-matched model was developed to predict the contact areas on the articulating surfaces for Pinnacle THR, which were then used to compare with the contact areas measured experimentally.

The experimentally-matched model used femoral head-polyethylene liner-metal shell-cement construction (Figure 5.6), which replicated the experimental set-up. The methodology used to generate the experimentally-matched model, i.e., the mechanical properties and mesh for the components, as well as the friction properties and contact formulation for the contact surfaces, was the same as that used to generate the anatomic Pinnacle THR model, which was detailed in **Chapter 2**. The mechanical properties and mesh for the cement in the experimentally-matched model were the same with that in the anatomic Charnley THR model which was also described in **Chapter 2**. The nodes at the outside of the cement in the experimentally-matched model were fully constrained and the interface between the cement and the metal shell was fully bonded, simulating the fixation of the metal shell in the cup holder using PMMA cement, as processed in the experimental tests. The FE modelling and boundary conditions for the experimentally-matched model is shown in Figure 5.6.

Fully constrained
PMMA cement
Titanium shell
Polyethylene liner
Femoral head
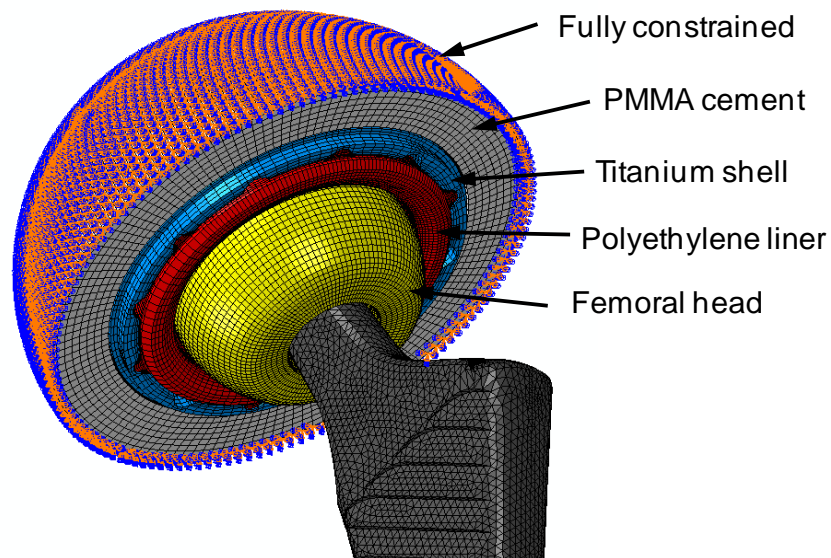
Figure 5.6 The FE modelling and boundary conditions for the simple Pinnacle THR model, which have the same construction and boundary conditions with the experimental set-up.

The outer diameters for the cement and metal shell in the experimentally-matched model were 76 mm and 52 mm respectively. Three polyethylene liners with three different clearances, corresponding to the specimens used in the experimental tests (Table 5.1), were reconstructed in the experimental-matched model. For the purpose of directly comparing with the

experimental tests, the liners used in the FE models were termed as "soak control liner", "load control liner", "worn liner" respectively as well. Vertical loads of 500 N, 1000 N, 1500 N, 2000 N and 2500 N, which were applied in the experimental tests, were applied at the centre of the femoral head in the experimentally-matched model. The acetabular cup was positioned at inclination angles of 35⁰ and 50⁰ to reproduce the experimental conditions. The models were solved using ABQUS (Version 6.9, Dassault Systèmes Simulia Corp., Providence, United States).

Parametric study

The parametric study was conducted to examine the effect of frictional characteristics at the metal shell/liner interface on the contact stresses on the articulating surface and backside surface of the liner. Different friction coefficients of 0.1, 0.15, 0.3, and 0.6 were applied at the metal shell/liner interface in the experimentally-matched model (Kurtz et al., 1997; Besong et al., 2001b; Ramero et al., 2007; Amirouche et al., 2008) and the contact mechanics of the Pinnacle THR were analysed.

5.3 Results

5.3.1 Comparison of Experimental Measurements and FE Predictions

Similar contact area patterns were observed between the experimental measurements and FE predictions from the simple Pinnacle THR model for soak control liner, load control liner and worn liner, although there were slight differences in the contact area values (Table 5.2 and 5.3). For all loading conditions and cup angles, the differences of contact areas between the experimental measurements and FE predictions from the simple Pinnacle THR model were within 3.5% for soak control liner, which was the lowest among the three specimens. The maximum differences of 14% was observed for worn liner. The differences of contact areas between the experimental measurements and FE predictions for load control liner was within 12% (Figure 5.7 and 5.8).

An increased load from 500 N to 2500 N resulted in an increased contact areas of approximately 85%-110% for cup inclination angles of 35⁰ and of

about 181%-262% for cup inclination angles of 50⁰ for both experimental measurements and FE predictions (Figure 5.7 and 5.8).

Table 5.2 The contact area patterns on the articulating surfaces between experimental measurements and FE predictions from experimentally-matched model under load of 2500 N and cup inclination angles of 35⁰.

	Soak control	Load control	Worn
Experimental measurements	370 mm^2	425 mm^2	535 mm^2
FE predictions from experimentally-matched model	388 mm^2	447 mm^2	565 mm^2
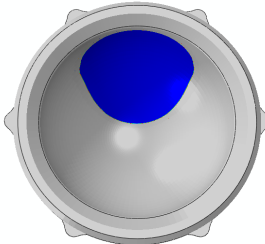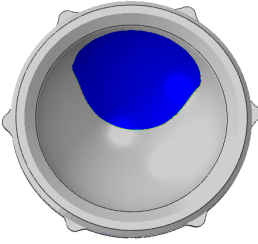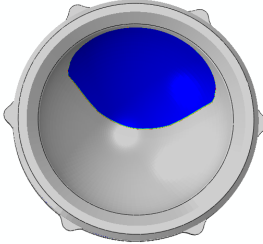
Table 5.3 The contact area patterns on the articulating surfaces between experimental measurements and FE predictions from experimentally-matched model under load of 2500 N and cup inclination angles of 50⁰.

	Soak control	**Load control**	**Worn**
Experimental measurements	325 mm^2	385 mm^2	425 mm^2
FE predictions from experimentally-matched model	341 mm^2	409 mm^2	465 mm^2
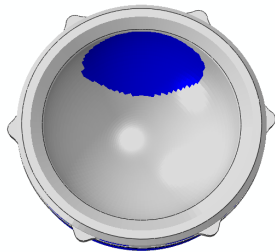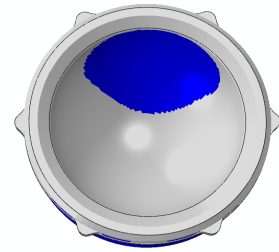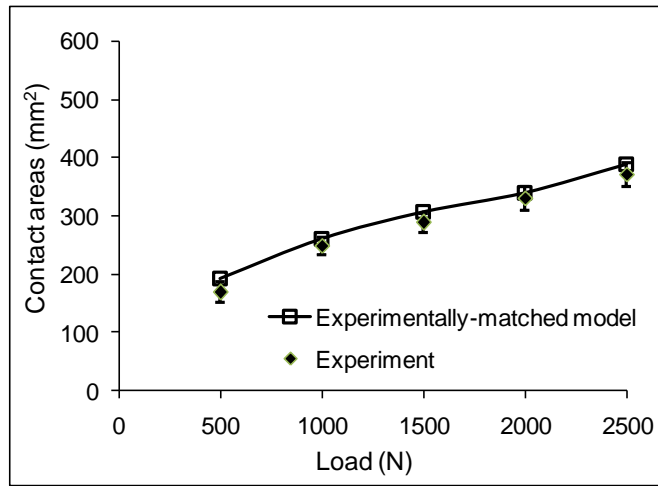
(a)
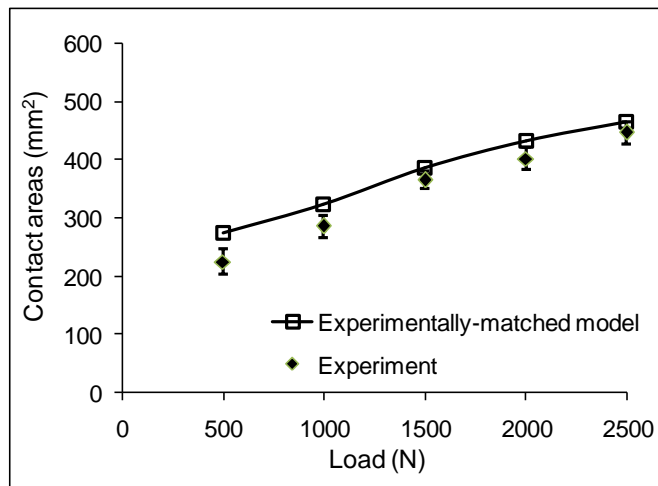
(b)
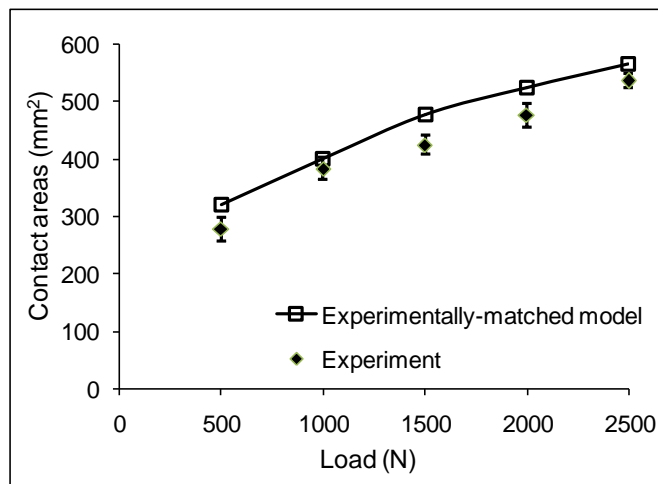
(c)

Figure 5.7 Comparison of the contact areas on the articulating surface between the experimental measurements and FE predictions from experimentally-matched model under cup inclination angles of 35º for different liners: (a) soak control liner, (b) load control liner, (c) worn liner. The error bars represent 95% confidence limit.
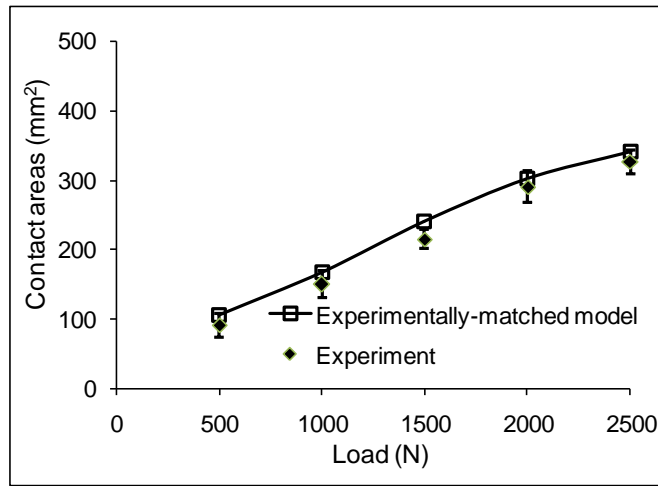
(a)
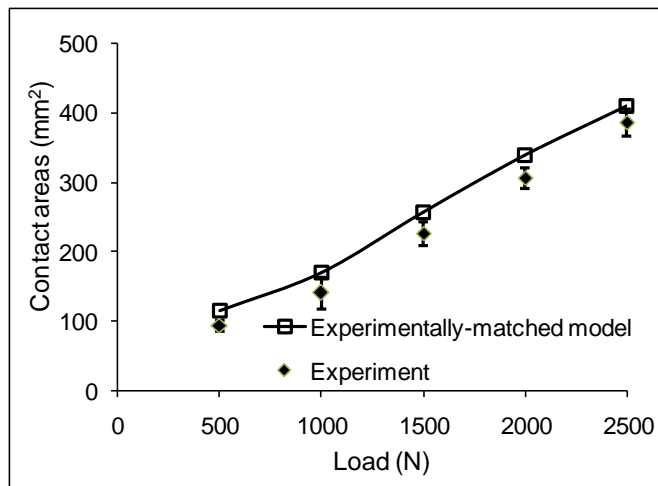
(b)
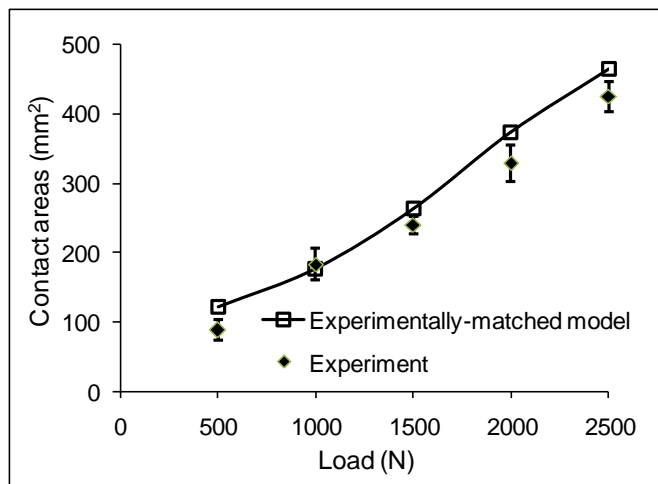
(c)

Figure 5.8 Comparison of the contact areas on the articulating surface between the experimental measurements and FE predictions from experimentally-matched model under cup inclination angles of 50⁰ for different liners: (a) soak control liner, (b) load control liner, (c) worn liner. The error bars represent 95% confidence limit.

5.3.2 Parametric Study

For all cup inclination angles and loading conditions considered, the differences in maximum contact stress on the frontside articulating surfaces were within 9% for cup inclination angle of 35⁰ and within 8% for cup inclination angle of 50⁰ when different friction coefficients (m) were considered at the metal shell/liner interface in the FE modelling (Figure 5.9). Under the same conditions, the differences in maximum contact stress on the backside surface of the liner were within 6% for cup inclination angle of 35⁰ and within 12% for cup inclination angle of 50⁰ (Figure 5.10).
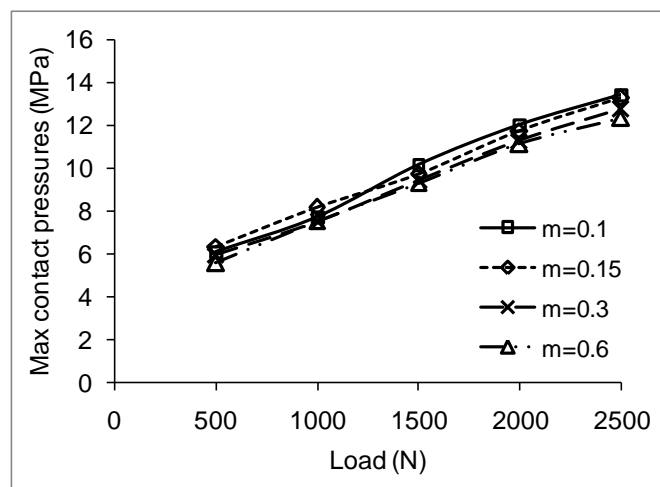
(a)
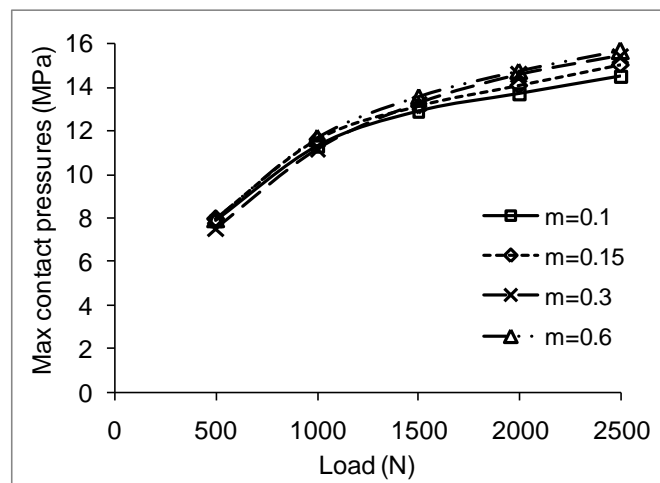
(b)

Figure 5.9 The predicted maximum contact pressures on the articulating surface with different friction coefficients (m) and loading under cup angles of (a) 35⁰ and (b) 50⁰.
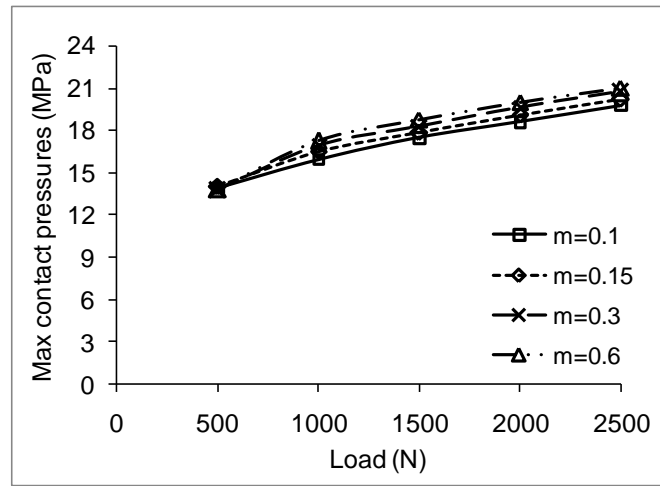
(a)
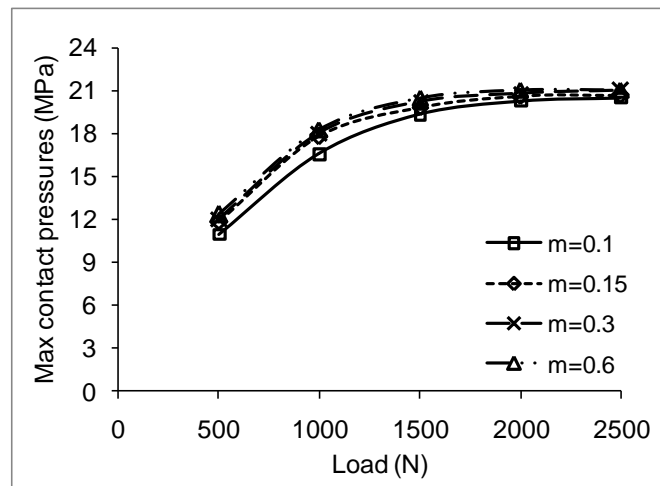
(b)

Figure 5.10 The predicted maximum contact pressures at the shell/liner interfaces with different friction coefficients (m) and loading under cup angles of (a) 35⁰ and (b) 50⁰.

5.4 Discussion

In this Chapter, an experimentally-matched model was developed as a bridge between the experimental measurements and the anatomic Pinnacle THR model, which applied the same methodology as the anatomic Pinnacle THR model on one hand, and had the same constructions, boundary conditions, and loading conditions as the experimental set-up on the other hand. The validity of anatomic Pinnacle THR model prediction was evaluated by directly comparing the contact areas between the experimental tests and FE predictions from the experimentally-matched model.

The anatomic Pinnacle THR model would be used in the future study to investigate the contact mechanics of Pinnacle THR under different conditions, which would be related to the contact pressures and contact areas. Therefore, the direct validation of the anatomic Pinnacle THR model would involve experimental measurements of contact pressure and contact area. The measurement of contact stress is challenging to some extent due to some reasons, such as the small radial clearance between the femoral head and acetabular cup and the geometric characteristics of the bearing surface for hip joint replacement restrict the effective use of pressures film or sensors. However, the measurement of contact area was conducted in this Chapter, and good agreement was obtained between the experimental measurements and FE predictions from the experimentally-matched model with respect to the contact area patterns and contact area magnitudes. This confirmed the validity of the experimentally-matched model to predict contact area, and provided great confidence in the validity of the experimentally-matched model to predict contact stresses. As the experimentally-matched model used the same constructions and methodology (i.e. contact formulation and conditions, mesh) as the anatomic Pinnacle THR model, this provided great confidence in the validity of the prediction of contact stress and contact area from anatomic Pinnacle THR model as well.

Although the results of the FE modelling showed good agreement with the experimental measurements, studies of this nature are not without their limitations. Indeed, errors from several sources may affect the final results and need to be examined with caution. Firstly, the material properties of the polyethylene liner in the FE modelling was from literatures (Liu et al., 2005a; Udofia, et al., 2007) which may be different from that used in the experimental tests. This is likely to be a major source of error. Although the load was removed immediately and each test was run for a short time, the polyethylene specimens still showed a degree of viscoelastic behaviour which can result in creep and material flow away from the contact region (Gauthier and Schirrer, 2000; Gauthier et al., 2001), this may have a marked effect on the contact areas measured. However, in the FE predictions, the creep and viscoelasticity was not considered. Moreover, the error may be generated during the calculation of the contact areas (i.e. how to choose the

fringe of the ink during the processing) as there was some ambiguity in the fringe of the ink for some measurement (Figure 5.3). An error of approximately 5% could be produced if the outside edge of the ambiguity was considered compared to that when the inside edge of the ambiguity was selected. Finally, only three experiments per polyethylene specimen were performed, it would have been desirable to conduct a series of experiments on each specimen and then take the average results to minimize the random errors.

In spite the several limitations and error sources listed above, as well as other potential error sources which have not been evaluated, the present study produced exceptionally positive outcome. The FE modelling produced very reasonable predictions with respect to the contact areas when compared to experimental measurements. This gives an encouraging indication about the accuracy of the anatomic Pinnacle THR model developed in this project, and provides great confidence in the use of the model to study the clinical applications across the hip implants such as edge loading, microseparation etc., and to evaluate the new hip implants designs.

Previous studies have demonstrated that a change of the friction coefficient at the articulating surfaces between the femoral and acetabular components was found to have a negligible effect on the predicted contact pressure and contact area for both cemented and cementless THRs (Besong et al., 2001b; Udofia et al., 2004). The friction coefficient for MoP was reported to range from 0.083 to 0.2 (Kurtz et al., 1997; Capitanu et al., 2005). Ramero and colleagues (Ramero et al., 2007) ran a series of FE models with friction coefficient values that varied between the given range (0.083 to 0.2), and compared the FE model prediction with the experimental data, they demonstrated that the results obtained in the FE models with different friction coefficients were between the maximum and minimum values obtained in the experiment. However, with a friction coefficient of 0.083, the FE prediction showed a close fit to the experimental data. Based on these, the coefficient of friction of 0.083 was chosen for the articulating surfaces in the full anatomic Pinnacle model in the current study as well as in the other FE models of modular THRs (Kurtz et al., 1997; Kurtz et al., 1998; Amirouche et al., 2008).

The results of this study also suggest that FE prediction of peak contact stresses at the articulating surface and backside of the liner at the shell/liner interface were not overly sensitive to changes in the friction coefficient at the liner/cup interface. When the friction coefficient at the liner/cup interface changed from 0.1 to 0.6, the maximum contact stresses were within 9% at the bearing surface and within 12% at the shell/liner interface. The same conclusion was drawn by Kurtz and colleagues (Kurtz et al., 1997) that there was a negligible change in the contact stresses both in the inner surface and outer surface of the liner as the coefficient of friction was changed from 0.08 to 0.16. This is indicated that polishing inside of the metal shell and the backside of the polyethylene will not substantially change the contact mechanics of the modular THR. Previous studies have demonstrated that the contact stresses in acetabular components were strongly dependent upon the manufacturing tolerances (conformity), the material properties, the thickness of the liner as well as the cup inclination angles for the modular THRs (Kurtz et al., 1994; Kurtz et al., 1998; Plank et al., 2007). The results of this study have an instructive significance to the surgeon and the engineer that, of the available design variables to be selectively modified, polishing the metal back plays the smallest role in lowering the contact stresses at the articulating surface and shell/liner interface for the modular THRs.

5.5 Summary

Experimental measurements of contact areas on the articulating surfaces of Three Pinnacle bearings were conducted in this Chapter. The measured contact areas were then compared with the FE predictions from an experimentally-matched model. Afterwards, the effect of friction coefficient on the contact stresses on the articulating surface and the backside surface of the liner were explored. The following conclusions can be drawn from this study:

1. Good agreement of the contact areas on the articulating surfaces with the maximum difference of 14% was obtained between the experimental

measurements and the corresponding FE predictions from the experimentally-matched model.

2. As the experimentally-matched model used the same constructions and methodology as the anatomic Pinnacle THR model, the positive outcome of the comparisons between the experimental measurements and the FE predictions provided great confidence in the use of experimentally-matched model, and the anatomic Pinnacle THR model as well.

3. The friction coefficient at the shell/liner interface was found to have only a slight effect on the contact stresses on the frontside articulating surface and backside surface of the liner for the Pinnacle THRs.

Chapter 6
Contact Mechanics Analysis of Pinnacle THR During Different Activities

6.1 Introduction

It is well known that the stresses experienced in the liner and on the articulating surface have been shown to be directly related to structural failure and fatigue-related wear mechanisms, which is closely linked to osteolysis and failure of the implant (Rostoker and Galante, 1979; Rose et al., 1983; McNie et al., 1998; Orishimo et al., 2003). Therefore, it is essential to estimate the stress levels and peak stress on the artificial hip joint in order to comprehensively understand the mechanics and the causes of failure of the joint.

The investigation of non-modular THR has been widely conducted and the contact mechanics have been extensively investigated (Jin et al., 1999; D'Lima et al., 2001; Korhonen et al., 2005). It is recognized that the contact stresses on the bearing surfaces for non-modular THR were affected by implant design, dimensions and materials of the components (Jin et al., 1994; Crowininshield et al., 2004; Lamvohee et al., 2009). Due to the conformity and integral support behind the acetabular component in non-modular THR, the cup inclination angles were found to have only a small influence on the contact mechanics if the contact area was within the bearing surface of the cup (Patil et al., 2003; Korhonen et al., 2005; Hua et al., 2012). However, for modular THR, the nonconformity between the shell and the liner has a marked effect on the stresses on both the frontside and backside surfaces of the liner (Kurtz et al., 1997; 1998). Additionally, the load and cup inclination angles were found to strongly affect the contact stresses on both the frontside articulating surfaces and backside shell/liner interfaces (Kurtz et al., 1997). However, for modular THRs such as the Pinnacle THR, few studies have been conducted that focus on the contact mechanics. The contact characteristics of the modular THRs are still not fully understood, especially under gait and also other daily activity conditions.

The muscle forces data has already been accounted for when converting the resultant contact forces to the FE model (Bergmann et al., 2001b). In order to consider the specific direction and orientation of the forces, the resultant hip joint forces were resolved to three components and converted to the FE model coordinate system, as shown in Figure 6.1. During the simulation process, the resultant hip joint forces were discretized into 21 steps and applied to the centre of the femoral head in a quasi-static manner. The resultant forces of different activities of daily living are shown in Figure 6.2.

The rotation of the head was constrained during the simulation process. In the first step, the femoral head was moved vertically by a small distance to allow contact with the acetabular component. The load vector corresponding to each step of the loading profile was applied one after the other in each step without changing any of the boundary conditions. A total of 16 orientations of cup angles were considered, with inclination angles varying between 35º and 65º and anteversion angles varying between 0º and 30º, both in 10º increments. The FE models were solved using ABAQUS (Version 6.9, Dassault Systèmes Simulia Corp., Providence, United States).
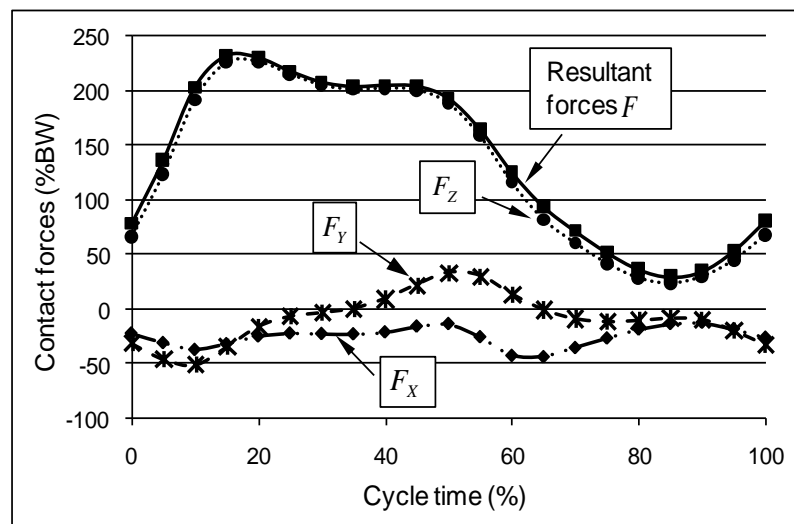
Figure 6.1 Resultant hip joint forces during normal walking. The resultant force was converted to three components (F_X, F_Y, F_Z) and computed as $F = \sqrt{F_X^2 + F_Y^2 + F_Z^2}$ (Bergmann et al., 2001b).

Table 6.1 The descriptions of six human routine activities (Bergmann et al., 2001a).

Activities	Descriptions	Cycle times (sec)
Normal Walking	Walking at normal speed on level ground, average speed: 3.9 km/h (1.09 m/s)	1.103
Ascending Stairs	Waking ascending stairs, stairs height 17 cm, no support at hand rail	1.593
Descending Stairs	Walking descending stairs, stairs height 17 cm, no support at hand rail	1.439
Standing Up	Standing up, chair height 50 cm, arms hold at the chest height	2.489
Sitting Down	Sitting down, chair height 50 cm, arms hold at the chest height	3.719
Knee Bending	Two-legged stance-bending knees-two-legged stance	4.665
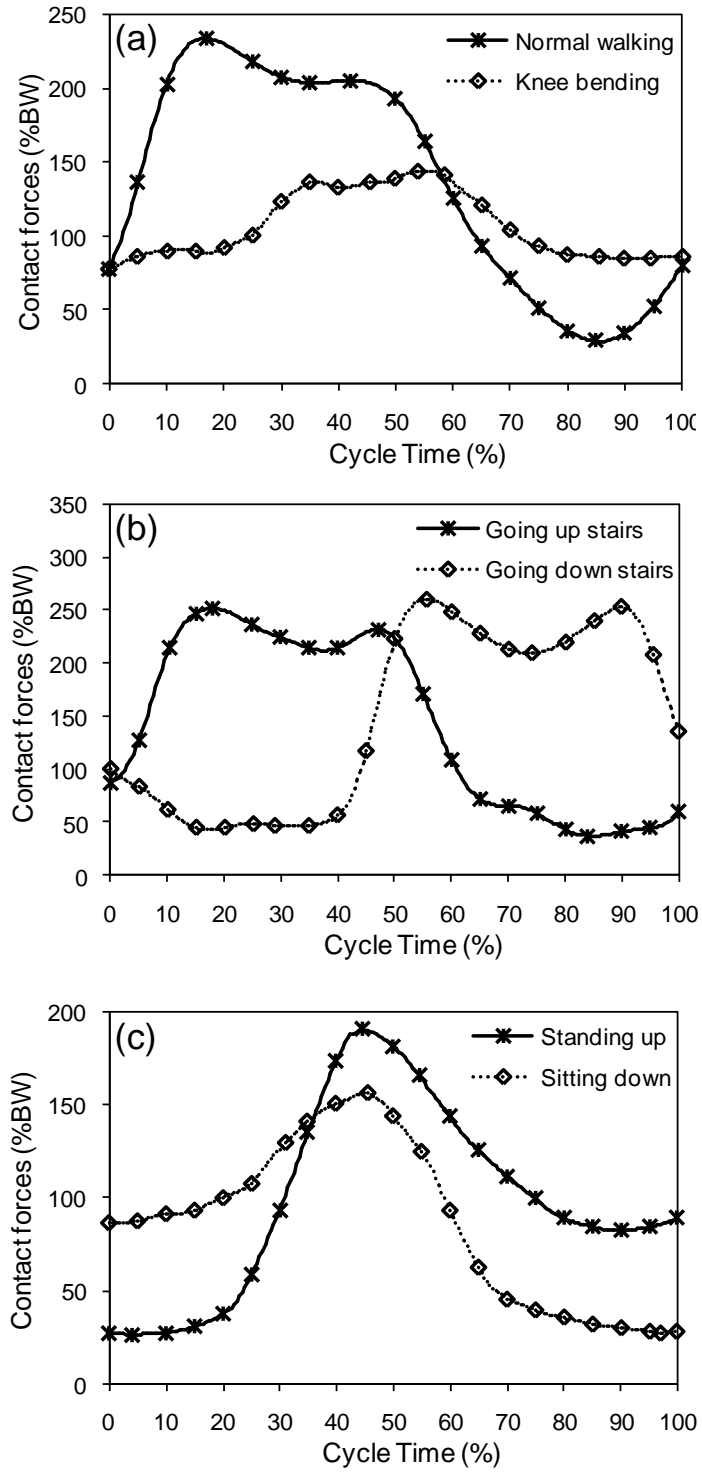
Figure 6.2 Hip joint contact forces during different activities of daily living (Bergmann et al., 2001b).

6.3 Results

6.3.1 Gait Analysis

Frontside contact stresses

The contact stress distribution on the frontside articulating surface at different stages of normal walking cycle under cup inclination angle of 45⁰ and anteversion angle of 10⁰ for radial clearance of 0.3 mm is shown in Figure 6.3. It can be seen that during the stance phase when the load was relatively high, the areas of contact were mostly located about the superior region of the liner. It was then shifted towards the medial region of the liner during the swing phase. The maximum contact pressure of approximately 11 MPa was predicted at 17% of walking cycle. The corresponding contact areas were less than 40% of the total inner surface of the liner during the whole cycle. No edge loading on the frontside articulating surface of the liner was observed during the whole cycle in this case.
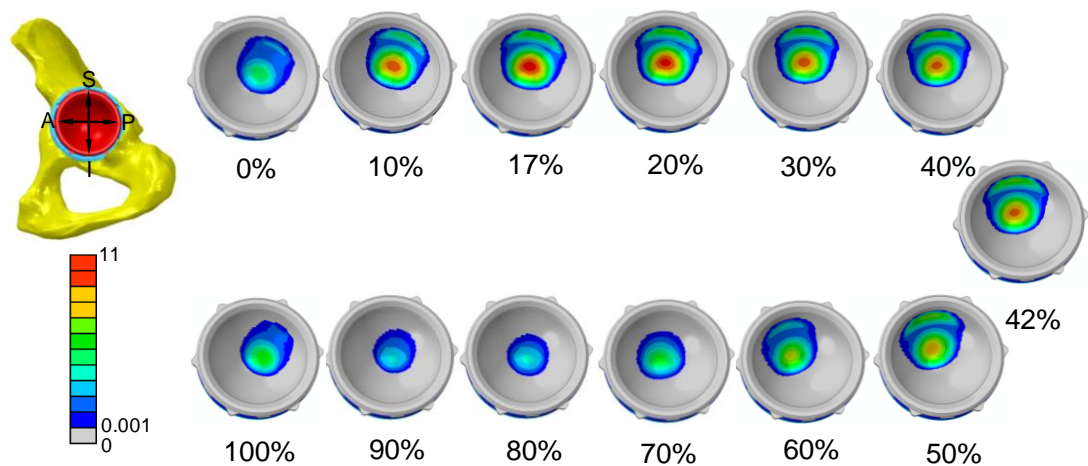
Figure 6.3 Contact stress (MPa) distribution on the frontside articulating surface of the liner during different phases of normal walking at the cup inclination angle of 45⁰ and anteversion angle of 10⁰ (A-Anterior; S-Superior; P-Posterior; I-Inferior) (clearance: 0.3 mm).

Generally, the peak contact stress on the frontside articulating surface for different activities showed the same time-dependent trend to that of the contact forces (Figure 6.4). For all activities considered, the peak contact

stress for radial clearance of 0.542 mm were predicted to be 2-3 times that for radial clearance of 0.1 mm during the whole cycles (Figure 6.4).

Under cup inclination angle of 45⁰ and anteversion angle of 10⁰, the maximum value of peak von Mises stress in the liner during the whole cycle among six activities were 10.84 MPa, 9.48 MPa and 8.15 MPa for the radial clearances of 0.542 mm, 0.3 mm and 0.1 mm respectively, which were all found to occur during the stair descending case. For the peak contact stress on the articulating surface, the maximum value among six activities were predicted to be 13.95 MPa (during ascending stair), 11.30 MPa (during descending stair) and 7.97 MPa (during descending stair) for the three radial clearances respectively (Figure 6.5).
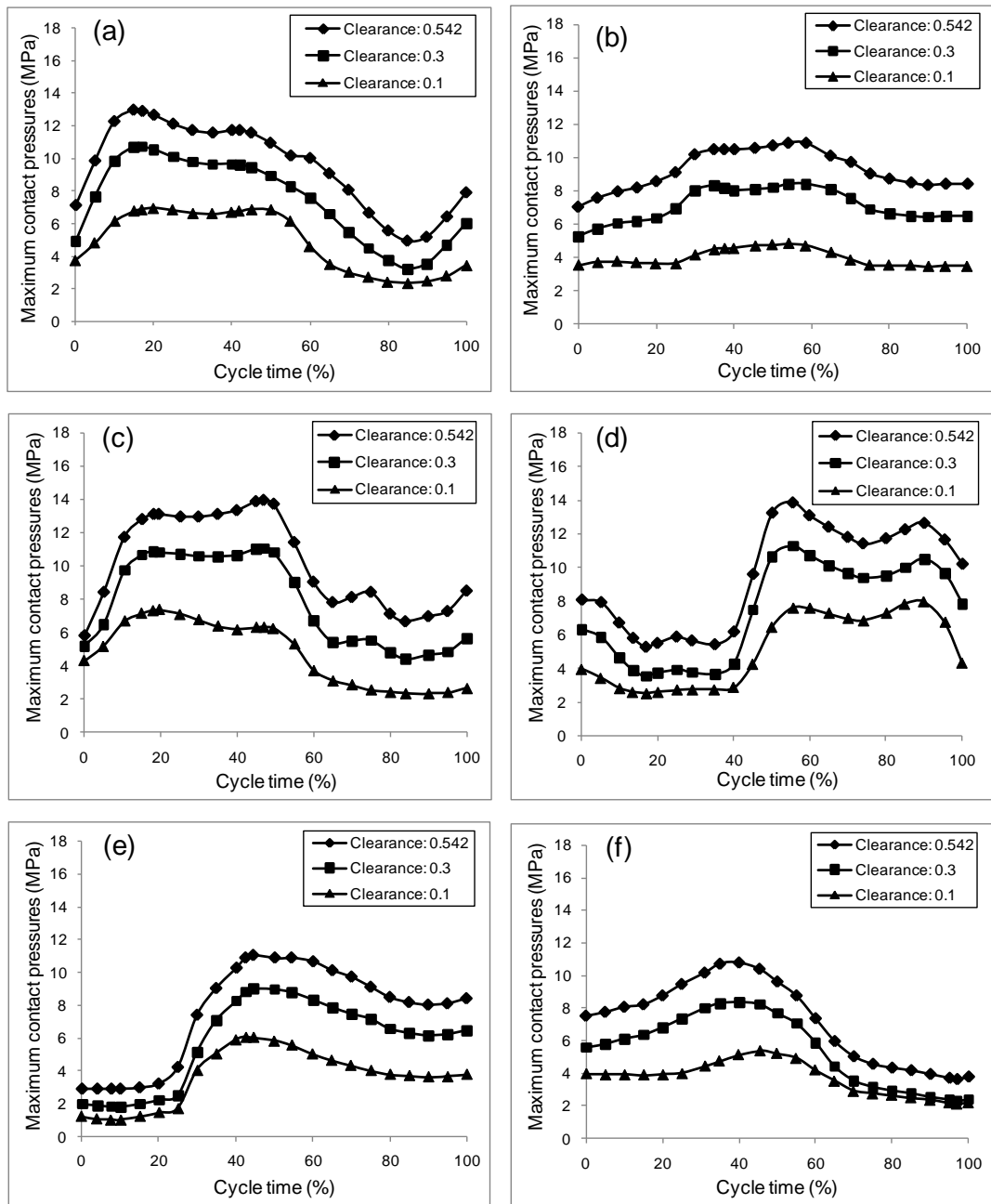
Figure 6.4 The predicted maximum contact pressure (MPa) on the frontside articulating surface of liner for three radial clearances of 0.542 mm, 0.3 mm and 0.1 mm under cup inclination angle of 45⁰ and anteversion angle of 10⁰ during different activities: (a) normal walking, (b) knee bending, (c) ascending stairs, (d) descending stairs, (e) standing up, (f) sitting down.
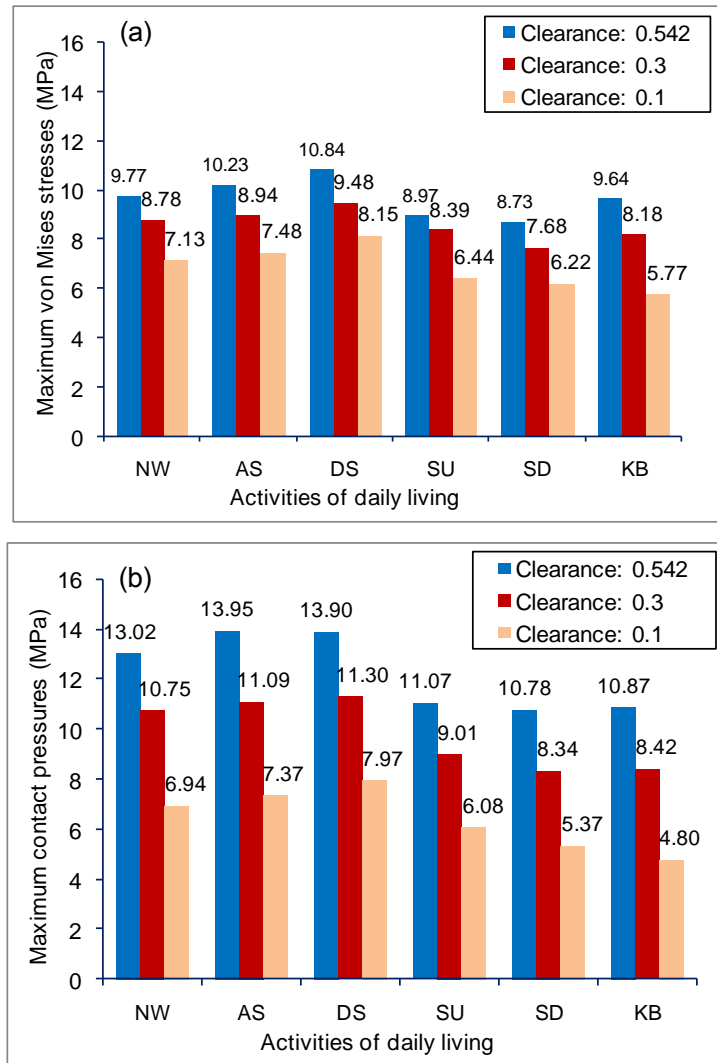
Figure 6.5 The predicted maximum stress (MPa) in the liner for different radial clearances during six different activities under cup inclination angle of 45⁰ and anteversion angle of 10⁰: (a) maximum von Mises stress in the liner, (b) maximum contact pressure on the frontside surface (NW: normal walking, AS: ascending stairs, DS: descending stairs, SU: standing up, SD: sitting down, KB: knee bending).

Backside contact stresses

The backside contact at the shell/liner interface was observed in two regions: the equatorial region and the spherical region (Figure 6.6). It is important to note the concentrated contact stresses in the equatorial region and in the spherical region, which were observed from 10% to 60% of cycle time for radial clearance of 0.3 mm under cup inclination angle of 45⁰ and anteversion of 10⁰. The maximum contact stress of 15 MPa in the equatorial

region at 50% of cycle time and 12.35 MPa in the spherical region at 17% of cycle time were predicted for this condition (Figure 6.6).

As with the frontside contact stresses, the peak contact stresses in the equatorial region of the backside surface of the liner for different activities showed a similar time-dependent trend to that of the contact forces. However, the peak contact stresses in the spherical region were found to be different from that of the contact forces (Figure 6.7). No contact between the spherical region of liner and the metal shell was observed for standing up case before the 20% of cycle.
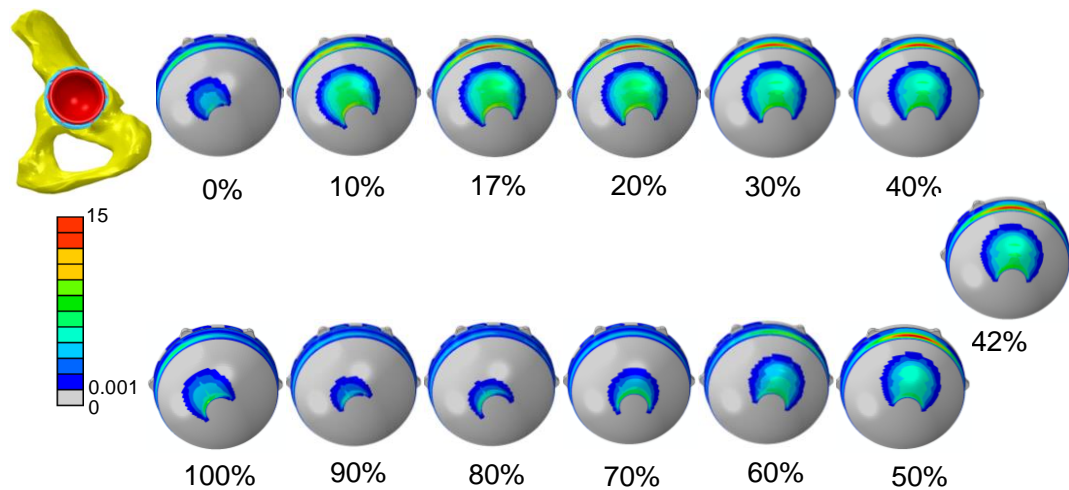
Figure 6.6 Contour plots of contact stresses (MPa) at the backside surface of UHMWPE liner during different phases of normal walking at the cup inclination of 45º and anteversion angle of 10º (clearance: 0.3 mm).
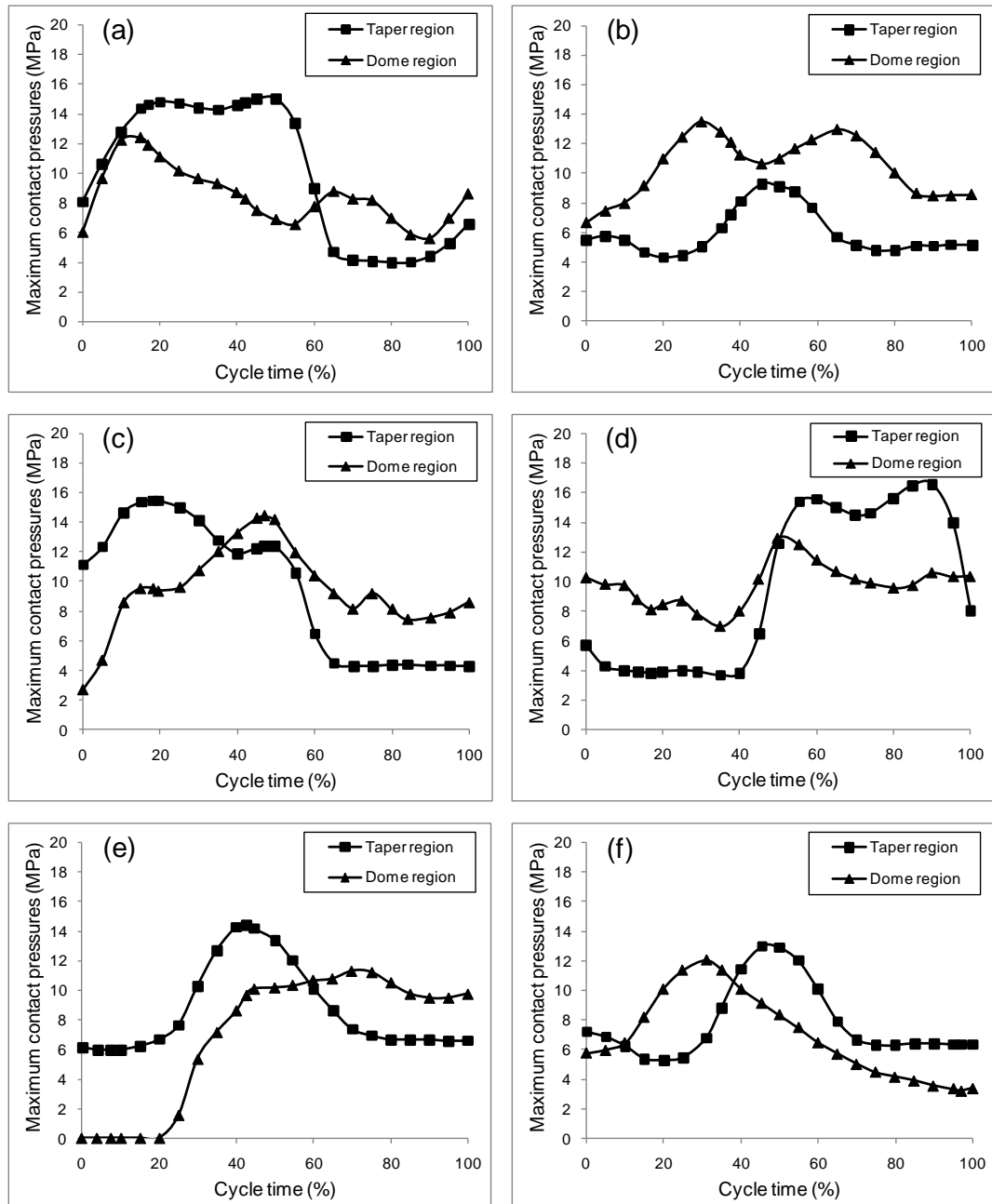
Figure 6.7 The predicted contact pressures (MPa) at two regions of the backside surface of liner under cup inclination angle of 45⁰ and anteversion angle of 10⁰ during different activities: (a) normal walking, (b) knee bending, (c) ascending stairs, (d) descending stairs, (e) standing up, (f) sitting down (clearance: 0.3 mm).

6.3.2 Edge Loading During Different Activities

Frontside edge loading

Figure 6.8 shows an example of edge loading on the frontside articulating surface of the liner for Pinnacle THR during normal walking. It should be pointed out that the edge loading on the articulating surface illustrated in this

chapter refers to the condition where the contact patch between the liner and the femoral component extends over the rim of the liner, as shown in Figure 6.9. Using this definition, edge loading on the frontside articulating surface of the liner for the Pinnacle THR with a radial clearance of 0.3 mm was identified during different daily activities. The proportion of the cycle and the specific instances where edge loading occurred during different activities as a function of the cup angles are shown in Figure 6.10.

It can be seen that edge loading in frontside surface of the liner was observed with steep cup inclination angles for normal walking, ascending stair, and descending stairs cases. No edge loading was predicted for standing up, sitting down and knee bending cases. For normal walking and ascending stair cases, the combination of steep cup inclination angle and lower anteversion angle was more inclined to cause edge loading, while for descending stair case, the combination of the steep cup inclination and high anteversion angle prone to induce edge loading.

Taking the normal walking case as an example (Figure 6.10 a), with cup inclination angle of 55⁰, edge loading occurred in specific instances of 45%-55% of cycle time (proportion of 5% of the cycle) with cup anteversion angle of 0⁰ while no edge loading was observed with cup anteversion angle of 30⁰. When the cup inclination angle increased to 65⁰, the proportion of the cycle where edge loading occurred increased to 40% (in specific instances of 15%-55% of cycle time) with cup anteversion angle of 0⁰, however, the proportion decreased to 13% (in specific instances of 42%-55% of cycle time) with cup anteversion angle of 30⁰.
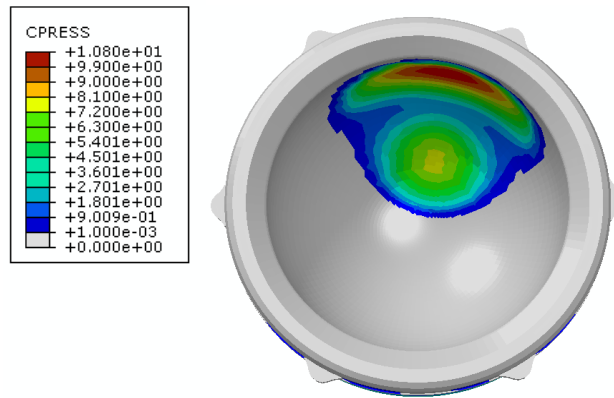
Figure 6.8 Contour plots of contact stresses (MPa) on the frontside articulating surface of liner at 17% of normal walking cycle at cup inclination of 65⁰ and anteversion of 0⁰ (clearance: 0.3 mm).

(a)   (b)
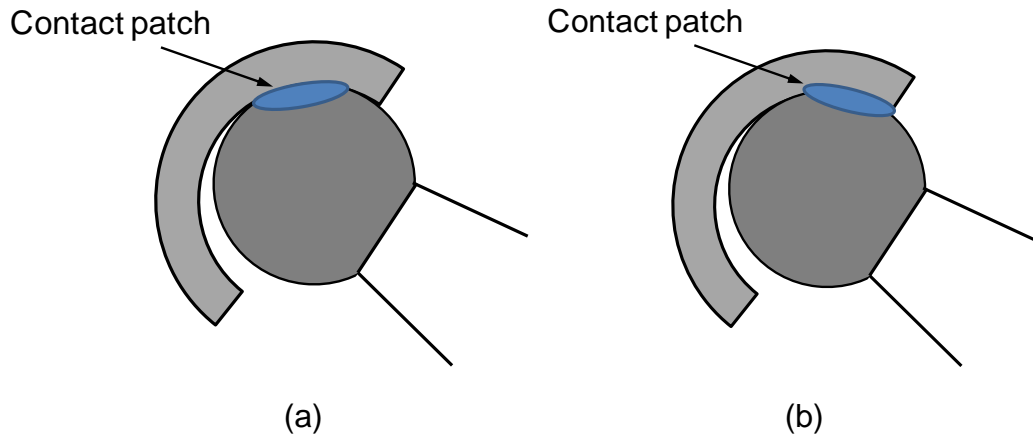
Figure 6.9 The definition of edge loading in MoP THR in the present study. (a) the case where edge loading does not occur because the contact patch is within the inner surface of the liner; (b) the case where edge loading occurs because the contact patch extends over the rim of the liner.
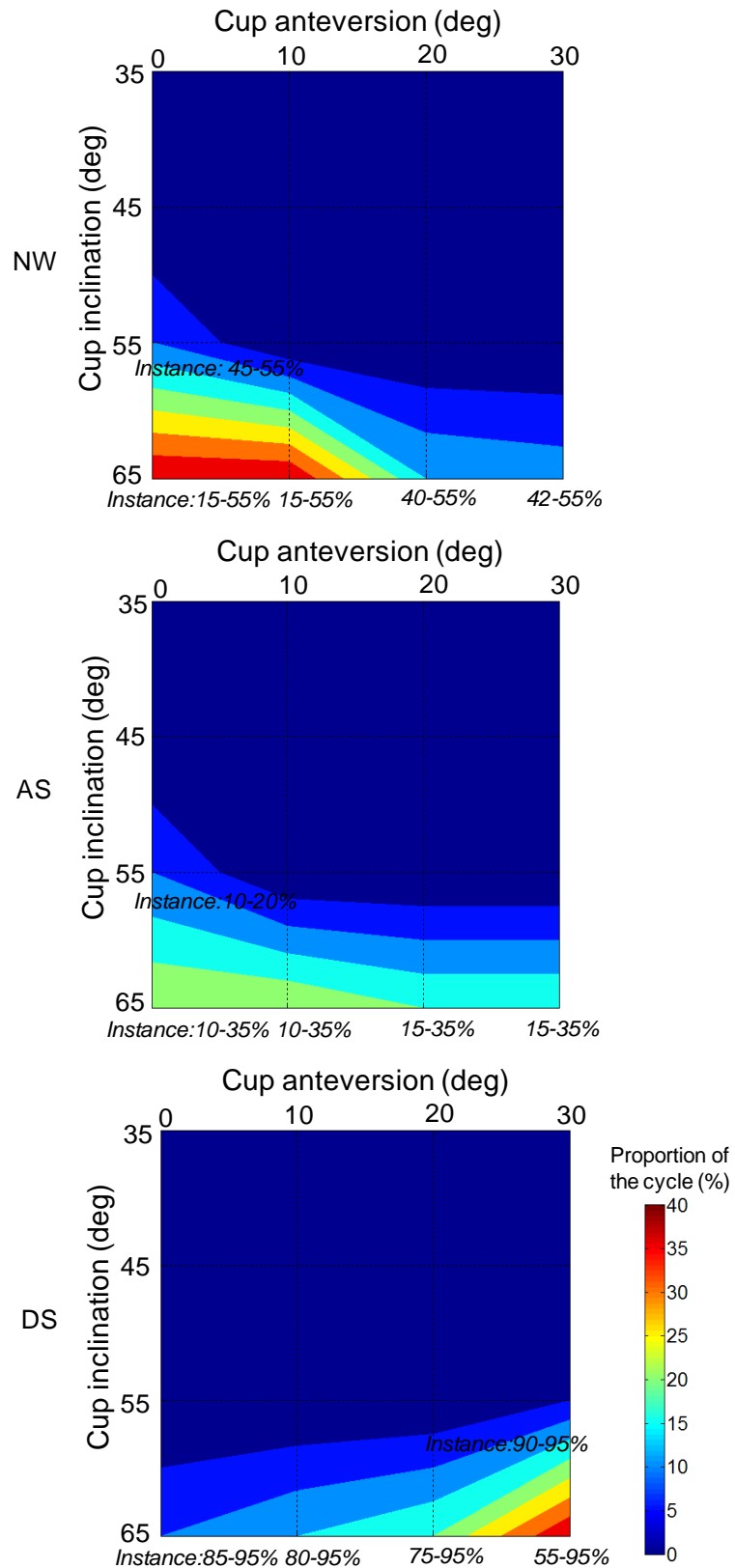
Figure 6.10 The proportion of the cycle and the specific instances over the cycle where edge loading occurred on the frontside articulating surface of the liner as a function of cup angles during different activities (NW: normal walking, AS: ascending stairs, DS: descending stairs. No edge loading in the frontside of liner was observed for standing up, sitting down and knee bending cases (clearance: 0.3 mm).

Backside edge loading

As mentioned above, concentrated stress in the equatorial region of the backside surface of the liner was observed in some instances of normal walking (Figure 6.6). This was probably due to the edge loading that occurred at the fringe of the taper on the backside surface of the liner, as shown in Figure 6.11 a. An example of such edge loading on the backside of the liner is shown in Figure 6.11 b. The proportion of the cycle and the specific instances when edge loading occurred in the taper of the backside surface of the liner during different activities as a function of the cup angles are presented in Figure 6.12.

Generally, edge loading in the taper of the backside surface of the liner was predicted at most instances of the cycle of activities and was more inclined to occur under steep cup inclination angle and lower anteversion angle conditions, except ascending stairs case, where edge loading prone to occur under high cup anteversion angles. Taking normal walking case as an example (Figure 6.12 a), with cup anteversion of 0°, the proportion of the cycle at which edge loading occurred at the taper of the liner was 60% under cup inclination of 35°, which increased to 100% when the cup inclination angle increased to 65°. Considering a cup inclination of 35°, the proportion of the cycle at which edge loading occurred was 60% under cup anteversion angle of 0° and decreased to 40% under cup anteversion angle of 30°. Under cup inclination angle of 35° and anteversion angle of 0°, edge loading occurred in the specific instances of 0-55% and 95%-100% of cycle time. It is important to note that edge loading in the taper of the backside surface of the liner occurred during the whole cycle under the cup inclination angle of 65° condition for all activities considered.

(a)
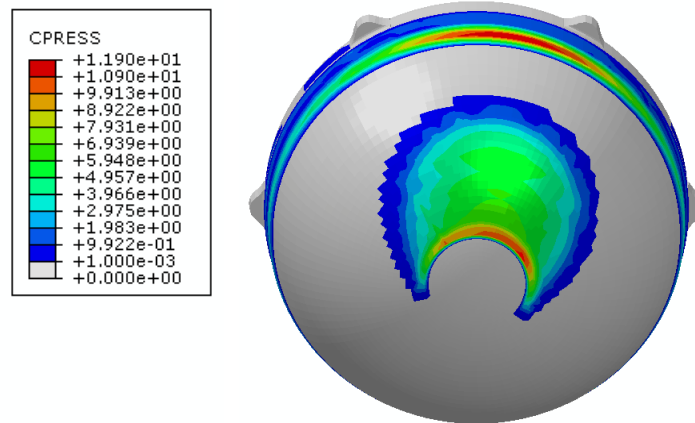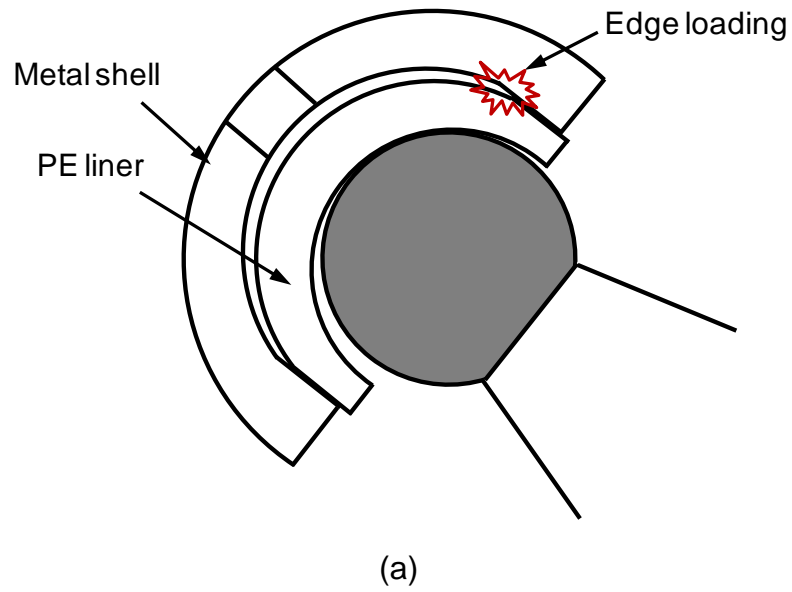
Figure 6.11 (a) The diagram shows the edge loading occurred at the fringe of the taper at the backside of UHMWPE liner, (b) Contour plots of contact stresses (MPa) at the backside surface of liner at 17% of normal walking cycle at cup inclination of 35⁰ (clearance: 0.3 mm), Note the concentrated stresses at the equatorial region and spherical region in the vicinity of the polar hole of the metal shell.

Cup anteversion (deg)

NW

Instance:0-55%   0-5%   17-55%   20-60%
95-100%   15-55%

Instance:0-60%   0-60%   0-60%   10-65%
85-100%   90-100%

Instance:0-70%   0-60%   0-70%   0-70%
85-100%   95-100% 95-100% 95-100%

Instance:0-100%   0-75%   0-75%   0-75%
                  95-100% 95-100% 95-100%

Cup anteversion (deg)

AS

Instance:0-55%   0-55%   0-60%   0-60%

Instance:0-60%   0-60%   0-60%   0-65%

Instance:0-65%   0-65%   0-65%   0-70%

Instance:0-75%   0-75%   0-75%   0-80%

Cup anteversion (deg)

DS

Instance:50-100% 50-100% 0-5%   0-5%

Instance:0-10%   0-5%   0-5%   0-5%
45-100%   45-100% 45-100% 40-100%

Instance:0-10%   0-10%   0-100%   0-10%
30-100%   30-100% 30-100% 30-100%

Instance:0-100%   0-100%   0-100%   0-100%

Figure 6.12 The proportion of the cycle and the specific instances over the cycle where edge loading occurred in the taper of the backside surface of the liner as a function of cup angles during different activities (NW: normal walking, AS: ascending stairs, DS: descending stairs, SU: standing up, SD: sitting down, KB: knee bending.(clearance: 0.3 mm).

6.3.3 Effect of Cup Angles on Contact Stresses

Frontside contact stress

Figure 6.13 shows the distribution of contact stress, the value and location of the peak contact stresses as well as the instance of the cycle when the peak contact stress occurred on the frontside articulating surface of liner with different cup inclination angles and anteversion angles during normal walking for radial clearance of 0.3 mm.

Generally, the areas of the predicted contact stresses were located about the superior region of the liner and shifted towards the superior edge as inclination angles were increased. The peak contact stress was located in the spherical region when the cup inclination angles were lower than 55°. It then moved to the equatorial region when the cup inclination angle was increased to 65°. With lower cup inclination angles, the peak contact stresses were predicted at 17% of the cycle for normal walking, at which point the maximum contact force exist. However, when the cup inclination angle increased to 65°, the peak contact stresses were predicted at 15% and 50% of normal walking cycle.

Cup anteversion (deg)
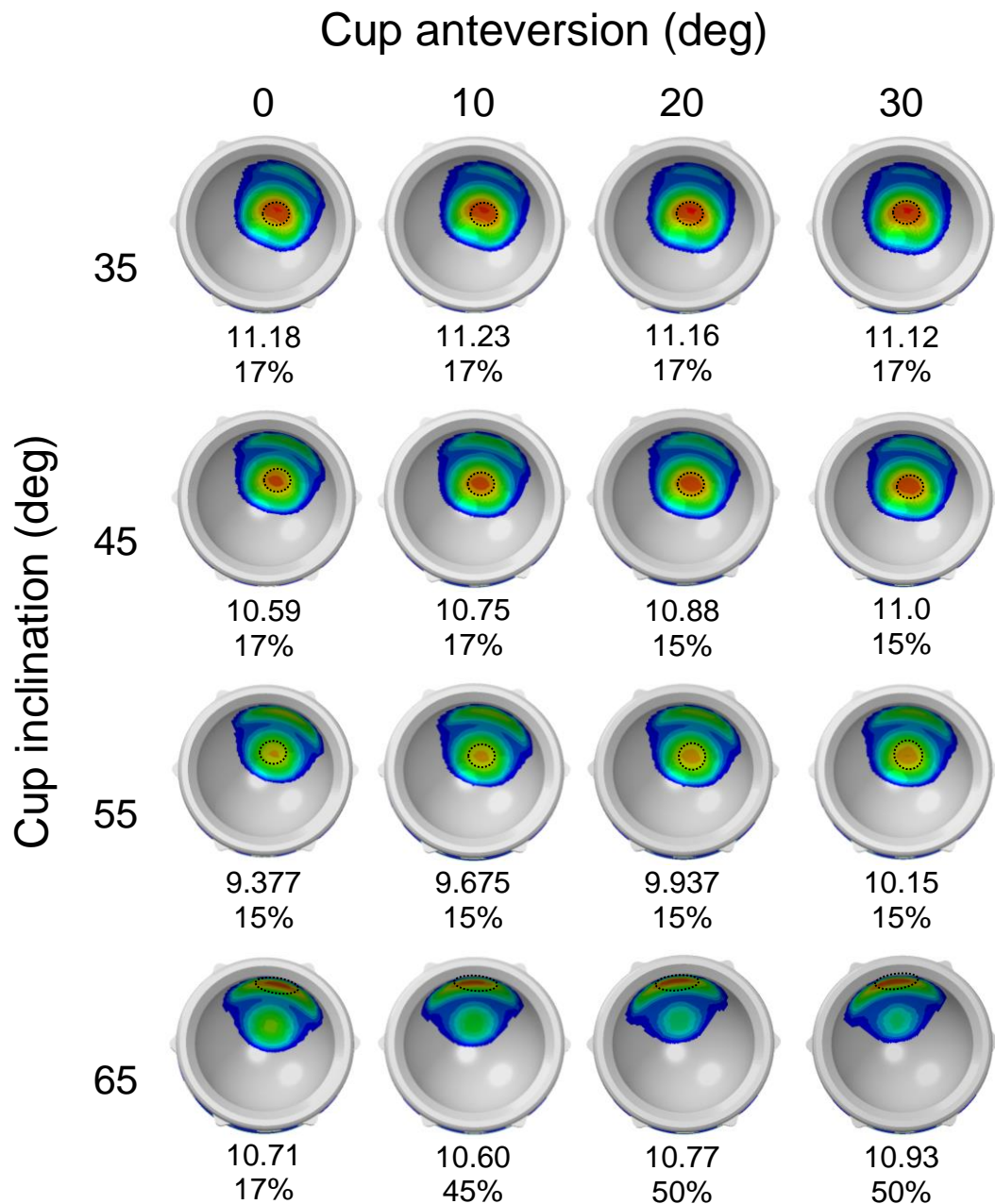
Figure 6.13 The distribution and maximum value of contact pressures (MPa) on the frontside surface of the liner and the corresponding instance of the cycle as a function of cup inclination angles and anteversion angles at the instance when the peak contact stress occur during normal walking (clearance: 0.3 mm).

The activities, cup angles and radial clearances were found to have a synergistic effect on the contact stress on the frontside articulating surface of the liner (Figure 6.14). For normal walking, ascending stairs and descending stairs cases, the cup inclination angles had marked effect on the contact stresses while the cup anteversion angles had limited effect. For large radial clearances of 0.542 mm and 0.3 mm, the maximum contact stress was

decreased moderately first and then increased slightly when the cup inclination angles increased from 35⁰ to 65⁰. However, for small radial clearance of 0.1 mm, the results were totally different. The maximum contact stress was increased continually when the cup inclination angles increased from 35⁰ to 65⁰.

In contrast, for standing up, sitting down and knee bending activities, the anteversion angles were found to have marked effect on the contact stress. The increased cup anteversion angles from 0⁰ to 30⁰ led to marked increase in the contact stress. The cup inclination angles had limited effect. However, there were increasing trend in contact stresses with increased cup inclination angles for these three activities.
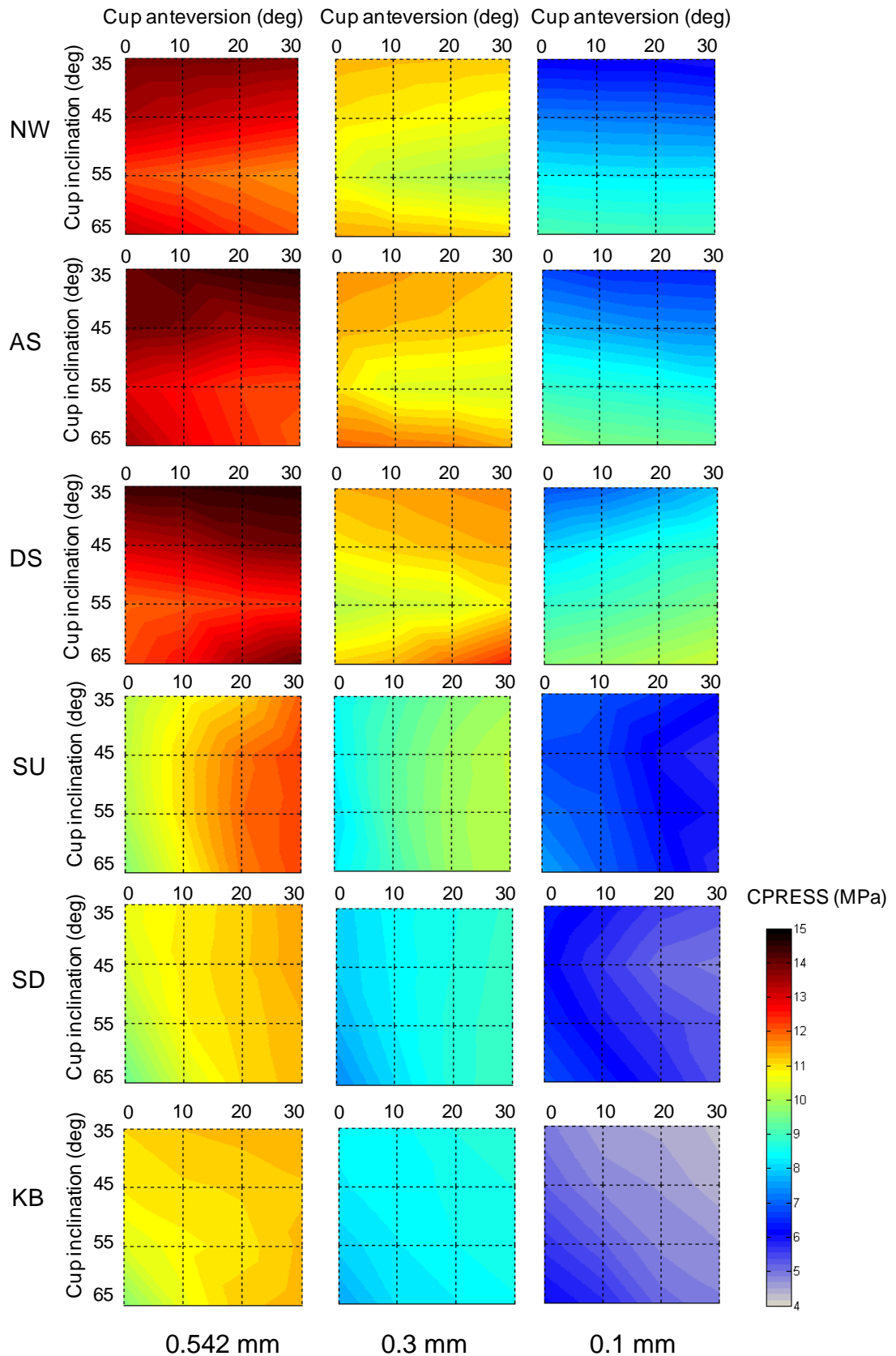
Figure 6.14 Peak contact stresses (MPa) on the frontside articulating surface of the liner as a function of cup inclination angle and anteversion angle during different activities (NW: normal walking, AS: ascending stairs, DS: descending stairs, SU: standing up, SD: sitting down, KB: knee bending) for different radial clearances.

Backside contact stress

For all activities considered, the cup inclination and anteversion angles were found to markedly affect the peak contact stresses in the equatorial region on the backside surface of the liner (Figure 6.15). For normal walking, ascending stairs and descending stairs activities, the cup inclination angles were found to have most effect on the contact stresses in this region. The contact stresses in the equatorial region of the backside surface of the liner increased markedly with increased cup inclination angles from 35° to 65°. In contrast, for standing up, sitting down and knee bending cases, the cup anteversion angles had most effect on the contact stress. There was marked decrease in the contact stress with increased cup anteversion angles from 0° to 30° (Figure 6.15).

The concentrated contact stresses were also observed in the vicinity of the hole of the metal shell on the backside surface of liner, as shown in Figure 6.11 b. Similar to the peak equatorial contact stresses, the peak contact stresses in the spherical region were found to be sensitive to the cup inclination angles and anteversion angles (Figure 6.16). However, as opposed to the peak equatorial contact stresses, the high contact stresses were predicted to be associated with lower cup inclination angles of 35°, which was approximately 2.5-3 times that for cup inclination angles of 65° for normal walking, ascending stairs and descending stairs cases (Figure 6.16).
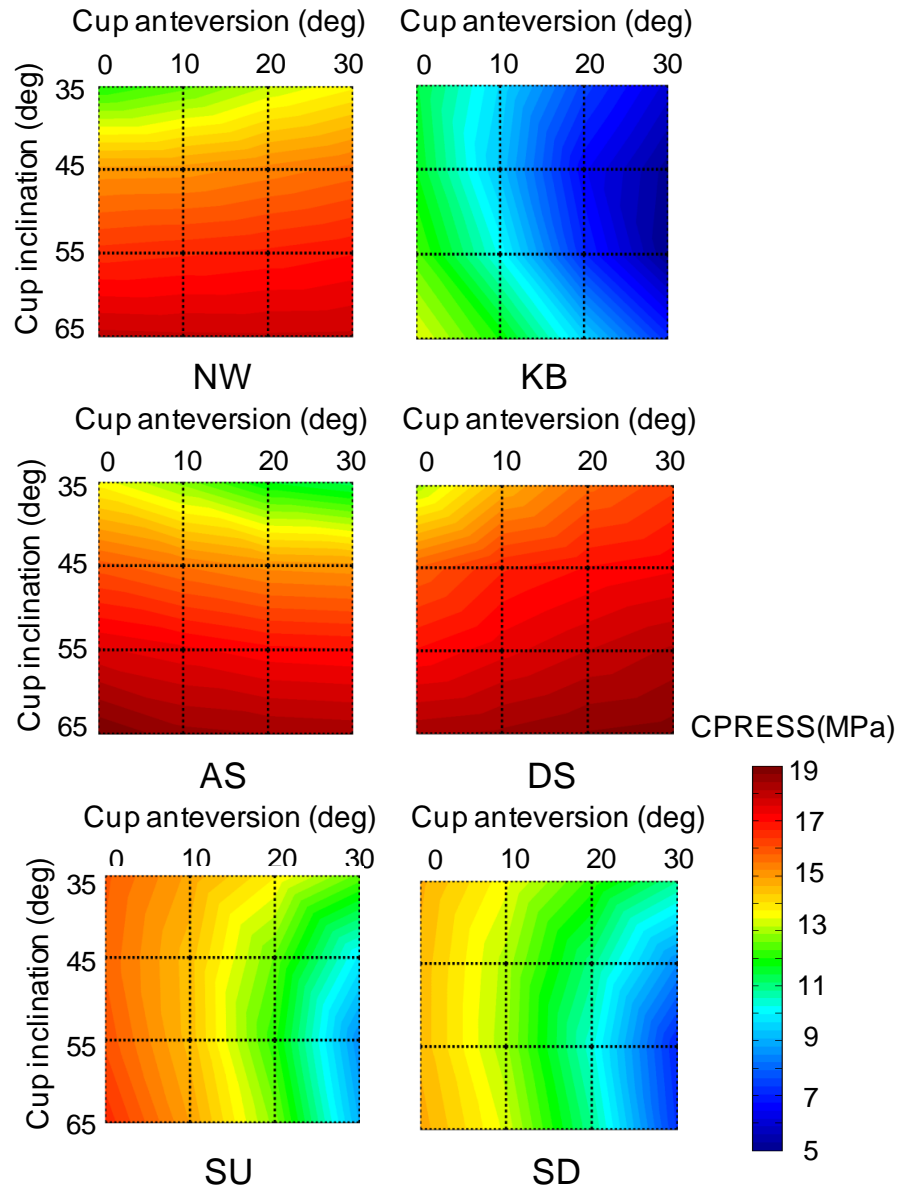
Figure 6.15 Peak contact stresses (MPa) at the equatorial region of backside surface of liner as a function of cup inclination angle and anteversion angle during different activities (NW: normal walking, AS: ascending stairs, DS: descending stairs, SU: standing up, SD: sitting down, KB: knee bending) (clearance: 0.3 mm).
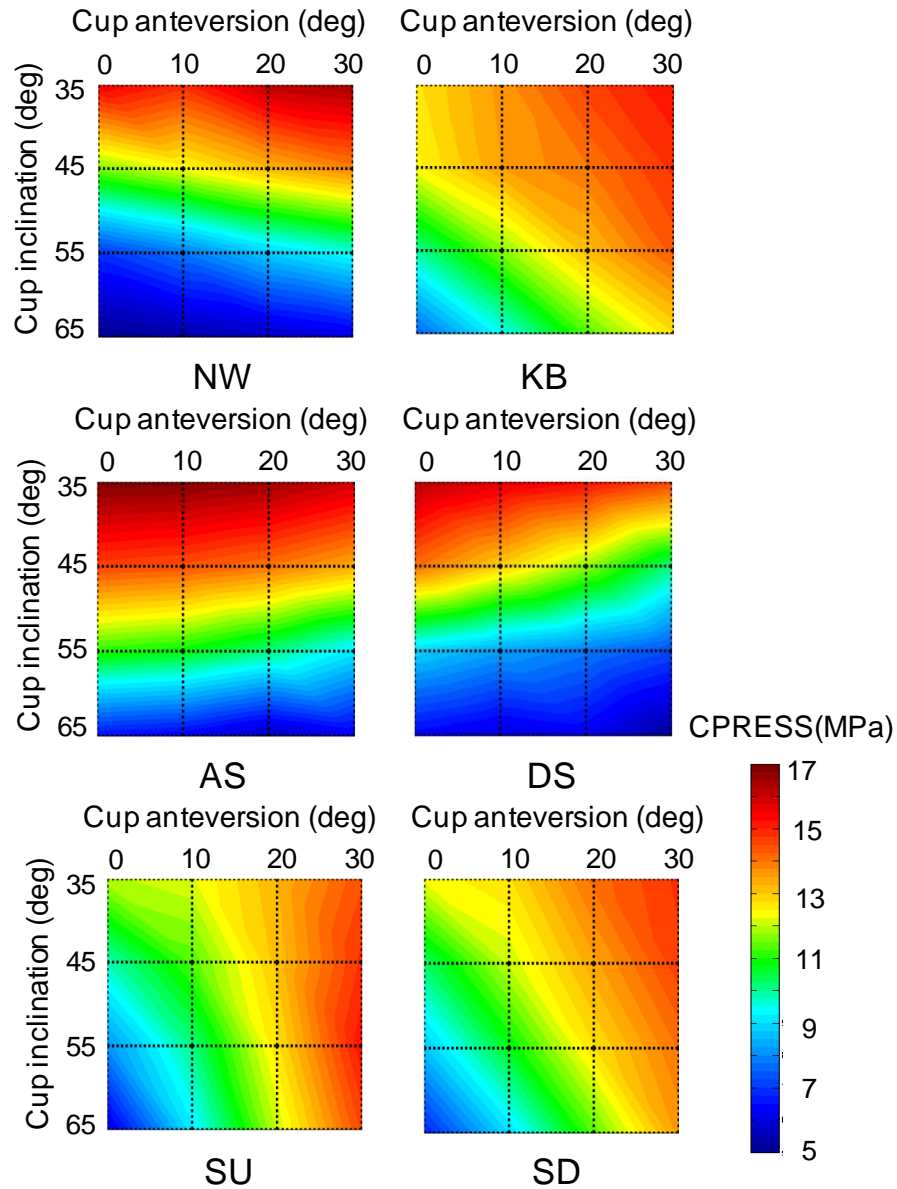
Figure 6.16 Peak contact stresses (MPa) at the spherical region of backside surface of liner as a function of cup inclination angle and anteversion angle during different activities (NW: normal walking, AS: ascending stairs, DS: descending stairs, SU: standing up, SD: sitting down, KB: knee bending) (clearance: 0.3 mm).

6.3.4 Effect of Cup Angles on Plastic Strain

Figure 6.17 shows the distribution of equivalent plastic strain in the liner in the instance of 17% of cycle during normal walking under cup inclination angle of 45° and anteversion angle of 10° for radial clearance of 0.1 mm. The maximum equivalent plastic strain was predicted as 1.618×10^{-3} in this case (Figure 6.17).

Plastic deformation in the liner was observed during most of the activities (Figure 6.18). The maximum equivalent plastic strain in the liner was found to be affected synergistically by activities, cup angles and radial clearances (Figure 6.18). Normally, the maximum equivalent plastic strains in the liner during normal walking, ascending and descending stairs activities were larger than those during standing up, sitting down and knee bending activities. The maximum equivalent plastic strain in the liner with a radial clearance of 0.542 mm was predicted to be about 4-5 times that with a radial clearance of 0.1 mm.

The effect of cup angles on the equivalent plastic strain in the liner was dependent upon the radial clearances (Figure 6.18). For example, for the normal walking case, the maximum equivalent plastic strain in the liner was increased moderately first and then increased markedly when the cup inclination angles increased from 35º to 65º for large radial clearance of 0.542 mm and 0.3 mm. However, for radial clearance of 0.1 mm, the maximum equivalent plastic strain increased continually with increased cup inclination angle from 35º to 65º. For normal walking, ascending and descending stairs activities, the cup inclination angles were found to have most effect on the maximum equivalent plastic strain while for standing up, sitting down and knee bending cases, the cup anteversion angles were found to have dominating effect.
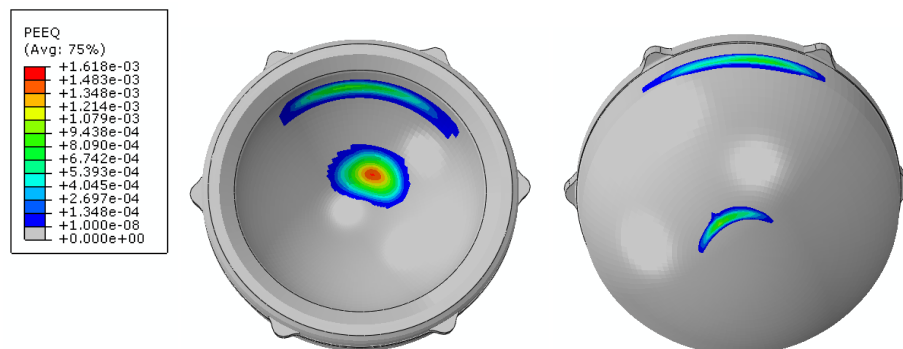
Figure 6.17 The equivalent plastic strain in the liner under cup inclination of 45º and anteversion of 10º in the instance of 17% of the cycle for normal walking (radial clearance: 0.3 mm).
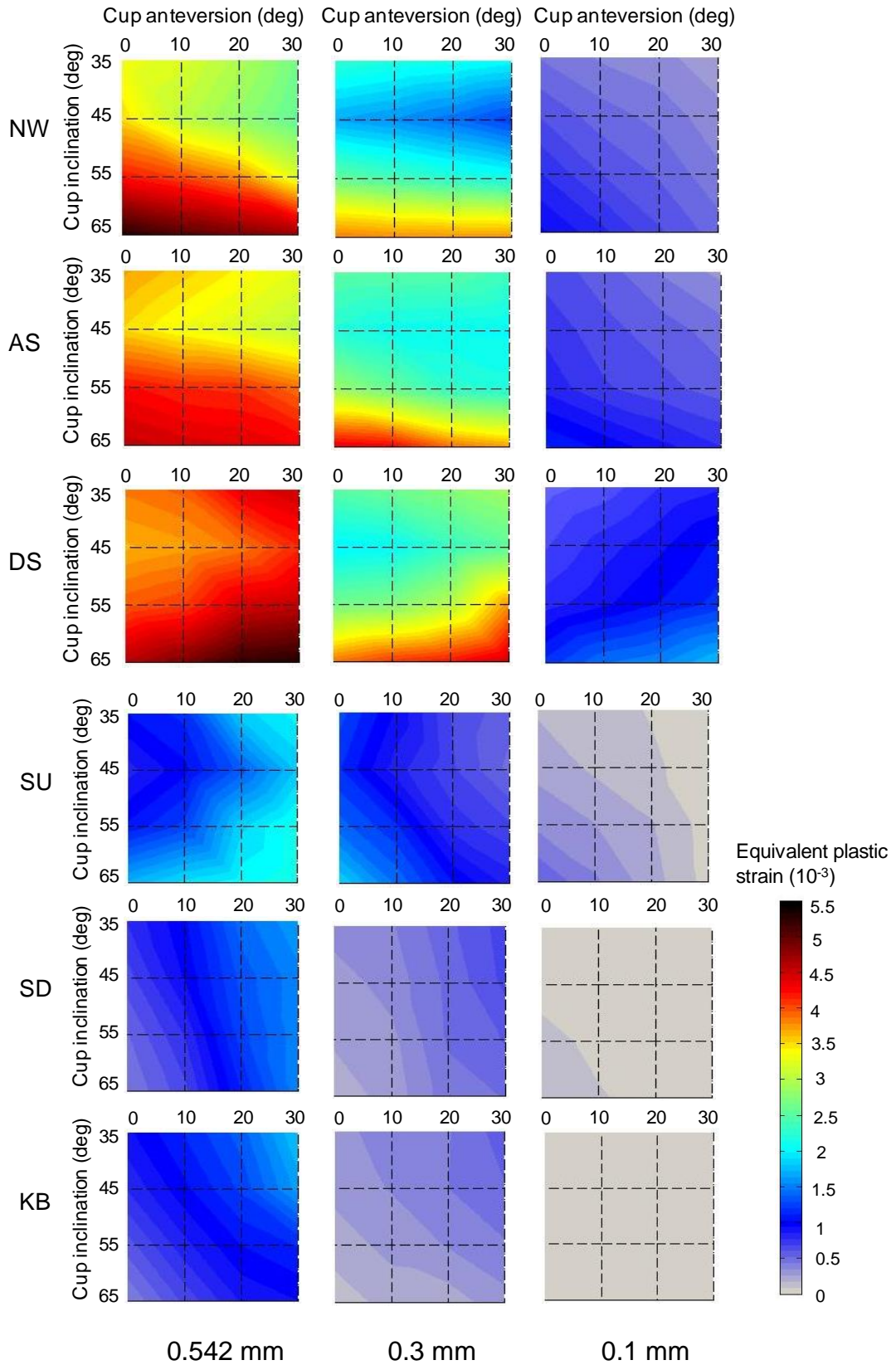
Figure 6.18 Peak equivalent plastic strain in the liner as a function of cup inclination angles and anteversion angles during different activities (NW: normal walking, AS: ascending stairs, DS: descending stairs, SU: standing up, SD: sitting down, KB: knee bending) for different radial clearances.

6.4 Discussion

The investigation of the contact mechanics for THR under different activities is very important because both the magnitude and direction of the contact forces vary during the cycle of the activities (Bergmann et al., 2001a). This variation in contact forces, together with the cup angles, were found to have a large effect on the contact mechanics of THRs, especially for modular THRs, where the gap between the metal shell and liner exists and the stiffness behind the liner in equatorial and spherical regions was different (Kurtz et al., 1997). This study aims to investigate the contact mechanics of modular THR during different daily activities and to examine the effect of the cup inclination and anteversion angles on the contact stresses on both the frontside and backside surface of liner for a modular THR. Particularly, the conditions under which edge loading occurred were predicted during different activities in this Chapter.

The gait analysis in this Chapter highlighted two aspects: first, the variation of the contact stresses on the frontside articulating surface of the liner followed that of hip contact forces in all activities considered, the magnitude of the maximum contact stress was found to be proportional to the applied hip contact force. Second, both the maximum von Mises stress in the liner material and the peak contact stress on the articulating surface showed their highest values for the stair descending case, when the implant was positioned at an anatomic position (i.e. inclination angle of 45⁰ and anteversion angle of 10⁰). This indicates that the descending stairs activity represented the worst case scenario among the six loading profiles examined in this Chapter. It should be noted that all the activities considered in this Chapter represented relatively mild conditions which would not cause adverse complications such as impingement and dislocation of the hip prostheses (Nadzadi et al., 2003; Stewart et al., 2004; Pedersen et al., 2005). However, they did represent the most frequent activities for human daily living (Bergmann et al., 2001a).

Edge loading of THRs has attracted more and more attention in biomechanical fields, especially for hard-on-hard bearings (Walter et al., 2004; Mellon et al., 2011; Elkins et al., 2012). The factors that cause the

edge loading have been identified and are generally associated with the component positions (such as cup angles, head offset/microlateralisation), prosthetic design (such as the radial clearance, cup coverage), impingement and activities (Fisher, 2011; Underwood et al., 2012). The edge loading that occurred on the articulating surface of the Pinnacle THR during routine activities was explored, and the effect of the cup inclination and anteversion, as well as the radial clearances on the occurrence of edge loading were examined in this study. The FE simulations showed that no edge loading was observed for the radial clearance of 0.542 mm for all activities and cup angles considered. However, for a radial clearance of 0.3 mm, edge loading did occur in some instances during normal walking, ascending and descending stairs activities under steep cup inclination angle conditions. Despite this, no edge loading was predicted for the remaining activity cases. This highlighted the contribution of the radial clearances, cup angles as well as the activities to the occurrence of the edge loading for modular THRs. The cup anteversion angles were found to have a crucial effect on the occurrence of edge loading as well. For example, for radial clearance of 0.3 mm under steep cup inclination angles of 65°, edge loading occurred over 40% of the cycle for normal walking under an anteversion angle of 0°, but reduced to 13% under an anteversion angle of 30°.

It is reassuring that the contact stresses in the articulating surfaces did not increase markedly even when the edge loading existed, which is markedly different from hard-on-hard articulations (Elkins et al., 2011; Sanders et al., 2011; Wang et al., 2012). This highlighted the robustness of the hard-on-soft articulations, which was less sensitive to the edge loading than hard-on-hard ones (Elkins et al., 2011; Wang et al., 2012). It is also indicated from the study that at the early stage after implantation of modular MoP, when the radial clearance was relatively large, edge loading would not be likely to occur. The radial clearance would then decrease during running-in and would increase the possibility of the occurrence of edge loading at this stage.

The analysis of the effect of cup angles on the contact stress on the articulating surface showed that the increase of the cup inclination angle seemed to induce decreased peak contact stress for larger radial clearances of 0.542 mm and 0.3 mm but increased stress for small radial clearance of

0.1 mm for most of activities. This was probably due to the fact that at lower cup inclination angle conditions, the peak contact stress was predicted along the direction of the applied load and mainly concentrated in the spherical area of the liner. However, with increased inclination angles, the peak contact stresses moved to the transition region between the spherical and equatorial areas. In this case, both spherical and equatorial regions would bear the peak contact stress, leading to an decrease of maximum contact stress (Figure 6.13). However, for the radial clearance of 0.1 mm, the contact areas were distributed on both equatorial and spherical regions for all cup inclination angle conditions. In this case, under steep cup inclination conditions, the peak contact stress was located in the equatorial region near the rim of the liner, where the stiffness behind the liner was larger than that in the spherical region, therefore leading to elevated stresses in this area. This indicated that at early stage of the hip implantation, the lower cup inclination was likely to produce higher stresses on the articulating surface for modular MoP THRs. However, the liner was expected to creep soon due to the high stresses, and the radial clearance would decrease markedly at the running-in stage, the lower cup inclination would then induce lower stress levels on the articulating surface at this stage. Therefore, the lower cup inclination would still be the recommendation for implant positioning for modular MoP THRs.

Edge loading would also occur at transition zone between the equatorial and spherical regions on the backside of the liner during all activities considered. The occurrence of the edge loading in this area was dependent upon the cup inclination and anteversion angles as well as the daily activities. Edge loading in this area was more inclined to occur at steep cup inclination angles. Different from the frontside articulating surface, the edge loading on the backside surface of liner would cause concentrated stresses, especially at steep cup inclination conditions. This is of significant interest as the damage and fracture of the liner would be induced by the high stress levels predicted in this area, which matched a retrieved case study that the rim of the liner was fractured at this location (Halley et al., 2004). However, it is expected that the local high stress levels predicted in this area represent

uniquely high values in this study, which would likely soon be reduced by creep at those locations.

Another noticeable observation in the present study was that concentrated stress was also predicted on the backside surface in the surrounding of the hole of the metal shell (Figure 6.11). The concentrated stress in this area was found to occur at lower cup angles, and was 2.5-3 times the value found for steep cup inclination angles. This increased contact stress in the surrounding of the hole of the metal shell would induce more backside wear, which was believed to aggravate the process of loosening of the hip implants, as debris generated at this location has direct access to subchondral bone through the dome holes (Kurtz et al., 1999; Krieg et al., 2009). This direct access may contribute to an increased prevalence of acetabular osteolysis around modular cups with holes (Kurtz et al., 1999; Young et al., 2002).

For all conditions and activities considered, the equivalent plastic strain was observed to increase with increased cup inclination angles. In particular, there was a substantial increase in the equivalent plastic strain for cup inclination angle of 65°. It is expected that the polyethylene would then creep due to the plastic deformation of the liner, leading to the decreased stress in the liner. Even though, the severe plastic deformation was still predicted under steep cup inclination angle conditions. Therefore, it is indicated that the positioning of the component is important clinically to avoid severe plastic deformation of the liner which is inclined to occur under steep cup inclination angle conditions.

Radial clearances of 0.542 mm, 0.3 mm and 0.1 mm were modelled in the present study. However, it should be noted that the larger radial clearance of 0.542 mm was modelled to represent the tolerance stack dimensional conditions while the smaller radial clearance of 0.1 mm was modelled to imply the joint replacements under steady-state stage after the running-in process. The present study suggests that the modular MoP THRs show different behaviour and sensitivity to the cup angles at different stages of the application of the THR. When the radial clearance decreased to 0.1 mm due to the creep and wear of the polyethylene liner, this study predicted that lower contact stresses occur under lower cup inclination angles compared to

steeper cup inclination angles, indicating that the lower cup angle remains a recommendation for implant positioning of the modular THRs.

6.5 Summary

The investigation of contact mechanics of Pinnacle THR under different daily activities has been conducted and the effect of cup inclination and anteversion angles on the contact mechanics for Pinnacle THR have been assessed in this Chapter. The following conclusions can be drawn from this study:

1. Both the peak contact stress on the frontside articulating surface and the backside shell/liner interface at the equatorial region showed the same time-dependent trend to the hip contact forces. The maximum values of peak von Mises stress in the liner material and contact stress on the frontside articulating surface were predicted to be the highest for cases of ascending and descending stairs, indicating that these two activities represent the worst case scenarios among the six loading profiles examined in this study.

2. The contact mechanics of the Pinnacle THR were found to be sensitive to the cup inclination angles and anteversion angles, as well as the type of daily activity.

3. Edge loading on the frontside articulating surface occurred during the activities of normal walking, and ascending and descending stairs when steep cup angles and a small radial clearance were considered. However, under all conditions considered, no edge loading was observed during standing up, sitting down and knee bending cases. Despite this, no significant increase in contact stresses was observed even when edge loading occurred.

4. Edge loading at the transition zone between the equatorial and spherical region at the backside of the liner also occurred during all activities considered, leading to a region of concentrated stress at this location.

5. Concentrated stresses on the backside surface of the liner in the surrounding of the hole of the metal shell were also observed, which would induce more backside wear at this location.

Chapter 7
Contact Mechanics Analysis of Pinnacle THR Under Microseparation Conditions: Effect of Cup Angles and Head Lateral Microseparation

7.1 Introduction

Edge loading has been one of the main concerns for THRs today, particularly for hard-on-hard articulations. It has been identified as an adverse factor that can negatively affect the biomechanics and long-term performance of THRs (Angadji et al., 2009; Harris, 2012; Elkins et al., 2012; Underwood et al., 2012). Edge loading can be caused by many factors, including the rotational and translational mal-positioning of components which have been recognized as two of the main reasons (Fisher, 2011). The rotational mal-positioning of the component is defined as the steep inclination and excessive anteversion of the acetabular component clinically and the translational mal-positioning of the component is classified as the microseparation of the centres of the head and cup, and has been demonstrated and recognized *in vivo* during gait (Dennis et al., 2001; Glaser et al., 2008). The microseparation occurs during the swing phase in the direction along the axis of the cup and has been associated with different factors such as laxity of the joint/soft tissues, femoral head offset deficiency or medialised cups (Nevelos et al., 2000). When a load is applied at heel strike, the femoral head is moved up and contacts the rim of the acetabular cup, leading to edge contact between the femoral head and rim of the acetabular cup and can have significant consequences on wear and biomechanics of the THRs (Nevelos et al., 2001a; Leslie et al., 2009).

The effect of edge loading on the biomechanics and performance of hard-on-hard articulations has been documented, as reviewed in **Section 1.4.5** (Manaka et al., 2004; Williams et al., 2006; Leslie et al., 2009; Al-Hajjar et al., 2010; Al-Hajjar et al., 2013). Edge loading can produce high rates of wear and high metal ions in the blood for MoM bearings (De Haan et al., 2008; Langton et al., 2008; Hussain et al., 2010), and high wear rates, stripe wear and fracture of the components as well as the squeaking of the implants for

CoC articulations (Stewart et al., 2001; Lusty et al., 2007; Jarrett et al., 2009; Restrepo et al., 2010). However, for MoP THRs, limited work has been done (Besong et al., 2001a; Netter et al., 2013). The limited experimental work to date with CoP bearings, does not indicate an increase in surface wear when inferior and lateral translations of 0.7 mm were introduced (Williams et al., 2003). However, for MoP hip prostheses, the average separation of the femoral head and acetabular cup during gait has been reported to be up to 2 mm (Lombardi et al., 2000; Dennis et al., 2001). This microseparation would produce concentrated stresses in the acetabular component and hence cause fatigue and damage of the soft material (Besong et al., 2001a). Despite this, the biomechanical behaviour of the hard-on-soft bearings under microseparation conditions is actually not clear and not extensively understood. Besides, the effect of edge loading on the contact mechanics and biomechanics of MoP THRs, especially for modular MoP THRs has not been comprehensively investigated. Therefore, the aim of the present study was to investigate the effect of cup angles and microseparation on the edge loading and contact mechanics of a current MoP modular THR using 3D anatomic Pinnacle THR model.

7.2 Materials and Methods

The Pinnacle THR used in **Chapter 6** was considered in this Chapter in order to predict the contact stresses and contact areas under an ideal centred regime and then under microseparation conditions. The effect of cup inclination angles and head lateral microseparation distances on contact mechanics of the Pinnacle THR were investigated.

The geometries and structures of the components for the Pinnacle THR have been described in **Chapter 2**. The nominal diameters of the femoral head and inner surfaces of the polyethylene liner were 36 mm and 36.6 mm respectively. The outer diameter of the acetabular component was assumed to be 54 mm. In order to examine the effect of the radial clearances, radial clearances of 0.542 mm and 0.1 mm were also considered in this Chapter.

The anatomic Pinnacle THR model was developed, as shown in Figure 2.7 and 2.9. The FE modelling processes, including the mechanical properties of

the components, the boundary conditions and meshing, as well as the mesh sensitivity analysis were described in **Chapter 2**. The FE analysis was performed with the ABAQUS software package (Version 6.9, Dassault Systèmes Simulia Corp., Providence, United States). A static analysis was used in the present study. Two steps were undertaken during the analysis: in the first step, a lateral displacement of the femoral head was performed to achieve a microseparation, in the second step, a specific load was applied through the centre of the head and vertically upwards onto the liner, as shown in Figure 7.1.
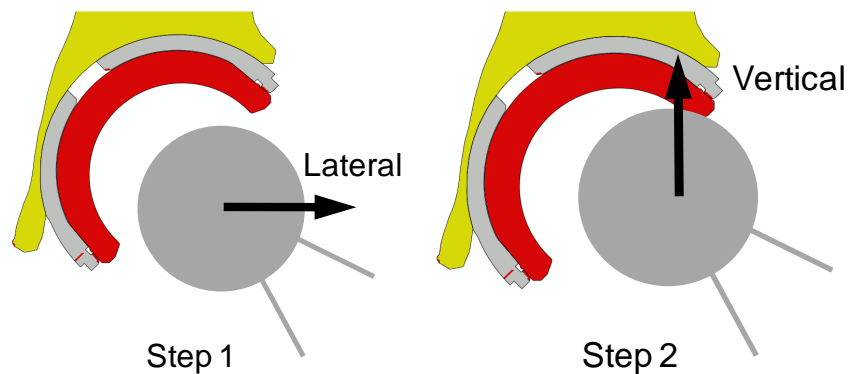
Figure 7.1 Schematic diagram shows the two steps used during the analysis in the study: the lateral displacement of the head was achieved in the first step and vertical load was applied in the second step.

A vertical load of 2,500 N, corresponding to about 3-4 times BW for an average weight (Bergmann et al., 2001), was applied through the centre of the femoral head. Four cup inclination angles, with inclination angles varying between 35⁰ and 65⁰ in 10⁰ increments, and 13 microseparation distances of 0 µm, 60 µm, 100 µm, 150 µm, 200 µm, 240 µm, 300 µm, 400 µm, 500 µm, 800 µm, 1000 µm, 1500 µm and 2000 µm were considered in this Chapter. The microseparation distance of the femoral head was defined as the lateral displacement of the femoral head from the centre of rotation of the acetabular cup, as shown in Figure 7.2.
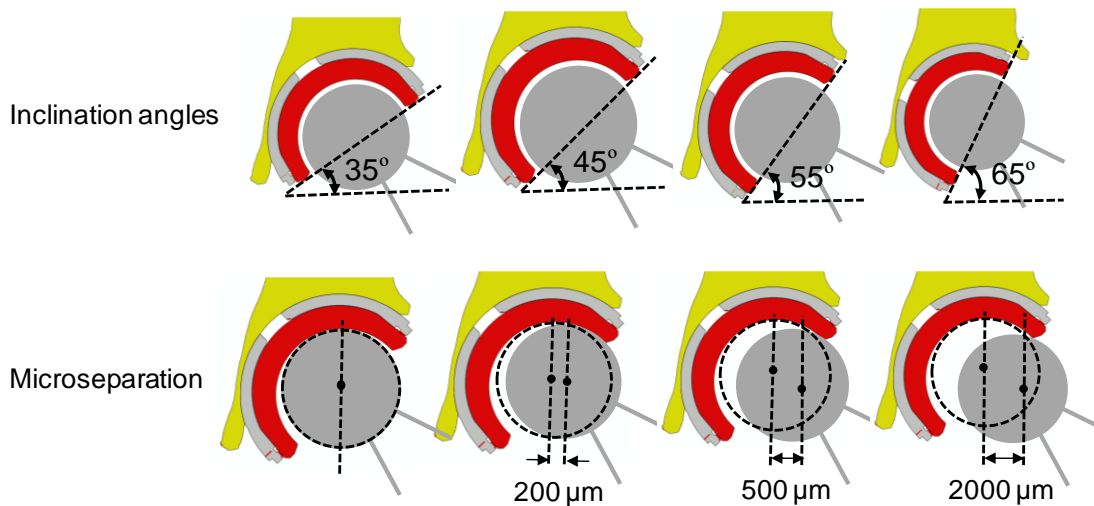
Figure 7.2 The definition of cup inclination angles and microseparation distances of the head, 4 orientation of cup inclination and 13 microseparation distances were considered in the present study.

7.3 Results

7.3.1 Contact Mechanics Analysis Under Cup Inclination Angle of 45º

Under standard conditions (no microseparation), the contact area was located about the superior region of the liner and the contact patch was within the inner surface of the liner. The contact areas were then moved towards the edge of the liner when the microseparation distances increased (Figure 7.3). When the microseparation distance increased to 100 μm, the femoral head was found to contact with the rim of the liner and edge loading occurred. A stripe shape contact area was observed around the rim of the liner when the microseparation distance was over 800 μm (Figure 7.3).

Under standard conditions, the maximum von Mises stress in the liner and peak contact pressure on the articulating surface were predicted as 11.71 MPa and 12.98 MPa respectively, and were increased by about 22% and 21% respectively when a microseparation distance of 150 μm was introduced (Figure 7.4). The maximum von Mises stress and peak contact pressure under a microseparation distance of 2000 μm were found to be more than four times that under standard conditions. The contact area under standard conditions was predicted to be ~504 mm^2 and decreased substantially by

~78% under a microseparation distance of 2000 μm. It is interesting to note that the contact area tended to converge to an asymptotic value of ~140 mm^2 when the microseparation distance increased to 2000 μm.
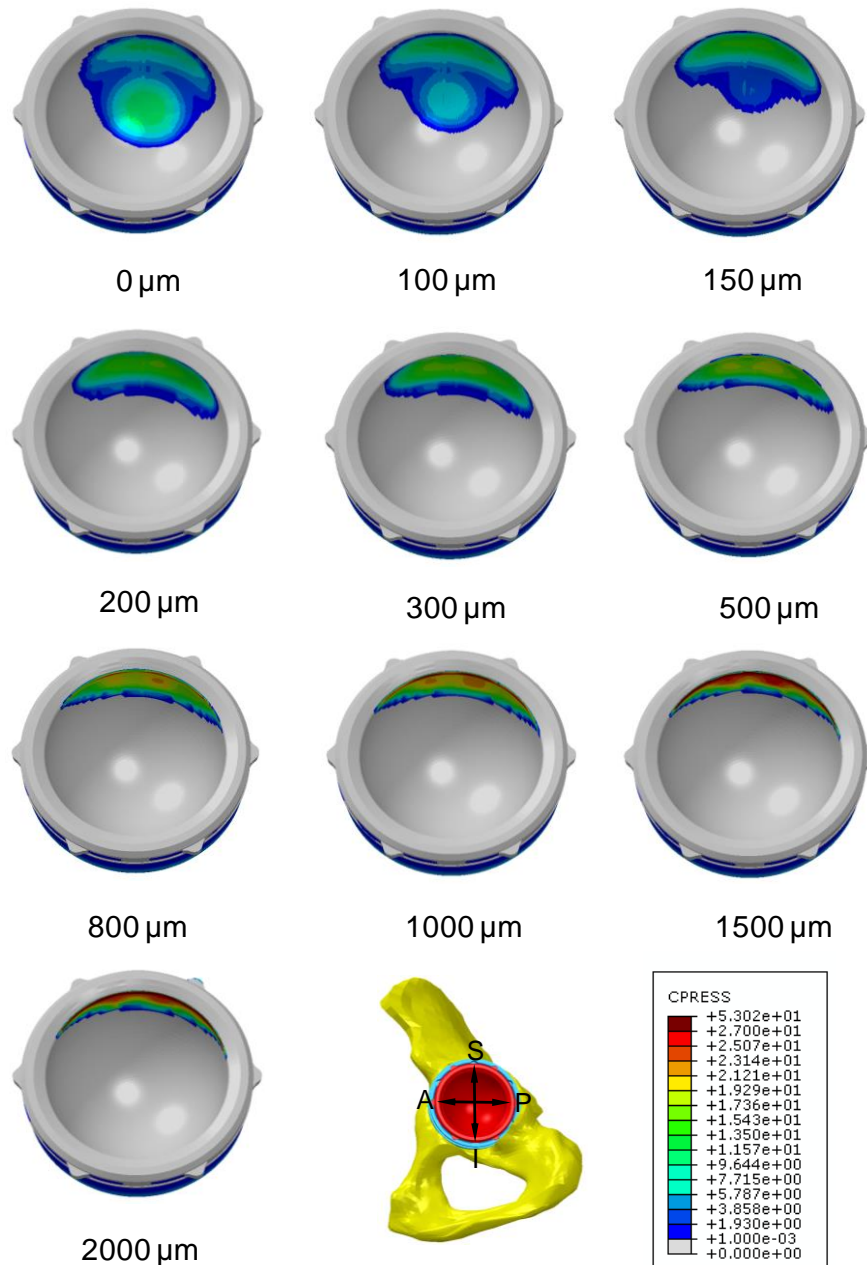
Figure 7.3 The distribution of predicted contact pressures (MPa) on the articulating surfaces for different microseparation distances under a cup inclination angle of 45⁰ for a radial clearance of 0.3 mm. Contact areas moved to the rim of the liner as the microseparation distances increased.
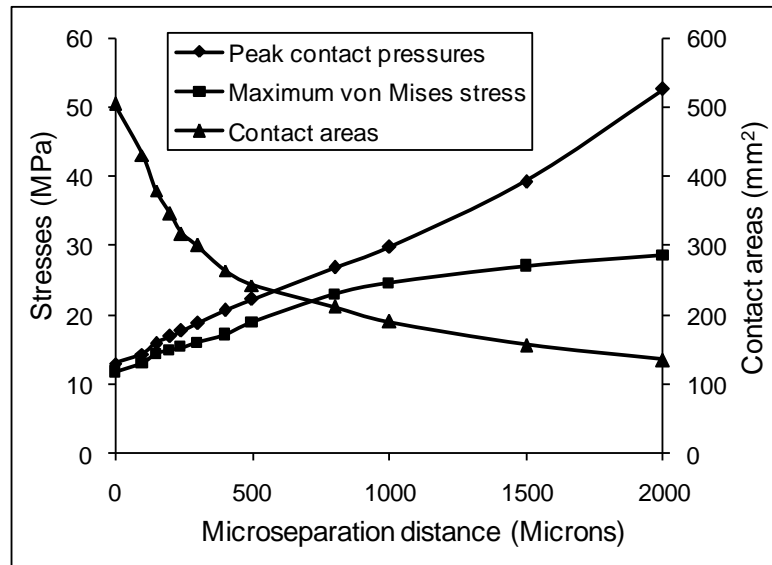
Figure 7.4 The predicted maximum von Mises stresses (MPa) in the liner, the predicted peak contact pressures (MPa) and contact areas on the articulating surfaces for different microseparation distances.

7.3.2 Effect of Cup Inclination Angles and Head Lateral Microseparation Distances on Von Mises Stresses and Frontside Contact Stresses

Under standard conditions, the areas of contact were located about the superior region of the liner for all cup inclination angle conditions. However, the areas were closer to the edge of the liner for steep cup inclination angles. The areas of contact were then moved towards the edge of the liner for all cup inclination angle conditions when the microseparation distances were increased, and finally converged to a stripe shape in the surrounding of the rim of the liner (Figure 7.5).

Edge loading was observed under microseparation conditions at certain microseparation levels (Figure 7.5). The occurrence of edge loading was found to be strongly dependent upon the cup inclination angles and radial clearances (Table 7.1, Table 7.2 and Table 7.3). For example, for a radial clearance of 0.542 mm, edge loading occurred initially at a microseparation distance of 300 μm for a cup inclination angle of 35° but 200 μm for cup inclination angle of 65°. For a cup inclination of 35°, the microseparation distances that caused the initial occurrence of edge loading were 300 μm, 200 μm and 60 μm for radial clearances of 0.542 mm, 0.3 mm and 0.1 mm

respectively (Table 7.1, Table 7.2 and Table 7.3). No substantial elevation of the peak contact stress was observed at the initial occurrence of edge loading. However, the peak contact stresses increased continuously when the microseparation distances increased.
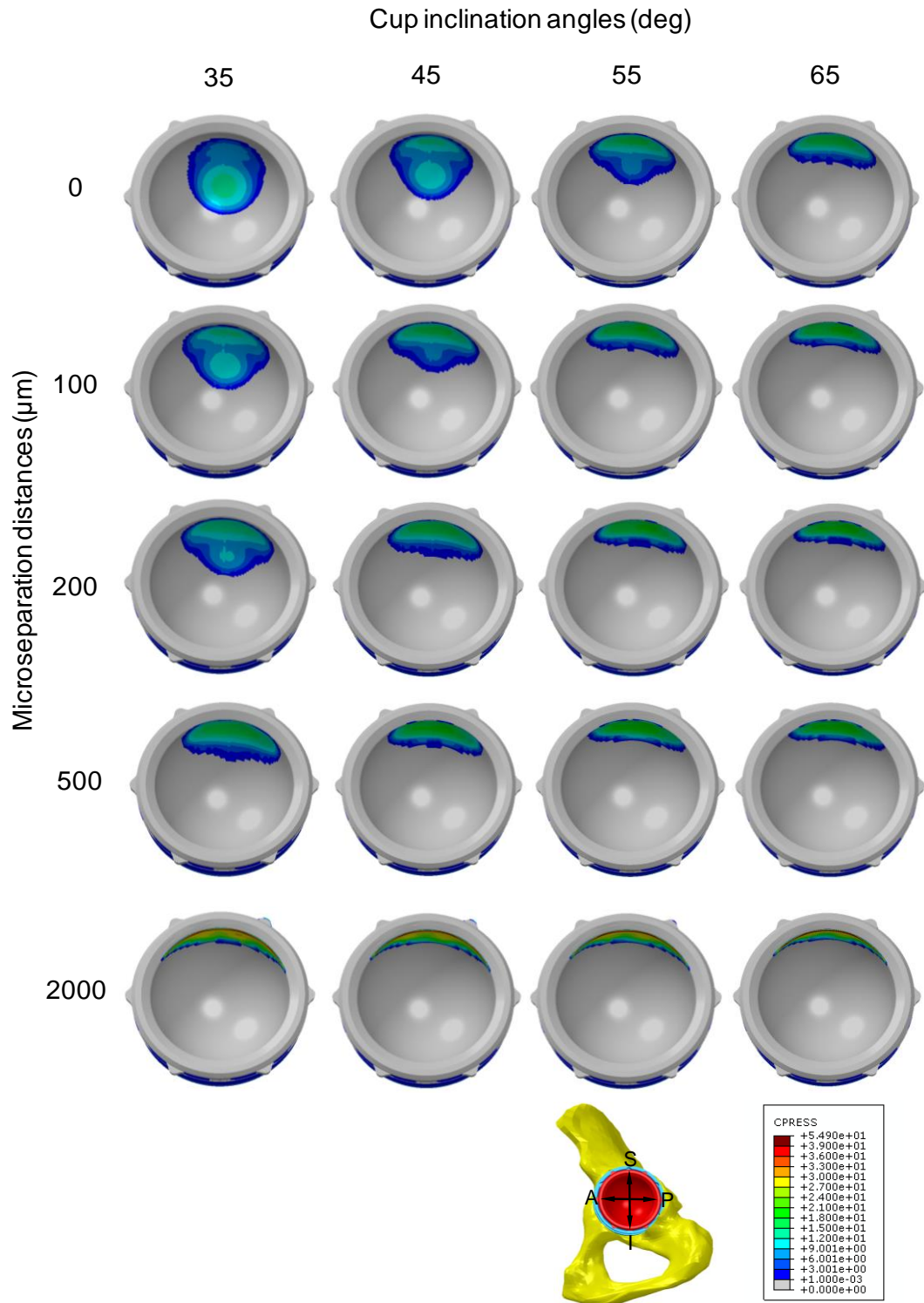
Figure 7.5 The distribution of contact stresses on the frontside articulating surface as a function of cup inclination angle and microseparation distance for a nominal radial clearance of 0.3 mm.

Table 7.1 The peak contact stresses (MPa) and edge loading states for different cup inclination angles and microseparation distances for radial clearance of 0.542 mm. The shadow in the table represents the occurrence of edge loading.

	Cup inclination angles (deg)			
	35	**45**	**55**	**65**
Microseparation (µm)				
0	13.77 (no edge contact)	13.94 (no edge contact)	16.6 (no edge contact)	18.09 (no edge contact)
200	13.92 (no edge contact)	16.72 (no edge contact)	18.95 (no edge contact)	22.05 (edge contact)
240	14.26 (no edge contact)	17.25 (no edge contact)	20.59 (edge contact)	22.9 (edge contact)
300	15.28 (edge contact)	19.3 (edge contact)	21.85 (edge contact)	24.11 (edge contact)
400	17.65 (edge contact)	20.61 (edge contact)	22.84 (edge contact)	25.01 (edge contact)
500	19.22 (edge contact)	21.71 (edge contact)	23.99 (edge contact)	25.98 (edge contact)

Table 7.2 The peak contact stresses (MPa) and edge loading states for different cup inclination angles and microseparation distances for radial clearance of 0.3 mm. The shadow in the table represents the occurrence of edge loading.

	Cup inclination angles (deg)			
	35	**45**	55	65
Microseparation (µm)				
0	10.75 (no edge contact)	12.98 (no edge contact)	15.08 (no edge contact)	16.77 (edge contact)
60	11.35 (no edge contact)	13.96 (no edge contact)	15.8 (edge contact)	18.51 (edge contact)
100	12.06 (no edge contact)	14.32 (no edge contact)	17.09 (edge contact)	19.03 (edge contact)
150	12.63 (no edge contact)	15.86 (edge contact)	18.13 (edge contact)	19.94 (edge contact)
200	14.02 (edge contact)	16.86 (edge contact)	19.09 (edge contact)	20.62 (edge contact)
240	14.74 (edge contact)	17.61 (edge contact)	19.95 (edge contact)	21.3 (edge contact)
300	15.91 (edge contact)	18.72 (edge contact)	20.84 (edge contact)	22.3 (edge contact)

Table 7.3 The peak contact stresses (MPa) and edge loading states for different cup inclination angles and microseparation distances for radial clearance of 0.1 mm. The shadow in the table represents the occurrence of edge loading.

Microseparation (µm)	Cup inclination angles (deg)			
	35	45	55	65
0	10.06 (no edge contact)	12.61 (no edge contact)	14.52 (no edge contact)	17.18 (no edge contact)
30	10.85 (no edge contact)	13.21 (no edge contact)	15.20 (edge contact)	18.05 (edge contact)
60	11.69 (edge contact)	14.02 (edge contact)	16.59 (edge contact)	18.95 (edge contact)
100	12.58 (edge contact)	15.65 (edge contact)	18.01 (edge contact)	19.8 (edge contact)
150	13.78 (edge contact)	17.15 (edge contact)	19 (edge contact)	20.67 (edge contact)
200	15.36 (edge contact)	18.37 (edge contact)	19.9 (edge contact)	21.81 (edge contact)

For all cup inclination angles considered, the maximum von Mises stresses in the liner increased markedly by ~67.5%-157.9%, ~87.7%-159.6% and ~74.1%-178.4% for radial clearances of 0.542 mm, 0.3 mm and 0.1 mm respectively when the microseparation distances increased to 1500 μm (from standard conditions) (Figure 7.6). Correspondingly, the peak contact stresses on the frontside articulating surface increased substantially by ~124.3%-161.6%, ~134.5%-255.6% and ~141.9%-290.1% for the three radial clearances respectively (Figure 7.7).

With increased cup inclination angles from 35⁰ to 65⁰, both the maximum von Mises stress and peak contact stress increased as well. However, this increase in von Mises stresses and contact stresses induced by higher cup inclination angles became negligible as the microseparation distance increased (Figure 7.7).

For all cup inclination angles considered, the contact areas on the frontside articulating surface were decreased markedly as the microseparation distance increased to 1000 μm, and slightly decreased to an asymptotic value of ~140-150 mm^2 for three radial clearances. Similarly to the stresses, the difference of contact areas induced by variation of cup inclination angles were found to decreased as microseparation distances increased (Figure 7.8).
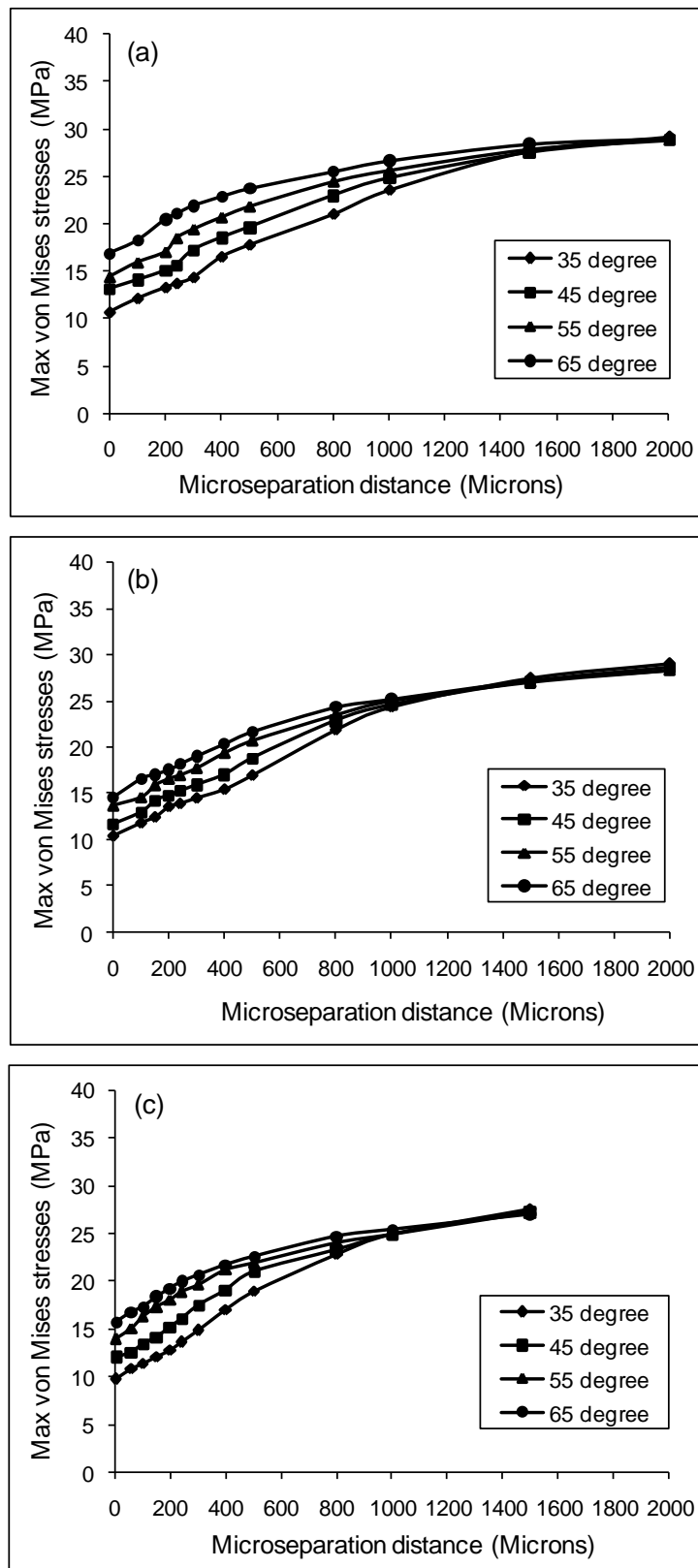
Figure 7.6 The variation of the maximum von Mises stresses (MPa) in the liner against cup inclination angle and microseparation distance for different radial clearances of (a) 0.542 mm, (b) 0.3 mm, (c) 0.1 mm.
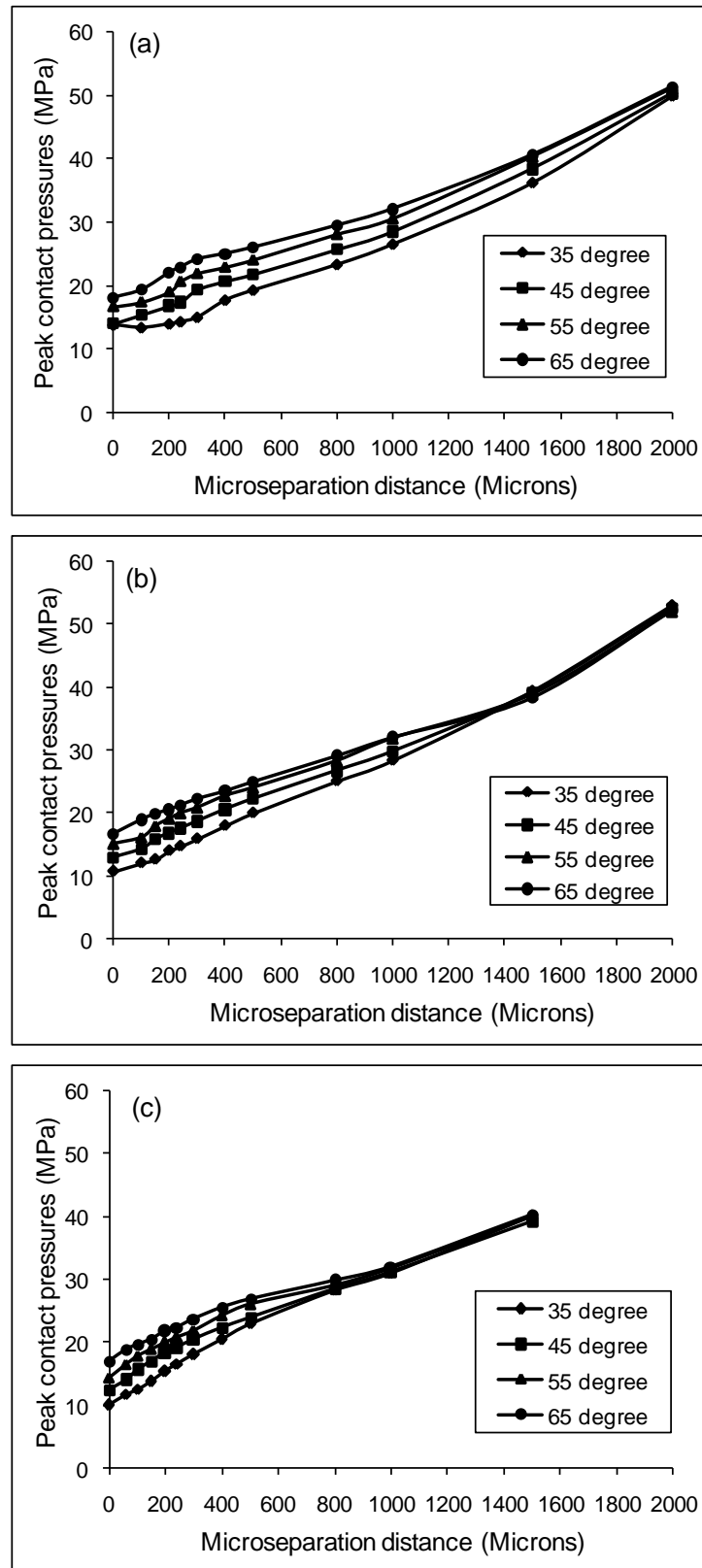
Figure 7.7 The variation of the peak contact pressure (MPa) on the articulating surfaces against cup inclination angle and microseparation distance for different radial clearances of (a) 0.542 mm, (b) 0.3 mm, (c) 0.1 mm.
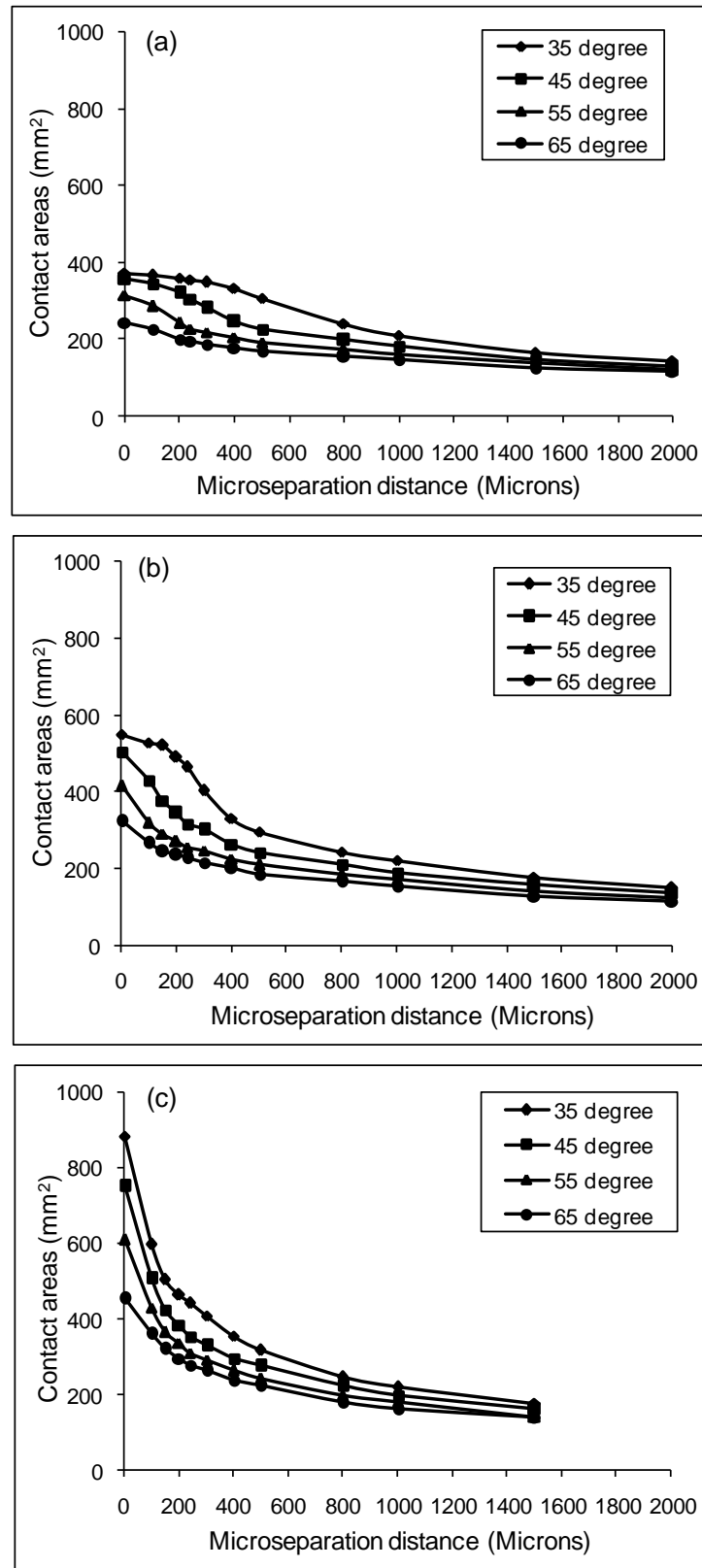
Figure 7.8 The variation of the contact areas (mm^2) on the articulating surfaces against cup inclination angle and microseparation distance for different radial clearances of (a) 0.542 mm, (b) 0.3 mm, (c) 0.1 mm.

7.3.3 Effect of Cup Inclination Angles and Head Lateral Microseparation on Backside Contact Stresses and Shear Stresses

For all cup inclination angles considered, the maximum contact stress on the backside surface of the liner increased markedly by ~90.6%-217.2%, ~117.4%-249.7% and ~119.2%-333.6% for radial clearances of 0.542 mm, 0.3 mm and 0.1 mm respectively when the microseparation distances increased to 1500 μm (from standard conditions) (Figure 7.9). Correspondingly, the peak shear stress at the shell/liner interface increased substantially by ~97.2%-179.1%, ~86.7%-135.3% and ~97.2%-122.2% for the three radial clearances respectively (Figure 7.10).

Both the peak contact stress on the backside surface of the liner and shear stress at the shell/liner interface increased with increased cup inclination angles under standard conditions and microseparation conditions. However, the difference of the backside contact stresses and shear stresses induced by the variation of cup inclination angles became insignificant when the microseparation distances increased to 1500 μm (Figure 7.9 and Figure 7.10).
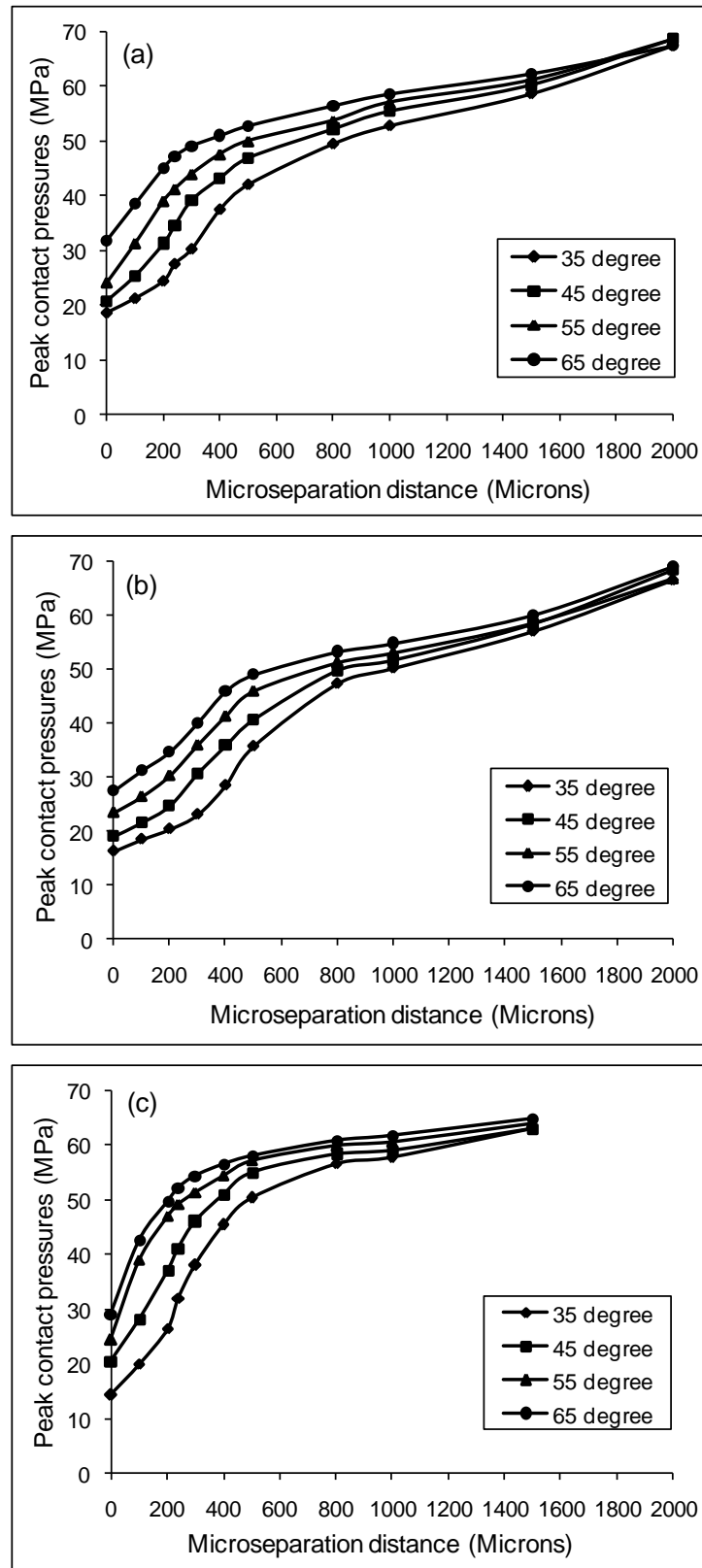
Figure 7.9 The variation of the peak contact pressure (MPa) on the backside surface of liner against cup inclination angle and microseparation distance for different radial clearances of (a) 0.542 mm, (b) 0.3 mm, (c) 0.1 mm.
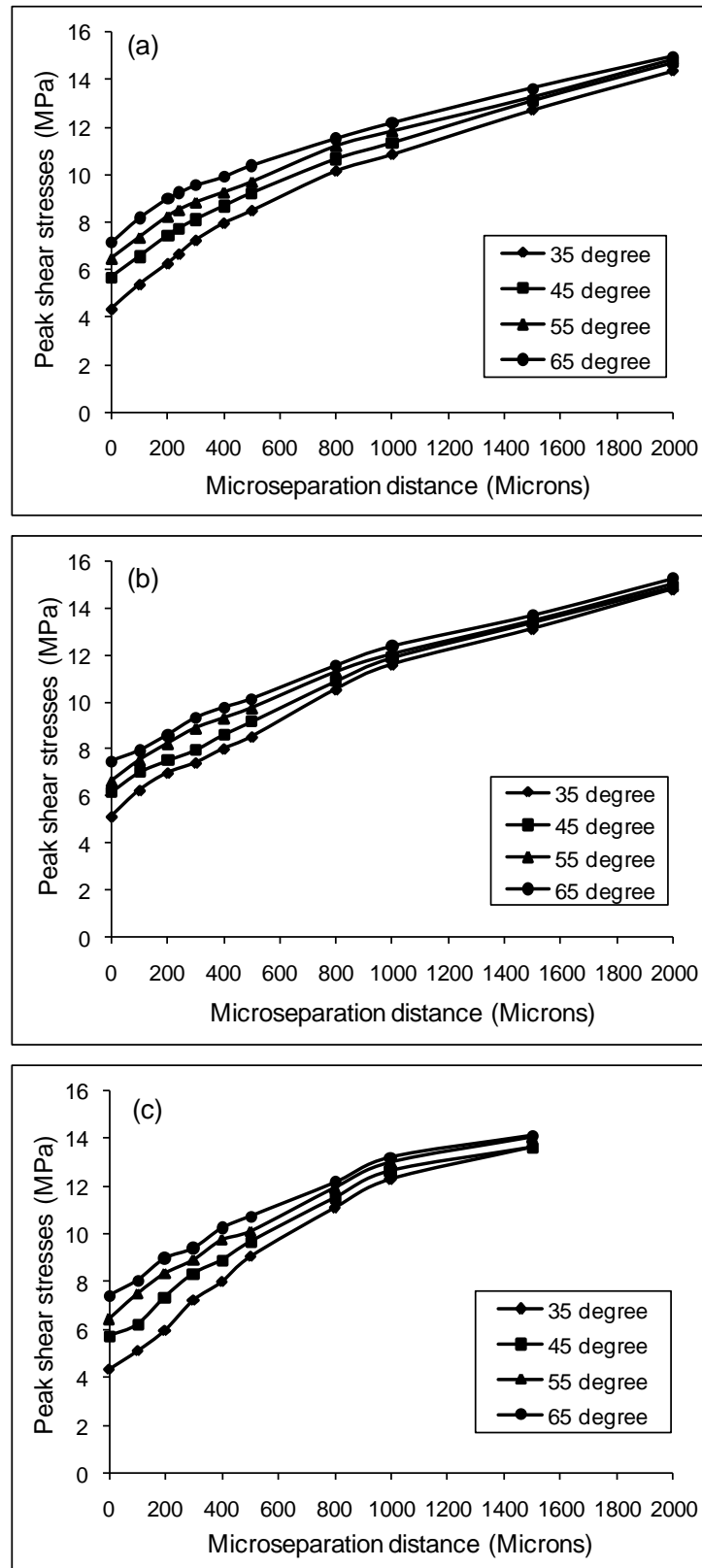
Figure 7.10 The variation of the peak shear stress (MPa) at the shell/liner interface against cup inclination angle and microseparation distance for different radial clearances of (a) 0.542 mm, (b) 0.3 mm, (c) 0.1 mm.

7.3.4 Effect of Cup Inclination Angles and Head Lateral Microseparation on Plastic Strain

Plastic deformation in the liner was observed for both standard conditions and microseparation conditions. The maximum equivalent plastic strain in the liner with radial clearance of 0.3 mm was predicted to be 21×10^{-3} for cup inclination angle of 45° at microseparation distance of 500 µm (Figure 7.11).

For all cup inclination angles considered, the maximum equivalent plastic strain in the liner increased substantially with increased microseparation distances (Figure 7.12). The maximum equivalent plastic strain in the liner was predicted to be around 10×10^{-3} under standard conditions, and increased markedly to around 60×10^{-3} when the microseparation distance increased to 1500 µm (Figure 7.12).
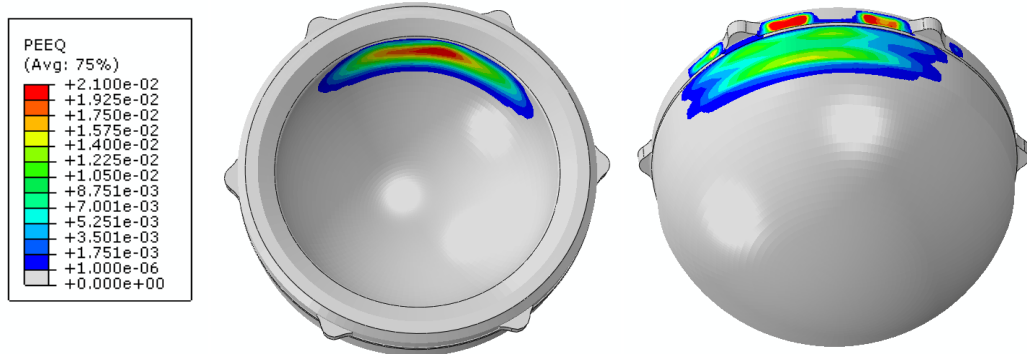
Figure 7.11 The equivalent plastic strain in the polyethylene liner under cup inclination angle of 45° and at microseparation distance of 500 µm (Radial clearance: 0.3 mm).
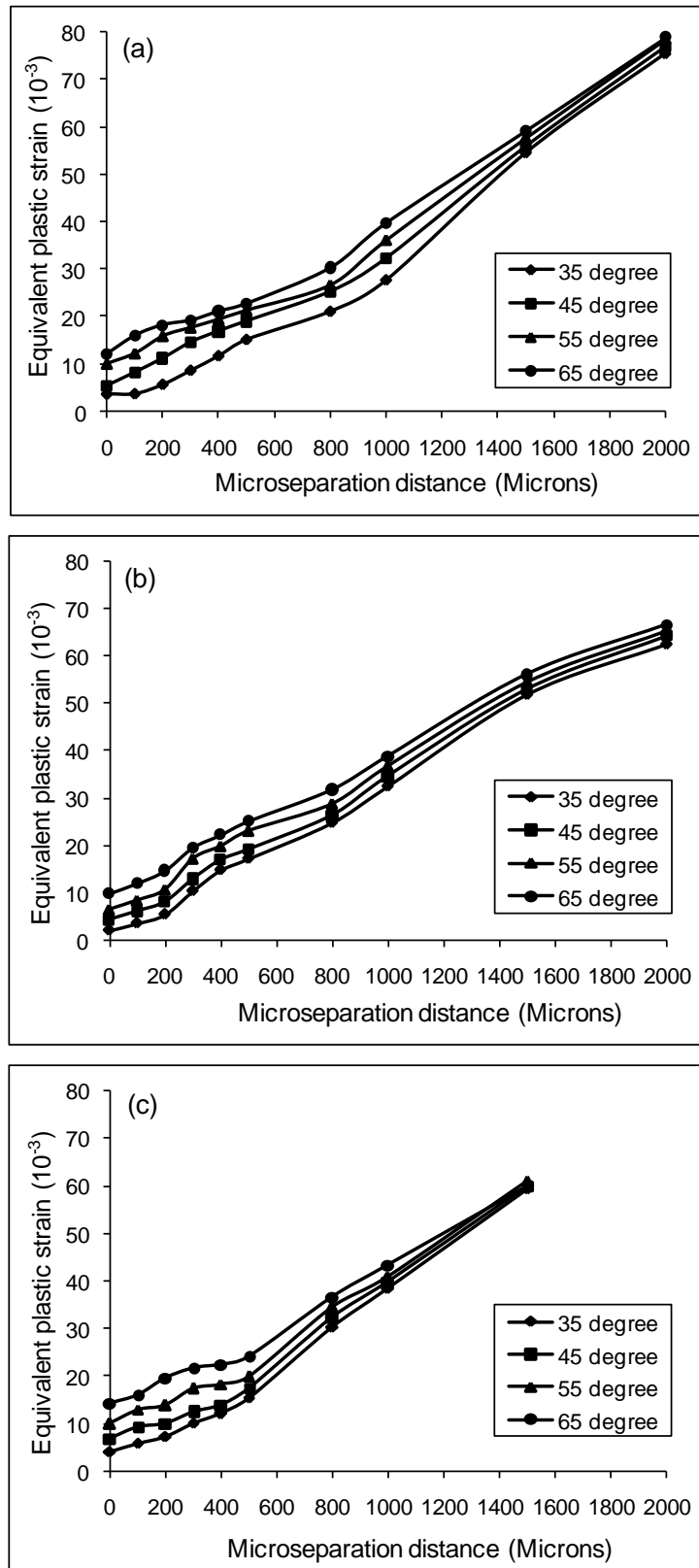
Figure 7.12 The variation of the peak equivalent plastic strain in the liner against cup inclination angle and microseparation distance for different radial clearances of (a) 0.542 mm, (b) 0.3 mm, (c) 0.1 mm.

7.4 Discussion

Current adverse tissue responses in MoM THRs and the presence of squeaking and stripe wear in CoC THRs have evoked interest in edge loading in these hard-on-hard articulations (Manaka et al., 2004; Williams et al., 2006; Leslie et al., 2009). Indeed, edge loading as an adverse condition which would cause accelerated wear and major clinical problems of the hip prostheses have been widely investigated for hard-on-hard articulations (Willert et al., 2005; Restrepo et al., 2010; Walter et al., 2010). However, for hard-on-soft combinations, limited work has been done and the effect of edge loading on the behaviour of these combinations deserves further attention. The aims of the present study were therefore to focus on edge loading in a current modular MoP THR, and to examine the effect of cup inclination angles and microseparation on the edge loading and contact mechanics of a current modular MoP THR.

This study showed that the microseparation distances required for generation of edge loading depended upon the cup inclination angles and radial clearances. In order to illustrate this, a mathematic analysis was carried out to determine the condition when microseparation leads to edge loading and how the microseparation distances that caused initial edge loading were related to the cup inclination angles and radial clearances, based on a simple 2D model, as shown in Figure 7.13.

The mathematic analysis showed that the theoretical lateral displacement of the head required for generation of edge loading decreased as the cup inclination angles increased and radial clearances decreased (Figure 7.14). Indeed, the theoretical microseparation distances that required for the generation of edge loading was 410 μm for a cup inclination angle of 35⁰ and radial clearance of 0.542 mm, and just 42 μm for a cup inclination angle of 65⁰ and radial clearance of 0.1 mm.
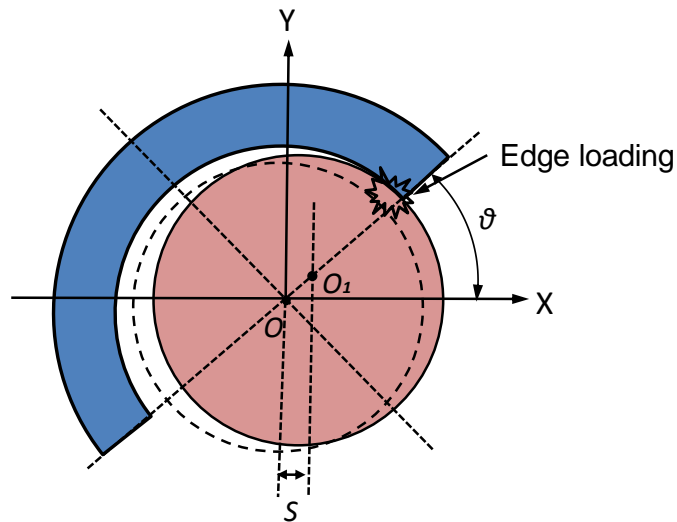
$$S = OO_1 * \cos\theta$$
$$= c * \cos\theta \tag{7.1}$$

Where c: radial clearance

θ: cup inclination angle

Figure 7.13 Simple 2D model of calculation of the microseration distances required for edge loading generation based on the geometry of the THR.
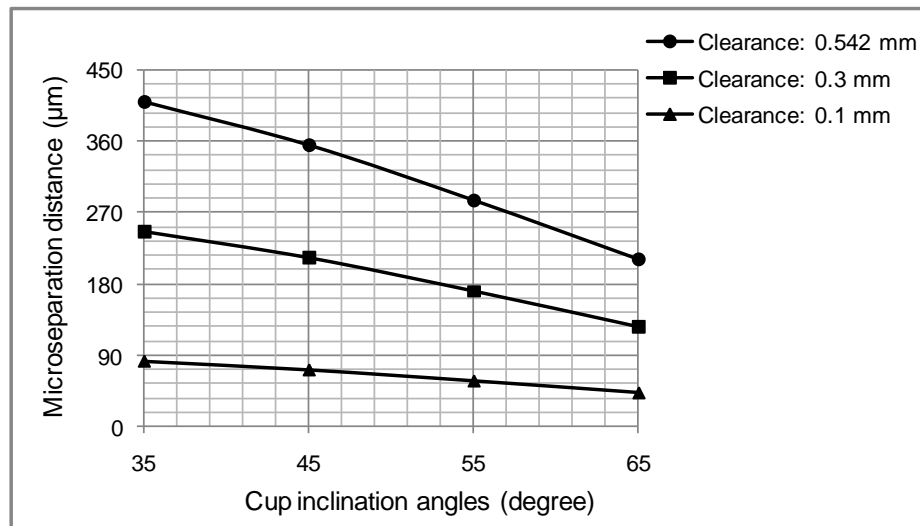
Figure 7.14 The microseparation distances required for edge loading generation as a function of cup inclination angle and radial clearance.

The results predicted by the FE simulations were consistent with this theoretical mathematic analysis. Both FE prediction and mathematical analysis showed that with increased cup inclination angles, the

microseparation distances required to generate the edge loading decreased, suggesting that a steep cup inclination angle potentially facilitates the occurrence of edge loading due to the head lateral microseparation. This therefore highlighted the relatively increased instability of the hip prostheses with steep cups *in vivo*. From another point of view, for a given microseparation distance, the component with a steep cup inclination angle was more inclined to suffer from edge loading. This was found to be consistent with the previous clinical studies, indicating that the cups positioned with high inclination angles tend to suffer from edge loading (Nevelos et al., 1999; Nevelos et al., 2000).

It is interesting to note that the maximum contact pressures on the bearing surface for articulation with radial clearance of 0.1 mm was found to be lower under standard conditions but a little higher under microseparation conditions (with microseparation distance of 1500 μm) compared to that with radial clearance of 0.542 mm. This can be explained from two competing factors. Under standard conditions, the bearing with smaller clearances has more conformity between the femoral head and acetabular cup, therefore leading to decreased contact pressure. However, under larger microseparation conditions, the liner with smaller clearances subjects to more lateral load under the same microseparation distances compared to the bearing with larger clearances, making the contact between the femoral head and liner more lateral and edge loading on the bearing surface more severe. The more severe edge loading would result in increased contact pressure on the bearing surface.

The contact areas on the articulating surface were located about the superior region of the liner under standard conditions, and were found to centralize at the rim of the liner when the microseparation distances were larger than 800 μm, leading to a stripe contact area at the rim of the liner and elevated stresses at this area. This elevation of the stresses would cause severe plastic deformation at this area. Indeed, the FE predictions from this study have shown that plastic deformation occurred in the liner under both standard conditions and microseparation conditions. However, there was a rapid increase in the equivalent plastic strain when the microseparation distances were over 500 μm. This substantial increase in the equivalent

plastic strain indicated that severe plastic deformation of the liner occurred when the microseparation distances increased. The severe plastic deformation at the rim of the liner would lead to the weakness of the mechanical properties of the material at this area in terms of elastic modulus and yield stress, making the material of the liner more susceptible to fatigue. The plastic deformation at the rim of the liner would also induce pitting and delamination of the surface at this area, leading to the fatigue damage and fracture of the material, which has been observed in an *in vitro* study (Williams et al., 2003).

The contact stresses on both the frontside articulating surface and the backside surface of the liner were found to increase as the cup inclination angles increased. This was consistent with the previous study (Kurtz et al., 1997). However, it is interesting to note from present study that the effect of cup inclination angles was found to be negligible in case of microseparation distances above 1500 μm. This indicated that in case of hip laxity, the dominating factor to affect the biomechanics of the modular MoP THR is the level of microseparation, rather than acetabular component position. However, the two factors are not independent. As discussed above, in cases of steep cup inclination, the microseparation distance of the head that caused edge loading was largely reduced. Additionally, clinically a steep cup angle may increase the frequency of occurrence of microseparation at a certain level.

The shear stresses at the shell/liner interface along the taper surface of the liner increased significantly when the microseparation was introduced. This has two implications. Firstly, when the head lateral microseparation occurred, the shear forces applied to the shell/liner interface increased, thus the risk of mechanical loosening of the liner may be increased. Secondly, under microseparation conditions, the increased shear stresses at the shell/liner interface induced the increase of the stresses associated with surface damage due to contact, which could result in the release of wear debris to the surrounding tissue that also increases the risk of loosening.

Microseparation is believed to generate both elevated localized wear and global wear for hard-on-hard articulations (Stewart et al., 2001; Leslie et al.,

2009; AI-Hajjar et al., 2010; Restrepo et al., 2010). However, it may not be true for hard-on-soft combinations (Williams et al., 2003). The limited experimental work to date with CoP bearing, did not indicated an increase in surface wear when a microseparation of 0.7 mm was introduced. Rather, four fold reduction in volume loss of material for the polyethylene were observed in that study (Williams et al., 2003). However, by contrast, a recent FE and experimental study of low and highly crosslinked polyethylene liners against metallic femoral head total hip arthroplasty has shown that wear rates increased by 15.59 mm^3/million cycles in the low crosslinked liner and by 1.12 mm^3/million cycles in the highly crosslined liner when lateral microseparation of 0.8 mm was introduced (Netter et al., 2013). Therefore, the effect of microseparation on the wear performance of hard-on-soft THR needs to be further confirmed. Nevertheless, this study has shown that the introduction of microseparation conditions to the gait cycle did significantly increase the von Mises stresses in the liner and contact stresses on the articulating surface, which was consistent with a previous study (Besong et al., 2001a). This highlighted the importance of the surgical technique in positioning the centre of the head in the centre of the axis of rotation to avoid head lateral displacement and thus reduce the component stress level.

This study has some limitations. First of all, a static analysis was performed and a fixed static load representing the mid-to-terminal stance loading of the gait cycle was used in the present study. As the head microseparation was actually a dynamic process (Lombardi et al., 2000; Dennis et al., 2001; Uribe et al., 2012), it did not consider the effect of dynamic impact on the contact stresses in the present study. However, a contact force of 2500 N was used in the present study, which was higher than physiological loading during daily activities (Bergmann et al., 1993; 2001a) and can be expected to include the dynamic impact loading. Besides, the creep behaviour of the polyethylene liner was not modelled in the present study, which is believed to occur during the application of modular THR and affect the contact mechanics of the THR (Penmetsa et al., 2006; Galvin et al., 2010).

Despite these limitations, this study did suggest that the head lateral microseparation would cause edge loading and induce a marked increase in von Mises stresses in the liner and contact stresses on the articulating

surfaces, as well as severe plastic deformation in the liner, and that the steep cup inclination angles would facilitate these phenomena. Therefore, clinically it is critically important to avoid conditions that may lead to edge loading, which means reducing the levels of rotational and translational mal-positioning of the head and cup.

7.5 Summary

In this Chapter, the contact mechanics of the Pinnacle MoP THR was analysed under both standard conditions and adverse conditions where the head lateral microseparation occurred. The effect of cup inclination angles and microseparation levels on the edge loading and contact mechanics of the Pinnacle THR have been examined. Based on the study, the following conclusions can be drawn:

1. The head lateral microseparation would cause edge loading on the articulating surface in Pinnacle THR and steep cup inclination could facilitate this edge loading.

2. The von Mises stresses in the liner and contact stresses both on the frontside articulating surface and backside shell/liner interface, as well as the shear stresses at the shell/liner interface increased significantly when the microseparation was introduced and increased.

3. The contact areas on the articulating surface were decreased and tended to converge to a constant value when the microseparation distance was increased. A stripe shape contact area was observed around the rim of the liner when the microseparation distances were over 800 μm.

4. The plastic deformation in the liner occurred under both standard conditions and microseparation conditions. The equivalent plastic strain increased substantially when the microseparation distances increased to 1500 μm. This severe plastic deformation of the liner would lead to the piiting and delamination of the material and finnaly the fatigue damage of the liner.

Chapter 8
Overall Discussion and Conclusions

8.1 Overall Discussion

The contact mechanics and biomechanical behaviour of MoP THR were investigated in this thesis using FE methods. Two types of design were focused on: cemented and cementless. For the cemented THR, the contact mechanics of the bearings and stresses states in the cement mantle were analysed and the effect of the cup inclination angles, the sizes of the components as well as the penetration depths and surface geometries on the worn cup were examined. For the cementless THR, the contact mechanics and biomechanical behaviour were assessed under different conditions, including normal daily activities, standard and microseparation conditions. The effect of cup angles and radial clearances between the femoral head and polyethylene liner were evaluated. The effect of microseparation levels was also examined in the microseparation studies.

8.1.1 Contact Mechanics and Cement Stresses for Cemented THR

As discussed in **Section 1.3.4**, aseptic loosening of the cemented THR, which is considered as the main reason that causes the revision and failure of hip prosthesis, can be the result of particulate-induced bone resorption and bone-cement interface failure due to the mechanical stresses upon it (Ingham and Fisher, 2005; Sundfeldt et al.; 2006). The underlying mechanical mechanism is closely related to the wear of the implant which has been shown to be related to the contact mechanics on the bearing surfaces (Rostoker and Galante, 1979; Rose et al., 1983). Therefore, the investigation of the contact mechanics on the bearing surfaces and stresses at the bone-cement interface as well as in the cement mantle can help better understand the failure mechanism of the hip prosthesis.

The investigation of contact mechanics and cement stresses for cemented THR was conducted by using a 3D anatomic Charnley THR model (**Chapter 3**). The model was detailed in **Chapter 2** and validated by

comparing the contact stresses and areas with a previous study (Jin et al., 1999) in which the model had the same structures of component and the same geometric parameters.

The effect of different factors on the contact mechanics and cemented stresses for cemented THR was examined (**Chapter 3**). Cup inclination angles, one key surgical related factor in the application of THR, were shown to have little effect on the contact mechanics if the cup inclination angles were lower than 65°. However, they had an important effect on the cement stresses. Both the von Mises stresses and shear stresses at the bone-cement interface increased markedly by 18% when the cup inclination angles increased from 45° to 65°.

Although the wear in the acetabular cup resulted in marked decrease of contact stresses on the bearing surface, the penetration depths had little effect on the contact mechanics of THR (**Chapter 3**). This could be inferred from two aspects. On the one hand, the conformity between the femoral head and acetabular cup was increased when wear in the acetabular cup occurred. However, on the other hand, even though the penetration depth of 4 mm resulted in marked decrease in the wall thickness of the aetabular cup, the improved conformity between the femoral head and the acetabular cup could compensate such a loss. In contrast, the penetration depths had an important effect on the stresses both at the bone-cement interface and in the cement mantle. This is because the stresses produced in the cement mantle depended on both the contact stresses on the bearing surface and how the contact stresses were transferred to the cement mantle.

It should be pointed out that the wear and penetration in the acetabular cup considered in this study as well as in the previous study (Coultrup *et al.*, 2010) was largely simplified by intersecting the cup using the femoral head in the direction of the resultant load, as described in **Chapter 3**. The wear direction for the worn cup was therefore modelled as medial and consistent with the direction of the resultant load. The clearance between the femoral head and the worn region of the cup (C_w) was therefore assumed as zero. However, this was not the normal situation clinically. Clinical studies have showed that the wear direction was always observed to be lateral and there

was actually a gap between the femoral head and worn region of the cup (Wroblewski et al., 1985; Hall et al., 1998). These parameters were therefore quantified in this thesis from two retrieved Charnley sockets in **Chapter 4**. CMM machine was used to collect data and surface fitting technique was applied to reconstruct the worn and unworn regions in the surface of the worn cup. The prediction results confirmed the clinical observations that the wear direction for the retrieved Charnley cups were predicted to be lateral by 12.5^o and the clearance C_w was close to the radial clearance between the femoral head and origin surface of the cup (C_o).

The effect of the wear directions and radial clearances C_w on the contact mechanics and cement stresses for cemented THR were then evaluated (**Chapter 4**). Given the load with medial direction, the change of wear directions from medial to lateral did not affect the contact mechanics and cement stresses substantially. However, there was an increasing trend for the contact stresses on the articulating surface with more lateral wear directions (i.e. over 30° lateral). In contrast, the radial clearance C_w had a marked effect on the contact mechanics and cement stresses for cemented THR, similar to the findings in **Chapter 3**.

The effect of wall thickness of the acetabular cup on the contact mechanics of THR is dependent on whether the cup is thick sufficiently. If the acetabular cup has sufficient thickness, the effect of the wall thickness is negligible, otherwise, the effect is apparent (Bartel et al., 1985). This conclusion was confirmed further in this thesis (**Chapter 3**). Keeping all other parameters constant, the change of the outer diameters of the acetabular cup from 40 mm to 43 mm, hence an increase of the wall thickness from 8.7 mm to 10.2 mm, did not affect the contact mechanics on the articulating surface. However, the increased head diameters from 22.225 mm to 36 mm, therefore a decreased wall thickness from 8.7 mm to 1.72 mm, resulted in a decrease of contact stresses on the bearing surface by nearly 50%. However, it should be pointed out that when the head diameters increased to 36 mm, the thickness of the cup goes below approximately 2 mm, which will become slightly irrelevant in practice.

The effect of wall thickness on the cement stresses was largely different. Both the outer sizes of the cup and the diameters of the femoral head had marked effect on the stresses produced in the cement mantle (**Chapter 3**). This again highlighted the conclusion that the stresses produced in the cement mantle depended on both the contact stresses on the bearing surface and how the stresses were transferred to the cement mantle.

Clinical studies have reported that under similar conditions, a cup with an outer diameter of 43 mm had approximately 20% lower aseptic loosening incidence compared to that with outer diameter of 40 mm with increasing penetration depths in the cup (Wroblewski, et al., 2009a). Correspondingly, the maximum von Mises stress at the bone-cement interface and the peak max principal stress in the cement mantle for the cup design with outer diameter of 43 mm were predicted to be approximately 15-19% and 15-22% lower compared to that of 40 mm for different cup inclination angles and penetration depths (**Chapter 3**). This provided a possible explanation on the difference of aseptic loosening incidence observed clinically between the two cup designs from a mechanical point of view.

8.1.2 Contact Mechanics for Modular THR Under Normal Activities

It has been shown that the contact mechanics of modular MoP THR was largely different from that of non-modular MoP THR, due to the nonconformity between the shell and liner in the modular bearings (Kurtz et al., 1998; 1999). However, whilst the contact mechanics has been extensively investigated for non-modular THRs, limited works have been done for modular THRs.

The contact mechanics and biomechanical behaviour for modular MoP THR were therefore investigated in this thesis by using a 3D anatomic Pinnacle THR model which was detailed in **Chapter 2**. In order to improve the confidence of using the anatomic Pinnacle THR model, the methodology used in this model was validated in **Chapter 5**. An experimental set-up was developed to allow the contact areas on the articulating surface for a modular MoP THR to be measured. An experimentally-matched model which applied the same methodology with that in the anatomic Pinnacle THR

model was developed to reproduce the experimental set-up, as described in **Chapter 5**. The contact areas measured from experiment and predicted from the experimentally-matched model were then compared. Good agreements were obtained between them in both patterns and values of contact areas, with a maximum difference of 14%, confirming that the methodology used in the anatomic Pinnacle THR model had a sound experimental footing.

There were, however, several limitations to the experimental validation which have been discussed in **Section 5.4**. A thorough and more accurate approach could be developed in the future, e.g. the material properties of the polyethylene liner used in the experiment should be tested and applied in the experimentally-matched model; the contact stresses on the articulating surface could be measured with the help of a transducer etc. Despite these limitations, the experimentally-matched model reproduced the experimental outcomes prospectively.

The anatomic Pinnacle THR model with validated methodology was then used to investigate the contact mechanics and biomechanical behaviour of a modular MoP THR (Pinnacle THR) during activities of daily living such as walking, ascending stairs etc. (**Chapter 6**). The loading data applied in the model was obtained from Bergmann's study (Bergmann, 2001b).

Contact stresses on the frontside articulating surface of the Pinnacle THR over the whole cycle for normal walking were predicted to distribute both at and away from equatorial regions, leading to a double-peak contact pattern (Figure 6.3), which was largely different from non-modular THR, such as the cemented THR discussed in **Chapter 3** (Figure 3.2). Contact was also predicted between the shell and the backside surface of the liner both at corresponding regions. This backside contact would produce backside wear which was considered to aggravate the aseptic loosening of the hip prosthesis (**Chapter 6**).

Edge loading on both the frontside articulating surface and backside surface of the liner for Pinnacle MoP THR was investigated and the contribution of cup angles, radial clearances and daily activities were examined in **Chapter 6**. It has been shown that the occurrence of edge loading on the

two surfaces of the liner was dependent on the cup angles, radial clearances as well as the daily activities. For radial clearance of 0.3 mm, edge loading on the frontside articulating surface was inclined to occur at steeper cup inclination angles and with smaller radial clearances for normal walking, ascending and descending stairs activities. In contrast, edge loading on the backside surface of the liner was predicted to occur for all activities considered. Similarly, it was inclined to occur at steeper cup inclination angles and with smaller radial clearances.

It is interesting to note that even though edge loading existed on the articulating surface, the contact stresses did not increase markedly. This indicated that this kind of hip prosthesis has less sensitivity to edge loading than hard-on-hard articulations (Wang et al., 2012). In contrast, the edge loading on the backside surface of liner led to concentrated stresses, which would induce damage and fracture of the liner at this region, as observed in a retrieved liner (Halley et al., 2004).

The study on the effect of cup angles suggested that both cup inclination angles and anteversion angles had a marked effect on the contact mechanics of modular MoP THR for all activities considered. However, how the cup angles affected the contact mechanics was dependent on the radial clearances. Take the normal walking activity as an example, the increased cup inclination angles resulted in decreased contact stresses on the articulating surface for radial clearances of 0.542 mm and 0.3mm, but led to increased contact stresses for radial clearance of 0.1 mm. The different behaviour of the modular MoP THR induced by varied cup angles for radial clearance of 0.1 mm suggested that lower cup angles remain a recommendation for implant positioning for the modular THRs.

8.1.3 Contact Mechanics for Modular THR Under Microseparation Conditions

As discussed in **Section 1.4.5**, microseparation of the femoral head and the acetabular cup can provoke adverse biomechanical and biotribological problems for THR, including the production of unexpected accelerated wear rates and stripe wear on hard-on-hard articulations, and fracture of the components as well as the squeaking of the implants for CoC bearings

(Manaka et al., 2004; Williams et al., 2006; Leslie et al., 2009). It can also lead to concentrated stresses and undesired deformation of the components, especially for MoP THR (Williams et al., 2003), which will cause damage of the components and promote the failure of the implants. Therefore, the investigation of microseparation for MoP THR is necessary in order to better assess the long-term performance of the THR.

The contact mechanics and biomechanical behaviour of a modular MoP THR (Pinnacle THR) under microseparation conditions were investigated by using the 3D anatomic Pinnacle THR model used in **Chapter 6**. The effect of cup inclination angles, microseparation distances and radial clearances between the femoral head and liner were evaluated (**Chapter 7**).

The microseparation study showed that the introduction of microseparation resulted in marked increase in the peak von Mises stress in the liner and contact stress on the articulating surface. With increased microseparation distances, the maximum von Mises stress and contact stress increased continually. Plastic deformation for the polyethylene liner occurred under both standard conditions and microseparation conditions, and the plastic deformation became more severe with increased microseparation distances. This plastic deformation on the polyethylene liner due to the microseparation was also observed in an *in vitro* study (Williams et al., 2003) (**Chapter 7**).

Edge loading would occur on the bearing surface due to microseparation. Previous studies have shown that the generation of edge loading was strongly dependent on the cup inclination angles and radial clearances (Mak et al., 2002; Sariali et al., 2012). This was further confirmed in this study (**Chapter 7**). It was suggested that the microseparation distances required to generate edge loading decreased with increasing cup inclination angles, indicating that the implants with higher cup inclination angles were more inclined to suffer from edge loading and had potentially increasing instability.

This study also suggested that all the stresses tested in this study increased markedly with increased cup inclination angles. However, the difference of the stresses induced by varied cup inclination angles became negligible when the microseparation distances increased to a certain level (**Chapter 7**). This indicated the leading role of microseparation level to the biomechanical

behaviour of the modular THR in case of hip laxity, highlighting the importance of aligning the position of the components to avoid head lateral microseparation clinically.

There are a number of limitations to the models used in this study. Firstly, in both antomic Charnley THR model and antomic Pinnacle THR model, the bone was modelled as a cancellous region surrounded by a cortical shell with fixed thickness, the mechanical properties in terms of elastic modulus and Poisson's ratio were considered to be uniform. However, in reality, the thickness of the cortical shell and the elastic modulus and Poisson's ratio of the bone are site-dependent and bone density-dependent (Leung et al., 2009). These were not considered in both models. Additionally, the pelvic bone in both models was constrained rigidly at the sacroiliac joint and at the pubic symphysis, these were not true for the pelvis in the human body. The real constraint for the pelvis at the sacroiliac joint and at the pubic symphysis was elastic by soft tissues such as ligaments and tendons (Hao et al., 2011). Furthermore, the soft tissues surrounding the hip joint such as capsule, muscles and ligaments were not considered in the anatomic models (Elkins et al., 2011). The loadings applied in both models were simplified to a point force. All these limitations may have a certain impact on the FE predictions and should be addressed in future studies.

8.2 Overall Conclusions

In summary, the following major conclusions can be made from this study.

For cemented THR (Charnely THR):

- The cup inclination angles had little effect on the contact pressures on the articulating surface but had marked effect on the cement stresses.
- The wear in the acetabular cup resulted in marked decrease in the contact pressures on the acetabular surface, however, the penetration depths had little effect on the contact pressures. By contrast, the penetration depths had marked effect on the cement stresses.
- Assuming the cup was positioned at an inclination angle of 45⁰, the wear directions for the two retrieved Charnley sockets were predicted to be lateral, rather than medial. However, the change of the wear directions

from medial to lateral did not affect the contact pressures and cement stresses substantially.

- The radial clearances between the femoral head and the worn region of the cup (C_w) for the two retrieved Charnley sockets were found to be close to the radial clearances between the femoral head and original surface of the cup (C_0). The radial clearances C_w had an important effect on the contact pressures and cement stresses. A larger radial clearance C_w produced higher contact pressures and cement stresses.

- The difference of the contact pressures on the bearing surface between the two cups with outer diameters of 40 mm and 43 mm was negligible. However, the cement stresses for the cup with outer diameter of 40 mm were predicted to be higher compared to that of 43 mm.

- Increased diameters of the femoral head from 22.225 mm to 38 mm resulted in decreased contact stresses by nearly 50% but increased cement stresses by about 30%, 25% and 11% with respect to peak von Mises stress, shear stress and max principal stress.

For modular THR (Pinnacle THR):

- Good agreements in contact areas were obtained between the experimental measurements and the FE predictions from the experimentally-matched model. This provides some level of confidence in using the anatomic Pinnalce THR model which applied the same methodology as the experimentally-matched model.

- Both the cup inclination angles and anteversion angles, as well as the type of daily activities had marked effects on the contact mechanics of the modular MoP THR. However, how the cup angles affected the contact mechanics was dependent on the radial clearances.

- Edge loading on the frontside articulating surface for the modular MoP THR was predicted during the activities of normal walking, ascending and descending stairs for radial clearance of 0.3 mm. Edge loading was more inclined to occur for the prosthesis with steeper cup inclination angles and smaller radial clearances.

- Edge loading in the equatorial region on the backside surface of the liner for modular THR was also observed for all activities considered, leading to a region of concentrated stress at this area.

- Edge loading on the frontside articulating surface would occur due to the lateral microseparation of the femoral head. The starting point of occurrence of edge loading was strongly dependent on the cup inclination angles and radial clearances between the femoral head and acetabular cup.

- The introduction of microseparation resulted in a significant increase of von Mises stresses in the liner material and contact stresses on the bearing surface. The material yielding of the polyethylene liner occurred under both standard conditions and microseparation conditions, leading to the plastic deformation for the polyethylene liner, which became increasingly more severe with increased microseparation distances.

- The contact stresses on the backside surface of the liner and shear stresses at the shell/liner interface increased significantly as well when the microseparation was introduced.

8.3 Future Work

The contact mechanics and biomechanical behaviour of a cemented MoP THR and a modular MoP THR were investigated in this thesis by using computational models. Meaningful and encouraging conclusions have been made based on the investigation. However, there are a few limitations in this thesis and need to be addressed in the future works.

- In order to investigate the macro mechanical behaviour of the cement mantle, the bone-cement interface was modelled at a continuum level in this thesis, where the bone-cement interface was considered as a bilayer which consists of the cement on one side and bone on the other. However, the true interface layer between the bone and the cement is actually a transition region of a bone-cement composite (Lewis, 1997). Therefore, in order to better understand the failure process of the interface, the bone-cement interface is recommended to be modelled at

a microstructural level which includes the bone-cement interdigitated region in the future study.

- The load applied in the anatomic Charnley THR model was static with a direction of 10⁰ medially. However, the magnitudes and directions of the load may have a marked effect on the contact mechanics of the bearing and mechanical behaviour of the cement mantle, especially the wear with lateral direction was modelled in the acetabular cup. Therefore, loads with varied magnitudes and directions for gait and other activities are recommended in the future study.

- The contact mechanics for modular THR was shown to be different from that for non-modular THR, which was attributed to the non-conformity between the shell and liner in the modular THR (Kurtz et al., 1998; 1999). This can be confirmed by investigating the effect of conformity between the shell and the liner in modular THR in the future study.

- The dynamic process of microseparation of the femoral head includes separation during swing phase, rim contact at heel-strike and relocation during the stance phase. These processes can be simulated dynamically to better understand the biomechanics of the hip prosthesis under microseparation conditions in the future study.

- The final recommendation for the future study is to investigate the impingement and dislocation of the hip prosthesis. The impingement and dislocation of the hip implants can also cause concentrated stresses and damage of the components, and finally the instability of the hip arthroplasty (Woo and Morry, 1982; Scifert et al., 1998). Therefore, the investigation of impingement and dislocation for the THR will be a good complementary for understanding the edge loading and the failure of the hip prosthesis.

References

Affatato, S., Bersaglia, G., Foltran, I., Emiliani, D., Traina, F. and Toni, A. (2004) The influence of implant position on the wear of alumina-on-alumina studied in a hip simulator. *Wear*, 256(3): 400-405.

Al-Hajjar, M., Leslie, I. J., Tipper, J., Williams, S., Fisher, J. and Jennings, L. M. (2010) Effect of cup inclination angle during microseparation and rim loading on the wear of BIOLOX® delta ceramic-on-ceramic total hip replacement. *Journal of Biomedical Materials Research Part B: Applied Biomaterials*, 95(2): 263-268.

Al-Hajjar, M. (2012) Wear of hard-on-hard hip prostheses: influence of head size, surgical position, material and function. PhD Thesis, *University of Leeds*, UK.

Al-Hajjar, M., Fisher, J., Williams, S., Tipper, J. L. and Jennings, L. M. (2013) Effect of femoral head size on the wear of metal on metal bearings in total hip replacements under adverse edge-loading conditions. *Journal of Biomedical Materials Research Part B: Applied Biomaterials*, 101(2): 213-222.

Amirouche, F., Romero, F., Gonzalez, M. and Aram, L. (2008) Study of micromotion in modular acetabular components during gait and subluxation: a finite element investigation. *Journal of biomechanical engineering*, 130(2): 021002: 1-9.

Amstutz, H. C., Campbell, P., Kossovsky, N. and Clarke, I. C. (1992) Mechanism and clinical significance of wear debris-induced osteolysis. *Clinical Orthopaedics and Related Research*, (276): 7-18.

Anderson, A. E., Ellis, B. J., Maas, S. A., Peters, C. L. and Weiss, J. A. (2008) Validation of finite element predictions of cartilage contact pressure in the human hip joint. *Journal of Biomechanical Engineering*, 130(5): 051008: 1-10.

Anderson, A. E., Peters, C. L., Tuttle, B. D. and Weiss, J. A. (2005). Subject-specific finite element model of the pelvis: development, validation and sensitivity studies. *Journal of Biomedical Engineering-Transactions of the ASME,* 127(3): 364-373.

Angadji, A., Royle, M., Collins, S. and Shelton, J. (2009) Influence of cup orientation on the wear performance of metal-on-metal hip

replacements. *Proceedings of the Institution of Mechanical Engineers Part H: Journal of Engineering in Medicine*, 223(4): 449-457.

Apkarian, J., Naumann, S. and Cairns, B. (1989) A three-dimensional kinematic and dynamic mode of the lower limb. *Journal of Biomechanics*, 22(2): 143-155.

Arola, D. Stoffel, K. A. and Yang, D. T. (2005) Fatigue of the cement/bone interface: the surface texture of bone and loosening. *Journal of Biomedical Materials Research Part B: Applied Biomaterials*, 76B(2): 287-297.

Bader, R., Steinhauser, E., Zimmermann, S., Mittelmeier, W., Scholz, R. and Busch, R. (2004) Differences between the wear couples metal-on-polyethylene and ceramic-on-ceramic in the stability against dislocation of total hip replacement. *Journal of Materials Science: Materials in Medicine*, 15(6): 711-718.

Banchet, V., Fridrici, V., Abry, J. C. and Kapsa, P. (2007) Wear and friction characterization of materials for hip prosthesis. *Wear*, 263(7): 1066-1071.

Barrack, R. L. (2003) Dislocation after total hip arthroplasty: implant design and orientation. *Journal of the American Academy of Orthopaedic Surgeons*, 11(2): 89–99.

Barreto, S., Folgado, J., Fernandes, P. R. and Monteiro, J. (2010) The influence of the pelvic bone on the computational results of the acetabular component of a total hip prosthesis. *Journal of Biomechanical Engineering*, 132(5): 054503: 1-4.

Bartel, D. L., Bicknell, V. L. and Wright, T. M. (1986) The effect of conformity, thickness, and material on stresses in ultra-high molecular weight components for total joint replacement. *Journal of Bone and Joint Surgery Am*, 68(7):1041-1051.

Bartel, D. L., Burstein, A. H., Toda, M. D. and Edwards, D. L. (1985) The effect of conformity and plastic thickness on contact stresses in metal-backed plastic implants. *Journal of Biomechanical Engineering*, 107(3): 193-199.

Bergmann, G., Graichen, F. and Rohlmann, A. (1993) Hip joint loading during walking and running, measured in two patients. *Journal of Biomechanics*, 26(8): 969-990.

Bergmann, G., Deuretzbacher, G., Heller, M., Graichen, F., Rohlmann, A., Strauss, J. and Duda. G. N. (2001a) Hip contact forces and gait patterns from routine activities. *Journal of Biomechanics*. 34(7): 859-871.

Bergmann, G. (2001b) Hip98. *Free University*, Berlin.

Bergmann, G., Graichen, F. and Rohlmann, A. (2004) Hip joint contact forces during stumbling. *Langenbeck's Archives of Surgery*, 389(1): 53-59.

Berry, D. J., von Knoch, M., Schleck, C. D. and Harmsen, W. S. (2005) Effect of femoral head diameter and operative approach on risk of dislocation after primary total hip arthroplasty. *Journal of Bone and Joint Surgery Am*, 87(11): 2456-2463.

Besong, A. A., Jin, Z. M., and Fisher, J. (2001a) Analysis of micro-separation and contact mechanics between the femoral head and the acetabular cup in artificial hip joint replacements. *47th Annual Meeting, Orthopaedic Research Society*, February 25-28, San Francisco, California, USA.

Besong, A. A., Lee, R., Farrar, R. and Jin, Z. M. (2001b) Contact mechancis of a novel metal-on-metal total hip replacement. *Proceedings of the Institution of Mechanical Engineers Part H: Journal of Engineering in Medicine*, 215(6): 543-548.

Bhushan, B. (2002) Introduction to Tribology. New York: *John Wiley & Sons, Ltd*.

Blewis, M. E., Nugent-Derfus, G. E., Schmidt, T. A., Schumacher, B. L. and Sah, R. L. (2007) A model of synovial fluid lubrication composition in normal and injured joints. *European cells and materials*, 13: 26-39.

Bobyn, J. and Engh, C. (1984) Human histology of the bone-porous metal implant interface. *Orthopaedics*, 7: 1410-1421.

Boger, A., Bohner, M., Heini, P., Verrier, S. and Schneider, E. (2008a) Properties of a low modulus PMMA bone cement for osteoporotic bone. *Journal of Biomedical Materials Research Part B: Applied Biomaterials*, 86B(2): 474-482.

Boger, A., Bohner, M., Heini, P., Schwieger, K. and Schneider, E. (2008b) Performance of vertebral cancellous bone augmented with compliant PMMA under dynamic loads. *Acta Biomaterialia*, 4(6): 1688-1693.

Boger, A., Heini, P., Windolf, M. and Schneider, E. (2007) Adjacent vertebral failure after vertebroplasty: a biomechanical study of low-modulus PMMA cement. *European Spine Journal*, 16(12): 2118-2125.

Brand, R. A., Pedersen, D. R., Davy, D. T., Kotzar, G. M., Heiple, K. G. and Goldberg, V. M. (1994) Comparison of hip force calculations and measurements in the same patient. *Journal of Arthroplasty*, 9(1): 45-51.

Brockett, C., Williams, S., Jin, Z., Isaac, G. and Fisher, J. (2007) Friction of total hip replacements with different bearings and loading conditions. *Journal of Biomedical Materials Research Part B: Applied Biomaterials*, 81(2): 508-515.

Brown, S. S. and Clarke, I. C. (2006) A review of lubrication conditions for wear simulation in artificial hip replacements. *Tribology Transactions*, 49(1): 72-78.

Bowsher, J. G. and Shelton, J. C. (2001) A hip simulator study of the influence of patient activity level on the wear of crosslinked polyethylene under smooth and roughened femoral conditions. *Wear*, 250(1): 167-179.

Burroughs, B. R., Hallstrom, B., Golladay, G. J., Hoeffel, D. and Harris, W. H. (2005) Range of motion and stability in total hip arthroplasty with 28-, 32-, 38-, and 44-mm femoral head sizes: an *in vitro* study. *The Journal of Arthroplasty*, 20 (1): 11-19.

Callaghan, J. J., Bracha, P., Liu, S. S., Piyaworakhun, S., Goetz, D. D. and Johnston, R. C. (2009) Survivorship of a Charnley Total Hip Arthroplasty. A Concise Follow-up, at a Minimum of Thirty-five Years, of Previous Reports. *Journal of Bone and Joint Surgery*, 91(11): 2617-2621.

Campbell, P., Ma, S., Yeom, B., McKellop, H., Schmalzried, T. P. and Amstutz, H. C. (1995) Isolation of predominantly sub-micron sized UHMWPE wear particles from periprosthetic tissues. *Journal of Biomedical Materials Research*, 29(1): 127-131.

Capitanu, L., Iarovici, A. and Onisoru, J. (2005) Tribological behaviour of a total hip prosthesis during normal walking active cycle. *Tribology in Industry*, 27(1): 27-33.

Carter, D. R., Vasu, R., and Harris, W. H. (1982) Stress distributions in the acetabular region-II. effect of cement thickness and metal backing of the total hip acetabular component. J*ournal of Biomechanics*, 15(3): 165-170.

Charlish, A. (1996) The Complete Arthritis Handbook. *London, Carnel Ltd*.

Charnley, J. (1961) Arthroplasty of the hip : a new operation. *The Lancet*, 1(7187): 1129-1132.

Charnley, J., Kamangar, A. and Longfiel, M. D. (1969) Optimum size of prosthetic head in relation to wear of plastic sockets in total replacement of hip. *Medical & Biological Engineering*, 7(1): 31-39.

Chen, W. C., Liu, Y. L., Lin, K. J., McClean, C. J., Lai, H. J., Chou, C. W., Chang, T. W., Yang, C. T., Huang, C. H., Lai, Y. S. and Cheng, C. K. (2012) Concave polyethylene component improves biomechanical performance in lumbar total disc replacement--modified compressive-shearing test by finite element analysis. *Medical Engineering and Physics*, 34(4): 498-505.

Clohisy, J. C., Calvert, G., Tull, F., McDonald, D. and Maloney, W. J. (2004) Reasons for revision hip surgery: a retrospective review. *Clinical Orthopaedics and Related Research*, (429): 188-192.

Coultrup, O. J., Browne, M., Hunt C. and Taylor, M. (2009) Accounting for inclusions and voids allows the prediction of tensile fatigue life of bone cement. *Journal of Biomechanical Engineering*, 131(5): 051007.

Coultrup, O. J., Hunt, C., Wroblewski, B. M. and Taylor, M. (2010) Computational assessment of the effect of polyethylene wear rate, mantle thickness, and porosity on the mechanical failure of the acetabular cement mantle. *Journal of Orthopaedic Research*, 28(5): 565-570.

Crowninshield, R. D., Johnston, R. C., Andrews, J. G. and Brand, R. A. (1978) A biomechanical investigation of the human hip. *Journal of Biomechanics*, 11(1-2): 75-85.

Crowninshield, R. D., Brand, R. and Pedersen, D. (1983) A stress analysis of acetabular reconstruction in protrusio acetabuli. *Journal of Bone and Joint Surgery*, 65(4): 495-499.

Crowininshield, R. D., Maloney, W. J., Wentz, D. H., Humphrey, S. M. and Blanchard, C. R. (2004) Biomechanics of large femoral head: what they do and don't do. *Clinical Orthopaedics and Related Research*, 429: 102-107.

Dalstra, M., Huiskes, R., Odgaard, A. and van Erning, L. (1993) Mechanical and textural properties of pelvic trabecular bone. *Journal of Biomechanics*, 26(4-5): 523-535.

Dalstra, M., Huiskes, R. and van Erning, L. (1995). Development and validation of a 3-dimensional finite-element model of the pelvic bone. *Journal of Biomechanical Engineering-Transactions of the ASME*, 117(3): 272-278.

Davy, D. T., Kotzar, G. M., Brown, R. H., Heiple, K. G., Goldberg, V. M., Heiple, K. G., Berilla, J. and Burstein, A. H. (1988) Telemetric force measurements across the hip after total arthroplasty. *Journal of Bone and Joint Surgery Am*, 70(1): 45-50.

De Haan, R., Pattyn, C., Gill, H. S., Murray, D. W., Campbell, P. A. and De Smet, K. (2008) Correlation between inclination of the acetabular component and metal ion levels in metal-on-metal hip resurfacing replacement. *Journal of Bone and Joint Surgery Br*, 90(10): 1291-1297.

Dennis, D. A., Komistek, R. D., Northcut, E. J., Ochoa, J. A. and Ritchie, A. (2001) "*In vivo*" determination of hip joint separation and the forces generated due to impact loading conditions. *Journal of Biomechanics*, 34(5): 623-629.

Diwan, A. and Drummond, R. (1997) Unusual case of third-body wear in total hip arthroplasty. *Journal of Arthroplasty*, 12(5): 586-588.

D'Lima, D. D., Chen, P. C. and Colwell, C. W. Jr. (2001) Optimizing acetabular component position to minimize impingement and reduce contact stress. *Journal of Bone and Joint Surgery Am*, 83A(Suppl. 2): 87-91.

Dorr, L. D., Lewonowski, K., Lucero, M., Harris, M. and Wan, Z. (1997) Failure mechanisms of anatomic porous replacement I cementless total hip replacement. *Clinical Orthopaedics and Related Research*, (334): 157-167.

Dowson, D. (2001) New joints for the Millennium: wear control in total replacement hip joints. *Proceedings of the Institution of Mechanical Engineers Part H: Journal of Engineering in Medicine*, 215(4): 335-358.

Dowson, D. and Jin, Z. M. (2006) Metal-on-metal hip joint tribology. *Proceedings of the Institution of Mechanical Engineers Part H: Journal of Engineering in Medicine*, 220(2): 107-118.

Dowson, D. and Wright, V. (1973) Bio-Tribology. *Proceedings of the conference on the rheology of lubrication. The Institute of petroleum, The Institution of Mechanical Engineers and the British Society of Rheology*, 81-85.

Duda, G. N., Schneider, E. and Chao, E. Y. (1997) Internal forces and moments in the femur during walking. *Journal of Biomechanics*, 30(9): 933-941.

Dunne, N. J., Mushipe, M. T. and Eveleigh, R. J. (2003) The relationship between porosity and fatigue characteristics of bone cements. *Biomaterials*, 24: 239-245.

Eberhardt, A. W., Keer, L. M., Lewis, J. L. and Vithoontien, V. (1990) An analytical model of joint contact. *Journal of Biomechanical Engineering*, 112(4): 407-413.

Eberhardt, A. W., Lewis, J. L. and Keer, L. M. (1991) Contact of layered elastic spheres as a model of joint contact - effect of tangential load and friction. *Journal of Biomechanical Engineering*, 113(1): 107-108.

Edidin, A. A., Pruitt, L., Jewett, C. W., Crane, D. J., Roberts, D. and Kurtz, S. M. (1999) Plasticity-induced damage layer is a precursor to wear in radiation-cross-linked UHMWPE acetabular components for total hip replacement. Ultra-high-molecular-weight polyethylene. *Journal of Arthroplasty*, 14(5): 616-627.

Elkins, J. M., Kruger, K. M., Pedersen, D. R., Callaghan, J. J and Brown, T. D. (2012) Edge-loading severity as a function of cup lip radius in metal-on-metal total hips--a finite element analysis. *Journal of Orthopaedic Research*, 30(2): 169-177.

Elkins, J. M., Stroud, N. J., Rudert, M. J., Tochigi, Y., Pedersen, D. R., Ellis, B. J., Callaghan, J. J., Weiss, J. A. and Brown, T. D. (2011) The capsule's contribution to total hip construct stability--a finite element analysis. *Journal of Orthopaedic Research*, 29(11): 1642-1648.

Engh, C. A., Hooten, J. P. J., Zettl-Schaffer, K. F., Ghaffarpour, M., McGovern, T. F. and Bobyn, J. D. (1995) Evaluation of bone ingrowth in proximally and extensively porous coated anatomic medullary locking protheses retrieved at autopsy. *Journal of Bone and Joint Surgery*, 77(6): 903-910.

English, T. A. and Kilvington, M. (1979) *In vivo* records of hip loads using a femoral implant with telemetric output (a preliminary report). *Journal of Biomedical Engineering*, 1(2): 111-115.

Fisher, J. (2001) Biomedical applications. In Modern tribology handbook, Volume II, *CRC Press*, NewYork.

Fisher, J. (2011) Bioengineering reasons for the failure of metal-on-metal hip prostheses: an engineer's perspective. *Journal of Bone and Joint Surgery Br*, 93(8): 1001-1004.

Fisher, J., Ingham, E. and Jin, Z. M. (2006) Biotribology. Handbook of Lubrication and Tribology, Volume I Application and Maintenance, *CRC Press*, NewYork.

Frayssinet, P., Hardy, D., Hanker, J. S. and Giammara, B. L. (1995) Natural history of bone response to hydroxyapatite-coated hip prostheses implanted in humans. *Cells and Materials*, 5(2): 128-138.

Fraysse, F., Dumas, R., Cheze, L. and Wang, X. (2009) Comparison of global and joint-to-joint methods for estimating the hip joint load and the muscle forces during walking. *Journal of Biomechanics*, 42(14): 2357-2362.

Fuziansyah, B., Xian, C. and Toshiaki, H. (2006) Finite element contact analysis of the hip joint. *Medical & Biological Engineering & Computing*, 44(8): 643-651.

Gaffey, J. L., Callaghan, J. J., Pedersen, D. R., Goetz, D. D., Sullivan, P. M. and Johnston, R. C. (2004) Cementless acetabular fixation at fifteen years. A comparison with the same surgeon's results following acetabular fixation with cement. *Journal of Bone and Joint Surgery*, 86-A(2): 257-261.

Galvin, A. L., Jennings, L. M., Tipper, J. L., Ingham, E. and Fisher, J. (2010) Wear and creep of highly crosslinked polyethylene against cobalt chrome and ceramic femoral heads. *Proceedings of the Institution of Mechanical Engineers Part H: Journal of Engineering in Medicine*, 224(10): 1175-1183.

Gardiner, C. and Hozack, W. J. (1994) Failure of the cement-bone interface. A consequence of strengthening the cement-prosthesis interface? *Journal of Bone and Joint Surgery*, 76(1): 49-52.

Gauthier, C., Lafaye, S. and Schirrer, R. (2001) Elastic recovery of a scratch in a polymeric surface: experiments and analysis. *Tribology International*, 34(7): 469-479.

Gauthier, C. and Schirrer, R. (2000) Time and temperature dependence of the scratch properties of poly(methylmethacrylate) surfaces. *Journal of Materials Science*, 35(9): 2121-2130.

Geesink, R. G., de Groot, K. and Klein, C. P. (1987) Chemical implant fixation using hydroxyapatite coatings: the development of a human total hip prosthesis for chemical fixation to bone using hydroxyapatite coatings on titanium substrates. *Clinical Orthopaedics and Related Research*, 225 (12): 147-170.

Glaser, D., Komistek, R. D., Cates, H. E. and Mahfouz, M. R. (2008) Clicking and squeaking: *in vivo* correlation of sound and separation for different bearing surfaces. *Journal of Bone and Joint Surgery Am*, 90(Suppl. 4): 112-120.

Goldring, S. R., Clark, C. R. and Wright, T. M. (1993) The problem in total joint arthroplasty: aseptic loosening. *Journal of Bone and Joint Surgery Am*, 75(6): 799-801.

Goldring, S. R., Schiller, A. L., Roelke, M., Rourke, C. M., O'Neill, D. A. and Harris, W. H. (1983) The synovial-like membrane at the bone-cement interface in loose total hip replacements and its proposed role in bone lysis. *Journal of Bone and Joint Surgery Am*, 65(5): 575-584.

Goldsmith, A. A. and Dowson, D. (1999) Development of a ten-station, multi-axis hip joint simulator. *Proceedings of the Institution of Mechanical Engineers Part H: Journal of Engineering in Medicine*, 213(4): 311-316.

Gore, T. A., Higginson, G. A. and Steven, J. (1984). The kinematics of hip joints: normal functioning. *Clinical Physics and Physiological Measurement*, 5(4): 233-252.

Gray, H. (2000) Gray's Anatomy of the Human Body, *New York, Bartleby.com*.

Hale, J. E. and Brown, T. D. (1992) Contact stress gradient detection limits of Pressensor film. *Journal of Biomechanical Engineering*, 114(3): 352-357.

Hall, R. M., Siney, P., Wroblewski, B. M. and Unsworth, A. (1998) Observations on the direction of wear in Charnley sockets retrieved at revision. *Journal of Bone and Joint Surgery Br*, 80(6): 1067-1072.

Halley, D., Glassman, A. and Crowninshield, R. D. (2004) Recurrent dislocation after revision total hip replacement with a large prosthetic femoral head. *Journal of Bone and Joint Surgery Am*, 86(4): 827-830.

Hammerberg, E. M., Wan, Z., Dastane, M. and Dorr, L. D. (2010) Wear and range of motion of different femoral head sizes. *The Journal of Arthroplasty*, 25(6): 839-843.

Hao, Z., Wan, C., Gao, X. and Ji, T. (2011) The effect of boundary condition on the biomechanics of a human pelvic joint under an axial compressive load: a three-dimensional finite element model. *Journal of Biomechanical Engineering,* 133(10):101006-1-9.

Hardidge, A. J, Hooper, J. and McMahon, S. (2003) Current attitudes to total hip replacement in younger patients: a comparison of two nations. *ANZ Journal of Surgery*, 73(5): 280-283.

Harris, M. D., Anderson, A. E., Henak, C. R., Ellis, B. J., Peters, C. L. and Weiss, J. A. (2012) Finite element prediction of cartilage contact stresses in normal human hips. *Journal of Orthopaedic Research*, 30(7): 1133-1139.

Harris, M. L., Morberg, P., Bruce, W. J. M. and Walsh, W. R. (1999) An improved method for measuring tibiofemoral contact areas in total knee arthroplasty: a comparison of K-scan sensor and Fuji film. *Journal of Biomechanics*, 32(9): 951-958.

Harris, W. H. (1995) The problem is osteolysis. *Clinical Orthopaedics and Related Research*, (311): 46-53.

Harris, W. H. (2012) Edge loading has a paradoxical effect on wear in metal-on-polyethylene total hip arthroplasties. *Clinical Orthopaedics and Related Research*, 470(11): 3077-3082.

Hashimoto, N., Ando, M., Yayama, T., Uchida, K., Kobayashi, S., Negoro, K. and Baba, H. (2005) Dynamic analysis of the resultant force acting on the hip joint during level walking. *Artificial Organs*, 29(5): 387-392.

Heaton-Adegbile, P., Zant, N. P. and Tong, J. (2006) *In vitro* fatigue behaviour of a cemented acetabular reconstruction. *Journal of biomechanics*, 39(15): 2882-2886.

Heller, M. O., Bergmann, G., Deuretzbacher, G., Dürselen, L., Pohl, M., Claes, L., Haas, N. P. and Duda, G. N. (2001) Musculo-skeletal loading conditions at the hip during walking and stair climbing. *Journal of Biomechanics*, 34(7): 883-893.

Hellio, M. P. and Graverand-Gastineau, L. (2009) OA clinical trials: current targets and trials for OA. Choosing molecular targets: what have we learned and where we are headed? *Osteoarthritis and Cartilage*, 17(11): 1393-1401.

Hertzberg, R. W. and Manson, J. A. (1980) Fatigue of engineering plastics. *New York: Academice press*.

Hirakawa, K., Jacobs, J. J., Urban, R. and Saito, T. (2004) Mechanisms of failure of total hip replacements: lessons learned from retrieval studies. *Clinical Orthopaedics and Related Research*, 420: 10-7.

Hua, X., Wroblewski, B. M., Jin, Z. M. and Wang, L. (2012) The effect of cup inclination and wear on the contact mechanics and cement fixation for ultra high molecular weight polyethylene total hip replacements. *Medical Engineering and Physics*, 34(3): 318-325.

Huiskes, R. (1993) The Current State and Future of Cemented and Non-Cemented Total Hip Replacement. *Post Graduate Lectures, 1st European Congress of Orthopaedic Surgery*.

Huiskes, R. and Chao, E. Y. (1983) A Survey of finite element analysis in orthopedic biomechanics: the first decade. *Journal of Biomechanics*, 16(6): 385-409.

Hummel, M. T., Malkani, A. L., Yakkanti, M. R. and Baker, D. L. (2009) Decreased dislocation after revision total hip arthroplasty using larger femoral head size and posterior capsular repair. *Journal of Arthroplasty*, 24(Suppl. 6): 73-76.

Hussain, A., Counsell, L. and Kamali, A. (2010) Clinical effects of edge loading on metal-on-metal hip resurfacings. *Journal of Bone and Joint Surgery Br*, 92(suppl III): 399.

Iglic, A., Antolic, V. and Srakar, F. (1993) Biomechanical analysis of various operative hip joint rotation center shifts. *Archives of Orthopaedic and Trauma Surgery*, 112(3): 124-126.

Inghama, E and Fisher, J. (2005) The role of macrophages in osteolysis of total joint replacement. *Biomaterials*, 26(11): 1271-1286.

Isacson, J., Gransberg, L. and Knutsson, E. (1986) Three-dimensional electrogoniometric gait recording. *Journal of Biomechanics*, 19(8): 631-635.

Jagatia, M., Jalali-Vahid, D. and Jin, Z. M. (2001) Elastohydrodynamic lubrication analysis of ultra-high molecular weight polyethylene hip joint replacements under squeeze-film motion. *Proceedings of the Institution of Mechanical Engineers Part H: Journal of Engineering in Medicine,* 215(2): 141-152.

Jarrett, C. A., Ranawat, A. S., Bruzzone, M., Blum, Y. C., Rodriguez, J. A. and Ranawat, C. S. (2009) The squeaking hip: a phenomenon of

ceramic-onceramic total hip arthroplasty. *Journal of Bone and Joint Surgery Am*, 91(6): 1344-1349.

Jasty, M., Maloney, W. J., Bragdon, C. R., O'Connor, D. O., Haire, T. and Harris, H. H. (1991) The initiation of failure in cemented femoral components of hip arthroplasties. *Journal of Bone and Joint Surgery Br*, 73(4): 551-558.

Jeffers, J. R. T. (2005) In silico simulation of long term cement mantle failure in total hip replacement. PhD Thesis, *University of Southampton, UK*.

Jeffers, J. R., Roques, A., Taylor, A. and Tuke, M. A. (2009) The problem with large diameter metal-on-metal acetabular cup inclination. *Bulletin of the NYU Hospital for Joint Diseases*, 67(2): 189-192.

Jin, Z. M., Dowson, D. and Fisher, J. (1994) A parametric analysis of the contact stress in ultra-high molecular weight polyethylene acetabular cups. *Medical Engineering and Physics*, 16(5): 398-405.

Jin, Z. M., Dowson, D. and Fisher, J. (1997) Analysis of fluid film lubrication in artificial hip joint replacements with surfaces of high elastic modulus. *Proceedings of the Institution of Mechanical Engineers Part H: Journal of Engineering in Medicine*, 211(3): 247-256.

Jin, Z. M., Heng, S. M., Ng, H. W. and Auger, D. D. (1999) An axisymmetric contact model of ultra high molecular weight polyethylene cups against metallic femoral heads for artificial hip joint replacement. *Proceedings of the Institution of Mechanical Engineers Part H: Journal of Engineering in Medicine*, 213(4): 317-327.

Jin, Z. M., Stone, M., Ingham, E. and Fisher, J. (2006) Biotribology. *Current Orthopaedics*, 20(1): 32-40.

Johnson, K. L. (1985), Contact mechanics, *Cambridge University Press*, Cambridge, UK.

Johnston, R. C. and Smidt, G. L. (1969) Measurement of hip-joint motion during walking. Evaluation of an electrogoniometric method. *Journal of Bone and Joint Surgery Am*, 51(6): 1083-1094.

Jones, L. C. and Hungerford, D. S. (1987) Cement disease. *Clinical Orthopaedics and Related Research*, (225): 192-206.

Joshi, M. G., Santare, M. H. and Advani, S. G. (2000) Survey of stress analysis of the femoral hip prosthesis. *Applied Mechanics Reviews*, 53(1): 1-18.

Kadaba, M. P., Ramakrishnan, H. K. and Wootten, M. E. (1990). Measurement of lower extremity kinematics during level walking. *Journal of Orthopaedic Research*, 8(3): 383-392.

Kadoya, Y., Kobayashi, A. and Ohashi, H. (1998) Wear and osteolysis in total joint replacements. *Acta Orthop Scand Suppl.* 278: 1-16.

Kang, L., Galvin, A. L., Brown, T. D., Fisher, J. and Jin, Z. M. (2008) Wear simulation of ultra-high molecular weight polyethylene hip implants by incorporating the effects of cross-shear and contact pressure. *Proceedings of the Institution of Mechanical Engineers Part H: Journal of Engineering in Medicine.* 222(7): 1049-1064.

Kang, L., Galvin, A. L., Fisher, J. and Jin, Z. M. (2009) Enhanced computational prediction of polyethylene wear in hip joints by incorporating cross-shear and contact pressure in additional to load and sliding distance: Effect of head diameter. *Journal of Biomechanics.* 42 (7): 912-918.

Keiji, I., Yukihito, K. and Hiroomi, M. (2005) A method of calculation for contact pressure between femoral head and cup of artificial hip joint. *Tribology Transaction*, 48(2): 230-237.

Kerschbaumer, F., Kerschbaumer, G. and Deghani, F. (2007) Is a dorsal access associated with an elevated luxation rate following total hip replacement? *Orthopade*, 36(10): 928-934.

Kienapfel, H., Sprey, C., Wilke, A. and Griss, P. (1999) Implant fixation by bone ingrowth. *Journal of Arthroplasty*, 14(3): 355-368.

Kim, D. G., Miller, M. A. and Mann, K. A. (2004) A fatigue damage model for the cement–bone interface. *Journal of Biomechanics*, 37(10): 1505-1512.

Kleinhans, J. A., Jakubowitz, E., Seeger, J. B., Heisel, C. and Kretzer, J. P. (2009) Macroscopic third-body wear caused by porous metal surface fragments in total hip arthroplasty. *Orthopedics*, 32(5): 364.

Kluess, D. (2010) Finite element analysis in orthopaedic biomechanics, finite element analysis, David Moratal (Ed.), ISBN: 978-953-307-123-7, InTech, Available from: http://www.intechopen.com/books/finite-element-analysis/finite-element-analysis-in-orthopaedic-biomechanics.

Komistek, R. D., Dennis, D. A., Ochoa, J. A., Haas, B. D. and Hammill, C. (2002) *In vivo* comparison of hip separation after metal-on-metal or

metal-on-polyethylene total hip arthroplasty. *Journal of Bone and Joint Surgery Am,* 84-A(10): 1836-1841.

Komistek, R. D., Sedel, L., Northcut, E. and Anderson, D. (2004) *In vivo* Determination of hip joint separation in subjects having variable bearing surfaces. *Journal of Bone and Joint Surgery Br*, 86-B(Supp. IV): 412.

Konan, S., Rhee, S. J. and Haddad, F. S. (2009) Total hip arthroplasty for displaced fracture of the femoral neck using size 32 mm femoral head and soft tissue repair after a posterior approach. *Hip International*, 19(1): 30-35.

Korhonen, R. K., Koistinen, A., Konttinen, Y. T., Santavirta, S. S. and Lappalainen, R. (2005) The effect of geometry and abduction angle on the stress in cemented UHMWPE acetabular cups-finite element simulations and experimental tests. *BioMedical Engineering Online*, 4(32): 1-14.

Krieg, A. H., Speth, B. M. and Ochsner, P. E. (2009) Backside volumetric change in the polyethylene of uncemented acetabular components. *Journal of Bone and Joint Surgery Br*, 91(8):1037-1043.

Kuehn, K. D., Ege, W. and Gopp, U. (2005) Acrylic bone cements: mechanical and physical properties. *Orthopedic Clinics of North America*, 36(1): 29-39.

Kurtz, S. M., Bartel, D. L. and Edidin, A. A. (1994) The effects of gaps on contact stress and relative motion in a metal-backed acetabular component. *Transactions of Orthopaedics Research Society*, 19: 243

Kurtz, S. M., Edidin, A. A. and Bartel, D. L. (1997) The role of backside polishing, cup angle, and polyethylene thickness on the contact stresses in metal-backed acetabular components. *Journal of Biomechanics*, 30(6): 639-642.

Kurtz, S. M., Ochoa, J. A., Hovey, C. B. and White C. V. (1999) Simulation of initial frontside and backside wear rates in a modular acetabular component with multiple screw holes. *Journal of Biomechanics*, 32(9): 967-976.

Kurtz, S. M., Ochoa, J. A., White, C. V., Srivastav, S. and Cournoyer, J. (1998) Backside nonconformity and locking restraints affect liner/shell load transfer mechanisms and relative motion in modular acetabular components for total hip replacement. *Journal of Biomechanics*, 31(5): 431-437.

Kurtz, S. M., Muratoglub, O. K., Evansc, M. and Edidind, A. (1999) Advances in the processing, sterilization, and crosslinking of ultra-high molecular weight polyethylene for total joint arthroplasty. *Biomaterials*, 20(18): 1659-1688.

Kurtz, S. M., Pruitt, L., Jewett, C. W., Crawford, R. P., Crane, D. J. and Edidin, A. A. (1999) The yielding, plastic flow, and fracture behavior of ultra-high molecular weight polyethylene used in total joint replacements. *Biomaterials*, 19(21): 1989-2003.

Kurtz, S. M., Rimnac, C. M. and Bartel, D. L. (1998) Predictive model for tensile true stress-strain behavior of chemically and mechanically degraded ultrahigh molecular weight polyethylene. *Journal of Biomedical Materials Research*, 43(3): 241-248.

Lamvohee, J. M. S., Mootanah, R., Dowell and Ingle, P. (2007) Patients' bone morphology and bone quality affect the performance of fixation techniques in cemented total hip replacements. *Journal of Biomechanics*, 40(Suppl. 2): 228

Lamvohee, J. M. S., Mootanah, R., Ingle, P., Cheah, K. and Dowell, J. K. (2009) Stresses in cement mantles of hip replacements: effect of femoral implant sizes, body mass index and bone quality. *Computer Methods in Biomechanics and Biomedical Engineering,* 12(5): 501-510.

Langton, D. J., Jameson, S. S., Joyce, T. J., Webb, J. and Nargol, A. V. (2008) The effect of component size and orientation on the concentrations of metal ions after resurfacing arthroplasty of the hip. *Journal of Bone and Joint Surgery Br*, 90B(9): 1143-1151.

Lavernia, C., Barrack, R., Thornberry, R. and Tozakoglou, E. (1998) The effects of component position on the motion to impingement and dislocation in total hip replacement. *Scientific exhibit presented at AAOS meeting*, New Orleans.

Laz, P. J. and Browne, M. (2010) A review of probabilistic analysis in orthopaedic biomechanics. *Proceedings of the Institute of Mechanical Engineers Part H: Journal of Engineering in Medicine*, 224(8): 927-943.

Lerch, M., Kurtz, A. Stukenborg-Colsman, C., Nolte, I., Weigel, N., Bouguecha, A.and Behrens, B. A. (2012) Bone remodeling after total hip arthroplasty with a short stemmed metaphyseal moading implant: finite element analysis validated by a prospective DEXA investigation.. *Journal of orthopaedic research*, 30(11): 1822-1829.

Leslie, I. J., Williams, S., Isaac, G., Ingham, E. and Fisher, J. (2009) High cup angle and microseparation increase the wear of hip surface replacements. *Clinical Orthopaedics and Related Research*, 467(9): 2259-2265.

Leung, A. S., Gordon, L. M., Skrinskas, T., Szwedowski, T. and Whyne, C. M. (2009) Effects of bone density alterations on strain patterns in the pelvis: Application of a finite element model. *Proceedings of the Institution of Mechanical Engineers Part H: Journal of Engineering in Medicine*, 223(8): 965-979.

Lewis, G. (1997) Properties of acrylic bone cement: state of the art review. *Journal of Biomedical Materials Research*, 38(2): 155-182.

Lewis G. (2003) Fatigue testing and performance of acrylic bone-cement materials: state-of-the-art review. *Journal of Biomedical Materials Research Part B: Applied Biomaterials*, 66(1): 457-486.

Li. S and Burstein, A. H. (1994) Ultra-high molecular weight polyethylene. The material and its use in total joint implants. *The Journal of Bone and Joint Surgery Am,* 76(7): 1080-1090.

Li, G., Sakamoto, M. and Chao, E. Y. S. (1997) A Comparison of Different Methods in Predicting Static Pressure Distribution in Articulating joints. *Journal of Biomechanics*, 30(6): 635-638.

Li, P. L., Ingle, P. J. and Dowell, J. K. (1996) Cement-within-cement revision hip arthroplasty: should it be done? A biomechanical study. *Journal of Bone and Joint Surgery Br*, 78B(5): 809-811.

Liau, J. J., Cheng, C. K., Huang, C. H. and Lo, W. H. (2002) Effect of Fuji pressure sensitive film on actual contact characteristics of artificial tibiofemoral joint. *Clinical Biomechanics (Bristol, Avon),* 17(9-10): 698-704.

Liu, F., Udofia, I. J., Jin, Z. M., Hirt, F., Rieker, C., Roberts, P. and Grigoris, P. (2005a) Comparison of contact mechanics between a total hip replacement and a hip resurfacing with a metal-on-metal articulation. *Proceedings of the Institution of Mechanical Engineers Part C: Journal of Mechanical Engineering Science*, 219(7): 727-732.

Liu, F. (2005b) Contact mechanics and elastohydrodynamic lubrication analysis of metal-on-metal hip implant with a sandwich acetabular cup under transient walking condition. PhD Thesis, *University of Bradford*, UK.

Liu, F., Jin, Z. M., Grigoris, P., Hirt, F. and Rieker, C. (2003) Contact mechanics of metal-on-metal hip implants employing a metallic cup with a UHMWPE backing. *Proceedings of the Institution of Mechanical Engineers Part H: Journal of Engineering in Medicine*, 217(3): 207-213.

Liu, F., Leslie, L., Wiliams, S., Fisher, J. and Jin, Z. (2008) Development of computational wear simulation of metal-on-metal hip resurfacing replacement. *Journal of biomechanics*, 41(3): 686-694.

Liu, F., Fisher, J. and Jin, Z. M. (2012) Computational modelling of polyethylene wear and creep in total hip joint replacements: Effect of the bearing clearance and diameter. *Proceedings of the Institution of Mechanical Engineers, Part J: Journal of Engineering Tribology*, 0(0): 1-12.

Lombardi, A. V., Mallory, T. H., Dennis, D. A., Komistek, R. D., Fada, R. A. and Northcut, E. J. (2000) An *in vivo* determination of total hip arthroplasty pistoning during activity. *Journal of Arthroplasty*, 15(6): 702-709.

Lord, J. K., Langton, D. J., Nargol, A. V. F. and Joyce, T. J. (2011) Volumetric wear assessment of failed metal-on-metal hip resurfacing prostheses. *Wear*, 272(1): 79-87.

Lusty, P. J., Watson, A., Tuke, M. A., Walter, W. L., Walter, W.K. and Zicat, B. (2007) Wear and acetabular component orientation in third generation alumina-on-alumina ceramic bearings: an analysis of 33 retrievals [corrected]. *Journal of Bone and Joint Surgery Br*, 89(9): 1158-1164.

Mai, M. T., Schmalzried, T. P., Dorey, F. J., Campbell, P. A. and Amstutz, H. C. (1996) The contribution of frictional torque to loosening at the cement-bone interface in tharies hip replacements. *Journal of Bone and Joint Surgery Am*, 78(4): 505-511.

Mak, M. M., Besong, A. A., Jin, Z. M. and Fisher, J. (2002) Effect of microseparation on contact mechanics in ceramic-on-ceramic hip joint replacements. *Proceedings of the Institution of Mechanical Engineers Part H: Journal of Engineering in Medicine*, 216(6): 403-408.

Mak, M. M. and Jin, Z. M. (2002) Analysis of contact mechanics in ceramic-on-ceramic hip joint replacements. *Proceedings of the Institution of Mechanical Engineers Part H: Journal of Engineering in Medicine*, 216(4): 231-236.

Mak, M. M., Jin, Z. M., Fisher J and Stewart, T. D. (2011) Influence of acetabular cup rim design on the contact stress during edge loading in ceramic-on-ceramic hip prostheses. *Journal of Arthroplasty*, 26(1): 131-136.

Maloney, W. J. and Smith, R. L. (1995) Periprosthetic osteolysis in total hip arthroplasty: the role of particulate wear debris. *Journal of Bone and Joint Surgery Am*, 77(9): 1448-1461.

Maloney, W. J., Smith, R. L., Hvene, D., Schmalzried, T. P. and Rubash, H. (1994) Isolation and characterisation of wear particles generated in patients who have had failure of a hip arthroplasty without cement. *Journal of Bone and Joint Surgery Am*, 77(9): 1301-1310.

Manaka, M., Clarke, I. C., Yamamoto, K., Shishido, T., Gustafson, A. and Imakiire, A. (2004) Stripe wear rates in alumina THR - comparison of microseparation simulator study with retrieved implants. *Journal of Biomaterials Research Part B: Applied Biomaterials*, 69(2): 149-157.

Manley, M. T. and Serekian, P. (1994) Wear debris. An environmental issue in total joint replacement. *Clinical Orthopaedics and Related Research*, 298: 137-146.

Mann, K. A., Mocarski, R., Damron, L. A., Allen, M. J. and Ayers, D. C. (2001) Mixed-mode failure response of the cement-bone interface. *Journal of Orthopaedic Research*, 19(6): 1153-1161.

Margevicius, K. J., Bauer, T. W., McMahon, J. T., Brown, S. A. and Merritt, K. (1994) Isolation and characterisation of debris in membranes around total joint prostheses. *Journal of Bone and Joint Surgery*, 76(11): 1664-1675.

Maxian, T. A., Brown, T. D., Pedersen, D. R. and Callaghan, J. J. (1996a) A sliding-distance-coupled finite element formulation for polyethylene wear in total hip arthroplasty. *Journal of Biomechanics*, 29(5): 687-692.

Maxian, T. A., Brown, T. D., Pedersen, D. R. and Callaghan, J. J. (1996b) Adaptive finite element modelling of long-term polyethylene wear in total hip arthroplasty. *Journal of Orthopaedic Research*, 14(4): 668-675.

Mazzucco, D. and Spector, M. (2003) Effects of contact area and stress on the volumetric wear of ultrahigh molecular weight polyethylene. *Wear*, 254(5): 514-522.

McCormack, B. A. and Prendergast, P. J. (1999) Microdamage accumulation in the cement layer of hip replacements under flexural loading. *Journal of Biomechanics*, 32(5): 467-475.

McKee, G. K. (1982) Total hip replacement--past, present and future. *Biomaterials*, 3(3): 130-135.

McKellop, H., Shen, F. W., Lu, B., Campbell, P. and Salovey, R. (2000) Effect of sterilization method and other modifications on the wear resistance of acetabular cups made of ultra-high molecular weight polyethylene. A hip-simulator study. *The Journal of bone and joint surgery Am*, 82(12): 1708-1725.

McNie, C., Barton, D. C., Stone, M. H. and Fisher, J. (1998) Prediction of plastic strains in ultra-high molecular weight polyethylene due to microscopic asperity interactions during sliding wear. *Proceedings of the Institution of Mechanical Engineers Part H: Journal of Engineering in Medicine*, 212(1): 49-56.

Mellon, S. J., Kwon, Y. M., Glyn-Jones, S., Murray, D. W. and Gill, H. S. (2011) The effect of motion patterns on edge-loading of metal-on-metal hip resurfacing. *Medical Engineering and Physics*, 33(10): 1212-1220.

Moore, K. L. and Agur, A. M. R. (2002) Essential clinical anatomy. *Lippincott Williams and Wilkins*.

Morlock, M. M., Bishop, N., Zustin J, Hahn, M., Rüther, W. and Amling, M. (2008) Modes of implant failure after hip resurfacing: morphological and wear analysis of 267 retrieval specimens. *Journal of Bone and Joint Surgery Am*, 90(3): 89-95.

Morrey, B. and Ilstrup, D. (1989) Size of the femoral head and acetabular revision in total hip-replacement arthroplasty. J*ournal of Bone and Joint Surgery Am*, 71(1): 50-55.

Muehleman, C. and Arsenis, C. H. (1995) Articular cartilage. Part II. The osteoarthritic joint. *Journal of the American Podiatric Medical Association*, 85(5): 282-286.

Müllera, O., Parak, W. J, Wiedemann, M. G. and Martini, F. (2004) Three-dimensional measurements of the pressure distribution in artificial joints with a capacitive sensor array. *Journal of Biomechanics*, 37(10): 1623-1625.

Murray, D. W. and Rushton, N. (1990) Macrophages stimulate bone resorption when they phagocytose particles. *Journal of Bone and Joint Surgery*, 72(6): 988-992.

Murphy, B. P. and Prendergast, P. J. (1999) Measurement of non-linear microcrack accumulation rates in polymethylmethacrylate bone cement under cyclic loading. *Journal of Materials Science: Materials in Medicine*, 10(12): 779-781.

Nadzadi, M. E., Pedersen, D. R., Yack, H. J., Callaghan, J. J. and Brown, T. D. (2003) Kinematics, kinetics, and finite element analysis of commonplace maneuvers at risk for total hip dislocation. *Journal of Biomechanics*, 36(4): 577-591.

Neill, A. L. (2008) The A to Z of Bones, Joints and Ligaments and the Back. *St. Leonards, NSW: Aspen Pharmacare Australia*.

Netter, J. D., Steklow, N., Hermida, J. C., Chen, P. C., Nevelos, J. and D'Lima, D. D. (2013) Increased wear in low and high Crosslinked polyethylene due to microseparation of total hip arthroplasty component. *59th Annual Meeting, Orthopaedic Research Society*, January 26-29, San Antonio, US.

Nevelos, J. E., Ingham, E., Doyle, C., Fisher, J. and Nevelos, A. B. (1999) Analysis of retrieved alumina ceramic components from Mittelmeier total hip prostheses. *Biomaterials*, 20(19): 1833-1840.

Nevelos, J. E., Ingham, E., Doyle, C., Streicher, R., Nevelos, A. and Fisher, J. (2001a) Micro-separation *in vitro* produces clinically relevant wear of ceramic–ceramic total hip replacements. *Key Engineering Materials*, 192-195: 529-532.

Nevelos, J. E., Prudhommeaux, F., Hamadouche, M., Doyle, C., Ingham, E., Meunier, A., Nevelos, A., Sedel, L. and Fisher, J. (2001b) Comparative analysis of two different types of Alumina-Alumina hip prostheses retrieved for aseptic loosening. *Journal of Bone and Joint Surgery Br*, 83(4): 598-603.

Nevelos, J. E., Ingham, E., Doyle, C., Streicher, R., Nevelos, A., Walter, W. and Fisher, J. (2000) Microseparation of the centers of alumina-alumina artificial hip joint during simulator testing produces clinically relevant wear rateand patterns. *Journal of Arthroplasty*, 15(6): 793-795.

Ng, F. Y., Zhang, J. T., Chiu, K. Y. and Yan, C. H. (2011) A cadaveric study of posterior dislocation after total hip replacement-effects of head

diameter and acetabular anteversion. *International Orthopaedics (SICOT)*, 35(3): 325-329.

Norkin, C. and Levangie, P. K. (1992) Joint structure and function. A comprehensive analysis. *Philadelphia, F. A. Davis Company*.

Ogden, C. L., Fryar, C. D., Carroll, M. D. and Flegal, K. M. (2004) Mean body weight, height and body mass index, United States 1960-2002. *Advance data from Vital and Health Statistics US Department of Health & Human Services*, 347: 1-20.

Okrajni, J., Plaza, M. and Ziemba, S. (2007) Validation of computer models of an artificial hip joint. *Archives of Materials Science and Engineering*, 28(5): 305-308.

Orishimo, K. F., Claus, A. M., Sychterz, C. J. and Engh, C. A. (2003) Relationship between polyethylene wear and osteolysis in hips with a second-generation porous-coated cementless cup after seven years of follow-up. *Journal of Bone and Joint Surgery Am*, 85A(6): 1095-1099.

Õunpuu, S, . (1995). Clinical gait analysis. Evaluation and Management of Gait Disorders.

Paul, J. P. (1966) Forces transmitted by joints in the human body. *Proceedings of the Institution of Mechanical Engineers, Conference Proceedings*, 181(8): 8-15.

Paul, J. P. (1976) Force actions transmitted by joints in the human body. *Proceedings of the Royal Society of London. Series B, Biological Sciences*, 192(1107): 163-172.

Palastanga, N. P., Field, D. and Soames, R. (2006) Anatomy and Human Movement: Structure and Function. *Butterworth Heinemann*.

Patil, S., Bergula, A., Chen, P. C., Colwell, C. W. Jr. and D'Lima, D. D. (2003) Polyethylene wear and acetabular component orientation. *Journal of Bone and Joint Surgery Am*, 85A(Suppl.4): 56-63.

Pedersen., D. R., Crowninshield., R. D., Brand, R. A. and Johnston, R. C. (1982) An axisymmetric model of acetabular components in total hip arthroplasty. *Journal of biomechanics*, 15(4): 305-345.

Pedersen, D. R., Callaghan, J. J. and Brown, T. D. (2005) Activity-dependence of the "safe zone" for impingement versus dislocation avoidance. *Medical Engineering & Physics*, 27: 323-328.

Penmetsa, J. R., Laz, P. J., Petrella, A. J. and Rullkoetter, P. J. (2006) Influence of polyethylene creep behavior on wear in total hip arthroplasty. *Journal of Orthopaedic Research*, 24(3): 422-427.

Plank, G. R., Estok, D. M., Muratoglu, O. K., O'Connor, D. O., Burroughs, B. R. and Harris, W. H. (2007) Contact stress assessment of conventional and highly crosslinked ultra high molecular weight polyethylene acetabular liners with finite element analysis and pressure sensitive film. *Journal of Biomedical Materials Research Part B: Applied Biomaterials*, 80(1): 1-10.

Rabinowicz, E. (1995). Friction and Wear of Materials. *John Wiley and Sons*, New York, USA.

Race, A., Miller, M. A., Ayers, D. C. and Mann, K. A. (2003) Early cement damage around a femoral stem is concentrated at the cement/bone interface. *Journal of Biomechanics*, 36(4): 489-496.

Ramero, F., Amirouche, F., Aram, L. and Gonalez, M. H. (2007) Experimental and analytical validation of a modular acetabular prosthesis in total hip arthroplasty. *Journal of Orthopaedic Surgery and Research*, 2(7): 1-9.

Restrepo, C., Matar, W. Y., Parvizi, J., Rothman, R. H. and Hozack, W. J. (2010) Natural history of squeaking after total hip arthroplasty. *Clinical Orthopaedics and Related Research*, 468(9): 2340-2345.

Ries, M. D., Young, E., Al-Marashi, L., Goldstein, P., Hetherington, A., Petrie, T. and Pruitt, L. (2006) *In vivo* behavior of acrylic bone cement in total hip arthroplasty. *Biomaterials*, 27(2): 256-261.

Rose, R. M., Goldfarb, H. V., Ellis, E. and Crugnola, A. N. (1983) On the pressure dependence of the wear of UHMWPE. *Wear*, 92(1): 99-111.

Rostoker, W. and Galante, J. O. (1979) Contact pressure dependence of wear rates of UHMWPE. *Journal of Biomedical Materials Research*, 13(6): 957-964.

Rothman, R. H. and Cohn, J. C. (1990) Cemented versus cementless total hip arthroplasty. A critical review. *Clinical Orthopaedics and Related Research*, (254): 153-169.

Rydell, N. W. (1966) Forces acting on the femoral head-prosthesis. A study on strain gauge supplied prostheses in living persons. *Acta Orthopaedica Scandinavica*, 37(Suppl. 88): 1-132.

Sakalkale, D. P., Eng, K., Hozack, W. J. and Rothman, R. H. (1999) Minimum 10-year results of a tapered cementless hip replacement. *Clinical Orthopaedics and Related Research*, (362): 138-144.

Saha, S. and Roychowdhury, A. (2009) Application of the finite element method in orthopedic implant design. *Journal of Long-Term Effects of Medical Implants*,19(1): 55-82.

Salek, E. (2012) Handbook of lubrication and tribology: theory and design. *Technology & Engineering, CRC Press*.

Sanders, A. P., and Brannon, R. M. (2011) Assessment of the applicability of the Hertzian contact theory to edge-loaded prosthetic hip bearings. *Journal of Biomechanics*, 44(16): 2802-2808.

Sariali, E., Stewart, T. D., Jin, Z. M. and Fisher, J. (2012) Effect of cup abduction angle and head lateral microseparation on contact stresses in ceramic-on-ceramic total hip arthroplasty. *Journal of Biomechanics*, 45(2): 390-393.

Scholes, S. C. and Unsworth, A. (2000) Comparison of friction and lubrication of different hip prostheses. *Proceedings of the Institution of Mechanical Engineers Part H: Journal of Engineering in Medicine*, 214(1): 49-57.

Schulte, K. R., Callaghan, J. J., Kelley, S. S. and Johnston, R. C. (1993) The outcome of Charnley total hip arthroplasty with cement after a minimum twenty-year follow-up. The results of one surgeon. *Journal of Bone and Joint Surgery Am*, 75(7): 961-975.

Scifert, C. F., Brown, T. D., Pedersen, D. R. and Callaghan, J. J. (1998) A Finite element analysis of factors influencing total hip dislocation. *Clinical Orthopaedics and Related Research*, 355: 152-162.

Scifert, C. F., Brown, T. D., Pedersen, D. R., Heiner, A. D., Callaghan, J. J. (1999) Development and physical validation of a finite element model of total hip dislocation. *Comput Methods in Biomechnics and Biomedical Engineering*, 2(2): 139-147.

Sedel, L., Nizard, R. S., Kerboull, L. and Witvoet, J. (1994) Alumina-alumina hip replacement in patients younger than 50 years old. *Clinical Orthopaedics and Related Research*, (298): 175-183.

Semlitsch, M. and Willert, H. G. (1997) Clinical wear behaviour of ultra-high molecular weight polyethylene cups paired with metal and ceramic ball heads in comparison to metal-on-metal pairings of hip joint

replacements. *Proceedings of the Institution of Mechanical Engineers, Part H: Journal of Engineering in Medicine*, 211(1): 73-88.

Shishido, T., Yamamoto, K., Clarke, I. C., Masaoka, T., Manaka, M. and Tateiwa, T. (2006) Comparison of the results of a simulator study and retrieval implants in ceramic THA. *Key Engineering Materials*, 309-311: 1277-1280.

Silva, M., Shepherd, E. F., Jackson, W. O., Dorey, F. J. and Schmalzried, T. P. (2002) Average patient walking activity approaches 2 million cycles per year: pedometers under-record walking activity. *Journal of Arthroplasty*, 17(6): 693-697.

Simonsen, E. B., Dyhre-Poulsen, P., Voigt, M., Aagaard, P., Sjøgaard, G. and Bojsen-Møller, F. (1995) Bone-on-bone forces during loaded and unloaded walking. *Acta Anatomic (Basel)*, 152(2): 133-142.

Smidt, G. L. (1971) Hip motion and related factors in walking. *Physical Therapy*, 51(1): 9-21.

Smith, D. C. (2005) The genesis and evolution of acrylic bone cement. *Orthopaedic Clinics of North America*, 36 (1): 1-10.

Smith, S. L., Goldsmith, A. A. J. and Dowson, D. (2002) Lubrication and wear of zirconia-on-metal total hip replacements. *Tribology Series*, 40: 377-386.

Stachowiak, G. W. and Batchelor, A. W. (2005). Engineering Tribology. *Butterworth-Heinemann*.

Stansfield, B. W., Nicol, A. C., Paul, J. P., Kelly, I. G., Graichen, F. and Bergmann, G. (2003) Direct comparison of calculated hip joint contact forces with those measured using instrumented implants. An evaluation of a three-dimensional mathematical model of the lower limb. *Journal of Biomechanics*, 36(7): 929-936.

Stewart, K. J., Pedersen, D. R., Callaghan, J. J. and Brown, T. D. (2004) Implementing capsule representation in a total hip dislocation finite element model. *Iowa Orthopaedic Journal*, 24: 1-8.

Stewart, T., Tipper, J., Streicher, R., Ingham, E. and Fisher, J. (2001) Long-term wear of HIPed alumina on alumina bearings for THR under microseparation conditions. *Journal of Materials Science: Materials in Medicine,* 12(10-12): 1053-1056.

Stolk, J., Verdonschot, N. J. J., Murphy, B. P., Prendergast, P. J. and Huiskes, H. W. J. (2004) Finite element simulation of anisotropic damage accumulation and creep in acrylic bone cement. *Engineering Fracture Mechanics*, 71: 513-528.

Stolk, J., Verdonschot, N., Murphy, B. P., Prendergast, P. J. and Huiskes, H. W. J. (2004) Finite element simulation of anisotropic damage accumulation and creep in acrylic bone cement. *Engineering Fracture Mechanics*, 71: 513–528.

Sundfeldt, M., Carlsson, L. V., Johansson, C. B., Thomsen, P. and Gretzer, C. (2006) Aseptic loosening, not only a question of wear: a review of different theories. *Acta Orthopaedica*, 77(2): 177-197.

Sutherland D. H., Olshen, R., Cooper, L. and Woo, S. L. (1980) The development of mature gait. *The Journal of Bone & Joint Surgery Am*, 62(3): 336-353.

Tipper, J. L., Ingham, E., Hailey, J. L., Besong, A. A., Fisher, J., Wroblewski, B. M. and Stone, M. H. (2000) Quantitative analysis of polyethylene wear debris, wear rate and head damage in retrieved Charnley hip prostheses. *Journal of Materials Science: Materials in Medicine*. 11(2): 117-124.

Tong, J., Zanta, N. P., Wanga, J. Y., Heaton-Adegbilea, P. and Hussella, J. G. (2008) Fatigue in cemented acetabular replacements. *International Journal of Fatigue*, 30(8): 1366-1375.

Tozzi, G., Zhang, Q. H. and Tong, J. (2012) 3D real-time micromechanical compressive behaviour of bone-cement interface: Experimental and finite element studies. *Journal of Biomechanics*, 45(2): 356-363.

Ulrich-Vinther, M., Carmody, E. E., Goater, J. J., Sballe, K., O'Keefe, R. J. and Schwarz, E. M. (2002) Recombinant adeno-associated virus-mediated osteoprotegerin gene therapy inhibits wear debris-induced osteolysis. *Journal of Bone and Joint Surgery Am*, 84-A(8): 1405-1412.

Udofia, I. J., Liu, F.; Jin, Z. M.; Roberts, P. and Grigoris, P. (2005) Contact mechanics analysis and initial stability of press-fit metal-on-metal hip resurfacing prostheses. *World Tribology Congress III*. Washington, DC, USA.

Udofia I, J., Liu F, Jin, Z. M., Roberts, P. and Grigoris, P. (2007) The initial stability and contact mechanics of a press-fit resurfacing arthroplasty of the hip. *Journal of Bone and Joint Surgery Br*, 89B(4): 549-556.

Udofia, I. J., Yew, A. and Jin, Z. M. (2004) Contact mechanics analysis of metal-on-metal hip resurfacing prostheses. *Proceedings of the Institution of Mechanical Engineers Part H: Journal of Engineering in Medicine*, 218(5): 293-305.

Underwood, R. J., Zografos, A., Sayles, R. S., Hart, A. and Cann, P. (2012) Edge loading in metal-on-metal hips: low clearance is a new risk factor. *Proceedings of the Institution of Mechanical Engineers Part H: Journal of Engineering in Medicine*, 226(3): 217-226.

Uribe, J., Hausselle, J., Geringer, J. and Forest, B. (2011) Finite element modelling of shock-induced damages on ceramic hip prostheses. *ISRN Materials Science*, 121486 : 1-14.

Vasu, R., Carter, D. R. and Harris, W. H. (1982) Stress distribution in the acetabular region-I. before and after total joint replacement. *Journal of Biomechanics*, 15(3): 155-164.

Verdonschot, N., Vena, P., Stolk, J. and Huiskes, R. (2002) Effects of metal-inlay thickness in polyethylene cups with metal-on-metal bearings. *Clinical Orthopaedics and Related Research*, (404): 353-361.

Wang, A., Stark, C. and Dumbleton, J. H. (1995) Role of cyclic plastic deformation in the wear of UHMWPE acetabular cups. *Journal of Biomedical Materials Research,* 29(5): 619-626.

Wang, J. T., Harada, Y. and Goldring, S. R. (1993) Biological mechanisms involved in the pathogenesis of aseptic loosening after total joint replacement. *Seminars in Arthroplasty*, 4: 215-222.

Wang, J. Y., Heaton-Adegbile, P., New, A., Hussell, J. G. and Tong, J. (2009) Damage evolution in acetabular replacements under long-term physiological loading conditions. *Journal of Biomechanics* 42(8): 1061-1068.

Wang, J. Y., Tozzi, G., Chen, J., Contal, F., Lupton, C. and Tong, J. (2010) Bone-cement interfacial behaviour under mixed mode loading conditions. *Journal of the Mechanical Behavior of Biomedical Materials*, 3(5): 392-398.

Wang, L., Williams, S., Udofia, I., Isaac, G., Fisher, J. and Jin, Z. M. (2012) The effect of cup orientation and coverage on contact mechanics and range of motion of metal-on-metal hip resurfacing arthroplasty. *Proceedings of the Institution of Mechanical Engineers Part H: Journal of Engineering in Medicine*, 226(11): 877-886.

Walter, W. L., Insley, G. M., Walter, W. K. and Tuke, M. A. (2004) Edge loading in third generation alumina ceramic-on-ceramic bearings: stripe wear. *Journal of Arthroplasty*, 19(4): 402-413.

Walter, W. L., Yeung, E. and Esposito, C. (2010) A review of squeaking hips. *Journal of the American Academy of Orthopaedic Surgeons*, 18(6): 319-326.

Willert, H. G., Bertram, H. and Buchhorn, G. H. (1990) Osteolysis in alloarthroplasty of the hip. The role of bone cement fragmentation. *Clinical Orthopaedics and Related Research*, (258): 108-121.

Willert, H. G., Buchhorn, G. H., Fayyazi, A., Flury, R., Windler, M., Koster, G. and Lohmann, C. H. (2005) Metal-on-metal bearings and hypersensitivity in patients with artificial hip joints: a clinical and histomorphological study. *Journal of Bone and Joint Surgery Am*, 87(1): 28-36.

Williams, S., Butterfield, M., Stewart, T., Ingham, E., Stone, M. and Fisher, J. (2003) Wear and deformation of ceramic-on-polyethylene total hip replacements with joint laxity and swing phase microseparation. *Proceedings of the Institution of Mechanical Engineers Part H: Journal of Engineering in Medicine*, 217(2): 147-153.

Williams, S., Jalali-Vahid, D., Brockett, C., Jin, Z. M., Stone, M. H., Ingham, E. and Fisher, J. (2006) Effect of swing phase load on metal-on-metal hip lubrication, friction and wear. *Journal of Biomechanics*, 39(12): 2274-2281.

Williams, S., Leslie, I., Isaac, G., Jin, Z. M., Ingham, E. and Fisher, J. (2008) Tribology and wear of metal-on-metal hip prostheses: influence of cup angle and head position. *Journal of Bone and Joint Surgery Am*, 90(Suppl. 3):111-117.

Williams, S., Stewart, T. D., Ingham, E., Stone, M. H. and Fisher, J. (2004) Metal-on-metal bearing wear with different swing phase loads. *Journal of Materials Research Part B: Applied Biomaterials*, 70(2): 233-239.

Wilson, D. R., Apreleva, M. V., Eichler, M. J. and Harrold, F. R. (2003) Accuracy and repeatability of a pressure measurement system in the patellofemoral joint. *Journal of Biomechanics*, 36(12): 1909-1915.

Woo, R. Y. and Morrey, B. F. (1982) Dislocations after total hip arthroplasty. *Journal of Bone and Joint Surgery Am*, 64(9): 1295-1306.

Wroblewski, B. M. (1985) Direction and rate of socket wear in Charnley low-friction arthroplasty. *Journal of Bone and Joint Surgery Br*, 67B(5): 757-761.

Wroblewski, B. M., Siney, P. D. and Fleming, P. A. (2007) Charnley low-friction arthroplasty: survival patterns to 38 years. *Journal of Bone and Joint Surgery Br*, 89B(8): 1015-1018.

Wroblewski, B. M., Siney, P. D. and Fleming, P. A. (2009a) The principle of low frictional torque in the Charnley total hip replacement. *Journal of Bone and Joint Surgery Br*, 91(7): 855-858.

Wroblewski, B. M., Siney, P. D. and Fleming, P. A. (2009b) Effect of reduced diameter neck stem on incidence of radiographic cup loosening and revisions in Charnley lowfrictional torque arthroplasty. *The Journal of Arthroplasty*, 24(1): 10-14.

Wroblewski, B. M., Siney, P. D. and Fleming, P. A. (2009c) Charnley low-frictional torque arthroplasty: follow-up for 30 to 40 years. *Journal of Bone and Joint Surgery Br*, 91(4): 447-450.

Wu, J. Z., Herzog, W. and Epstein, M. (1998) Effects of inserting a pressensor film into articular joints on the actual contact mechanics. *Journal of Biomechanical Engineering*, 120(5): 655-659.

Yamada, H., Yoshihara, Y., Henmi, O., Morita, M., Shiromoto, Y., Kawano, T., Kanaji, A., Ando, K., Nakagawa, M., Kosaki, N. and Fukaya, E. (2009) Cementless total hip replacement: past, present, and future. *Journal of Orthopaedic Science*, 14(2): 228-241.

Yamamoto, T., Saito, M., Ueno, M., Hananouchi, T., Tokugawa, Y. and Yonenobu, K. (2005) Wear analysis of retrieved ceramic-on-ceramic articulations in total hip arthroplasty: Femoral head makes contact with the rim of the socket outside of the bearing surface. *Journal of Biomaterials Research Part B: Applied Biomaterials,* 73(2): 301-307.

Young, A. M., Sychterz, C. J., Hopper, R. H. J. and Engh, C. A. (2002) Effect of acetabular modularity on polyethylene wear and osteolysis in total hip arthroplasty. *Journal of Bone and Joint Surgery Am*, 84A(1): 58-63.

Zant, N. P., Heaton-Adegbile, P., Hussell, J. G. and Tong, J. (2008) *In vitro* fatigue failure of cemented acetabular replacements: a hip simulator study. *Journal of Biomechanical Engineering*, 130(2): 021019.

Zant, N. P., Wong, C. K. Y. and Tong, J. (2007) Fatigue failure in the cement mantle of a simplified acetabular replacement model. *International Journal of Fatigue*, 29(7): 1245-1252.

Zhang, Q. H., Wang, J. Y., Lupton, C., Heaton-Adegbile, P., Guo, Z. X., Liu, Q. and Tong, J. (2010) A subject-specific pelvic bone model and its application to cemented acetabular replacements, *Journal of biomechanics*, 43(14): 2722-2227.

Appendix A
Matlab Code For Surface Fitting

```
% Select the X,Y,Z coordinate for the CMM data

x = A(:,1);
y = A(:,3);
z = A(:,2);
o=[x,y,z];

% Remove the data on the rim of the cup

k=1;
m=length(o);
  for j=1:m
      if  o(j,3)<-6;
          n(k,:)=o(j,:);
          k=k+1;
      end
  end

x1=n(:,1);
y1=n(:,2);
z1=n(:,3);

% Split the data into 36 tracks

t(1,:)=n(1,:);
nrow=2;

track=1;
   for row=2:length(n)
       if abs(n(row,3)-n(row-1,3))<5;
           t(nrow,track*3-2)=n(row,1);
           t(nrow,track*3-1)=n(row,2);
           t(nrow,track*3)=n(row,3);
           nrow=nrow+1;
       else
           track=track+1;
           nrow=2;
           t(nrow-1,track*3-2)=n(row,1);
           t(nrow-1,track*3-1)=n(row,2);
           t(nrow-1,track*3)=n(row,3);
        end
     end


% tracks plot

    for j1=1:36
        p(j1,:)=t(j1,:);
```

```
    end

pstrack=1;
ptrack=36;

    for j2=pstrack:pstrack+ptrack-1
        plot(sqrt(p(:,3*j2-2).^2+p(:,3*j2-1).^2),p(:,3*j2));
        hold on;
    end


% Choose tracks on unworn surface for surface fitting (one group track)

ftrack=1;               % the first tracks of the tracks chosen for surface fitting
nftrack=17;              % the number of tracks chosen for surface fitting

xdata0=t(:,3*ftrack-2);
ydata0=t(:,3*ftrack-1);
zdata0=t(:,3*ftrack);

    for a=ftrack+1:ftrack+nftrack-1
        xdata0=cat(1,xdata0,t(:,3*a-2));
        ydata0=cat(1,ydata0,t(:,3*a-1));
        zdata0=cat(1,zdata0,t(:,3*a));
        plot(sqrt(p(:,3*a-2).^2+p(:,3*a-1).^2),p(:,3*a));
        hold on;
    end

grid on;
figure;

xdata0(find(xdata0==0))=[];
ydata0(find(ydata0==0))=[];
zdata0(find(zdata0==0))=[];

data0=[xdata0,ydata0,zdata0];

% first surface fitting

f=@(p,data0)(data0(:,1)-p(1)).^2+(data0(:,2)-p(2)).^2+(data0(:,3)-p(3)).^2-p(4)^2;
p=nlinfit(data0,zeros(size(data0,1),1),f,[0 0 0 1]')        %Surface fitting

[X,Y,Z]=meshgrid(linspace(-18,18),linspace(-18,18),linspace(-18,-5,50));
V1=(X-p(1)).^2+(Y-p(2)).^2+(Z-p(3)).^2-p(4)^2;

c(1,:)=[p(1),p(2),p(3),p(4)];          %  the original centre of the cup

R1=abs(sqrt((data0(:,1)-p(1)).^2+(data0(:,2)-p(2)).^2+(data0(:,3)-p(3)).^2)-p(4));
[R1max,pos1]=max(R1)            % the sphericity of the surface fitting

% second surface fitting

s1=0.37;       % threshold for the data selection for the second surface fitting
k1=1;
[m1 n1]=size(data0);
```

```
    for i1=1:m1
        if R1(i1,1)<s1;
                data1(k1,:)=data0(i1,:);
                k1=k1+1;
        end
    end

f=@(p,data1)(data1(:,1)-p(1)).^2+(data1(:,2)-p(2)).^2+(data1(:,3)-p(3)).^2-p(4)^2;
p=nlinfit(data1,zeros(size(data1,1),1),f,[0 0 0 1]')            %Surface fitting
hold on

V2=(X-p(1)).^2+(Y-p(2)).^2+(Z-p(3)).^2-p(4)^2;

c(2,:)=[p(1),p(2),p(3),p(4)];

R2=abs(sqrt((data1(:,1)-p(1)).^2+(data1(:,2)-p(2)).^2+(data1(:,3)-p(3)).^2)-p(4));
[R2max,pos2]=max(R2)                        % the sphericity of the surface fitting

% to decide the wear depths and directions, and choose the worn surface data

rt=11;
kd=round(rt)+1;

x2=x1(:)-p(1);
y2=y1(:)-p(2);
z2=z1(:)-p(3);

[theta,phi,r]=cart2sph(x2,y2,z2);

pene=r(:)-p(4);
[maxpene,pos]=max(pene)
angle=(theta(pos))*180/pi

    for s=1:length(r)
            R(s)=p(4);
    end

[mtheta,mphi]=meshgrid(linspace(min(theta),max(theta),200),linspace(min(phi),max(phi),200));

mr=griddata(theta,phi,r,mtheta,mphi,'v4');
mR=griddata(theta,phi,R,mtheta,mphi,'v4');
err=mr-mR;

[s1 s2]=size(err);

    for s1=1:s1
        for s2=1:s2
            if err(s1,s2)<0;
                    err(s1,s2)=0;
            end
        end
    end

[mx,my,mz]=sph2cart(mtheta,mphi,mr);
```

```
surf(mx,my,mz,err);
colormap(jet);
shading interp;
xlabel('X'),ylabel('Y'),zlabel('Z');
axis([-kdkd -kdkd -kd 0]);
set(gca,'XTick',[-kd:4:kd],'YTick',[-kd:4:kd],'ZTick',[-kd:2:0]);
view(-12,42);
colorbar('YTick',0:0.2:2.0);


% to choose worn surface data and fitting the worn area

R=abs(sqrt((x1(:)-p(1)).^2+(y1(:)-p(2)).^2+(z1(:)-p(3)).^2)-p(4));

deviation=0.1;
s4=1;

    for s3=1:length(R)
            if R(s3)>deviation
                    w(s4,1)=x1(s3);
                    w(s4,2)=y1(s3);
                    w(s4,3)=z1(s3);
                    s4=s4+1;
            end
    end

f=@(p,w)(w(:,1)-p(1)).^2+(w(:,2)-p(2)).^2+(w(:,3)-p(3)).^2-p(4)^2;
p=nlinfit(w,zeros(size(w,1),1),f,[0 0 0 1]')

[wX,wY,wZ]=meshgrid(linspace(-18,18),linspace(-18,18),linspace(-18,-5,50));
Vw=(wX-p(1)).^2+(wY-p(2)).^2+(wZ-p(3)).^2-p(4)^2;

plot3(w(:,1),w(:,2),w(:,3),'o');
isosurface(wX,wY,wZ,Vw,0);
alpha.5;camlight;axis equal;gridon;view(3);
title(sprintf('(x-%f)^2+(y-%f)^2+(z-%f)^2=%f',p(1),p(2),p(3),p(4)^2))

grid on;
figure;

plot3(x1,y1,z1,'o');
isosurface(wX,wY,wZ,Vw,0);
grid on;
figure;
```

Appendix B
List of Publications

Journal papers

[1] **Hua, X.**, Wroblewski, B. M., Jin, Z. and Wang, L. The effect of cup inclination and wear on the contact mechanics and cement fixation for ultra high molecular weight polyethylene total hip replacements. Medical Engineering & Physics, 2012 , 34(3): 318-25.

[2] **Hua, X.**, Wroblewski, B. M., Wang, L., Jin, Z. and Fisher, J. The cup outer diameter influences the cement fixation of Charnley total hip replacement, 2012, Journal of Biomechanics, 45(S1): S82.

[3] **Hua, X**., Wang, L., Al-Hajjar, M., Jin, ZM., Wilcox, R., Fisher, J. Experimental Validation of Finite Element Modelling of a Modular Metal-on-Polyethylene Total Hip Replacement. Proceedings of the IMechE Part H: Journal of Engineering in Medicine, under review.

[4] **Hua, X**., Li, J., Wang, L., Jin, Z., Wilcox, R, Fisher, J. Contact mechanics of modular metal-on-polyethylene total hip replacement under edge loading conditions. Journal of Biomechanics. under review.

Conference proceedings

[1] **Hua, X.**, Jin, Z., Wilcox, R. and Fisher, J. Edge loading in metal-on-polyethylene modular total hip replacement: effect of cup angles and microseparation. 59th Annual Meeting of the Orthopaedic Research Society (ORS), San Antonio, USA, January 26-29, 2013. Oral presentation.

[2] **Hua, X.**, Wroblewski, B. M., Wang, L., Fisher, J. and Jin, Z. The cup outer diameter influence the cement fixation of Charnley total hip replacement. European Society of Biomechanics (ESB), Lisbon, Portugal, July 1-4, 2012. Oral presentation.

[3] **Hua, X.**, Wang, L., Jin, Z. and Fisher, J. The effect of cup angles on the contact stress in modular metal-on-polyethylene total hip replacement. UK

Society for Biomaterials Annual Conference (UKSB), Nottingham, UK, June 27-28, 2012. Oral presentation.

[4]   **Hua, X.**, Wang, L. and Jin, Z. The effect of head diameter and cup thickness on the contact mechanics and cement fixation for ultra high molecular weight polyethylene total hip replacement. International Tribology Conference (ITC), Hiroshima, Japan, October 30-November 3, 2011. Oral presentation.